Towards reliable reconstructions of Pliocene terrestrial temperatures using branched glycerol dialkyl glycerol tetraethers

Emily Dearing Crampton-Flood

ISBN 978-90-6266-545-7

Printed by Ipskamp Printing, Enschede

Graphic design cover: Margot Stoete

Cover photo: North Sea Pliocene paleogeography. Figure modifed from Gibbard and Lewin (2016).

Towards reliable reconstructions of Pliocene terrestrial temperatures using branched glycerol dialkyl glycerol tetraethers

Op weg naar betrouwbare reconstructies van de gemiddelde luchttemperatuur tijdens het Plioceen op basis van vertakte glycerol dialkyl glycerol tetraethers
(met een samenvatting in het Nederlands)

Proefschrift

ter verkrijging van de graad van doctor aan de
Universiteit Utrecht
op gezag van de
rector magnificus, prof.dr. H.R.B.M. Kummeling,
ingevolge het besluit van het college voor promoties
in het openbaar te verdedigen op
woensdag 3 juli 2019 des middags te 12.45 uur
door

Emily Katherine Louise Honora Dearing Crampton Flood

geboren op 11 april 1992
te Liverpool, Verenigd Koninkrijk

Promotoren:

Prof. dr. J.S. Sinninghe Damsté

Prof. dr. S. Schouten

Copromotor:

Dr. F. Peterse

This work has been financially supported by the Netherlands Earth System Science Center (NESSC) through a gravitation grant (NWO 024.022.001) from the Dutch Ministry for Education, Culture and Science.

“I am always doing that which I cannot do, in order that I may learn how to do it” – Pablo Picasso

For Granddad Ric

Table of contents

Summary

The current and imposing climate crisis caused in part by anthropogenic greenhouse gas emissions bears strong implications for the future of the earth's natural resources and forms of life. For example, the current unprecedented rise in temperatures is likely to result in sea level rise that affects the homes of a large proportion of the world's population that live in coastal areas. In order to inform policy-makers and prepare better for future climate scenarios, a detailed understanding of past climates that bear strong resemblances to the near-future is desirable. In particular, a period that is recognized by the Intergovernmental Panel on Climate Change (IPCC) as an analogue for the near future is the mid-Pliocene Warm Period (ca. 3.3–3.0 million years ago). Although carbon dioxide concentrations were similar to those of today, temperatures were approximately 2–3 °C higher than present during this period. Reconstructing the absolute values of land and sea temperatures and greenhouse gas concentrations, among others, in this time slice better informs climate models and thus could generate more reliable projections of climate in the near future. In the absence of instrumental records of climate during the Pliocene, these reconstructions are achieved through the application of a climate proxy (a stand-in measurement) on a suitable climate archive. Climate archives for the Pliocene are mostly limited to marine sediments and outcrop areas on land.

The current state of knowledge on the mid-Pliocene Warm Period climate is mostly centered on the marine realm, as that is the location where most of the complete and best preserved climate archives in the form of sediment cores are located. As such, less is known about terrestrial climate in the form of quantitative temperatures. The focus of this thesis is to reconstruct terrestrial temperatures using a group of biomarker lipids from bacteria preserved as molecular fossils in Pliocene-age marine sediments. These lipids form part of the cell membrane in bacteria which thrive in soils and peats, and upon cell death

they are released and fossilized in the sedimentary record. The abundance and distribution of these so-called branched glycerol dialkyl glycerol tetraethers (brGDGTs) in global soils and peats has been found to correlate with mean air temperature, probably as a result of the bacterial response to different environmental conditions. These observations form the basis of the so-called brGDGT paleothermometer which can be used as a proxy for terrestrial temperatures. BrGDGTs have been observed in coastal marine sediment records, where their presumed transport pathway from the continent to the sediment is via river and runoff processes. Thus, the temperature of whole river catchments can theoretically be reconstructed from marine sediments close to major river outflows containing large amounts of terrestrial material. In this thesis, coastal marine sediment archives close to major river outlets in the Pliocene were analysed and the brGDGT paleothermometer was applied to attempt to reconstruct Pliocene terrestrial temperatures on the nearby continent. In doing so, a number of caveats associated with the brGDGT paleothermometer in the context of record generation are examined, and methods to overcome these caveats are presented.

The generation of Pliocene terrestrial temperatures was first attempted at two coastal marine locations with (presumed) large input of soil-derived brGDGTs: the Ceará Rise, draining the Amazon River, and the Gulf of Mexico, draining the Mississippi River. At both sites, brGDGTs were analysed and the resulting records were critically evaluated for their reliability as records of past terrestrial temperatures. Through comparison of the brGDGT distributions from the Pliocene marine sediments with typical brGDGT distributions seen in modern soils, it is quite clear that the majority of the brGDGTs in the Gulf of Mexico and Ceará Rise sediments are not soil-derived. This observation ties in with recent evidence for production of brGDGTs in modern marine sediments and rivers. Indeed, the brGDGT signatures in sediments from the Gulf of Mexico and Ceará Rise are characteristic for marine water column and/or sedimentary production,

and the Amazon River system, respectively. This study presents the challenges associated with terrestrial temperature reconstruction using the brGDGT paleothermometer and identifies severe caveats with proxy that should be resolved before application to Pliocene sediment sequences.

In order to gain insight into the marine brGDGT production environment in more detail, the production of brGDGTs was examined in modern surface sediments from the Kongsfjorden and Krossfjorden in Svalbard. This site was the first marine site where the occurrence of *in situ* brGDGT production was suggested 10 years ago. The fjord sediments were (re)analysed with an upgraded chromatography method to better understand shifts in the suite of brGDGTs and glean insight into the phenomenon of marine *in situ* brGDGT production. This study affirms the findings of the initial study at the same site, however novel insights are gleaned from the separated analyses of the 'living' and 'dead' brGDGT distributions. The living and dead brGDGT distributions raise interesting implications regarding the possible change in production manifested in the brGDGT distributions throughout the year. Furthermore, a tentative link with the natural salinity gradient of the glacier terminus to outer fjord transect is proposed.

A next attempt to generate a brGDGT temperature record was targeted at a borehole located in the southern North Sea, which spans the Early Pliocene (~4.5 million years ago) to the Pleistocene (~2.5 million years ago). However, the proxies for *in situ* marine brGDGT production indicate that a fraction of the brGDGTs in the deeper (Pliocene age) part of the borehole are produced *in situ*, which impedes the creation of a terrestrial temperature record for the site. Using marine sites with reported *in situ* brGDGT production (including Svalbard) to create a marine brGDGT calibration, in combination with a mixing model formulated to determine the percentage contribution of terrestrial and marine brGDGTs in the borehole, a method was created to subtract the contribution from marine-derived brGDGTs. This method resulted in the first absolute terrestrial

temperature record for North Western Europe during the Pliocene, and shows that temperatures were approximately 1–3 °C higher than present. The record also reveals the presence of two cooler periods that interrupt the presumably stable warm Pliocene. The method is adaptable and can be applied to other marine sediment sequences. Furthermore, the method represents the first attempt for correcting the known bias of *in situ* brGDGT production in marine settings.

In order to put the Pliocene temperature record for North Western Europe into a global context, a good age model is crucial. Loose age control and suspected hiatuses in the borehole record could seriously undermine the impact of the temperature record and hinder the incorporation of the temperature data into climate models. A key challenge with this site is the coastal location, which presents difficulties for generating continuous records, as well as for the influence of fresh water on the oxygen isotope composition of benthic foraminifera that are generally used to construct an age model. First, hiatuses were identified using seismostratigraphy for the region. Secondly, the oxygen isotopic composition of endobenthic foraminifera that are less sensitive to disturbances and freshwater inputs, were used to make the match with a global reference stack for the Pliocene. This interdisciplinary approach allows the temperature record to be placed in the mid-Pliocene Warm Period. A subsequent multi-proxy study shows that the evolution of marine and terrestrial climate in the North Sea basin was asynchronous during the mid-Pliocene Warm Period.

Finally, a key aspect in the reliability of any climate proxy is the strength of the calibration that is used. Traditional linear regressions of brGDGT distributions and mean air temperatures results in a statistical phenomenon which leads to overestimation of temperature when the proxy is used to reconstruct temperatures in high latitude soils. A calibration using Bayesian statistics on an extended global soil and peat dataset remedies this phenomenon and increased the upper temperature limit of the proxy from approximately 25 °C to 29 °C, which allows the reconstruction of temperature records for lower latitude sites, which

are key to understanding future climate change. Despite this step forward, the lack of information regarding the specific bacterial producer(s) of brGDGTs impedes the creation of a calibration that encompasses this specific information and is a major stopgap in the understanding of this climate proxy.

The results and research presented in this thesis provide a re-assessment of the way in which the brGDGT paleothermometer can be applied to generate quantitative terrestrial temperature records for key periods in earth's history. The caveats associated with the proxy are thoroughly explored and a new methodology for extracting more accurate terrestrial temperatures from coastal marine sediments with mixed sources is presented. The final dated record for North Western Europe presents one of the first quantitative terrestrial temperature records covering the mid-Pliocene Warm Period in the literature, and sets a precedent for future applications of the brGDGT paleotemperature proxy for other periods. Finally, the work presented in this thesis has implications for brGDGT-based paleoclimate reconstructions not only in the Pliocene but for other marine sediments from various ages.

Samenvatting

De huidige opwarming van de aarde die wordt veroorzaakt door de uitstoot van broeikasgassen heeft grote consequenties voor de voorraad natuurlijke grondstoffen en verschillende vormen van leven op aarde. De ongekende snelheid waarmee de aarde nu opwarmt, zal bijvoorbeeld resulteren in een stijging van de zeespiegel, waardoor een groot deel van de mensen die in kustgebieden wonen met overstromeningen te maken zal krijgen. Om ervoor te zorgen dat beleidsmakers goed geïnformeerd zijn en ons goed kunnen voorbereiden op toekomstige klimaatveranderingen is een goed begrip van het klimaatsysteem erg belangrijk. Het Intergovernmental Panel on Climate Change (IPCC) wijst specifiek naar een warme periode tijdens het mid-Plioceen, de 'mid-Pliocene Warm Period' (mPWP), ongeveer 3,3 tot 3,0 miljoen jaar geleden, als analoog voor ons toekomstige klimaat. Hoewel de concentratie broeikasgassen in de atmosfeer in deze periode ongeveer gelijk was aan die van vandaag, lag de gemiddelde luchttemperatuur ongeveer 2–3 °C hoger. Reconstructies van onder andere lucht- en zeewatertemperaturen en broeikasgasconcentraties tijdens deze periode zijn nodig om klimaatmodellen te testen en dragen bij aan de betrouwbaarheid van de voorspellingen die ze maken voor het toekomstige klimaat. Aangezien er geen meetgegevens beschikbaar zijn voor het Plioceen, worden deze gegevens verkregen met behulp van zogeheten proxy's en beschikbare geologische archieven. Klimaatarchieven voor het Plioceen zijn vooral te vinden in sedimenten op de zeebodem en ontsluitingen op het land.

Het grootste deel van onze kennis over de mPWP is afkomstig uit het mariene bereik, aangezien de sedimenten op de zeebodem tot nog toe de meest complete en best bewaarde geologische archieven zijn gebleken. Als gevolg hiervan is er eigenlijk nog maar weinig bekend over het klimaat op het land, en dan met name de absolute luchttemperatuur, tijdens deze periode. De nadruk in dit proefschrift ligt daarom op het reconstrueren van de luchttemperatuur tijdens

het Plioceen aan de hand van organische chemische verbindingen die deel uitmaken van het celmembraan van bodembacteriën en als fossiele moleculen in sedimenten bewaard blijven. Het is gebleken dat variatie in de samenstelling van deze zogeheten vertakte glycerol dialkyl glycerol tetraethers (brGDGTs) in bodems en venen wereldwijd afhankelijk is van de jaargemiddelde luchttemperatuur (MAT), wat waarschijnlijk een aanpassing is van de bacterie aan andere leefomstandigheden. Deze relatie ligt ten grondslag aan de 'brGDGT-paleothermometer', die kan worden gebruikt als proxy voor luchttemperatuur. BrGDGTs zijn ook gevonden in mariene sedimenten in het kustgebied, waar ze na erosie en transport van land naar zee door rivieren worden afgezet. Door het bestuderen van veranderingen in de samenstelling van brGDGTs in kustsedimenten in de buurt van grote rivieren kan een reconstructie worden gemaakt van temperatuurvariabiliteit in het stroomgebied van de rivier in het verleden. In dit proefschrift worden kustsedimenten in de buurt van grote rivieren geanalyseerd op hun brGDGT-samenstelling, waarna de brGDGT-paleothermometer wordt toegepast om de MAT van het nabije continent tijdens het Plioceen te reconstrueren. Tijdens deze exercitie kwamen enkele beperkingen van de proxy aan het licht, zodat allereerst nieuwe methodes moesten worden ontwikkeld om die te omzeilen.

Voor de eerste pogingen om MAT voor het Plioceen te reconstrueren, werden kustsedimenten van de Ceará Rise, voor de monding van de Amazone, en de Golf van Mexico, voor de monding van de Mississippi, geselecteerd. Voor beide locaties werden de brGDGTs geanalyseerd. Door de samenstelling van de brGDGTs in de kustsedimenten te vergelijken met die in bodems werd duidelijk dat het grootste deel van de brGDGTs in de sedimenten van de Ceará Rise en de Golf van Mexico waarschijnlijk niet uit bodems afkomstig is. Dit is in overeenstemming met de recente ontdekking dat brGDGTs niet alleen in bodems, maar ook in rivieren en kustgebieden worden geproduceerd. De samenstelling van de brGDGTs in de sedimenten van de Golf van Mexico en de Ceará Rise

komt dan ook beter overeen met die van brGDGTs die in kustgebieden (Golf van Mexico) of de Amazone (Ceará Rise) zijn geproduceerd. De brGDGT-paleothermometer is hierdoor niet toepasbaar op deze locaties. Deze studie belicht de beperkingen in de toepasbaarheid van de proxy in kustsedimenten, en geeft een overzicht van de inzichten die zullen moeten worden verkregen voordat de brGDGT-paleothermometer algemeen kan worden gebruikt voor het reconstrueren van MAT tijdens het Plioceen.

Om beter inzicht te krijgen in de productie van brGDGTs in kustgebieden zijn brGDGTs in oppervlaktesedimenten van de Kongsfjord en de Krossfjord in Spitsbergen geanalyseerd. Op deze locatie is mariene productie van brGDGTs tien jaar geleden voor het eerst vastgesteld. Dezelfde sedimenten zijn nu opnieuw geanalyseerd met een verbeterde chromatografische methode, waardoor veranderingen in de samenstelling van brGDGTs in meer detail kunnen worden bestudeerd. Deze studie bevestigt dat brGDGTs in het mariene bereik worden geproduceerd, maar laat daarnaast ook zien dat de samenstelling van 'levende' en 'fossiele' brGDGTs in de sedimenten niet overeenkomt. Dit suggereert dat de samenstelling waarin brGDGTs worden geproduceerd, verandert gedurende het jaar. Daarnaast lijkt de saliniteit van het zeewater een bepalende factor te zijn in de samenstelling van mariene brGDGTs.

Een volgende poging om een temperatuurreconstructie te maken van het Plioceen richtte zich op brGDGTs in een sedimentkern uit de zuidelijke Noordzee die de periode tussen het vroeg Plioceen (~4.5 miljoen jaar geleden) tot het begin van het Pleistoceen (~2.5 miljoen jaar geleden) omspant. Ook hier liet de samenstelling van de brGDGTs zien dat een groot deel van deze verbindingen in het kustgebied is geproduceerd, vooral in het Pliocene gedeelte van de kern, wat het gebruik van de brGDGT-paleothermometer in de weg staat. In dit hoofdstuk wordt daarom een methode ontwikkeld waarmee het brGDGT signaal in kustsediment gecorrigeerd kan worden voor de bijdrage van mariene brGDGTs, daarbij gebruik makend van de kennis over mariene brGDGTs (zoals die in

Svalbard) en een mixing model. Met behulp van deze nieuwe methode kan alsnog de eerste kwantitatieve MAT reconstructie voor Noordwest-Europa worden gemaakt, die laat zien dat het tijdens het Plioceen 1-3 °C warmer was dan vandaag. Daarnaast wordt de toepasbaarheid van de brGDGT-paleothermometer in kustgebieden door het ontwikkelen van deze nieuwe methode substantieel vergroot.

Om vervolgens de klimaatreconstructie voor Noordwest-Europa in een wereldwijde context te plaatsen, is een goede ouderdomsbepaling van cruciaal belang. Immers, reconstructies die zweven in de tijd en mogelijk hiaten bevatten, zijn van veel minder waarde voor de validatie van klimaatmodellen. Een van de grote uitdagingen van een goede ouderdomsbepaling voor de sedimentkernen in de Noordzee is de geringe afstand van de kust tot de boorlocatie. Hierdoor kunnen er grote verschillen optreden in de sedimentatiesnelheid van het materiaal, maar ook speelt de invloed van zoet water een rol in de zuurstofisotopenverhouding in de benthische foraminiferen die vaak gebruikt worden voor ouderdomsbepaling. Eerst is de aanwezigheid van mogelijke hiaten bepaald met behulp van het seismische profiel van de regio. Daarna zijn de zuurstofisotopen van foraminiferen die relatief dieper in het sediment leven, en daardoor minder gevoelig zijn voor de invloed van zoet water en verstoringen, gemeten om alsnog de ouderdom van het sediment te kunnen bepalen. Door deze multidisciplinaire aanpak kan een deel van de reconstructie met zekerheid gekoppeld worden aan de mPWP. Een multi-proxy studie laat vervolgens zien dat temperatuurvariaties boven land niet synchroon verliepen met die van het zeewater tijdens deze periode.

Een belangrijk aspect dat bijdraagt aan de betrouwbaarheid van elke proxy is de sterkte van de correlatie die aan de proxy ten grondslag ligt. Tot nu toe wordt meestal een lineaire regressie tussen de brGDGT-samenstelling en MAT gebruikt als uitgangspunt, al leidt deze benadering tot een statistische afwijking waardoor de proxy MAT overschat bij bodems van hogere

breedtegraden. Deze afwijking kan worden verholpen door het gebruik van Bayesiaanse statistiek. Toepassing van deze methode op een grote wereldwijde dataset van brGDGTs in bodems en venen leidt inderdaad tot verbetering, en zorgt er tegelijk voor dat de bovengrens van de proxy van 25 °C naar 29 °C stijgt. Dit zorgt ervoor dat de proxy veel gevoeliger wordt in het hogere bereik en dus ook temperaturen voor locaties in de tropen veel nauwkeuriger kan reconstrueren. Ondanks deze grote stap voorwaarts is het allergrootste obstakel dat ons ervan weerhoudt om de proxy nog beter te maken dat we nog steeds niet weten welk(e) specifieke organisme(n) brGDGTs produceren.

De data die in dit proefschrift worden gepresenteerd, hebben geleid tot een evaluatie van de toepasbaarheid van de brGDGT-paleothermometer in kustsedimenten. Alle beperkingen van de proxy in kustgebieden zijn uitgebreid in kaart gebracht, waarna een methode is ontwikkeld om een bijdrage van mariene brGDGTs te herkennen en het brGDGT-signaal daar vervolgens voor te corrigeren. De uiteindelijke temperatuurreconstructie voor Noordwest-Europa tijdens het Plioceen is de eerste kwantitatieve reconstructie met betrouwbare ouderdomsbepaling in de literatuur. Ten slotte opent het werk van dit proefschrift de deur voor het reconstrueren van MAT op basis van brGDGTs in kustsedimenten van andere locaties en ouderdom.

Chapter 1

Introduction

1.1 Temporal perspectives on climate change

Global climate is currently changing, due in part to anthropogenic carbon dioxide (CO_2) emissions caused by deforestation and fossil fuel consumption (IPCC, 2014). The concentration of CO_2 in the atmosphere has been rising steadily since *in situ* measurements started in 1958 at the Mauna Loa observatory in Hawaii (Keeling et al., 2017). At present, the CO_2 concentration in the atmosphere is ~410 ppmv (parts per million per volume; scripps.ucsd.edu/programs/keelingcurve), but is projected to reach 490–1370 ppmv in 2100, depending on the chosen representative concentration pathway (RCP; Fig. 1; Van Vuuren et al., 2006, 2007; Riahi et al., 2007). Increasing atmospheric CO_2 concentration leads to ocean acidification and climate warming, which can consequently exert severe effects on human civilization such as droughts and food shortages in the near future (O'Brien et al., 2006; IPCC, 2014). To project the climate feedbacks in a world with higher atmospheric CO_2 concentrations, it is crucial to understand climate evolution during periods in the Earth's history with CO_2 concentrations similar to that of the (near) future. Furthermore, studying past climates may also constrain the Earth system response to future climate forcing by enabling the identification of the relative contribution of natural and anthropogenic climate perturbations.

Instrumental records for temperature and CO_2 provide the most accurate data to study past climate, due to the relatively small error associated with instrumental measurement techniques. However, instrumental records are relatively short, only ranging back ~260 years for land surface temperatures (Rohde et al., 2013), and ~55 years for atmospheric CO_2 concentrations (Keeling et al., 2017). Thus, other methods are needed to acquire information about pre-instrumental record era climate. For example, physical and chemical features stored in climate archives can be measured in order to infer past changes in environmental parameters such as temperature, precipitation, and concentrations of gases in the atmosphere, among others. This forms the basis of a climate

proxy, which is a stand in measurement used to reconstruct past climate. To illustrate, calcareous fossils stored in marine sediment archives can be studied for their isotopic content, which reflects the seawater composition at the time of carbonate formation (Urey, 1947; Emiliani, 1955). Using the oxygen isotopic composition of pelagic foraminifera in Pleistocene sediments, Emiliani (1955) reconstructed seawater temperatures and furthered the understanding of Pleistocene 'ice ages' by demonstrating that periodic seawater temperature minima occurred in tandem with continental glaciation events. Other proxies for temperature reconstruction using marine sediments include the magnesium/calcium (Mg/Ca) content of foraminifera (Nürnberg et al., 1996), and the unsaturation index of alkenones ($U^{K'}_{37}$), produced by marine phytoplankton (Brassell et al., 1986), among others.

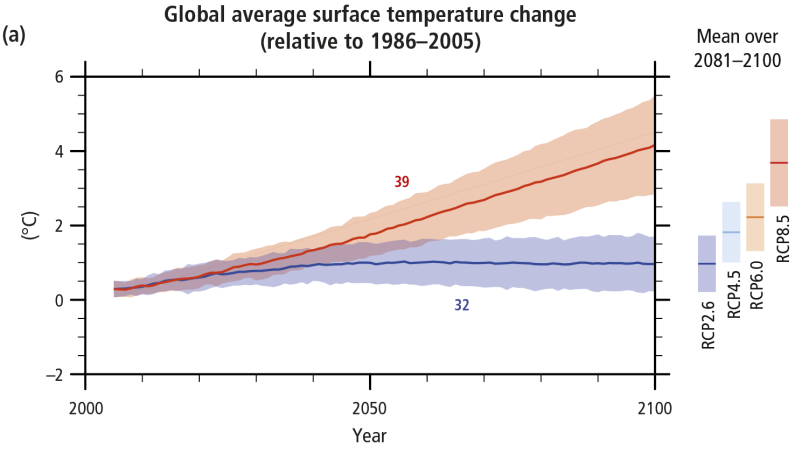

Fig. 1. IPCC 2014 projected global average surface temperature change until 2100 (IPCC, 2014). Representative concentration pathway (RCP) 2.6 and 8.5 refer to stringent and very high emissions, respectively. The number next to each curve indicates the number of coupled model intercomparison project Phase 5 (CMIP5) models used to calculate the multi-modal mean.

Past climate changes are also recorded in Arctic and Antarctic ice cores, where isotopes of air trapped in the ice reflect changes in global temperatures and

CO_2 composition (Dansgaard et al., 1984; Lorius 1984; Jouzel et al., 1987). On the continent, fossil plant remnants and organic molecules extracted from outcrops and paleosol deposits can be studied to reveal information on past vegetation, temperature, and CO_2 levels (Bailey and Sinnott, 1916; Woodward, 1987; Wolfe, 1995; Xie et al., 2003). For example, plant waxes stored in loess-paleosol sequences at the Chinese Loess Plateau have been used to reconstruct vegetation change and monsoon variability in East Asia over the last 35 ka (Liu et al., 2005). More continuous but relatively younger-aged deposits on the continents are lake sediments, whose biomarker and fossil flora/fauna content, among others, can impart information on lake water temperature, terrestrial temperature, and biological productivity (see Castañeda and Schouten, 2011 for a review).

1.2 The Pliocene and mid-Piacenzian Warm Period as analogues for future climate

The Pliocene (5.33–2.58 Ma) is a relatively stable period that preceded the onset of large interglacial/glacial climate shifts that characterize the climate of the Quaternary (Fig. 2). Pliocene paleoclimate research specifically focuses on the so-called mid-Pliocene Warm Period, or mid-Piacenzian Warm Period (mPWP; 3.264–3.025 Ma), as an analogue for current climate for two main reasons: firstly, atmospheric CO_2 levels were estimated to have been between 400–450 ppmv (Seki et al., 2010; Badger et al., 2013; Haywood et al., 2016a), comparable to present day and the near future; and secondly, continental figurations, ocean bathymetry, and land elevations were largely similar to the present (Crowley, 1996; Dowsett et al., 2010). However, proxies and models show that global temperatures in the mPWP were 2–4 °C warmer than pre-industrial temperatures (Dowsett et al., 2010; Haywood et al., 2013). Thus, these reconstructions suggest

that modern climate has not yet reached equilibrium, and that the mPWP may likely reflect the projected climate of the middle of the 21st century.

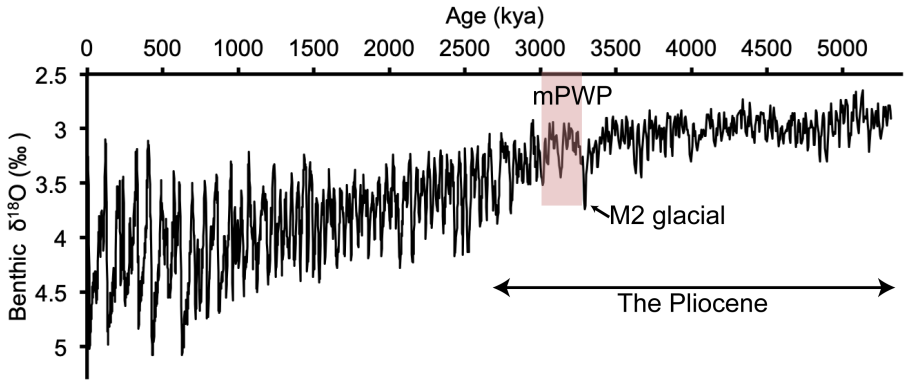

Fig. 2. Benthic oxygen isotope stack of Lisiecki and Raymo (2005) from 5.33 Ma to present. Key intervals of Pliocene climate discussed in the text are indicated.

A globally recognized cooler interval during the relatively stable Pliocene is the M2 event (Marine Isotope Stage M2, ~3.3 Ma; Lisiecki and Raymo, 2005), which is considered a failed attempt by the Earth to transfer into the glacial-interglacial cycles of the Pleistocene (Haug and Tiedemann, 1998). The recovery of the M2 event into the mPWP is especially targeted in order to study the rates of temperature change and the spatial variation of these rates. This interval represents the lower boundary of the time interval selected by the Pliocene Research Interpretation and Synoptic Mapping Project (PRISM). The PRISM project is a significant effort to compile all Pliocene climate data to provide global boundary conditions and verification data to the climate modeling community (Dowsett et al., 1994, 2010, 2013). A large proportion of this data pertains to the reconstruction of sea surface temperatures (SSTs), due to the recovery of marine archives as part of the numerous ocean drilling project (ODP) and international ocean drilling project (IODP) expeditions. The mPWP SST records in Fig. 3 compiled and confidence assessed by Dowsett et al. (2012), of which there are 95 in total, illustrate the global scope of the PRISM project.

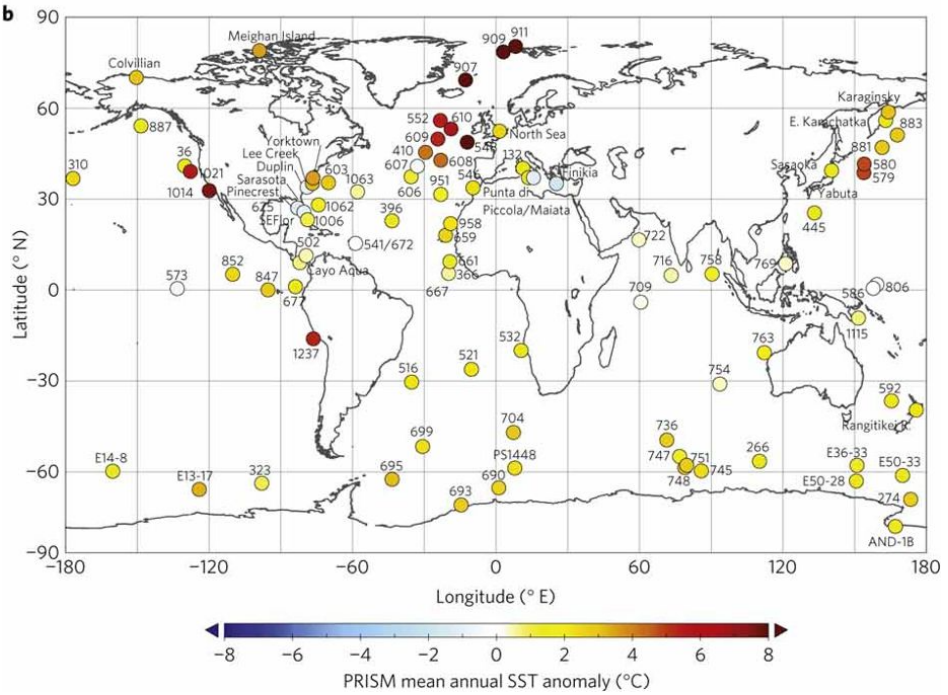

Fig. 3. Compilation of 95 sea surface temperature (SST) records of the Pliocene Research Interpretation and Synoptic Mapping project (PRISM; Dowsett et al., 2012). SSTs are presented as anomalies compared to pre-industrial values.

The SST records in Fig. 3 are mainly based on three proxies: faunal assemblages, Mg/Ca of foraminifera, and lipid biomarkers (Dowsett et al., 2012). Faunal assemblages, such as fossilized diatoms and foraminifers, can be used to estimate water temperatures under the assumption that the paleo-assemblages respond to SST in a similar way as the modern assemblages (e.g. Keller, 1978). In contrast, the Mg/Ca paleothermometer is based on the observation that more magnesium is incorporated into a calcareous shell of planktic foraminifera at higher temperatures (Lear et al., 2000). Biomarker paleothermometry is based on the premise that the distribution of lipids in marine organisms responds to sea surface temperature (Brassell et al., 1986; Schouten et al., 2002; Rampen et al., 2012). The first biomarker paleothermometer used to reconstruct past SSTs is the alkenone unsaturation index, U^{K}_{37}, which is based on unsaturated ketones

synthesized by haptophyte algae (Brassell et al., 1986). An increased degree of unsaturation in the C_{37} alkenones correlates with an increase in temperature (Brassell et al., 1986). Another established SST proxy is based on isoprenoidal glycerol dialkyl glycerol tetraethers (isoGDGTs) produced by marine archaea, which are used in the Tetraether index of 86 carbon atoms, or TEX_{86} (Schouten et al., 2002). The relative increase in the number of rings in isoGDGTs was found to correlate with increasing seawater temperature, in both the natural environment and mesocosm experiments (Schouten et al., 2002; Wuchter et al., 2004; Schouten et al., 2007). The latest calibration of this proxy is based on isoGDGTs in 426 globally distributed core-top sediments (Kim et al., 2010).

The multi-proxy SST compilation of Dowsett et al. (2012) is an advantageous tool for gaining insights from examining regions in the world where the proxies agree (or disagree) with each other. For example, the SST records in Fig. 3 indicate that the North Atlantic was particularly sensitive to warming in the Pliocene, which is also recognized in present day patterns of global warming (Keigwin et al, 1994; Xie et al., 2010).

1.3 Pliocene terrestrial temperature reconstructions

In contrast to the large collection of Pliocene SST records, there is a relative scarcity of terrestrial temperature reconstructions. The lack of a quantitative terrestrial temperature compilation similar to that for the marine realm is due in part to the paucity of well-dated, continuous archives on land and the lack of proxies that reliably reconstruct terrestrial temperatures. Regardless, terrestrial temperatures are a vital component to understanding Pliocene climate for several reasons. Firstly, a direct comparison of SSTs and terrestrial temperatures gives insight into the distribution of heat in the oceans and atmosphere, and is a powerful way to reconstruct regional hydroclimate Secondly, paleorecords of terrestrial air temperatures are severely underrepresented in Pliocene climate models prohibiting a proper evaluation of model output. Finally, the use of the

mPWP as a future climate analogue indicates that terrestrial temperatures are an important parameter to constrain given the fact that the majority of humans live on the continents and will be impacted by ongoing warming and associated consequences.

Only a limited number of proxies exist that can be used to reconstruct mean annual temperatures (MATs) on the continent. The isotopic composition of ice cores (Jouzel et al., 1987) and speleothems (Hendy and Wilson, 1968) can be used as a proxy to reconstruct MAT. However, the most extensive ice sheets on Antarctica only cover the last ~1 Ma (Jouzel et al., 2007). Speleothems of Pliocene-age may exist, however, the absence of absolute-dating methodologies for speleothems outside the range of U/Th dating (400,000–800,000 years; Dorale et al., 2004) renders them unsuitable for Pliocene MAT reconstruction. Other methods that are generally used to reconstruct MATs are based on tree rings (Libby and Pandolfi, 1974), fossil pollen assemblages (Bernabo, 1981), leaf remnants (Ach and Spicer, 1996), and chironomids (Walker et al., 1991). Terrestrial temperature reconstruction using tree rings is generally advantageous due to the tight age constraints provided by dendrochronology (Hughes, 2002), however, the role of other climate factors such as precipitation can obscure the temperature signal (Graumlich and Brubaker, 1986). Furthermore, the proxy is not suitable to reconstruct Pliocene temperatures due to the poor preservation of intact plant material over these timescales, and tree ring temperature records only cover the past three millennia (Lara and Villalba, 1993).

Fossil pollen assemblages and leaf remnants stored in sedimentary archives are a reflection of the plant community at the time of deposition, and thus give insights into past environmental conditions. These proxies are especially useful for terrestrial temperature reconstruction during more recent periods because many species in recent archives are extant. Pollen and leaf remnants are also preserved over long timescales; however, they often suffer from a ‘no-modern analogue’ problem (Davis et al., 2003; Birks and Seppa, 2004a).

Proxies based on plant remains are qualitative for the most part, and the effects of humidity and temperature cannot easily be differentiated (Guiot, 1990). This issue also applies to chironomids preserved in lake sediments (Velle et al., 2010). Furthermore, chironomids are more skewed toward reconstructing summer temperatures than MATs (Heiri et al., 2003). The errors associated with leaf remnants, fossil pollen, and chironomids as proxies for MAT are often high because they produce ranges of reconstructed temperature rather than absolute values (Coope, 1970; Guiot, 1990; Mosbrugger and Utescher, 1997). However, they are the only applicable proxies for Pliocene MAT reconstruction and as such, make up the bulk of Pliocene terrestrial data (Salzmann et al., 2008, 2013).

A compilation of paleobotanical site pollen data reveals that the continental climate was generally warmer and moister during the Pliocene, with smaller deserts and expanded warm-temperate forests (Salzmann et al., 2008). Pollen-inferred temperature anomalies indicate that MAT was 1–10 °C higher compared to pre-industrial (Salzmann et al., 2013), particularly in the Northern Hemisphere, although this may be because most of the sampling sites are located there. The compilation of Salzmann et al. (2013) provides a first glance into the Pliocene terrestrial climate. However, most of the archives in the compilation are discontinuous and thus cannot be used to infer long-term climate trends. This factor and the semi-quantitative nature of pollen temperature estimates indicate that the need for quantitative, continuous, well-dated temperature records is not yet fulfilled.

1.4 brGDGT-paleothermometry

Branched alkyl glycerol dialkyl glycerol tetraethers (brGDGTs; Fig. 4a) are membrane lipids of bacteria that have been documented in soils and peats worldwide (Sinninghe Damsté et al., 2000; Weijers et al., 2007a). Unlike the isoGDGTs, the alkyl backbone of brGDGTs is not isoprenoidal, but is branched. BrGDGTs can have 4-6 methylations in total, with four methyl groups at the 13

and 16 positions, and one or two methyl groups at the 5- or 6- positions on the alkyl chain (Sinninghe Damsté et al., 2000; De Jonge et al., 2013). They can also be composed of up to two internal cyclisations. They were first discovered in a Dutch peat bog (Sinninghe Damsté et al., 2000), and are surmised to have a bacterial origin, based on the 1,2-di-*O*-alkyl-*sn*-glycerol stereo-configuration of the glycerol moiety (Weijers et al., 2006). The exact biological source of brGDGTs is unknown, but they are sourced from (presumably) heterotrophic bacteria (Pancost and Sinninghe Damsté, 2003; Weijers et al., 2010). So far, at least one brGDGT, Ia, was found in a strain of Acidobacteria (Sinninghe Damsté et al., 2011), though the assignment of individual brGDGTs to their exact producers is an ongoing effort (Sinninghe Damsté et al., 2011; 2018).

An empirical study that examined the distribution of brGDGTs in globally distributed soils revealed that temperature explained a large part of the variation in brGDGT signature (Weijers et al. 2007a). The Methylation of Branched Tetraethers (expressed as MBT) is related to MAT and soil pH, and the cyclisation of branched tetraethers (CBT) is related to soil pH (Weijers et al., 2007a). The presence of more methyl branches on the alkyl chains correlates with lower temperatures (Fig. 4b), and is hypothesized to be an adaptation of the cell to retain membrane fluidity in changing environments such as observed with cyclopentane moieties in archaea (Van de Vossenberg et al., 1995, 1999). These relations are at the base of a paleotemperature proxy that translates brGDGT distributions into MAT (Weijers et al., 2007a). The first proof of concept of the proxy in a paleo-setting is the reconstruction of the deglaciation of tropical Africa using brGDGTs associated with fluvially discharged soil organic matter (OM) archived in Congo River fan sediments (Weijers et al., 2007b), where they are presumed to represent an integrated climate signal of the catchment area of the river. Soil-derived brGDGTs are also used to determine the relative contribution of soil OM to marine sediments, quantified in the Branched and Isoprenoid Tetraether (BIT) index (Hopmans et al., 2004). The BIT index is a ratio of the

sum of brGDGTs with crenarchaeol (Fig. 4a), a characteristic biomarker for marine Thaumarchaeota (formerly known as Crenarchaeota; Sinninghe Damsté et al., 2002), where high BIT implies a significant amount of soil terrestrial input and vice versa for a low BIT. However, several studies have shown that brGDGTs may also be produced in coastal marine environments (e.g. Peterse et al., 2009a; Zhu et al., 2011). Thus, *in situ* produced brGDGTs may alter the initial soil brGDGT signal in coastal sediments characterized by a low BIT value. Hence, coastal marine sediments need to be screened prior to using brGDGTs in these sediments to infer paleotemperatures of the adjacent continent (Zell et al., 2014a).

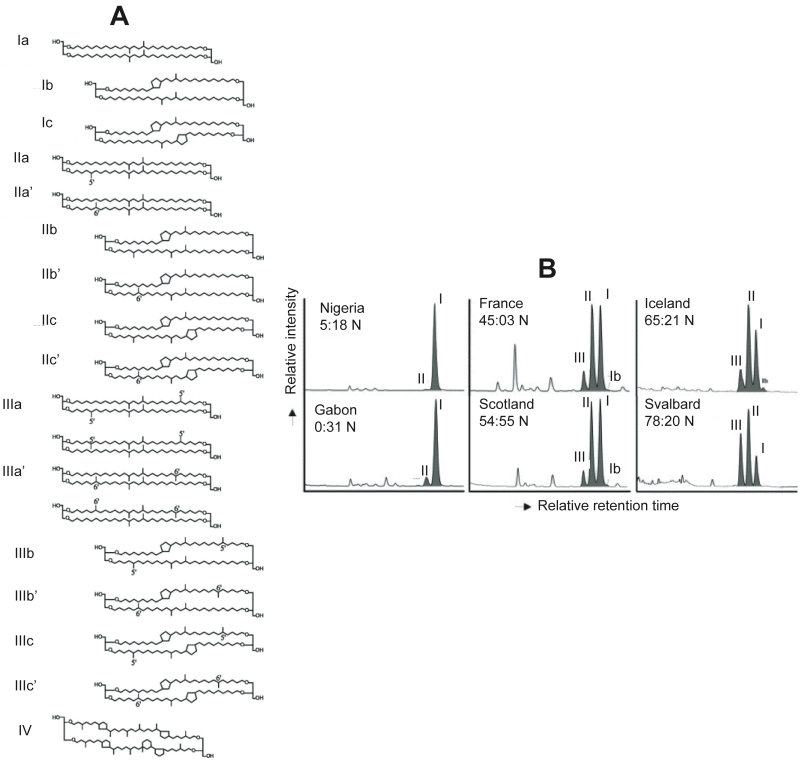

Fig. 4. (A) Structures of the fifteen brGDGTs used in the brGDGT paleothermometer (after De Jonge et al., 2014a). The structure of crenarchaeol used in the calculation of the BIT index is also shown (IV). (B) HPLC chromatograms showing the temperature dependence of the major brGDGTs over low, mid and high latitudes (modified from Weijers et al., 2007a).

Although the brGDGT paleothermometer is one of the few proxies that can quantitatively reconstruct terrestrial temperatures over a wide range of temporal scales (e.g. Weijers et al., 2007c; Schouten et al., 2008; Donders et al., 2009; Peterse et al., 2011), the accuracy of the absolute temperature estimates can still be improved as the error on the latest calibration is relatively large, 4.8 °C (De Jonge et al., 2014a). Recent advances in chromatography techniques resulted in the identification of previously co-eluting isomers distinguishable by the position of the peripheral methyl group located on the 6-position of the alkyl branch (De Jonge et al., 2013; Fig. 4A). Reanalysis of the global soil calibration set indicated that only the 5-methylated isomers responded to temperature, whereas the 6-methylated varieties correlated better with soil pH (De Jonge et al., 2014a). This led to a new index, MBT′5Me, which removes the pH dependency of the MBT and is defined by a decrease in scatter of the relationship between brGDGT distributions and MAT (De Jonge et al., 2014a).

1.5 Scope and framework of this thesis

This thesis aims to generate quantitative, continuous terrestrial temperature records for the Pliocene using brGDGTs in coastal marine sediments near various large river outflows in the world. All targeted sites were assessed for the influence of *in situ* production on brGDGT signals stored in the sedimentary records. Moreover, ways to disentangle marine versus terrestrial brGDGTs and to correct for a potential aquatic overprint were investigated to improve the reliability of brGDGT-based paleotemperature records derived from coastal marine sediment archives. The Pliocene climate records generated in this thesis are placed in a global perspective by developing an age framework for the Pliocene North Sea area. Finally, a calibration exercise for the brGDGT paleothermometer was also carried out in order to assess the effect of

confounding factors such as seasonality on the proxy and to improve the accuracy of the transfer function.

In **Chapter 2**, the brGDGT paleothermometer was applied to sediment sequences in the Gulf of Mexico and the Ceará Rise (Amazon Fan) in order to reconstruct Pliocene continental temperatures of the adjacent river basins. The proximity to the Mississippi and Amazon Rivers was thought to yield sufficient terrestrial input to these sites. Surprisingly, application of the brGDGT paleothermometer to both sites resulted in disparate absolute temperatures compared to Pliocene model estimates, and temperatures were in some cases severely underestimated compared to the present day. Furthermore, the trends in both records did not indicate any variability associated with major Pliocene climate events (e.g. the M2 event). Through a comparison with brGDGT distributions in modern coastal settings, a high degree of marine *in situ* brGDGT production was found to alter the soil signal in the Gulf of Mexico sediments, and the Ceará Rise sediments were influenced by aquatic brGDGTs produced in the lower Amazon River. Based upon these results, the need for a method to identify and correct for the effects of *in situ* brGDGT production in these, and other, settings is highlighted.

The issue of *in situ* production of brGDGTs in coastal marine environments is therefore studied in **Chapter 3** by re-visiting the Svalbard fjords, where this production was first described (Peterse et al., 2009a). The fjord sediments from Peterse et al. (2009a) as well as those collected at the same sites one year later, were (re-)analysed using the new HPLC method with improved chromatography to study spatial trends and patterns of both 5- and 6-methylated isomers (De Jonge et al., 2014a; Hopmans et al 2016) of living (intact polar lipid-derived) and fossil (core lipid) brGDGTs in the same sediment. The high (>0.7) weighted average of the number of rings of the tetramethylated brGDGTs (Ia, Ib, Ic), $\#rings_{tetra}$, confirmed the predominantly *in situ* origin of brGDGTs in fjord sediments. Substantial differences in the $\#rings_{tetra}$ between 'living' and 'fossil'

brGDGTs in the same sediment sample indicated that brGDGTs are produced in different configurations throughout the year. Furthermore, the spatial variation in $\#rings_{tetra}$ suggests that brGDGT production may be influenced by the natural salinity gradient and associated microbial community changes in the fjord to open ocean transect.

In **Chapter 4** brGDGTs in a borehole from Hank, located in the western Netherlands, were analysed to generate a temperature record for North Western Europe during the Pliocene. Shifts in the total organic carbon (TOC) content of the sediments and its stable carbon isotopic composition ($\delta^{13}C_{org}$) show a transition from marine organic matter (OM) during the Pliocene to terrestrial OM towards the Pleistocene, suggesting that the source of brGDGTs has changed over time. *In situ* brGDGT production was identified using the $\#rings_{tetra}$ index. The use of a mixing model and a new transfer function for coastal marine brGDGTs enabled the removal of the *in situ* overprint on the terrestrial temperature record. The corrected temperature record shows that NW Europe was indeed 1–2 °C warmer than present during the Pliocene, confirming previous pollen-based estimates. Importantly, this novel correction method extends the applicability of this proxy to other coastal marine settings influenced by *in situ* brGDGT production.

In order to provide a global context for the Pliocene temperature record for North Western European climate generated in Chapter 4, **Chapter 5** focuses on the generation of an age framework for the Pliocene North Sea Basin. To circumvent the influence of freshwater input on the $\delta^{18}O$ values of benthic foraminifera generally used for age model reconstruction, the endobenthic foraminifera species *Cassidulina laevigata* was targeted for $\delta^{18}O$ analysis. In combination with seismic records, an age model was derived for the interval ~3.2–2.8 Ma, covering most of the mPWP. The M2 event is marked by a hiatus that is also recognized in a range of records from the southern North Sea to the

Nordic Seas. Finally, the brGDGT-based terrestrial temperature record (from Chapter 4) is complemented with climate records based on lipid biomarker SST proxies, pollen, and dinoflagellate cyst assemblages. The multi-proxy records show that the mPWP climate was stable on land, however, the marine climate was more variable, and SSTs were probably influenced by changes in the strength and direction of the North Atlantic Current.

Despite analytical improvements and various attempts at re-calibrating the brGDGT paleothermometer, the calibration error on the proxy remains relatively large, adding uncertainty to the temperature records it produces. In **Chapter 6** a Bayesian approach is used to investigate potential confounding factors that may be responsible for the large scatter of residuals in the previous global surface soil calibrations. The different models used to assess the confounding factors indicated that temperature seasonality explains a large part of the scatter, and that excluding soils with seasonality >20 °C substantially decreased the root mean squared error (RMSE) and the variance of the model residuals. The $BayMBT_0$, which excludes the temperatures of all months below 0 °C in the calculation of MAT, best captures the relation of brGDGTs with temperature, and also possesses the lowest RMSE (3.8 °C). Furthermore, the addition of soils from high temperature regions to the calibration dataset increased the upper temperature limit of the models from ~25 to 27–29 °C. Finally, testing the $BayMBT_0$ on two published climate records illustrated that the trends and timing of the records are preserved, and the absolute values are slightly higher than those reconstructed using previous calibrations.

In summary, the results of this thesis show that brGDGTs in coastal archives can be used to generate reliable records of terrestrial Pliocene climate. However, a sufficient input of terrestrial material to a site and a thorough assessment of the sources of brGDGTs to the sediments should be carried out. This thesis indicates that *in situ* brGDGT contribution can be recognized by the $\#rings_{tetra}$ index, and a method to correct for potential marine *in situ* production

using this index is provided. By generating an age framework for the Pliocene North Sea, a final Pliocene terrestrial temperature record for North Western Europe was presented that currently represents the most accurate absolute Pliocene terrestrial temperature record for the mPWP to date. Moreover, the error on the proxy was reduced using Bayesian statistics, which also indicates that seasonality has a strong bearing on the RMSE of the calibration.

Chapter 2

Marine and riverine production of branched GDGTs prohibits the reconstruction of Pliocene continental temperatures from Mississippi and Amazon River fan sediments

Emily Dearing Crampton-Flood, Francien Peterse, Guido van de Molen, Carolien van der Weijst, Francesca Sangiorgi, Appy Sluijs, Jaap S. Sinninghe Damsté.

In preparation for *Organic Geochemistry*.

Abstract

The mid-Piacenzian Warm Period (mPWP, 3.3–3.0 Ma) shares several common features with the present, such as similar continental configurations and ocean bathymetry. Moreover, the range of reconstructed atmospheric CO_2 concentrations in the mPWP is comparable to the present concentration of ~410 ppmv. These reasons make the mPWP an appealing interval to consider as an analogue for our current climate. However, proxy data indicate that temperatures in the mPWP were 2–3 °C warmer than present, which implies that the current climate is not yet in equilibrium. Thus, studying the mPWP can give insights into future climate. Despite the large number and global scope of mPWP sea surface temperature reconstructions, terrestrial temperatures are largely overlooked, mostly due to a lack of quantitative proxies for mean air temperature (MAT). Here, we analysed branched glycerol dialkyl glycerol tetraethers (brGDGTs) in coastal marine sediments near the outflow of the Mississippi (Gulf of Mexico; GoM) and Amazon (Ceará Rise) Rivers to reconstruct terrestrial temperatures of the river catchments during the mPWP. Extremely low branched to isoprenoid tetraether (BIT) index values of 0.02–0.13, and the near absence of pollen and long chain plant waxes in the Gulf of Mexico sediments suggest that the Mississippi River did not have a strong influence at the study location during the Pliocene and soil input was limited. Indeed, the high weighted average of cyclopentane containing tetramethylated brGDGTs ($\#rings_{tetra}$) in the GoM sediments (0.50 ±0.09) relative to that of modern soils from the Mississippi catchment (0.34 ±0.22) indicates that the brGDGTs in the GoM sediments are produced *in situ* in the marine realm, hampering reliable temperature reconstruction using the global soil calibration. Despite high BIT index values (average 0.46 ±0.21) and low $\#rings_{tetra}$ (average 0.25 ±0.15) that indicate a soil-origin of the brGDGTs, reconstructed temperatures in the Ceará Rise sediments were lower than expected and trends were difficult to interpret. Subsequent comparison of the relative abundance of the 6-methylated brGDGTs in the sediments to that in catchment soils and Amazon River suspended particulate matter (SPM) reveals that brGDGTs in the Ceará Rise sediments resemble the brGDGT signal of the SPM rather than that of the catchment soils. Thus, the majority of the brGDGTs in both the GoM and Ceará Rise sediments are produced *in situ*, in the marine or river realms, which precludes application of the brGDGT paleothermometer. Hence, to reconstruct changes in past terrestrial temperatures using this proxy, the relative contributions of soil-derived and aquatic brGDGTS in coastal marine sediment archives must be disentangled.

1. Introduction

The Pliocene (5.33–2.58 Ma) was an epoch of relatively stable, warm climate conditions prior to the onset of Northern Hemisphere glaciation and the transition into the glacial-interglacial cycles that characterize the Pleistocene. Despite the generally stable climate, manifested by the relatively low fluctuations in the benthic $\delta^{18}O$ stack record of Lisiecki and Raymo (2005), several cooling events take place in the Pliocene, one of which is Marine isotope stage M2, or the 'M2 event' from 3312–3264 ka. The M2 event is recognized globally (De Schepper et al., 2014), and thus it may represent a pioneer attempt of the earth system to initiate a glaciation similar to that of the more severe glaciations that followed in the Pleistocene (Haug and Tiedemann, 1998).

The Pliocene, and in particular the mid-Piacenzian warm period (mPWP; 3264–3025 ka), is considered as an analogue for (near) future climate change scenarios caused by anthropogenic global warming (Masson-Delmotte et al., 2013). This is because the Pliocene is the most recent period in which carbon dioxide (CO_2) concentrations in the atmosphere, estimated to have been 400–450 ppmv, were similar to modern values (Seki et al., 2010; Badger et al., 2013; Haywood et al., 2016). Furthermore, continental configurations were largely similar to present. In contrast, global temperatures were 2–3 °C warmer (Haywood et al., 2016), and the sea level was approximately 20 m higher (Miller et al., 2012), indicating that current climate has not reached equilibrium. Thus, studying the climate system during the Pliocene and mPWP intervals could provide crucial insight on climate processes in a warmer world, similar to the warming advisory 'limits' of 1.5–2 °C that the Intergovernmental Panel for Climate Change has suggested for the end of the century (IPCC, 2018).

Over the last decades, a significant effort has been directed toward the reconstruction of Pliocene and mPWP climate, which has been the focus of the Pliocene Research, Interpretation and Synoptic Mapping (PRISM) initiative (Dowsett et al., 1994). The PRISM data compilation shows that global sea surface

temperatures (SSTs) were on average 2–3 °C higher than pre-industrial values, but were as much as 6 °C higher in the North Atlantic (Dowsett et al., 2012). Furthermore, SST evidence suggests that the meridional temperature gradient was reduced from 8 °C to 2 °C in the Pacific (Brierley et al., 2009). Although there is a wealth of data in the marine realm, there is a lack of precise and accurate terrestrial temperature reconstructions. This is in part due to the unavailability of quantitative terrestrial temperature proxies. Our current knowledge regarding Pliocene terrestrial temperatures is primarily derived from pollen assemblages (see compilation in Salzmann et al., 2008), which can be translated into biome types and terrestrial temperature ranges. However, pollen-based temperatures are often biased towards the summer or growing season. Also, pollen assemblages rely on extrapolated information from the modern system, which introduces uncertainty in cases where no modern analogue exists for Pliocene taxa (Birks and Seppa, 2004a; Velle et al., 2010). In addition, next to temperature, precipitation also influences pollen assemblages and thus may influence the signal (Guiot, 1990). Overall, there is too little quantitative data available to determine boundary conditions for climate models of the Pliocene, assess equator to pole temperature gradients needed to determine climate sensitivity during the Pliocene, or to compare land-sea surface temperature evolution to reconstruct the hydrological cycle during the Pliocene (Brierley et al., 2009; Martínez-Boti et al 2015).

Over the past decade, a quantitative proxy for mean air temperatures (MATs) has been developed based on membrane lipids of soil bacteria (Weijers et al., 2007a). The so-called branched glycerol dialkyl glycerol tetraethers (brGDGTs) are composed of two alkyl chains bound to two glycerol moieties by ether bonds, and can vary in the number of methyl branches (4–6), and cyclopentane moieties (0–2; see Appendix A for structures). Although the exact producer(s) of brGDGTs is unknown, their abundance in soils varies with that of *Acidobacteria* (Weijers et al., 2006, 2009, 2010), and brGDGT Ia was even

identified in two species of *Acidobacteria* (Sinninghe Damsté et al., 2011). An empirical study on their occurrence in soils and peats worldwide showed that the degree of methylation of brGDGTs relates to MAT and soil pH, whereas the degree of cyclisation was linked to soil pH (Weijers et al. 2007a). Subsequently combining these two relations resulted in an empirical transfer function to reconstruct MAT. A recent improvement in high performance liquid chromatography (HPLC) analysis of brGDGTs led to the structural identification of isomers of the penta- and hexamethylated brGDGTs, which are distinguished by the varying position of the methyl group present on either the 5- or 6-position of the alkyl chain (De Jonge et al., 2013, 2014a). A reinvestigation of the soil calibration for the separated brGDGTs showed that the distribution of the 5-methylated variety in soils is related solely to temperature, leading to a new transfer function that removes the influence of pH on temperature estimates (De Jonge et al., 2014a).

Upon mobilization, fluvial transport, and discharge, soil brGDGTs can be archived in coastal marine sediments and can thus be used as proxy for the relative input of river-transported soil material to marine sediments. This can be quantified by the Branched and Isoprenoid Tetraether (BIT) index, in which the abundance of soil-derived brGDGTs is taken relative to that of the isoprenoidal GDGT crenarchaeol, produced by marine Thaumarchaeota (Hopmans et al 2004). Hence, sites with a high BIT index are indicative of substantial input of terrestrial organic matter to the site, rendering the sedimentary archive suitable for application of the brGDGT-paleothermometer and thus the reconstruction of past air temperatures of the nearby continent. Indeed, analysis of brGDGTs stored in the Congo River fan resulted in a temperature record for tropical east Africa over the last deglaciation (Weijers et al., 2007b). Since then, MAT records have been generated for a variety of sites of different geological age, the oldest to our knowledge being the Cretaceous (Kemp et al., 2014; Super et al., 2018), indicating excellent preservation of these molecular fossils.

Here, we aim to use brGDGTs stored in sediments near the Mississippi and Amazon River outflows to reconstruct Pliocene terrestrial temperatures in the respective drainage basins. The Mississippi and Amazon are among the largest rivers worldwide, and have a modern annual sediment discharge of ~6.21 x 10^{11} kg (Coleman, 1988) and 700–800 x 10^{9} kg (Martinez et al., 2009), respectively. Previous studies have indicated that both rivers were active during the Pliocene (Coleman, 1988; Figueiredo et al., 2009). The influence of the Pliocene Mississippi River on sediments on the continental shelf and slope of the Northern Gulf of Mexico was confirmed by the presence of pollen in sediments from offshore Louisiana, from which the assemblage was used to reconstruct climate change from the Miocene to the Pleistocene (Elsik, 1969). In addition, the paleo-discharge of the Mississippi River system is estimated to have been six to eight times larger during the Pliocene than it is now (Cox et al., 2014). Ocean drilling program (ODP) site 925 on the Ceará Rise near the Amazon outflow is located on the shelf, and should thus have received enough terrestrial material to allow application of the brGDGT-paleothermometer. Indeed, the activity of the Amazon River is inferred from a low resolution BIT index record spanning the last 30 Ma for this site (van Soelen et al., 2017), which shows high BIT values (0.4–0.7) during the Pliocene interval, indicating a substantial input of fluvially discharged soil material.

2. Methods

2.1 Study sites

2.1.1 Mississippi River delta

ODP site 625B (28°49.9′N, 87°09.6′W; Leg 100) is located on the west Florida continental slope in the North Eastern Gulf of Mexico, approximately 300 km from the current mouth of the Mississippi River, and was drilled at a water depth of 889 m (Fig. 1A). Based upon the preliminary age model of Joyce et al. (1990)

constructed using biostratigraphy, the interval from 129 to 165 metres below sea floor (mbsf) was selected, which should cover the period from ~2.5 to 4.0 Ma. The average sedimentation rate of the interval is 0.42 kyr/cm, and the mean temporal resolution between samples is ~ 13 kyr.

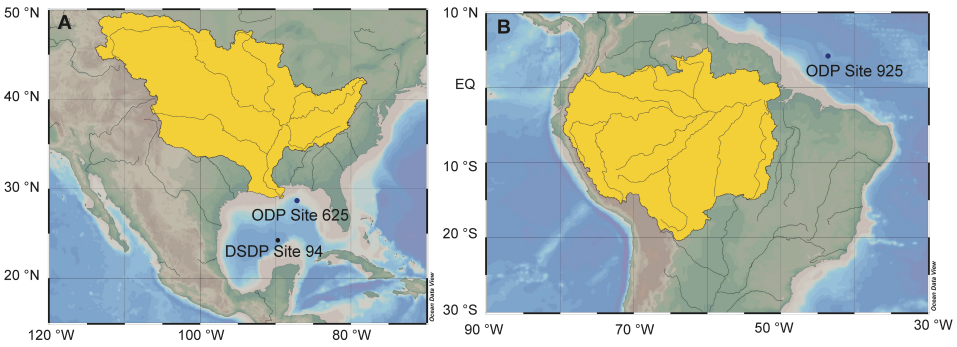

Fig. 1. Locations of (A) ODP site 625 and DSDP site 94 in the Gulf of Mexico, and (B) ODP site 925 on the Ceará Rise. The modern watersheds of the (A) Mississippi and (B) Amazon Rivers are shaded in yellow.

2.1.2 Amazon River delta

ODP site 925B (4°12.248′N, 43°29.349′W; Leg 154) is located on the Ceará Rise and was drilled at a water depth of 3,040 m (Fig. 1B). Site 925 is located approximately 800 km away from the current mouth of the Amazon River. The relative positions of the Ceará Rise and South America did not change significantly over the Cenozoic (Curry et al., 1995). The age model based on benthic oxygen isotope data for sites 925, 927, 928, and 929 (Wilkens et al., 2017) was used to target the interval between 75 and 133 mbsf, corresponding to the Pliocene and Pleistocene (2.3–5.3 Ma). Fourteen sediment samples were selected and complemented with data from nine samples previously published by van Soelen et al. (2017) from the same interval. The average sedimentation rate for the targeted interval is 0.5 kyr/cm. The temporal resolution between samples is highly variable due to the collation of two datasets, but is ~75 kyr on average.

2.2 Oxygen isotope analysis

For the age model reconstruction of ODP site 625, 190 samples corresponding to a sampling resolution of 0.1–0.5 m/sample were washed and fractions were collected at >210 μm. The washed samples were dried at 40 °C. Foraminifera tests of *Cibicides wuellerstorfi* were picked and cleaned ultrasonically before crushing. $\delta^{18}O$ isotopes were measured on a Thermo Gas Bench II (Thermofisher Scientific) with a Delta V mass spectrometer. An NBS-10 standard ($\delta^{18}O$ = -2.20‰, $\delta^{13}C$ = 1.95‰) and in house NAXOS standard were used to calibrate the sample isotope ratios to the Vienna Pee Dee Belemnite (VPDB) standard. Oxygen isotope ratios were calculated according to the following equation:

$$\delta^{18}O = \frac{\delta^{18}Os - \delta^{18}O_{\text{standard}}}{\delta^{18}O_{\text{standard}}} * 1000‰ \quad (1)$$

Where:

- $\delta^{18}O$ is the isotopic composition (in ‰) used for comparison with the benthic oxygen isotope stack (Lisiecki and Raymo; 2005).
- $\delta^{18}O_s$ was the isotope value of the sample measured by the mass spectrometer.
- $\delta^{18}O_{standard}$ were the isotope values measured on the standards.

2.3 GDGT extraction and analysis

Sediments from ODP site 625 (n = 93) and site 925 (n = 14) cores were freeze dried and ground prior to extraction (3x) using a dichloromethane (DCM):methanol (9:1, *v/v*) solvent mixture in an accelerated solvent extractor (ASE 350, Dionex). The ASE extraction method consisted of a 5 minute extraction at 100 °C and 7.6 x 10^6 Pa. The total lipid extract (TLE) was dried under nitrogen and separated into apolar, ketone, and polar fractions using activated Al_2O_3 in a small column using hexane:DCM (9:1, *v/v*), hexane:DCM

(1:1, *v/v*) and DCM:methanol (1:1, *v/v*) as eluents, respectively. Polar fractions were prepared for GDGT analysis first by the addition of an internal standard (C_{46} GTGT; Huguet et al., 2006), then by dissolving the (dry) fraction in hexane:isopropanol 99:1 (*v/v*) prior to filtering using a 0.45 µm PTFE filter.

Samples from ODP site 925, including those of van Soelen et al. (2017; n = 9), were analysed at the Royal Netherlands Institute for Sea Research (NIOZ). All samples from ODP site 625 were measured at Utrecht University. At both institutes, brGDGTs were analysed following Hopmans et al. (2016). In short, an Agilent 1260 Infinity ultra high performance liquid chromatography (UHPLC) instrument coupled to an Agilent 6130 single quadrupole mass detector was used for analysis. Two silica Waters Acquity UPLC BEH Hilic columns (1.7 µm, 2.1 mm x 150 mm) at 30 °C and a guard column was used for chromatographic separation. The solvent program, for which hexane (A) and hexane:isopropanol 9:1 (B) were used, followed isocratic elution at a flow rate of 0.2 ml/min with 82% A and 18% B for 25 min, followed by a linear gradient to 70% A and 30 B for 25 min. 10 µL of sample was injected. Ionisation of GDGTs was achieved using atmospheric pressure chemical ionisation (APCI) using the following source conditions: gas temperature 200 °C, vaporizer temperature 400 °C, capillary voltage 3500 V, nebulizer pressure 25 psi, drying gas (N_2) flow 6L/min, corona current 5.0 µA. Selected ion monitoring (SIM) model was used to identify the GDGTs using their $[M\text{-}H]^+$ ions: *m/z* 1032, 1300, 1298, 1296, 1292, 1050, 1048, 1046, 1036, 1034, 1032, 1022, 1020, 1018. The internal standard was identified using *m/z* 744. GDGTs were integrated using Chemstation software B.04.02.

2.4 GDGT proxy calculations

The MBT′5Me index was calculated using the following equation (De Jonge et al., 2014a):

$$\mathrm{MBT'5Me} = \frac{\mathrm{Ia+Ib+Ic}}{\mathrm{Ia+Ib+Ic+IIa+IIb+IIc+IIIa}} \quad (2)$$

Temperatures were calculated using the MAT_{mr} transfer function of De Jonge et al. (2014a):

$$MAT_{mr} = 7.17 + 17.1 * [Ia] + 25.9 * [Ib] + 34.4 * [Ic] - 28.6 * [IIa] \quad (3)$$

BIT indices were calculated according to the following equation, which includes both 5- and 6-methyl GDGTs (Hopmans et al., 2004);

$$BIT = \frac{Ia+IIa+IIa'+IIIa+IIIa'}{IV+Ia+IIa+IIa'+IIIa+IIIa'} \quad (4)$$

Where IV refers to Crenarchaeol.

The isomer ratio (IR), which expresses the relative proportion of 6-methyl brGDGTs (De Jonge et al., 2014b, 2015), was calculated as follows:

$$IR = \frac{[IIa']+[IIb']+[IIc']+[IIIa']+[IIIb']+[IIIc']}{[IIa']+[IIb']+[IIc]+[IIIa']+[IIIb']+[IIIc']+[IIa]+[IIb]+[IIc]+[IIIa]+[IIIb]+[IIIc]} \quad (5)$$

Numbers refer to structures of brGDGTs in Appendix A.

3. Results & Discussion

3.1 Mississippi River basin

3.1.1 ODP site 625 Pliocene age model

The $\delta^{18}O$ values for *Cibicides wuellerstorfi* range between 2.27–3.83‰ (Fig. 2). In the deeper part of the core (133.75–160.0 mbsf) the $\delta^{18}O$ values for site 625 are lighter than those of the LR04 stack (Lisiecki and Raymo, 2005), whereas they converge to similar absolute values in the upper interval, 129.98–133.75 mbsf. The variability between warmer and colder periods of the record is 0.2–0.6‰, which is similar to that of the LR04 stack (Lisiecki and Raymo, 2005; Fig. 2). There is a clear trend toward heavier $\delta^{18}O$ values in the upper interval of the core, from 137 mbsf and up, similar to that observed in the LR04 stack, which is concurrent with the gradual build-up of ice in the Northern Hemisphere during the late Pliocene and early Pleistocene (Raymo et al., 2006).

The benthic $\delta^{18}O$ record at site 625 shows a clear period of heavier $\delta^{18}O$ values at 143–145 mbsf, which can be linked to the M2 event (Fig. 2). This

provides one of the initial tie-points for our age model (Table 1), and enables further correlation of our $\delta^{18}O$ *Cibicides wuellerstorfi* record with the global LR04 benthic $\delta^{18}O$ stack (Lisiecki and Raymo, 2005; Fig. 2 and Table 1). The oxygen isotopes of *Cibicides wuellerstorfi* in site 625 constrain the chronology of the core from marine isotope stage (MIS) Gi6 (3712 ka) to G16 (2913 ka). Sedimentation rates indicate an incremental increase over the studied interval from ~4.3 to ~4.6 cm/kyr (Fig. 2C).

Table 1. Table of tie-points used to establish the age model for the ODP site 625B.

Marine Isotope Stage	**LR04 ka**[1]	**ODP sample/reference**	**625B Tie points (mbsf)**
59/60	1696	Shakun et al. (2016)	89.68
G15/G16	2925	16 5W 61 – 63 cm	133.94
G20/G21	3015	17 1W 103 – 105 cm	137.63
KM1/KM2	3135	17 3W 43 – 45 cm	140.05
KM2/KM3	3155	17 3W 133 – 135 cm	140.95
KM4/KM5	3190	17 4W 72 – 74 cm	141.85
KM6/M1	3245	17 5W 72 – 74 cm	143.36
M2/MG1	3295	17 6W 63 – 65 cm	144.68
MG12/MC11	3585	18 6W 128 – 130 cm	154.58
Gi2/Gi3	3630	19 2W 38 – 40 cm	155.45
Gi4/Gi5	3670	19 3W 83 – 85 cm	157.48
Gi6/Gi7	3715	19 5W 23 – 25 cm	159.8

3.1.2 Temperature reconstruction

GDGTs are present throughout the chosen interval, where isoGDGTs are more abundant than brGDGTs. Of the brGDGTs, the most abundant compound is Ia

[1] Lisiecki and Raymo, 2005

(average fractional abundance 28.0 ±10%), followed by Ib (4.8 ±1.1%). BrGDGTs IIIc and IIIc′ were below detection limit in all but 2 samples. Application of the MAT_{mr} transfer function of De Jonge et al. (2014a) results in temperatures between 13.6–16.1 °C (Fig. 3B). The temperature record does not show a clear trend with time. The temperature drop associated with the M2 event (~3.3 Ma) that is clearly recorded in the benthic $\delta^{18}O$ record for this site seems to be dampened in the brGDGT-derived temperature record, where it is represented by a drop of only ~1 °C (Fig. 3B). The trend towards heavier $\delta^{18}O$ values seen in the global LR04 benthic stack and the $\delta^{18}O$ record of *Cibicides wuellerstorfi* from site 625 is not reflected in the brGDGT-based MAT_{mr} estimates (Fig. 3). In fact, the highest temperature of the record, ~16 °C, is recorded at 2.95 Ma (Fig. 3B). The variability of temperatures in the sediments aged 3.0 Ma and younger is 2 °C.

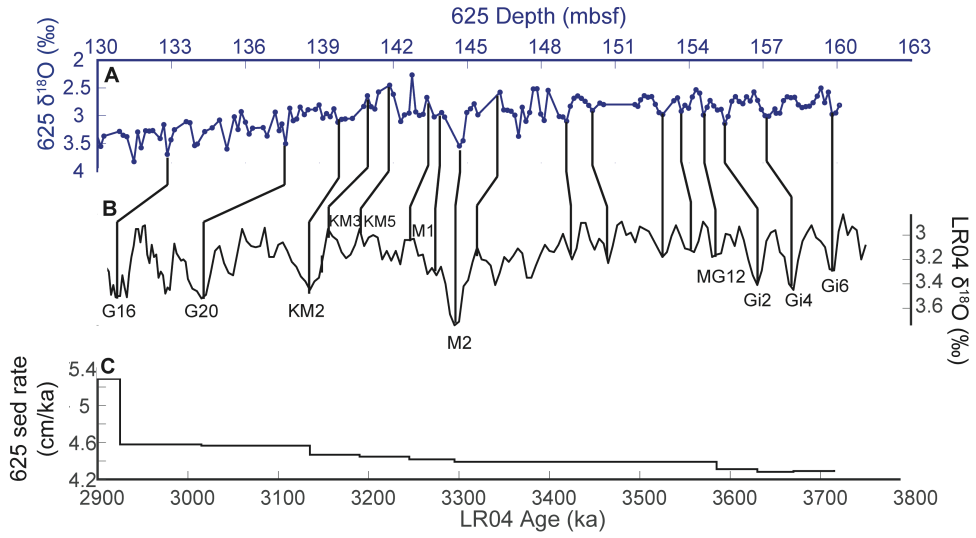

Fig. 2. Correlation of the (A) 625 benthic $\delta^{18}O$ record on its depth scale (top x-axis; blue) to the (B) LR04 stack and age scale (bottom x-axis, Lisiecki and Raymo, 2005; black), with (C) implied sedimentation rates. Tie points used for tuning and key marine isotope stages are indicated.

The absolute reconstructed temperatures are low compared to the modern annual MAT of the nearby state of Louisiana where the Mississippi discharges, which is 18–20 °C (Harris et al., 2014). The lower temperatures conflict with the general idea that global (and terrestrial) temperatures were 2–3 °C higher during the Pliocene (Haywood et al., 2016a, b). This could indicate that brGDGTs in the core derive from soil material from higher up the Mississippi catchment. However, recent studies of both particulate organic matter (POM; Richardson et al., 2013) and dissolved organic matter (DOM; Ward et al., 2013) in North American streams and rivers and the Amazon River demonstrate that fresh, labile OM is partially oxidized, degraded, and respired as CO_2 (Butman and Raymond, 2011). Thus, the OM component discharged into the ocean from these rivers is presumably mostly composed of material derived from the lower catchment area. This process is observed in the Yangtze River, where the mineral load of the river is similar throughout (He et al., 2013), whereas the distribution of brGDGTs in the outflow only reflects that of soils in the lower catchment (Li et al., 2015). In addition, brGDGT distributions discharged to the Black Sea by the Danube River appeared to be dominated by inputs from the lower Danube Basin, indicating that brGDGTs reflect a local rather than basin wide signal (Freymond et al., 2017). Hence, the underestimation of Pliocene temperatures in site 625 sediments indicates that the initial soil-derived brGDGT signal may have been altered during transport and burial.

A closer look at the total pool of GDGTs in the Gulf of Mexico sediments shows that the BIT index is low, varying between 0.02 and 0.13 (Fig. 3C) suggesting a dominance of marine OM (Schouten et al., 2013 and references cited therein). This implies that the majority of brGDGTs may have a marine origin, which could be attributed to a limited influence of the Mississippi River during this time interval. Indeed, the virtual absence of plant leaf wax biomarkers and pollen (not shown) in the same sediments suggests that the input of terrestrial material was minimal at this site. This either indicates that the axis of the

Mississippi outlet was different during the Pliocene, or that the river mouth was located further away from site 625 due to the higher sea level at the time, limiting the input of terrestrial material to the site. Recent studies indicate that the concentration of brGDGTs in modern continental margin sediments rapidly decreases with increasing distance from the coast at the East Siberian Arctic Shelf and the Tagus River outflow (Sparkes et al., 2015; Zell et al., 2015). Hence, a minor sea level increase (ca. 20 m according to Miller et al., 2012) may have led to a strong decrease in the amount of soil-derived brGDGTs that reached the site.

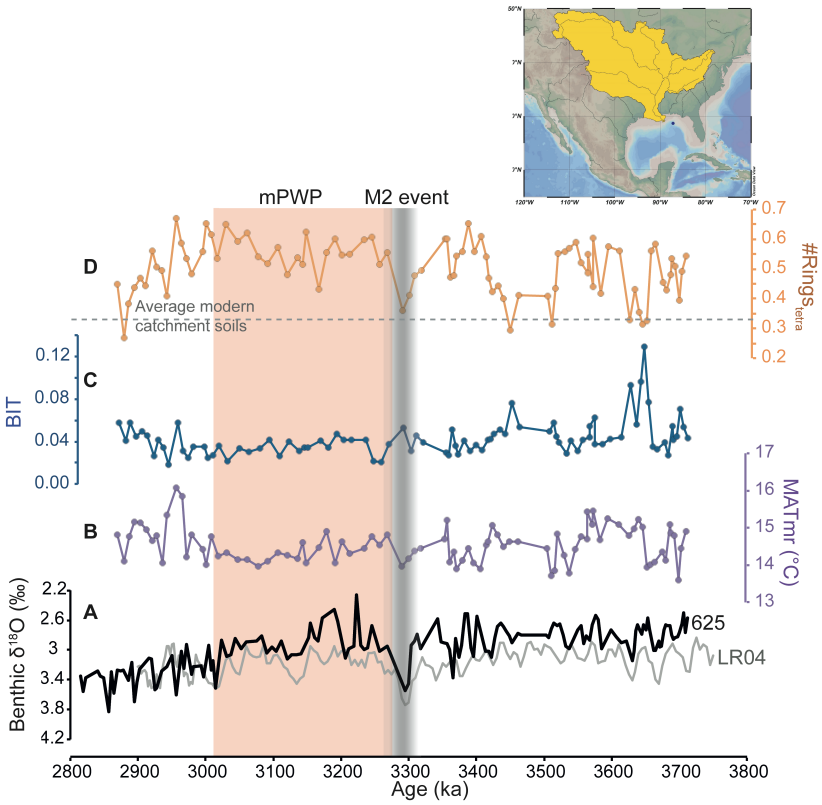

Fig. 3. Proxies for ODP site 625 in the Gulf of Mexico. (A) ODP 625 (black) and LR04 benthic $\delta^{18}O$ records (grey), (B) MATmr, (C) BIT, and (D) $\#rings_{tetra}$ plotted against the age scale.

However, a recent study reported carbon and hydrogen isotopic compositions of terrestrial leaf waxes over the last 35 Ma in a sediment core from the central Gulf of Mexico (DSDP site 94; Fig. 1A; Tipple and Pagani, 2010), indicating that terrestrial material did reach the central basin during the Pliocene. DSDP site 94 is located 300 km further away from the mouth of the Mississippi River than site 625, hence the lack of plant waxes at site 625 is startling since terrestrial material should pass by site 625 before reaching the central Gulf. This suggests that in contrast to a higher sea level, the virtual absence of terrestrial leaf waxes at site 625 is a result of a change in the direction of the Mississippi River outflow. Some evidence implies that the axis of the Mississippi outflow pointed more towards the west during the Miocene/Pliocene than at present, due to the location of the Pliocene Mississippi Gulf of Mexico depocenters in the North Western Gulf Margin near the Texas and Louisiana border, where the shelf edge prograded most rapidly (Woodbury et al., 1974; Galloway et al., 2011; Bentley Sr. et al., 2016). However, the evidence for terrestrial input from palynological assemblages in sediments from offshore Louisiana still suggests a limited influence of the Mississippi River to the area during the Pliocene (Elsik et al., 1969). In any case, abundant terrestrial palynomorphs in site 625 sediments from the late Pleistocene to the Holocene indicate that the Mississippi outflow was similar to its present position at that time (Limoges et al., 2014). This evidence suggests that a change in the direction of the Mississippi outflow is at least partly responsible for the low abundance of terrestrial material in the Pliocene site 625 sediments.

The limited amount of terrestrial material at 625 raises a question regarding the provenance of the brGDGTs, as brGDGTs in sediments that receive little terrestrial input were found to be overprinted by a marine signal that is substantially different from that in nearby soils (Peterse et al., 2009a; Zhu et al., 2011). This is visualized by the position of these sediments in a triplot with the relative amounts of tetra-, penta-, and hexamethylated brGDGTs, in which

sediments with an aquatic contribution plot away from soils (Fig. 4; cf. Sinninghe Damsté, 2016). Adding the Gulf of Mexico sediments to this triplot shows that they also plot offset from the typical soil pattern (Fig. 4), suggesting that a proportion of brGDGTS in site 625 has an aquatic origin. Peterse et al. (2009a) noted that these *in situ* produced brGDGT distributions are characterized by more cyclopentane-containing brGDGTs than soil derived brGDGTs, after which Sinninghe Damsté (2016) proposed to use the degree of cyclisation of the tetramethylated suite of brGDGTs, expressed as the $\#rings_{tetra}$, as an indicator of a marine brGDGT overprint in marine sediments. A value of $\#rings_{tetra}$ above 0.7 is used as a cutoff to indicate unequivocal marine *in situ* production.

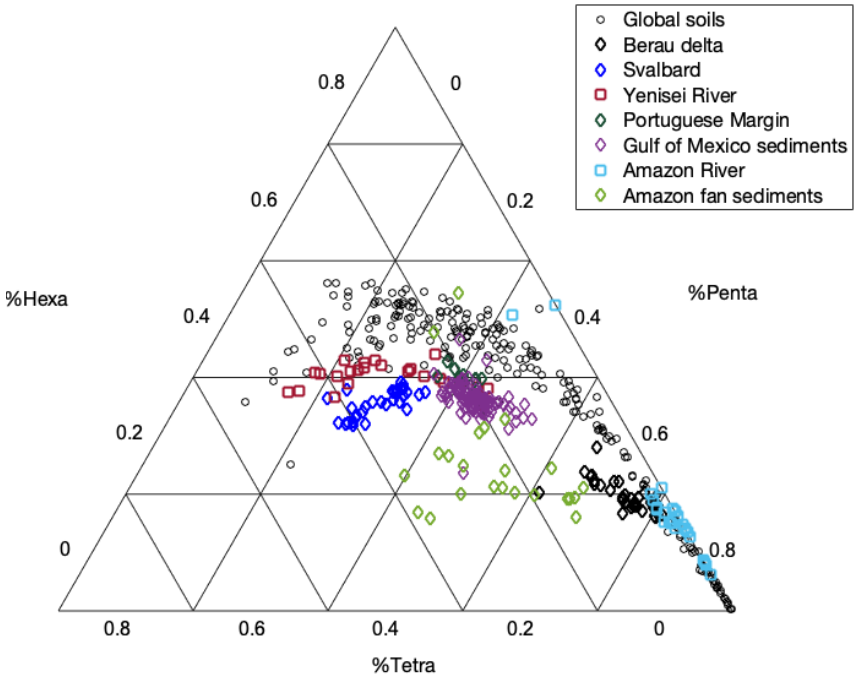

Fig. 4. Triplot showing abundances of the tetramethylated, pentamethylated, and hexamethylated brGDGTs for global soils (black circles, De Jonge et al., 2014a), Berau delta (black diamonds, Sinninghe Damsté, 2016), Svalbard fjord (blue diamonds, Peterse et al., 2009a), Yenisei River (maroon squares, De Jonge et al., 2015), Portuguese margin (green diamonds, Warden et al., 2016), Amazon River (blue squares, Zell et al., 2013a), Pliocene Gulf of Mexico sediments (purple diamonds, ODP site 625) and Pliocene Amazon Fan sediments (green diamonds, ODP site 925).

The $\#rings_{tetra}$ of the Gulf of Mexico sediments ranges from 0.26–0.67 (Fig. 3D), and the average value of 0.5 ±0.09 suggests that the brGDGTs have a mixed origin. This is further exemplified when comparing the average $\#rings_{tetra}$ values in the sediments to the average $\#rings_{tetra}$ of the soils in the modern catchment of the Mississippi, which is 0.34 ±0.22 (n = 9; De Jonge et al., 2014a). The $\#rings_{tetra}$ record is highly variable over time, and shows several minima and a trend toward lower $\#rings_{tetra}$ values after 3.0 Ma (Fig. 3D). The minima in the $\#rings_{tetra}$ record (at 3.66, 3.51–3.45, and 3.29 Ma) coincide with increases, albeit very small, in the BIT index (Fig. 3). Also, the decrease in $\#rings_{tetra}$ after 3.0 Ma coincides with a slight increase (0.04) in the BIT record (Fig. 3). These intervals suggest (i) more input of soil-derived brGDGTs, (ii) a reduced marine *in situ* produced brGDGT overprint, (iii) a change in the direction of the Mississippi outflow, or (iv) changing currents in the Gulf of Mexico, or a combination of those four factors. In particular, the M2 event and the Late Pliocene, two intervals characterized by a cooler (global) climate in the $\delta^{18}O$ records, are characterized by these coinciding trends in $\#rings_{tetra}$ and BIT (Fig. 3). The coinciding trends in the two records indicate an increased input of soil OM, which is probably a result of increased proximity to the Mississippi River mouth as a result of sea level fluctuations which occurred during both the M2 event and the Plio-Pleistocene transition when ice began to build up on the North American continent (De Schepper et al., 2014; Shakun et al., 2016).

Overall, the high $\#rings_{tetra}$ values and the offset distributions of the Gulf of Mexico sediments compared to global soils (Fig. 4) indicate that *in situ* marine brGDGT production contributes a great deal to the brGDGT pool in the Gulf of Mexico sediments, leading to a marine brGDGT 'overprint'. This makes it impossible to obtain a quantitative temperature record for Southern North America during the Pliocene based on brGDGT distributions in the sediments of ODP site 625.

3.2 Temperature reconstruction for the Amazon River basin

BrGDGTs are present in all samples of ODP site 925 (Ceará Rise) throughout the studied interval of ~2.3–5.3 Ma. In general, the most abundant brGDGT is Ia (44.0 ±12.2%), followed by the 6-methylated brGDGTs IIa′ (9.7 ±2.4%) and IIb′ (9.0 ±5.8%). In contrast, the least abundant brGDGTs, IIIc, IIc, and IIIb, are all 5-methylated isomers. Reconstructed temperature using MAT_{mr} (De Jonge et al., 2014a) in the Ceará Rise sediments ranges from 13.1–19.3 °C (Fig. 5B). The lowest temperatures in the record occur between 2.7–3.8 Ma (Fig. 5B). Interestingly, temperatures do not follow the same general trend for the Pleistocene as the benthic oxygen isotopes in the global stack (Lisiecki and Raymo, 2005), but instead stabilise at ~19 °C after 2.8 Ma (Fig. 5B). Furthermore, the variability in the MAT record (ca. 6 °C) is remarkable given the supposedly equable climate during the Pliocene, especially in the subtropics. Comparison with the modern day MAT of the Amazon River catchment (25–30 °C; Harris et al., 2014) shows that the brGDGT-based temperatures severely underestimate actual MAT, by 5–17 °C, and thus most likely also underestimate Pliocene temperatures that are expected to have been even higher. Given the lack of temperature seasonality in the modern Amazon Basin, it is unlikely that brGDGT-based MATs are biased towards austral winters, despite the fact that the currents delivering terrigenous material from the Amazon outflow to the Ceará Rise are mostly active in this time of year (May to October; Lammertsma et al., 2018).

The Ceará Rise sediments generally have high BIT index values, ranging from 0.40–0.83 (average 0.58 ±0.11; Fig. 5C), suggesting that brGDGTs stored in site 925 are primarily soil derived (cf. Schouten et al., 2013). In addition, brGDGTs are associated with a low $\#rings_{tetra}$ (0.12–0.59), especially after 3.6 Ma (Fig. 5D), that is well below the threshold value of 0.7 that identifies an aquatic source of brGDGTs (cf. Sinninghe Damsté, 2016). Comparison of the average

#rings$_{tetra}$ in this record with the average from the Amazon catchment soils in the soil calibration dataset, which is 0.14 ±0.15 (n = 13; De Jonge et al., 2014a), confirms that the majority of the brGDGTs in the Amazon fan sediments have a soil origin, and should thus reflect terrestrial temperatures. Moreover, van Soelen et al. (2017) showed that after 4.5 Ma, the sedimentation of mineral and organic terrigenous material at site 925 increases considerably due to Andean uplift. However, addition of the Ceará Rise sediments to the triplot of tetramethylated, pentamethylated, and hexamethylated brGDGTs (Fig. 4) reveals that they plot offset from global soils, implying that a proportion of the brGDGTs in site 925 sediments do not derive from soils. Strikingly, the pattern of the Ceará Rise sediments in the triplot is more widely distributed than that of other marine sediments, which tend to cluster together (Fig. 4).

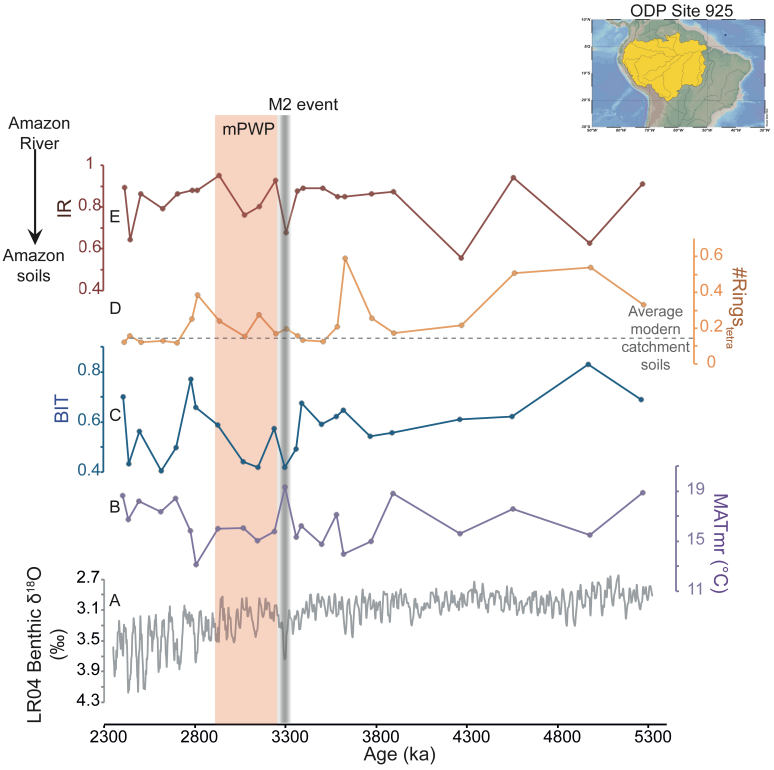

Fig. 5. Proxies for ODP site 925 on the Ceará Rise. (A) LR04 benthic δ^{18}O record, (B) MATmr, (C) BIT, (D) #rings$_{tetra}$, and (E) IR plotted against the age scale.

The alternative pattern of site 925 sediments in Fig. 4 suggests that these brGDGTs may be produced in an environment other than soils or the coastal marine water column. Recent studies have indicated that the production of brGDGTs can also take place in the Amazon River itself (Zell et al., 2013a, b). In particular, the presence of brGDGTs with phospho- and glyco-headgroups still attached in suspended particulate matter (SPM) from the Amazon provides strong evidence for brGDGT production within the river (Zell et al., 2013a), as these headgroups are presumed to be quickly lost upon cell death (White et al., 1979; Harvey et al., 1986). Furthermore, offsets in brGDGT distributions in soils and SPM from the Lower Amazon were explained by additional *in situ* river production (Zell et al., 2013a). In other studies, *in situ* brGDGT production has also been observed in the Pearl (Zhang et al., 2012), Yangtze (Yang et al., 2013), and the Yenisei Rivers (De Jonge et al., 2014b), where a high proportion of 6-methylated isomers characterizes *in situ* produced brGDGTs. In soils, the relative contribution of 6-methyl isomers, quantified in the isomerisation ratio (IR), is linked to pH (De Jonge et al., 2014b; Ding et al., 2015; Yang et al., 2015), where high pH soils contain a larger fraction of 6-methyl brGDGTs. In contrast, soils from the Amazon catchment are generally characterized by low soil pH values (Moreira and Fageria, 2009). Indeed, soils from the global brGDGT calibration (n = 13; De Jonge et al., 2014a) and the area surrounding the Madre de Dios tributary located in South Eastern Peru (Kirkels et al., in prep.), located in the Amazon catchment, are associated with low IR values of 0.18 ± 0.18 (n = 39; Fig. 6). Hence, the IR may be used to detect a riverine contribution to the brGDGT signal in the site 925 sediments.

The IR of the site 925 sediments is generally high (0.79 ±0.12; Fig. 6) throughout the record (Fig. 5), but temporarily shifts to lower values of ca. 0.5 at ~4.3 and ~5.0 Ma. However, these shifts are only based on one data point each. Regardless, the IR in the site 925 sediments is substantially higher than the IR of

the Amazon catchment soils (Fig. 6). Re-analysis of the SPM samples from Zell et al. (2013a) using the new HPLC method with improved separation of brGDGT isomers (Hopmans et al., 2016), shows that the IR signature in modern lower Amazon river SPM is 0.38 ±0.08, and shows little variation among the top or bottom water, and intact polar lipids (i.e. 'living') or core lipids ('dead'; Fig. 6). Furthermore, brGDGTS in SPM from the upper Amazon River have a similar IR of 0.43 ±0.14 (Kirkels et al., in prep.; Fig. 6). In particular, the SPM collected during the dry season has a high IR (0.56 ±0.10; Fig. 6), likely as a result of the decreased turbidity of the river water in the dry season, which allows for more light penetration enabling primary production, including that of brGDGTS (Kirkels et al., in prep.). The high IR value for the Ceará Rise sediments thus indicates that brGDGTS are derived from *in situ* river production, rather than a soil or coastal marine origin.

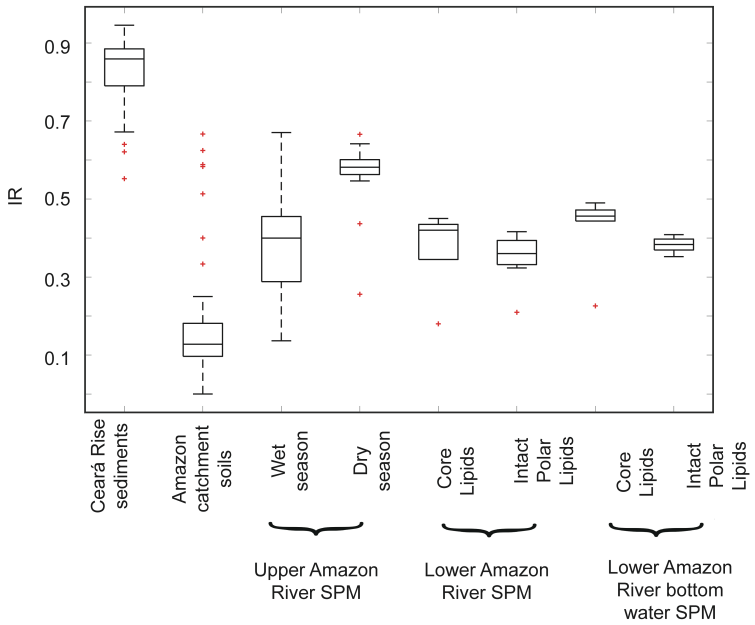

Fig. 6. Comparison of IR values across Ceará Rise sediments (ODP site 925), Amazon River catchment soils (including soils from Kirkels et al., in prep.), Upper Amazon River SPM (wet and dry season; Kirkels et al., in prep.), Lower Amazon River SPM (core and intact polar lipids), and Lower Amazon River bottom water SPM (core and intact polar lipids) reanalysed from Zell et al., (2013a).

Following from this, the decrease in IR at 4.3 and 5.0 Ma may reflect a change in brGDGT source from rivers to soils, perhaps linked to the transcontinental connection of the Amazon River to the Andes (van Soelen et al., 2017; Lammertsma et al., 2018). This connection would have led to a large amount of eroded material being transported in the river, decreasing the turbidity, thus decreasing the production of 6-methylated brGDGTs. Moreover, both the IR and $\#rings_{tetra}$ signatures around this time are more comparable to the signature to that of the Amazon catchment soils (Figs. 5, 6), indicating an increase in soil-derived brGDGT input to site 925. Regardless, the generally high IR signature of the Ceará Rise sediments (Fig. 6) indicates a substantial riverine brGDGT overprint that disqualifies this site for the creation of an absolute temperature record for the Pliocene Amazon Basin. Notably, a previous attempt to reconstruct paleotemperatures for the last deglaciation using brGDGTs in the Amazon River fan also resulted in a severe underestimation (~10 °C) of Holocene temperatures (Bendle et al., 2010), similar to the offset observed in our Pliocene record. Bendle et al. (2010) explained their underestimated temperatures by an increased input of soil material from the high Andes, mobilized by melting glaciers. Although their brGDGT data was generated using the classic HPLC method that does not separate 5- and 6-methyl isomers, our data suggest that a contribution of brGDGTs produced in the Amazon River may be responsible for their underestimated reconstruct temperatures. Where Zell et al. (2014a) advised that brGDGT paleothermometry should only be applied to marine sediments under a heavy river influence, we here notify that even the river influence itself can dominate the soil signal and obscure the resulting reconstructed temperatures.

4. Conclusions

The analysis of brGDGTs in marine Pliocene sediments from the Gulf of Mexico and the Ceará Rise failed to generate reliable records of Pliocene terrestrial climate from the adjacent river basins for different reasons. Low BIT and high

values of $\#rings_{tetra}$ indicate that the Gulf of Mexico sediments did not receive sufficient terrestrial material, likely due in part to the altered direction of the Mississippi River during the Pliocene. The primarily marine source of the brGDGTs rendered these sediments unsuitable for brGDGT paleothermometry. Although the brGDGTs recovered from the Ceará Rise sediments have high BIT index and low $\#rings_{tetra}$ values, reconstructed MATs underestimate the temperatures expected for the Pliocene Amazon Basin by 5–17 °C. We show that the large proportion of 6-methylated brGDGTS in the Ceará Rise sediments does not match the typical signature of modern soils from the Amazon watershed. Instead, the IR in the Ceará Rise sediments is closer to that of modern river SPM collected during the dry season, reflecting in river production. We postulate that a riverine contribution to the brGDGT pool in Amazon River fan sediments may have also complicated earlier attempts that used brGDGTs to generate temperature records for the Amazon Basin. This study shows that a mixed terrestrial/riverine/marine brGDGT source in coastal marine sediments complicates the use of the soil-based brGDGT calibration in these settings. Therefore, future studies that aim to reconstruct temperature changes on the continent using these biomarkers should focus on developing a method that can separate aquatic from terrestrial brGDGTs signals to correct for the aquatic overprint.

Acknowledgements

The authors would like to acknowledge the Ocean Drilling Program Core repositories at Bremen and Texas A&M for providing access to the core material. We also thank Anita van Leeuwen and Arnold van Dijk (UU), and Marianne Baas and Denise Dorhout (NIOZ) for analytical support. The work was supported by funding from the Netherlands Earth System Science Center (NESSC) through a gravitation grant (NWO 024.002.001) from the Dutch Ministry for Education, Culture and Science to JSSD.

Appendix A

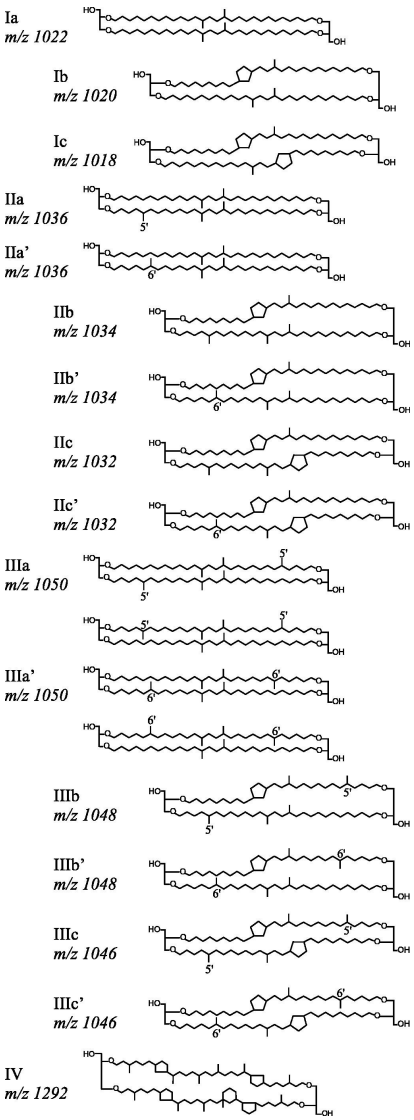

Fig. A1. Molecular structures of the tetramethylated (Ia – Ic), pentamethylated (IIa – IIc), hexamethylated (IIIa – IIIc) brGDGTS, and Crenarchaeol (IV). From De Jonge et al. (2014a).

Chapter 3

Production of branched tetraethers in the marine realm: Svalbard fjords revisited

Emily Dearing Crampton-Flood, Francien Peterse, Jaap S. Sinninghe Damsté.

A revised version of this manuscript under consideration for publication in *Organic Geochemistry*.

Abstract

Branched glycerol dialkyl glycerol tetraethers (brGDGTs) are bacterial membrane lipids predominantly found on the continent. They are used as continental paleothermometer based on the empirical relation between their molecular composition and air temperature in surface soils worldwide. The proxy is applied in continental margin sediments based on the assumption that all brGDGTs originate from land and are transported to marine sediments by rivers and runoff. However, this assumption has been challenged by the discovery of *in situ* brGDGT production in the coastal marine environment. To better understand marine brGDGT production we revisit soils and marine surface sediments from the Krossfjorden and Kongsfjorden in Svalbard, the first location where *in situ* brGDGT production was posited, this time including 5- and 6-methyl brGDGTs. 'Living' intact polar lipid (IPL)-derived and 'fossil' core lipid (CL) brGDGTs were also studied for a subset of fjord sediments. The amount of cyclopentane moieties in tetramethylated brGDGTs, used as indicator for brGDGT production in coastal marine settings, is much higher in the fjord sediments ($\#rings_{tetra}$ = 0.65–0.93 for CL and 0.24–0.79 for IPL-derived brGDGTs) compared to those in nearby soils ($\#rings_{tetra}$ = 0.00–0.37), and confirms the predominantly marine source of the brGDGTs in the fjords. Furthermore, IPL-derived brGDGTs have a substantially lower $\#rings_{tetra}$ (up to 0.52 offset) compared to that of CLs in the same sediment, suggesting that brGDGTs are produced in different configurations throughout the year, of which the CL distribution in the sediment is an integrated signal. The offset in $\#rings_{tetra}$ between IPL-derived and CL brGDGTs varies between 0.15–0.52 and increases towards the open ocean, possibly linking brGDGT production to the natural salinity gradient and associated microbial community changes.

1. Introduction

Branched glycerol dialkyl glycerol tetraethers (brGDGTs) are membrane lipids produced by bacteria that thrive in soils and peats worldwide (Weijers et al., 2007a). Specific brGDGT structures are distinguished by the varying number of cyclopentane moieties (0–2) and methyl branches (4–6) that are present on the alkyl chains. Furthermore, the position of the outer methyl branches in the pentamethylated and hexamethylated brGDGTs can vary from the fifth to the sixth position on the alkyl chain, giving rise to structural isomers, referred to as 5- and 6-methylated brGDGTs (De Jonge et al., 2013). Variations in the degree of methylation of brGDGTs (methylation of branched tetraethers, MBT) in a set of globally distributed soils have been linked to mean annual air temperature (MAAT; Weijers et al., 2007a; De Jonge et al., 2014a), whereas the position of the methyl branch, as well as the degree of cyclisation is related to soil pH (Weijers et al., 2007; Peterse et al., 2012; De Jonge et al., 2014a). Subsequently, these relations have been employed as a terrestrial paleothermometer. The first proof of concept of the proxy resulted in a temperature record for the last deglaciation in tropical Africa (Weijers et al., 2007b). Subsequently, it has been applied to reconstruct temperatures in the mid- to high-latitudes during the early Paleogene (Weijers et al., 2007c; Naafs et al., 2018), and the Arctic in the Pliocene (Keisling et al., 2017), among others.

Application of the brGDGT-based paleothermometer on continental margin sediments relies on the underlying assumption that soil-derived brGDGTs are washed into rivers and delivered into the marine realm. This assumption has been challenged by the recent findings that brGDGT production also takes place *in situ* in rivers (Zell et al., 2013a, b; De Jonge et al., 2014b), lakes (Tierney and Russell, 2009; Sinninghe Damsté et al., 2009; Weber et al., 2015), and continental margins (Peterse et al., 2009a; Zhu et al., 2011; Zell et al., 2014a, b; De Jonge et al., 2015; Liu et al., 2014, Xie et al., 2014; Sinninghe Damsté, 2016), altering the initial soil signal. However, the specific organism(s) responsible for producing

brGDGTs remain ambiguous. To date, one subgroup of the phylum *Acidobacteria* has been identified as the producer of at least one specific brGDGT (Ia, Sinninghe Damsté et al., 2011, 2014, 2018). However, recent work has proposed that the search for the biological sources of brGDGTs should be extended to other bacterial phyla, due to the absence of the gene cluster in many subdivisions of *Acidobacteria* that is responsible for the formation of the ether-bound variety of iso-diabolic acid, the surmised building block of brGDGTs (Sinninghe Damsté et al., 2018).

Evidence of *in situ* marine brGDGT production was first reported for the Kongsfjorden and Krossfjorden of Svalbard (Peterse et al., 2009a), where the concentration of brGDGTs in sediments increased the further away from land, which was opposite to the expected trend based on a soil origin of the brGDGTs, and in contrast to previous studies that have used brGDGTs to trace fluvially discharged soil OC into the marine realm (Hopmans et al., 2004; Herfort et al., 2006; Kim et al., 2006; Kim et al., 2007). Furthermore, brGDGTs in open ocean sediments contained more cyclopentane moieties compared to those in the Svalbard soils. The contrast between brGDGT distributions in marine sediments and soils led to the conclusion that at least part of the brGDGTs in the fjord sediments were produced *in situ*, and thus MAT reconstructions using these sediments would be unreliable. A similarly high proportion of ring-containing brGDGTs in modern coastal zones was later observed in the East China Sea, the Portuguese continental margin, and the Berau Delta (Zhu et al., 2011; Zell et al., 2015; Sinninghe Damsté et al., 2016). This led to the use of the weighted number of rings of the tetramethylated brGDGTs, quantified as $\#rings_{tetra}$, as an indicator for *in situ* marine brGDGT production. Based on the aforementioned three sites, a threshold of $\#rings_{tetra} > 0.7$ has been proposed as an indicator for a predominantly marine source of brGDGTs in marine sediments (Sinninghe Damsté, 2016).

A marine contribution obviously impedes the use of the brGDGT-based paleothermometer as a terrestrial temperature proxy, due to the fact that the

calibration is based upon a global soil dataset (De Jonge et al., 2014a). Therefore, Dearing Crampton-Flood et al. (2018) recently proposed a method to resolve the influence of mixed brGDGT sources on continental temperature reconstruction. This method uses an end-member mixing model that to disentangle the sources of brGDGTs in the paleo-record based on $\#rings_{tetra}$. Subsequently, a separate coastal marine transfer function was used to subtract the marine contribution from the terrestrial temperature signal. This correction method thus expands the use of brGDGTs as continental paleothermometer. However, the drivers of marine *in situ* brGDGT production, including temporal and spatial variations, still remain uncertain. To further elucidate trends in marine *in situ* brGDGT production we analysed new surface sediments collected from the same locations as the surface sediments in Peterse et al. (2009a) exactly one year later, using the new chromatography method to separate 5- and 6-methylated brGDGT isomers (cf. De Jonge et al., 2014a; Hopmans et al., 2016). To specifically investigate the signature of *in situ* produced brGDGTs, a subset of the sediments was separated into intact polar lipid (IPL)-derived and core lipids (CLs) using column chromatography, and analysed accordingly. IPLs are structurally different from CLs in the fact that they contain a polar headgroup (Koga et al., 1993). IPL-derived lipids are considered as biomarkers for living biomass, as the headgroup is thought to be rapidly lost upon cell death, leaving the 'fossil' core lipid structure (White et al., 1979). Following this approach, brGDGT distributions from both 'living' organisms and the pool of 'fossil' brGDGTs stored in sediments can be directly compared. The results are discussed in context with the hydrological conditions of the fjords and (intra-)annual variability in currents reaching Kongsfjorden and Krossfjorden.

2. Material and methods

2.1 Environmental setting and fjord hydrogeography

The environmental setting of Svalbard, and that of Kongsfjorden and Krossfjorden are described in detail in Peterse et al. (2009a). In short, the west coast of Spitsbergen is influenced by the West Spitsbergen Current (WSC; Fig. 1A), whose core is composed of Atlantic Water (AW). This relatively warm and saline AW leads to largely ice-free conditions throughout the year on the west coast of Spitsbergen. In contrast, the east coast is characterized by cooler conditions due to influence of the colder East Spitsbergen Current (ESC, Fig. 1A). In Kongsfjorden and Krossfjorden, two water masses create a hydrogeographical gradient: the relatively warm, saline AW fed in by the WSC, and the tidewater glaciers on land that input cooler, fresh water. The interaction between these two water masses leads to large intra-annual hydrological changes which strongly affects the variability of fauna in the fjords and the nearby coastal shelf (Jernas et al., 2018). The Atlantic water mainly enters Kongsfjorden in the summer, although episodic intrusions have been detected in winter as well (Svendsen et al., 2002; Jernas et al., 2018). On average, the salinity varies from 30 g kg^{-1} in the innermost fjord areas (Svendsen et al., 2002) to 35 g kg^{-1} out towards the mouth and the shelf area (Jernas et al., 2018). In the Kongsfjorden, and by extension the neighbouring Krossfjorden, temperature and salinity gradients can vary inter-annually, as well as sediment supply and turbidity of water close to the glacier terminus (Svendsen et al., 2002; Jernas et al., 2018). The water depth in the two fjords varies from less than 100 m deep in the inner part of Kongsfjorden and increases to 400 m at the intersection of the Kongsfjorden and Krossfjorden (Hop et al., 2002). Toward the open ocean the depth decreases slightly again to around 200–300 m (Hop et al., 2002). Sea surface water temperatures in August/September in the fjords range from 5–7 °C (Jernas et al., 2018). The bottom water temperatures are usually stable between 2–3 °C (Jernas et al., 2018). The MAAT for Ny Ålesund, at the interior of the Kongsfjorden, is -5.8 °C (Birks et al., 2004b).

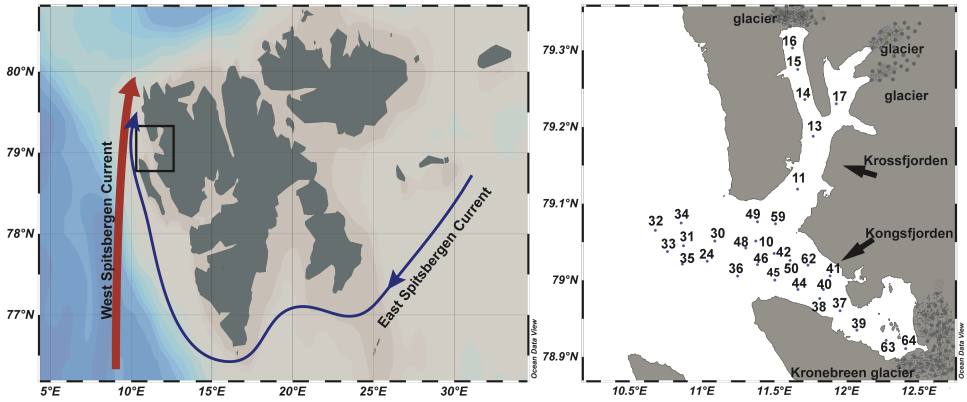

Fig. 1. Map showing (A) Svalbard and relative ocean currents and (B) locations of marine surface sediments (2008 cruise) in Kongsfjorden and Krossfjorden. For an overview of the sampling stations for the 2007 cruise, see Peterse et al. (2009a) and Supplementary Table 1 (sample label prefixes NP-08-16/NP-07-13). Maps were constructed using the Ocean Data View (odv.awi.de) software.

2.2 Soil and sediment sampling

The soil (n = 12) and surface sediment (n = 29, 0–1 cm) sampling on the R/V Lance cruise in September 2007, as well as the specifications of the sites and bulk properties of thesamples, are described in Peterse et al. (2009a). Additional surface sediments (n = 31, 0–1 cm) were collected in August 2008 with a multicorer from the R/V Lance at approximately the same locations as in 2007 (Fig. 1B). All sediments were stored on board at -20 °C, transported to the Royal NIOZ on dry ice, and stored at -40 °C until further analysis.

2.3 GDGT extraction

The extraction method for the soils and sediments from the 2007 cruise is described in Peterse et al. (2009a). The Svalbard soils were already analysed using the new chromatography method and are part of the soil database that De Jonge et al. (2014a). Freeze-dried and powdered surface sediments from the 2008 cruise were extracted in the same manner, using a DIONEX accelerated solvent extractor (ASE 200) with a mixture of dichloromethane (DCM):MeOH 9:1 (v/v)

at 100 °C and 7.6 x 10^6 Pa for 3 back-to-back extractions of 5 min. The subsequent column fractionation, addition of internal standard (cf. Huguet et al., 2006), and filtration steps are identical to those of Peterse et al. (2009a).

A spatially evenly distributed subset of samples (n = 14) of the freeze-dried sediments from the 2008 cruise was extracted with a modified Bligh-Dyer extraction (cf. Pitcher et al., 2009), in order to separate CLs from IPL-derived GDGTs. Samples were extracted (3x) ultrasonically using a single-phase solvent mixture of MeOH/DCM/phosphate buffer 10:5:4 (v/v/v) for 10 minutes. DCM and phosphate buffer were added to the combined extracts to obtain a new mixture of 1:1:0.9 (v/v/v) and achieve phase separation. The DCM phase was collected and passed over a silica column (modified procedure from Pitcher et al., 2009) to obtain IPL and CL fractions using hexane/ethyl acetate 1:1 (v/v) and MeOH as eluents, respectively. In order to cleave off the head groups on the IPLs, the IPL fraction was refluxed for 2 h with 1.5 N HCl in MeOH. An internal standard (C_{46}; Huguet et al., 2006) was added to the CL and IPL-derived GDGT fractions before filtration over a 0.45 µm PTFE filter.

2.4 GDGT analysis

BrGDGTs in the 2008 cruise sediments were analysed according to the latest method of Hopmans et al. (2016) using an Agilent 1260 Infinity ultra high performance liquid chromatography (UHPLC) coupled to an Agilent 6130 single quadrupole mass detector. Two silica Waters Acquity UPLC BEH Hilic (1.7 µm, 2.1 mm x 150 mm) columns with a guard column at 30 °C were used for separation. Injection volume for each sample was 10 µL. An isocratic gradient was used, starting with 82% A and 18% B at a flow rate of 0.2 ml/min for 25 min, then a linear gradient to 70% A and 30 B for 25 min, where A = hexane and B = hexane/isopropanol 9:1 (v/v). The following source conditions were used for the atmospheric pressure chemical ionisation (APCI): gas temperature 200 °C, drying gas (N_2) flow 6 L/min, vaporizer temperature 400 °C, nebulizer pressure 25 psi,

capillary voltage 3500 V, corona current 5.0 µA. Selected ion monitoring (SIM) mode was used to detect the $[M\text{-}H]^+$ ions of brGDGTs at *m/z* 1292, 1050, 1048, 1046, 1036, 1034, 1032, 1022, 1020, 1018 and at 744 for the internal standard.

The $\#rings_{tetra}$ was calculated as follows (Sinninghe Damsté, 2016):

$$\#rings_{tetra} = ([Ib]+2\times[Ic])/([Ia]+[Ib]+[Ic]) \quad (1)$$

The $\#rings_{penta}$ of the 5-methylated brGDGTs is calculated using same reasoning with the pentamethylated group (IIa, IIb, IIc) of brGDGTs.

The relative contribution of 6-methyl brGDGTs, i.e. the degree of isomerization, is quantified in the isomer ratio (IR), calculated according to the following equation:

$$IR = \frac{[IIa']+[IIb']+[IIc']+[IIIa']+[IIIb']+[IIIc']}{[IIa']+[IIb']+[IIc]+[IIIa']+[IIIb']+[IIIc']+[IIa]+[IIb]+[IIc]+[IIIa]+[IIIb]+[IIIc]} \quad (2)$$

The IR_{penta} and IR_{hexa} variants only use the pentamethylated and hexamethylated groups of brGDGTs, respectively.

The reanalysis of the 2007 sediments with the new chromatography method gave similar values for $\#rings_{tetra}$ as those using the old method (difference <0.07). A comparison of brGDGTs extracted from the sediments collected in 2008 using the ASE and Bligh-Dyer methods showed that values for $\#rings_{tetra}$ and $\#rings_{penta}$ remained <0.07 and that differences BIT values were <0.02. Two exceptions were station NP08-16-14 with a larger difference in $\#rings_{tetra}$ (0.27), $\#rings_{penta}$ (0.36), and station NP08-16-64 which had a difference in BIT of 0.1, both of which have reasons which are unclear.

3. Results

3.1 Svalbard Soils

The brGDGT distribution in the re-analysed Svalbard soils shows that brGDGT IIa′ is the most abundant compound (21.1 ±6.4%), followed by IIIa′, Ia and IIa (17.2 ±9.6, 16.6 ±7.4, and 16.0 ±8.5%, respectively; Fig. 2; Supplementary Table 1). BrGDGT IIIc′ was only detected in two soils, in all others it was below the

detection limit. Overall, the 6-methyl brGDGT isomers are dominant in the soils, and comprise on average 45% of the total brGDGT pool. This degree of isomerisation corresponds to isomer ratio (IR) values between 0.24 and 0.73. The $\#rings_{tetra}$ of the soils is low, and varies between 0 and 0.37.

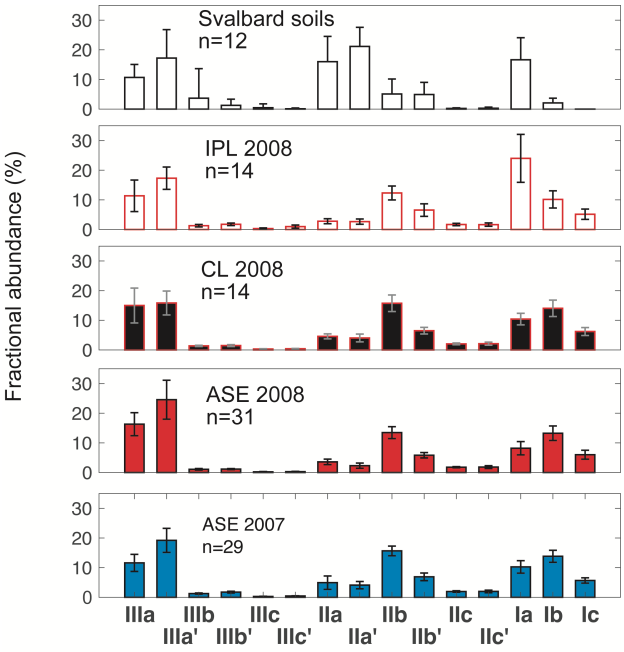

Fig. 2. Average fractional distributions of brGDGTs in Svalbard soils and fjord sediments. IPL-derived and CL brGDGT abundances are shown for a subset of the 2008 surface sediments. Error bars indicate standard deviation.

3.2 Kongsfjorden and Krossfjorden sediments

BrGDGTs in the ASE extracted sediments from Kongsfjorden and Krossfjorden have IIIa′ as the most dominant brGDGT (24.6 ±6.6% for sediments collected in 2007, 19.2 ±4.1% for those collected in 2008; Fig.2). BrGDGTs IIIc and IIIc′ were minor compounds in sediments collected in both 2007 and 2008, only being detected in a few sediments (Fig. 2). Minor differences in the relative abundances of brGDGTs Ib, IIb and IIIa occur between sediments collected in 2007 and 2008

(0.58, 2.2, and 4.7%, respectively). The average abundances of 6-methylated brGDGTs in the 2007 and 2008 sediments comprise 34–36% of the total brGDGT pool and are not statistically different between years (t-test, p = 1). The IR ranges from 0.35–0.55 (2007) and 0.30–0.54 (2008). The $\#rings_{tetra}$ of the ASE extracted surface sediments ranges between 0.66–1.01 (2007) and 0.56–0.92 (2008). The $\#rings_{tetra}$ for the CL brGDGTs is generally low (0.72 on average) in the inner fjords, increases towards the intersection of the fjords (0.88 on average), and then slightly decreases towards the open ocean (0.83 on average; Fig. 3B). In general, the highest values of $\#rings_{tetra}$ occur around the mouth of both of the fjords.

A selection of the Kongsfjorden and Krossfjorden sediments was extracted using Bligh-Dyer type extraction to separate IPL from CL brGDGTs. The brGDGT distribution in the CL fraction shows a similar pattern as the brGDGTs in the same sediment extracted using ASE (Fig. 2), indicating that their results can be compared. In the Bligh-Dyer extracts, the most abundant brGDGTs in the CL fraction are IIIa′, IIb, and IIIa (15.8 ±4.0, 15.7 ±2.7, and 15.0 ±5.9%, respectively). The IR of CL brGDGTs is 0.32–0.51 and the $\#rings_{tetra}$ ranges from 0.65–0.93.

The IPL-derived brGDGTs make up 5.8% on average of the total brGDGT pool in the sediments, with a high range of values: 1.7–25.8%. The site with the highest %IPL was located just outside the fjord mouth, whereas %IPL remained fairly low (≤8%) in other areas (Fig. 3A). The distribution of the IPL-derived brGDGTs differs from that of the CLs, and is characterized by a higher abundance of brGDGT Ia (24 ± 8.1%, Fig. 2). BrGDGT IIIa′ is only the second most abundant compound (17.3 ±3.8%). The IR of the IPL-derived fraction is 0.37–0.61 and $\#rings_{tetra}$ is overall lower than that of the CLs, ranging from 0.24–0.79. The $\#rings_{tetra}$ of the IPL-derived brGDGTs is highest in the mouth/interior part of the fjords, and decreases toward the open ocean. At the input of the Kronebreen glacier (Fig. 3C), the $\#rings_{tetra}$ of the IPL-derived brGDGTs is quite low (0.34), but is not the lowest (0.24) in the stations considered, which occurs at

the mouth of the fjords at station NP-08-16-48. The $\#rings_{tetra}$ of IPL-derived brGDGTs at the other glacier inputs in the Krossfjorden do not exhibit lower signatures (>0.44).

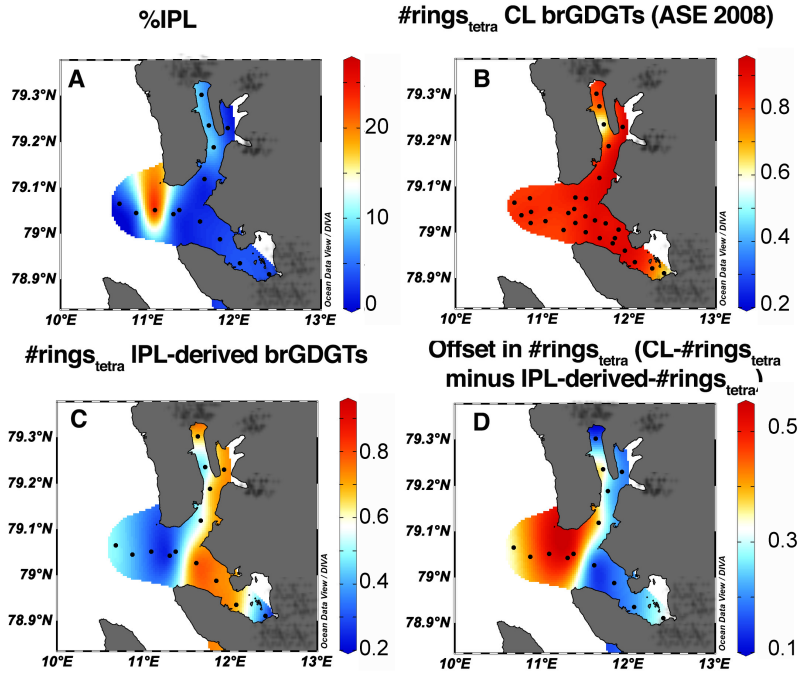

Fig. 3. The percent contribution of the (A) IPL-derived brGDGTs to the total GDGT pool in Svalbard sediments. Spatial variation of brGDGT distributions expressed in the $\#rings_{tetra}$ for (B) CLs and (C) IPL-derived brGDGTs in Svalbard sediments, and (D) the offset in $\#rings_{tetra}$ between these brGDGT pools. The hatched black texture indicates presence of glaciers. Surface plots were constructed using the Ocean Data View (odv.awi.de) software. DIVA (Data-Interpolating Variational Analysis) gridding was used to grid the fields of observations.

4. Discussion

4.1 Soil vs. marine CL-brGDGTs

The new chromatography method shows that Svalbard soils contain relatively high amounts of 6-methylated brGDGTs (up to 63%; De Jonge et al., 2014a). This fits with the generally alkaline pH of most of the Svalbard soils (pH>7 in 9 out of 12 soils), as the contribution of 6-methylated brGDGTs, captured in the IR,

generally increases with soil pH (De Jonge et al., 2014a). The IR_{hexa} vs. IR_{penta} plot of the global calibration set shows that the Svalbard soils follow the global pattern (Fig. 4A; De Jonge et al., 2014a). The same is true for their position in a ternary plot of the tetra-, penta- and hexamethylated brGDGTs and a plot of $\#rings_{tetra}$ vs. $\#rings_{penta}$ (Fig. 4B, C).

The distribution of brGDGTs in Svalbard sediments, however, differs substantially from those in soils (Fig. 2). This vast difference in brGDGT distributions was used as evidence by Peterse et al. (2009a) of aquatic *in situ* production of brGDGTs in the Krossfjorden and Kongsfjorden. The analysis of both 5-methyl and 6-methyl brGDGTs now indicates that also the IR_{penta} and IR_{hexa} in the Svalbard sediments differ from those in soils, and are generally slightly lower (average difference = 0.12 units) than those in the Svalbard soils (Fig. 4A). This is a further indication that the brGDGTs found in Svalbard sediments do not consist exclusively of soil-derived brGDGTs, and thus *in situ* production in the fjord aquatic system is responsible for the different IR values. Although somewhat lower than in the soils, the amounts of 6-methylated brGDGTs in the Svalbard sediments are still relatively high and could possibly be attributed to the alkaliphilic pore waters of marine sediments, whose pH often exceed 7.5 (Jourabchi et al., 2008) thus providing a similar high pH environment to that to the Svalbard soils (Reimers et al., 1996).

Addition of the brGDGT distribution of the Svalbard sediments to the ternary plot with the relative abundances of tetra-, penta-, and hexamethylated brGDGTs provides further confirmation for a marine source of the brGDGTs in the fjords (Fig. 4B). Sinninghe Damsté (2016) used this plot to show that sediments from the Berau delta plot increasingly offset from the global surface soils, and should thus receive an increasing contribution of *in situ* produced brGDGTs. Similarly, Dearing Crampton-Flood et al. (2018) used this plot to assess the qualitative contributions of soil-derived and marine *in situ* produced brGDGTs in a Pliocene sediment sequence from the Netherlands, and Warden et

al. (2018) did the same to investigate the provenance of brGDGTs in Baltic Sea Holocene sediments. The Svalbard fjord sediments are all substantially offset from the typical brGDGT distributions of Svalbard soils (black diamonds) and global soils (grey diamonds, Fig. 4B), clearly confirming their non-soil origin.

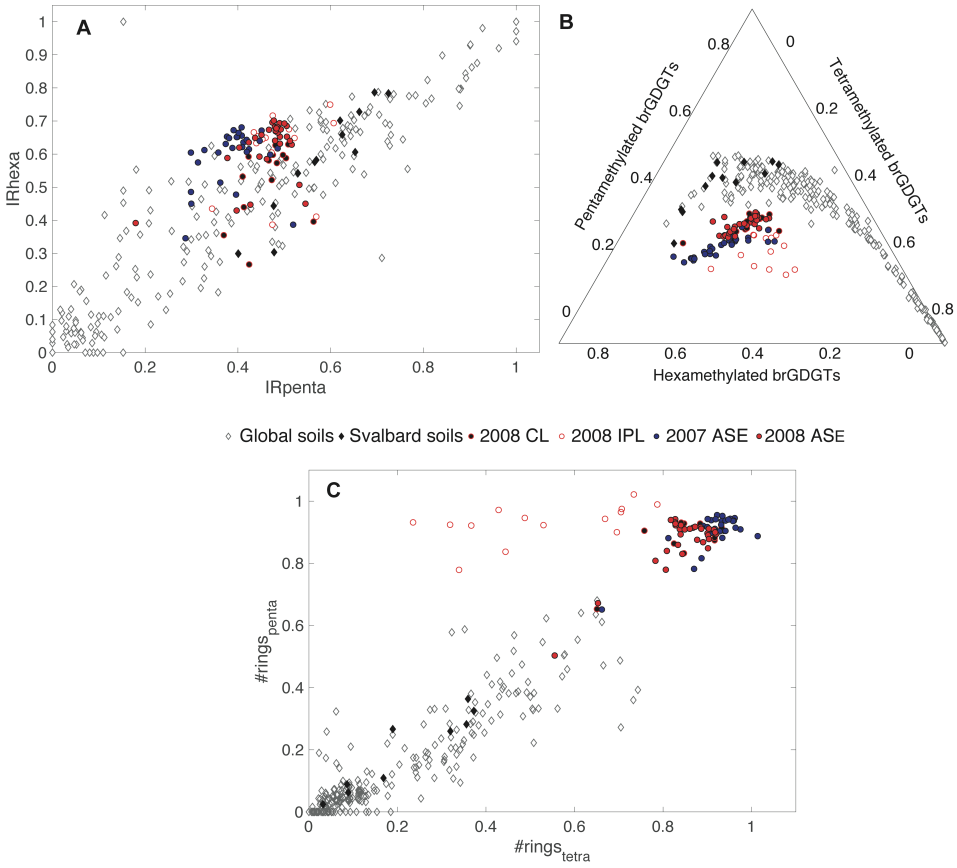

Fig. 4. (A) The degree of isomerisation of penta- versus hexamethylated brGDGTs, (B) ternary plot showing brGDGT distributions, and (C) the degree of cyclisation (#rings) of tetra- versus pentamethylated 5-methyl brGDGTs in Svalbard fjord sediments and soils collected in 2007 and 2008. BrGDGTs in soils from the global soil calibration set (De Jonge et al., 2014a) are plotted for comparison.

Finally, the average #rings$_{tetra}$ and #rings$_{penta}$ of brGDGTs in the marine sediments (2008) are 0.84 and 0.87, which are exceptionally high compared to Svalbard soils as well as global soils, where #rings$_{tetra}$ and #rings$_{penta}$ range

between 0.0–0.74, but have a median value of 0.12 (De Jonge et al., 2014a; Fig. 4C). In fact, the fjord sediments are associated with the highest $\#rings_{tetra}$ reported so far, which is well above the threshold of 0.7 proposed by Sinninghe Damsté (2016) to indicate a purely marine origin for brGDGTs. The water depth in almost the entire fjord system (average depths of 50 m in the inner glacial bays and ~400 m at the outer basins; Zhu et al., 2014) is similar to the depth range assumed to be most suitable for *in situ* brGDGT production (50–300 m; Sinninghe Damsté, 2016). The highest values of $\#rings_{tetra}$ (>0.9) in these fjords are found in the outer basin fjord area, especially in the depth range of 270–310 m (Fig. 4B). At slightly deeper sites outside the mouth of the fjords and into the open ocean, the $\#rings_{tetra}$ decreases slightly, but is still >0.8.

4.2 IPL-derived vs. CL brGDGTs in Svalbard fjord sediments

To obtain a clearer picture of the distribution of marine produced brGDGTs we analysed IPL-derived brGDGTs, assuming that they mostly reflect the brGDGT of living biomass and thus of the brGDGT-producers in marine sediments. The relative distribution of IPL-derived brGDGTs in the fjord sediments differs from that of the CLs, and is characterized by a higher abundance of brGDGT Ia in the IPL-derived pool (Fig. 2). This leads to a different order of abundance of the tetramethylated brGDGTs; where Ib>Ia in the CL pool, and Ia>Ib for IPL-derived brGDGTs. Consequently, the $\#rings_{tetra}$ of IPL-derived brGDGTs is substantially lower than that of the CLs in the same sediment, and can differ up to 0.52 (Fig. 4C). Likely, the IPL-derived brGDGTs reflect the membrane composition of the dominant microbial community present in the sediment at the time of collection, i.e. August/September, whereas the CL signature is an integration of long-term production throughout the year. This means that IPL-derived brGDGTs likely vary in distribution over the season. Interestingly, this finding suggests that brGDGT-producers in the marine environment are more sensitive to seasonally changing environmental conditions than in soils, where seasonal patterns are

absent in IPL-derived brGDGTs (Weijers et al., 2011). Despite the presumed seasonal variation in production, the variation between years is minor, given the similar brGDGT distributions in fjord sediments collected in 2007 and 2008 (Fig. 2).

The higher abundance of brGDGT Ia in the IPL-derived pool may be explained by warmer Atlantic Water that enters the fjord in the summer (i.e. at the time of sampling). This can introduce a warm bias to the 'living' brGDGT signal either directly, due to the higher temperature of the water and subsequent membrane adaptation by their producers, or indirectly, as a result of the introduction of a different brGDGT-producing microbial community with this water mass. Nevertheless, the higher abundances of Ia in the IPL-derived brGDGTs agree with a summer signal of brGDGT production, which must be averaged out over the whole year in order to match the brGDGT CL signal in the sediments.

4.3 Spatial variation in #rings

The spread in $\#rings_{tetra}$ values for CL-brGDGTs in the fjord sediments follows a distinct spatial pattern (Fig. 3B; Supplementary Figure S1), which is similar to that in the Berau delta, the East China Sea, and the Portuguese Margin, where $\#rings_{tetra}$ initially increases on the coastal shelf, and then decreases towards the open ocean (Zhu et al., 2011; Zell et al., 2015; Sinninghe Damsté, 2016). In Svalbard, the lower $\#rings_{tetra}$ in the inner fjords (average 0.72) may partly be the result of the input of soil material by glaciers. The slightly higher BIT and the more soil-like distribution of brGDGTs in the sediment (station NP08-16-64) in front of the Kronebreen glacier in Kongsfjorden (Supplementary Figure S2) were previously used as evidence for substantial input of soil material (Peterse et al., 2009a). The minor decrease in $\#rings_{tetra}$ towards the open ocean (from 0.88 at the mouth of the fjords to 0.83 at the open ocean) corresponds with depths at the deeper end of the zone where *in situ* production is expected (Sinninghe Damsté,

2016), suggesting that *in situ* production indeed changes at depths deeper than ~ 300 m.

The spatial pattern of $\#rings_{tetra}$ based on IPL-derived brGDGTs is broadly similar to that of the CLs, except for that the spread in $\#rings_{tetra}$ is much larger (0.24–0.79; Fig 4C). Plotting the offset between the $\#rings_{tetra}$ between the CL and IPL-derived brGDGTs indicates that the IPL-derived brGDGTs and CL signals are more comparable in the fjords than at the mouth of the fjords or towards the open ocean, where the discrepancy can be up to 0.52 (Fig. 4D). One environmental parameter that follows a similar gradient is salinity, which is lower in the fjords due to the input of glacial meltwater, and increases towards the open ocean. The salinity gradient is especially pronounced in the summer months due to the interaction between the tidewater glaciers, and the inflow of warm, saline Atlantic Water (Jernas et al., 2018). The spatial pattern of $\#rings_{tetra}$ of IPL-brGDGTs then suggests that the incorporation of cyclopentane moieties may be linked to decreasing salinity (Fig. 4C). Interestingly, the bacterial community in sediments close to the glacier mouth differs from that in sediments that are influenced by seawater (Conte et al., 2018). Close to the glacial front, the bacterial community in the fjord mainly consists of *Chloroflexi*, *Acidobacteria*, and *Nitrospirae*, whereas *Proteobacteria*, *Parcubacteria*, *Firmicutes*, and *Actinobacteria* become more abundant towards the open ocean (Conte et al., 2018). Hence, the shift in bacterial communities may explain the simultaneous changes in the $\#rings_{tetra}$ of the IPL-derived brGDGTs. Alternatively, the same bacterial community may be influenced by the salinity gradient, leading to membrane adaptation where more rings are incorporated at lower salinity, and vice versa. This may be a similar process to bacteria that experience acid stress that introduce cyclopropane rings in their alkyl chains to increase stability (Zhang and Rock, 2008).

5. Conclusions

BrGDGT distributions obtained with the new method indicate that 6-methyl brGDGTs are important brGDGTs in Svalbard soils. Subsequent comparison with brGDGT distributions in fjord sediments confirms the earlier conclusion of Peterse et al. (2009a) that most brGDGTs in the fjord sediments are produced *in situ*. The discrepancy in $\#rings_{tetra}$ values (up to 0.52 difference) between the IPL-derived brGDGTs and CLs in the same sediment indicates that brGDGTs in Svalbard are produced in seasonally varying distributions throughout the year. Furthermore, the increasing offset between $\#rings_{tetra}$ in CLs and IPL-derived brGDGTs from the inner fjord towards the open marine environment points toward a possible salinity influence on marine brGDGT production. This indicates that either membrane adaptation to increasing/decreasing salinity may be responsible for the degree of cyclisation of tetramethylated brGDGTs, or that the microbial community of brGDGT-producing bacteria changes on the glacio-marine transect. Further brGDGT studies in other modern systems are needed to confirm this possible salinity trend in $\#rings_{tetra}$ values.

Acknowledgements

The work was supported by funding from the Netherlands Earth System Science Center (NESSC) through a gravitation grant (NWO 024.002.001) from the Dutch Ministry for Education, Culture and Science to JSSD. The authors thank Alle-Tjipke Hoekstra for analytical support. Thanks also to the crew and participants of the 2007 and 2008 cruises on the R/V Lance of the Norwegian Polar Institute.

Supplementary Material

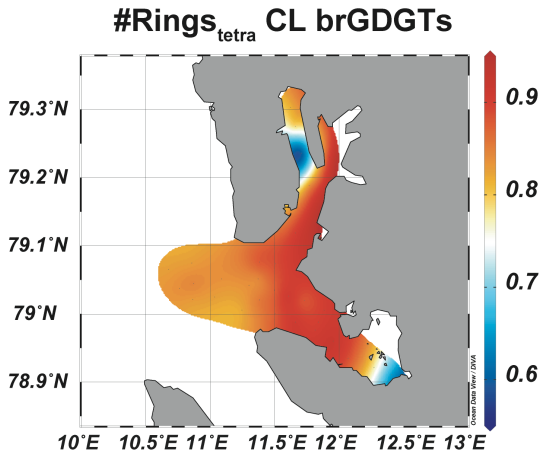

Fig. S1. Spatial variation in #rings$_{tetra}$ values for the core lipids (CLs) of the surface sediment samples collected on the 2008 cruise. Surface plot constructed using the Ocean Data View (odv.awi.de) software. DIVA (Data-Interpolating Variational Analysis) gridding was used to grid the fields of observations with default values in ODV.

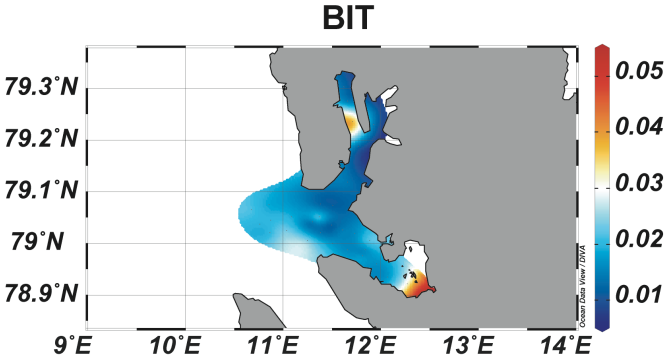

Fig. S2. Spatial variation in BIT index values for the surface sediment samples collected on the 2008 cruise. Surface plot constructed using the Ocean Data View (odv.awi.de) software. DIVA (Data-Interpolating Variational Analysis) gridding was used to grid the fields of observations with default values in ODV.

Table S1. Sample locations for the 2007 (CL) and 2008 cruises (IPL and CL).

Year	Station	Latitude	Longitude	Extraction/Lipid type
2007	NP-07-13-09	79°01.46'N	10°44.57'E	ASE
2007	NP-07-13-10	79°03.34'N	10°39.55'E	ASE
2007	NP-07-13-11	79°03.55'N	10°50.54'E	ASE
2007	NP-07-13-13	79°07.07'N	11°39.45'E	ASE
2007	NP-07-13-14	79°17.47'N	11°40.05'E	ASE
2007	NP-07-13-15	79°15.58'N	11°40.05'E	ASE
2007	NP-07-13-16	79°13.45'N	11°42.21'E	ASE
2007	NP-07-13-21	79°11.10'N	11°45.41'E	ASE
2007	NP-07-13-23	79°13.42'N	11°55.25'E	ASE
2007	NP-07-13-24	79°00.53'N	11°01.40'E	ASE
2007	NP-07-13-25	79°00.46'N	10°51.32'E	ASE
2007	NP-07-13-26	79°02.26'N	10°52.11'E	ASE
2007	NP-07-13-40	79°03.36'N	11°05.12'E	ASE
2007	NP-07-13-41	78°57.21'N	11°57.07'E	ASE
2007	NP-07-13-42	78°58.12'N	11°47.41'E	ASE
2007	NP-07-13-44	78°59.10'N	11°50.6'E	ASE
2007	NP-07-13-46	79°00.43'N	11°43.53'E	ASE
2007	NP-07-13-47	79°01.41'N	11°29.26'E	ASE
2007	NP-07-13-48	79°00.52'N	11°36.06'E	ASE
2007	NP-07-13-49	78°59.59'N	11°30.20'E	ASE
2007	NP-07-13-50	79°00.44'N	11°22.55'E	ASE
2007	NP-07-13-51	79°01.57'N	11°18.21'E	ASE
2007	NP-07-13-52	79°02.38'N	11°22.18'E	ASE
2007	NP-07-13-53	79°04.23'N	11°22.35'E	ASE
2007	NP-07-13-55	78°59.09'N	11°39.13'E	ASE
2007	NP-07-13-60	79°08.54'N	11°44.47'E	ASE
2007	NP-07-13-61	78°55.38'N	12°03.23'E	ASE
2007	NP-07-13-64	78°54.25'N	12°24.12'E	ASE
2007	NP-07-13-09	79°03.52'N	11°29.53'E	ASE
2008	NP08-16-10	79°02.65'N	11°22.18'E	ASE
				CL
				IPL
2008	NP08-16-11	79°07.08'N	11°39.38'E	ASE
				CL
				IPL
2008	NP08-16-13	79°11.17'N	11°45.67'E	ASE
				CL
				IPL
2008	NP08-16-14	79°13.69'N	11°42.37'E	ASE
				CL
				IPL
2008	NP08-16-15	79°15.91'N	11°39.41'E	ASE

2008	NP08-16-16	79°17.71'N	11°37.31'E	ASE
				CL
				IPL
2008	NP08-16-17	79°13.49'N	11°55.42'E	ASE
				CL
				IPL
2008	NP08-16-24	79°00.90'N	11°01.67'E	ASE
2008	NP08-16-30	79°03.05'N	11°05.17'E	ASE
				CL
				IPL
2008	NP08-16-31	79°02.42'N	10°52.18'E	ASE
				CL
				IPL
2008	NP08-16-32	79°03.55'N	10°39.96'E	ASE
				CL
				IPL
2008	NP08-16-33	79°01.75'N	10°44.96'E	ASE
2008	NP08-16-34	79°03.89'N	10°50.80'E	ASE
2008	NP08-16-35	79°00.76'N	10°51.51'E	ASE
2008	NP08-16-36	79°00.20'N	11°14.43'E	ASE
2008	NP08-16-37	78°57.37'N	11°57.14'E	ASE
2008	NP08-16-38	78°57.95'N	11°48.49'E	ASE
2008	NP08-16-39	78°55.66'N	12°03.72'E	ASE
				CL
				IPL
2008	NP08-16-40	78°59.17'N	11°50.22'E	ASE
				CL
				IPL
2008	NP08-16-41	79°00.21'N	11°52.64'E	ASE
2008	NP08-16-42	79°01.66'N	11°29.52'E	ASE
2008	NP08-16-44	78°59.17'N	11°39.45'E	ASE
2008	NP08-16-45	79°00.01'N	11°30.11'E	ASE
2008	NP08-16-46	79°00.74'N	11°23.01'E	ASE
2008	NP08-16-48	79°01.92'N	11°18.09'E	ASE
				CL
				IPL
2008	NP08-16-49	79°04.35'N	11°22.61'E	ASE
2008	NP08-16-50	79°00.94'N	11°35.92'E	ASE
				CL
				IPL
2008	NP08-16-59	79°03.85'N	11°29.87'E	ASE
2008	NP08-16-62	79°00.71'N	11°43.54'E	ASE
2008	NP08-16-63	78°55.18'N	12°15.79'E	ASE
2008	NP08-16-64	78°54.39'N	12°24.28'E	ASE
				CL
				IPL

Chapter 4

Using tetraether lipids archived in North Sea Basin sediments to extract North Western European Pliocene continental air temperatures

Emily Dearing Crampton-Flood, Francien Peterse, Dirk Munsterman, Jaap S. Sinninghe Damsté, 2018. *Earth and Planetary Science Letters*, 490, 193-205.

Abstract

The Pliocene is often regarded as a suitable analogue for future climate, due to an overall warmer climate (2–3 °C) coupled with atmospheric CO_2 concentrations largely similar to present values (~400 ppmv). Numerous Pliocene sea surface temperature (SST) records are available, however, little is known about climate in the terrestrial realm. Here we generated a Pliocene continental temperature record for Northwestern Europe based on branched glycerol dialkyl glycerol tetraether (brGDGT) membrane lipids stored in a marine sedimentary record from the western Netherlands. The total organic carbon (TOC) content of the sediments and its stable carbon isotopic composition ($\delta^{13}C_{org}$) indicate a strong transition from primarily marine derived organic matter (OM) during the Pliocene, to predominantly terrestrially derived OM after the transition into the Pleistocene. This trend is supported by the ratio of branched and isoprenoid tetraethers (BIT index). The marine-terrestrial transition indicates a likely change in brGDGT sources in the core, which may complicate the applicability of the brGDGT paleotemperature proxy in this setting. Currently, the application of the brGDGT-based paleothermometer on coastal marine sediments has been hampered by a marine overprint. Here, we propose a method to disentangle terrestrial and marine sources based on the degree of cyclisation of tetramethylated brGDGTs (#rings) using a linear mixing model based on the global soil calibration set and a newly developed coastal marine temperature transfer function. Application of this method on our brGDGT record resulted in a 'corrected' terrestrial temperature record (MAT_{terr}). This latter record indicates that continental temperatures were ~12–14 °C during the Early Pliocene, and 10.5–12 °C during the Mid Pliocene, confirming other Pliocene pollen based terrestrial temperature estimates from Northern and Central Europe. Furthermore, two colder (Δ 5–7 °C) periods in the Pliocene MAT_{terr} record show that the influence of Pliocene glacials reached well into NW Europe.

1. Introduction

Over the past decade, branched glycerol dialkyl glycerol tetraethers (brGDGTs) have emerged as a promising class of biomarker lipids used in paleoenvironmental reconstructions (Weijers et al., 2007a). BrGDGTs are bacterial membrane lipids present in soils and peats worldwide, and their structure consists of two alkyl chains (C_{30-32}) bound by ether bonds to two glycerol moieties (Fig. 1). Individual brGDGTs are distinguished by the number and position of methyl groups (4–6) and cyclopentane rings (0–2) on the alkyl chains (Fig. 1). Weijers et al. (2007a) analyzed brGDGTs in a global set of soils, and identified significant correlations between the degrees of cyclisation and methylation of brGDGTs with soil pH and mean air temperature (MAT). This observation formed the original basis for the brGDGT-based continental paleothermometer (Weijers et al., 2007a). A second brGDGT proxy builds upon the predominantly soil origin of brGDGTs; the Branched and Isoprenoid Tetraether (BIT) index measures the relative input of soil organic matter (OM) delivered to the marine environment by runoff processes (Hopmans et al., 2004). In short, the BIT index is a ratio of the most abundant brGDGTs to Crenarchaeol, an isoprenoid GDGT produced by marine Thaumarchaeota (Sinninghe Damsté et al., 2002; Hopmans et al., 2004).

Both the brGDGT paleotemperature proxy and the BIT index have been applied in various systems throughout geological time. For example, the first MAT record based upon brGDGT-paleothemometry was carried out on a marine sediment core from the Congo River outflow, and resulted in a continuous record of tropical African continental air temperatures during the last deglaciation (Weijers et al., 2007b). Similarly, terrestrial temperature records were reconstructed for the Miocene of North Europe (Donders et al., 2009) and the mid-Pleistocene of the Arctic (de Wet et al., 2016). Application of the BIT index has also indicated the early activation of European rivers during the last deglaciation in the Bay of Biscay (Ménot et al., 2006), and served as an indirect

method reflecting the amount of monsoon precipitation in Holocene sediments from Lake Challa (Verschuren et al., 2009). The BIT index is also employed in modern settings to trace OM transport from land to sea through rivers (Herfort et al., 2006).

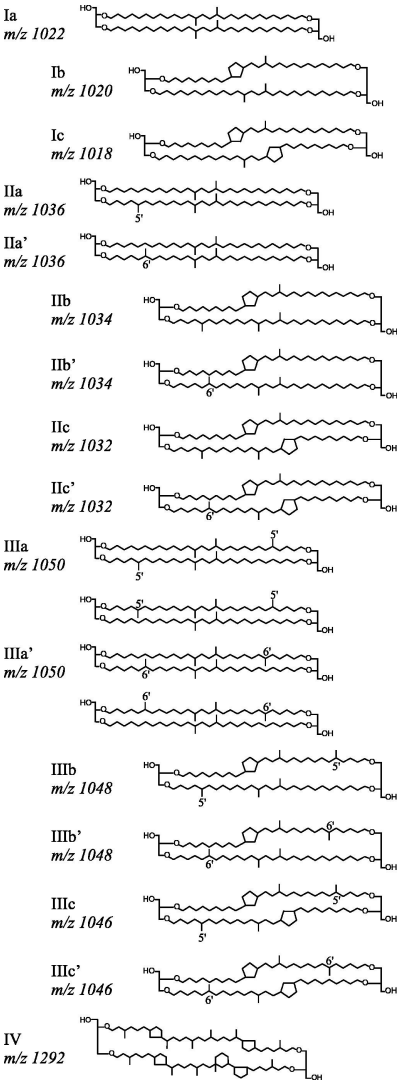

Fig. 1. Molecular structures of the brGDGTs analysed in this study (I–III), and Crenarchaeol (IV). The tetramethylated brGDGTs are represented by structures Ia–Ic, the pentamethylated by structures IIa–IIc, and the hexamethylated by structures IIIa–IIIc. From De Jonge et al. (2014a).

The foundation of these brGDGT proxies is grounded in the assumption that brGDGTs are transported from the continent to coastal marine sediments by rivers and runoff. In other words, the proxies can only be suitably applied if brGDGTs in marine sediments are allochthonous components. This assumption has been challenged recently with the discovery of aquatic brGDGT production in rivers (Zell et al., 2013a, b; De Jonge et al., 2014b), and coastal marine settings (Peterse et al., 2009a; Sinninghe Damsté, 2016). The influence of aquatically produced brGDGTs on the paleorecord can result in a slight underestimation (up to 3 °C recorded in the Amazon river; Zell et al., 2013b), or large overestimation (up to 11–19 °C recorded in marine sediments from Svalbard; Peterse et al., 2009a) of calculated MATs. Thus, a mixed source of brGDGTs in coastal marine sediments has strong implications for MAT reconstruction, as the current calibration (MAT_{mr}) is based solely upon brGDGTs in surface soils (De Jonge et al., 2014a). The wide applicability of the proxy, and thus the generation of terrestrial MAT records, is hampered by the lack of a method to disentangle these disparate sources and to correct for a possible aquatic overprint of the terrestrial brGDGT signal.

Recent analytical developments in liquid chromatography methods have permitted the discovery of structural isomers of penta- and hexamethylated brGDGTs, where the peripheral methyl group(s) varies from the 5- to the 6-carbon position of the alkyl chain (De Jonge et al., 2013; 2014a; Fig. 1). The identification and separation of the isomers led to an improved calibration of the brGDGT paleothermometer for soils (De Jonge et al., 2014a) and aided in the recognition of riverine brGDGT production (De Jonge et al., 2015), as revealed by high abundances of pH-sensitive 6-methyl brGDGTs in suspended particulate matter (SPM) from the Yenisei River. The better match of brGDGT-based pH with the higher pH of Yenisei River water rather than the pH of the Yenisei watershed soils suggested that substantial amounts of particularly 6-methyl brGDGTs in the Yenisei River are aquatically produced.

Similarly, the number of cyclopentane rings appears to indicate in situ brGDGT production in coastal marine settings (Peterse et al., 2009a; Sinninghe Damsté, 2016). In a transect of marine sediments from Svalbard, Peterse et al. (2009a) observed that brGDGT concentrations increased toward the ocean, particularly those containing a cyclopentane moiety. Due to the clear offset with brGDGT distributions found in Svalbard soils, the trends in the fjord sediments could only be explained by a large contribution of in-situ produced cyclopentane-containing brGDGTs to the fjord sediments (Peterse et al., 2009a). Sinninghe Damsté (2016) also observed a similar trend in two coast-shelf transects from the Berau River delta, and formulated an index based upon the weighted average number of cyclopentane moieties of tetramethylated brGDGTs, $\#rings_{tetra}$. The $\#rings_{tetra}$ shows a marked increase from the river mouth (0.22) toward the shelf break (0.83), reflecting the increased contribution of in-situ produced brGDGTs towards open sea. Thus, the new analytical method and identification of brGDGT isomers provides possibilities to disentangle soil vs. marine contributions to the climate signal archived in coastal marine sediments, providing an opportunity to reconstruct continental MAT for areas with mixed brGDGT sources.

The North Sea basin is an ideal test case to separate marine and terrestrial sources of brGDGTs, due to its coastal location and associated sensitivity to sea level change. Here we specifically target the interval covering the Pliocene (5.33–2.58 Ma), which is the most recent geological interval possessing CO_2 atmospheric concentrations similar to both present and projected levels for the near future (400–450 ppmv, Masson-Demotte et al., 2013; Haywood et al., 2016a, b). In addition, continents were in, or relatively close to, their present position (Dowsett et al., 2010; Haywood et al., 2016a, b). For these reasons, the Pliocene, in particular the mid-Piacenzian Warm Period (mPWP, 3.264–3.025 Ma; Dowsett et al., 2010) is studied to provide constraints on the magnitude and severity of future climate change.

Pliocene temperature estimates are primarily composed of sea surface temperature (SST) records generated using geochemical proxies. Comprehensive SST records of the MPWP have been compiled by the PRISM Group (Pliocene Research Interpretation and Synoptic Mapping; Dowsett et al., 1994, 2010). In contrast to the marine realm, terrestrial temperatures during the Pliocene remain poorly constrained, due to the limited number of proxies and a scarcity of continuous Pliocene terrestrial sedimentary archives. Currently, the bulk of temperature estimates are based on pollen assemblages (Head 1998; Pross and Klotz, 2001; Meijer et al., 2006; Salzmann et al., 2008, 2013 and references therein). Although this data has been used for data-model comparison studies (e.g. Salzmann et al., 2008, 2013), there is a lack of diversity in terrestrial temperature proxies, which highlights the need for more methods to infer past terrestrial temperatures to validate the temperature estimates generated thus far.

Here we aim to extract the terrestrial temperature signal of Pliocene North-western (NW) Europe from brGDGTs and OM bulk properties archived in sediments deposited in the North Sea Basin, using the improved chromatographic method separating 5-methyl and 6-methyl brGDGT isomers (De Jonge et al., 2014a; Hopmans et al., 2016). We use the $\#rings_{tetra}$ index and end-member modeling to correct for possible changes in brGDGT sources with time. The resulting record should thus primarily represent terrestrial air temperatures, providing a semi-quantitative Pliocene air temperature record for NW Europe.

2. Methods

2.1 Study Site and sampling

The study site lies within the Rhine-Meuse-Scheldt delta in North-western Europe, with a present-day climate characterized by mild, maritime conditions and an annual mean air temperature (MAT) of ~10 °C (van Engelen et al., 2001). The Hank core was drilled in 2001 in the Dutch province of Noord-Brabant (51°43'N, 4°55'E; Fig. 2) using air-lifting well technology to a base of 404 m.

Samples were collected at a resolution of 1 m. The air-lifting well technology provides mixed samples for every 1 m, leading to the generation of smoothed trends in a comparatively extensive record. There was no evidence of caving observed in the core. The interval from 404 m to 136 m was selected for this study.

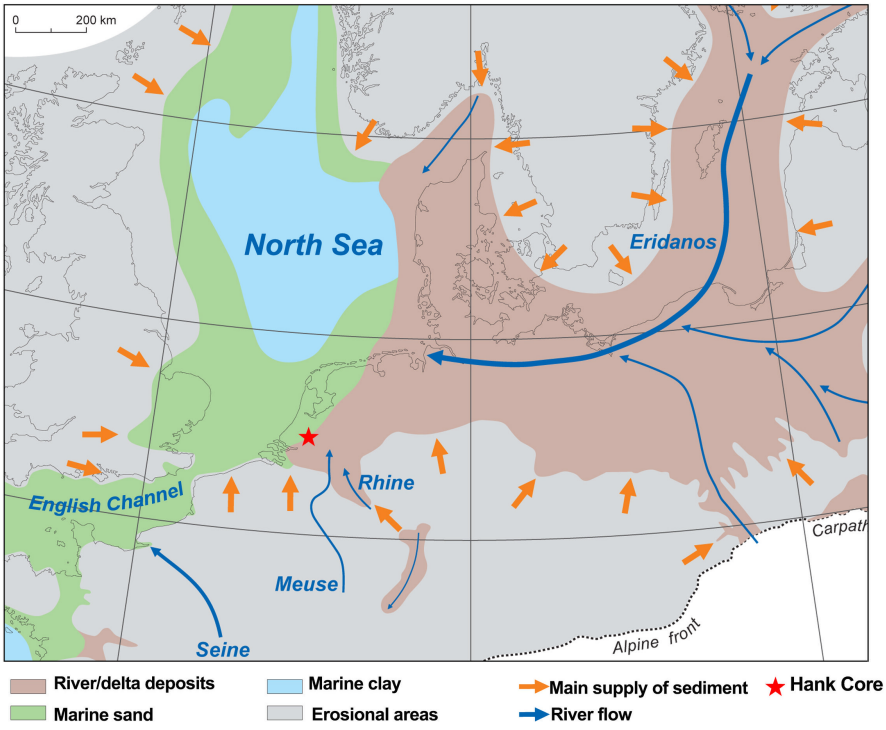

Fig. 2. Location of the Hank site in South-west Netherlands (red star). The early Pliocene paleogeography is modified after Gibbard and Lewin (2003) and Knox et al. (2010). Figure modified from Gibbard and Lewin (2016).

The lithostratigraphy of the succession spans the upper part of the Breda Formation, the Oosterhout Formation and the lower part of the Maassluis Formation (Fig. 3). The Breda Fm. consists of shallow marine glauconitic sands, silts and (sandy) clays. The Oosterhout Fm. predominantly consists of shallow to marginal marine (moderate to low glauconitic) sands and is relatively rich in shells. The Maassluis Fm. shows an alternation of shales, silts and sands and is

developed in a near coastal shallow-marginal marine setting (Van Adrichem Boogaert & Kouwe, 1993-1997).

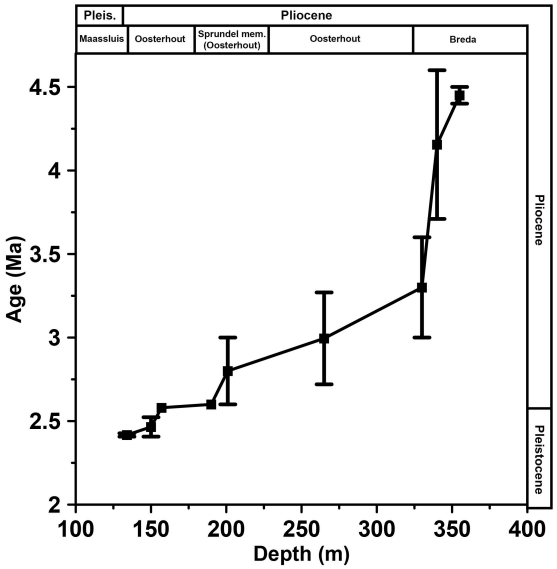

Fig. 3. Age-depth model for the Hank core, with corresponding formations. The closed squares denote Hank biostratigraphic dinocyst events summarized in Table 1. Briefly, the events are: the LOD of *Reticulatosphaera actinocoronata* (355 m), the LOD of *Operculodinium tegillatum* (340 m), the LOD of *Melitasphaeridium choanophorum* (330 m), the LOD of *Invertocysta lacrymosa* (265 m), the LOD of *Operculodinium? eirikianum* (201 m), the LOD of *Barssidinium pliocenicum* (190 m), the LOD of *Barssidinium* spp. (157 m), the acme of *Impagidinium multiplexum* (150 m), and the acme of *Operculodinium israelianum* (133–136 m).

2.2 Palynology and age-assessment

A selection of 82 samples (~20 g) was processed for palynological analysis following the standard techniques, involving HCl and HF digestion, no oxidation, and 15 µm sieving (Janssen and Dammers, 2008). The palynomorphs were counted until 200 specimens per sample were registered. The remainder of the microscope slide was then scanned for rare species. The dinocyst taxonomy is according to that cited in Williams et al. (2017).

Ages are assigned based on last occurrence datums (LODs), first occurrence datums (FODs), and acmes of dinoflagellate cyst species in the North

Sea (Table 1, Fig. 3). Key-references for the Plio-Pleistocene dinoflagellate cyst stratigraphy used for the North Sea age model are listed in Table 1. Recent stratigraphic publications on the Nordic Seas and North Atlantic are taken into account for the strong diachroneity between dinoflagellate cyst events, and applied only if discussed and correlated with their North Sea occurrences (De Schepper et al., 2015; 2017).

2.3 Bulk organic carbon analysis

Total organic carbon (TOC) content and stable carbon isotopes of the bulk OC ($\delta^{13}C_{org}$) were measured for 89 and 72 samples, respectively. Homogenized sediments were decalcified by overnight treatment with 1.0 M HCl. The samples were then rinsed 2x with demineralized water, and left to dry in an oven (60 °C). TOC content and $\delta^{13}C_{org}$ values were analyzed with a Fison NA 1500 CNS-analyzer connected to a Finnigan Mat Delta Plus isotope ratio mass spectrometer following standard procedures. TOC content values are expressed as the weight percentage of dried sediment (wt.%). $\delta^{13}C_{org}$ values are reported in the standard delta notation relative to the Vienna Pee Dee Belemnite (VPDB) standard.

2.4 GDGT extraction and analysis

In total, 155 samples were homogenized with a mortar and pestle for organic geochemical analysis. Samples (5–10 g) were extracted (3x) with dichloromethane (DCM):methanol (9:1, *v/v*) using an accelerated solvent extractor (ASE 350, Dionex™) at 100 °C and 7.7 x 10^6 Pa. Total lipid extracts (TLE) were dried under a stream of N_2. Separation into apolar, ketone and polar fractions was achieved by passing the TLE over an activated Al_2O_3 column using hexane:DCM (9:1, *v/v*), hexane:DCM (1:1, *v/v*), and DCM:methanol (1:1, *v/v*) as eluents, respectively. A known amount of internal standard (IS, $GDGT_{46}$) was added to the polar fraction (Huguet et al., 2006). Polar, GDGT-containing

fractions were re-dissolved in hexane:isopropanol (99:1, *v/v*), and filtered using a 0.45 µM PTFE filter.

GDGTs were analyzed according to Hopmans et al. (2016) using an Agilent 1290 Infinity ultra high performance liquid chromatography (UHPLC) coupled to an Agilent 6130 single quadrupole mass detector. In short, separation was achieved by two silica Waters Acquity UPLC HEB Hilic (1.7 µm, 2.1 mm x 150 mm) columns at 30 °C, with a guard column of the same material preceding both. Isocratic elution was used to separate the GDGTs, starting with 82% A and 18% B for 25 min at a flow rate of 0.2 ml/min, followed by a linear gradient to 70% A and 30% B for 25 min, where A = hexane and B = hexane:isopropanol 9:1. Injection volume was 10 µL. Ionization of the GDGTs was accomplished using atmospheric pressure chemical ionization with the following source conditions: gas temperature 200 °C, vaporizer temperature 400 °C, drying gas (N_2) flow 6 L /min, capillary voltage 3500 V, nebulizer pressure 25 psi, corona current 5.0 µA.

GDGTs were identified by detecting the $[M\text{-}H]^+$ ions in selected ion monitoring (SIM) mode at *m*/z 1292, 1050, 1048, 1046, 1036, 1034, 1032, 1022, 1020, 1018, using *m*/*z* 744 for the internal standard. Quantitation was achieved by peak area integration of the $[M\text{-}H]^+$ ions in Chemstation software B.04.02 and comparing that with the area of the IS, assuming that the response of the mass spectrometer was similar for brGDGTs, crenarchaeol, and the IS.

Replicate measurements of a subset of samples yielded similar index values for MBT′5Me and CBT′ indices (difference <0.03 for MBT'5Me and <0.05 for CBT'), corresponding with a difference of 1.0 °C and <0.1 pH units, respectively.

2.5 GDGT proxy calculations

Roman numerals in the following equations refer to the molecular structures of GDGTs shown in Fig. 1.

The BIT index was calculated using both 5- and 6-methyl GDGTs, in an equation adapted from Hopmans et al. (2004):

$$\mathrm{BIT} = \frac{\mathrm{Ia+IIa+IIa'+IIIa+IIIa'}}{\mathrm{IV+Ia+IIa+IIa'+IIIa+IIIa'}} \quad (1)$$

MBT′5Me values were calculated using fractional abundances of brGDGTs and the index defined by De Jonge et al. (2014a):

$$\mathrm{MBT'_{5Me}} = \frac{\mathrm{Ia+Ib+Ic}}{\mathrm{Ia+Ib+Ic+IIa+IIb+IIc+IIIa}} \quad (2)$$

MATs were calculated using fractional abundances of brGDGTs and the latest transfer function of De Jonge et al. (2014a):

$$\mathrm{MAT_{mr}} = 7.17 + 17.1 * [\mathrm{Ia}] + 25.9 * [\mathrm{Ib}] + 34.4 * [\mathrm{Ic}] - 28.6 * [\mathrm{IIa}] \quad (3)$$

The weighted average number of cyclopentane rings in tetramethylated brGDGTs ($\#\mathrm{Rings_{tetra}}$) was calculated cf. Sinninghe Damsté (2016):

$$\#\mathrm{Rings_{tetra}} = \frac{[\mathrm{Ib}]+2*[\mathrm{Ic}]}{[\mathrm{Ia}]+[\mathrm{Ib}]+[\mathrm{Ic}]} \quad (4)$$

2.6 Statistical analysis

To identify changes in the brGDGT assemblage and to assess variability in the brGDGT pool, principal component analysis (PCA) was performed with the software package SigmaPlot (Systat Software). Standardized fractional abundances of the major brGDGTs (excluding brGDGTs IIIb, IIIb′, IIIc and IIIc′) were used.

3. Results

3.1 Lithology and age model

The studied core section (404–136 m) consists of three formations, the Maassluis (157–136 m), the Oosterhout (333–157 m), and the Breda (404–333 m). The presence of marine dinocysts preferring outer neritic conditions (e.g. *Spiniferites*, *Operculodinium? eirikianum*) and bisaccates in common values (approx. 32% of the total sum of dinoflagellate cysts and sporomorphs) suggests an open-marine

offshore conditions of the Hank site at the time of deposition of the Breda Fm. The Oosterhout Fm. sediments (333–157 m) consist almost exclusively of sands, except for one clay interval between 291–271 m. The sands deposited above the clay layer (271–157 m) contain abundant shells, suggesting that the shore was closer to the Hank site during this period. The overlying Maassluis Fm. (157–136 m) mostly consists of silt deposits interspersed with thin clay and sand deposits. The emergence of freshwater algae species (e.g. *Pediastrum*) and organisms preferring brackish water conditions (*Botryococcus*) in this section indicates a development towards estuarine conditions. Thus, the shore gradually moved closer to the Hank site over the evolution of the Pliocene and early Pleistocene. Eventually, the core site attained a deltaic character. This is also reflected in the age-depth model (Fig. 3), where the observed sedimentation rate increases drastically just before the Plio-Pleistocene transition at approximately 200 m.

The Pliocene-Pleistocene transition (~154 m) is indicated by the increased proportion of cold-tolerant taxa such as *Habibacysta tectata* (Head et al., 1989; Jimenez-Moreno et al., 2006; Hennissen et al., 2017). Also, markers for the Piacenzian, (including taxa preferring relatively warmer conditions – like *Barssidinium pliocenicum, Invertocysta lacrymosa,* and *Melitasphaeridium choanophorum)* are absent above this depth.

The presence of hiatuses in the Hank core is unknown, however, the mixing of samples due to the core collection method leads to the smoothing out of hiatuses, if present. Thus, linear interpolation between the age tie-points is used to estimate the age of the Hank sediments (Fig. 3). The obtained age model indicates that the studied interval encompasses the Early Pliocene (Zanclean) to the early Pleistocene (Gelasian), although the coastal setting suggests that the sedimentation rate may not always have been constant between tie-points at this site.

3.2 Bulk properties of organic material in the Hank Core

TOC content ranges from 0.02 to 2.1 wt. % (Fig. 4B), where TOC is lower in the Pliocene (>161 m; 0.25 wt.% on average) than in the Pleistocene part of the core (average 0.92 wt.%). The lowest TOC values (0.02-0.09 wt.%) occur in four intervals: 386–381 m, 261–259 m, 211–192 m, and 176–163 m (Fig. 4B). In general, TOC content follows the lithology, with the lowest TOC values corresponding to the sand intervals (0.02–0.81 wt.%), the highest values in the loam intervals (0.26–1.95 wt.%), and the clay layers possessing intermediate TOC values (0.19–0.54 wt.%).

The $\delta^{13}C_{org}$ values vary between -28.4 and -22.2‰, and show an overall decreasing trend from the Pliocene towards the Pleistocene, except during two distinct intervals in the Pliocene at 386–376 m and 305–300 m, which show more depleted $\delta^{13}C_{org}$ values ($\Delta\ \delta^{13}C_{org}$ ~3 ‰; shaded in Fig. 4C).

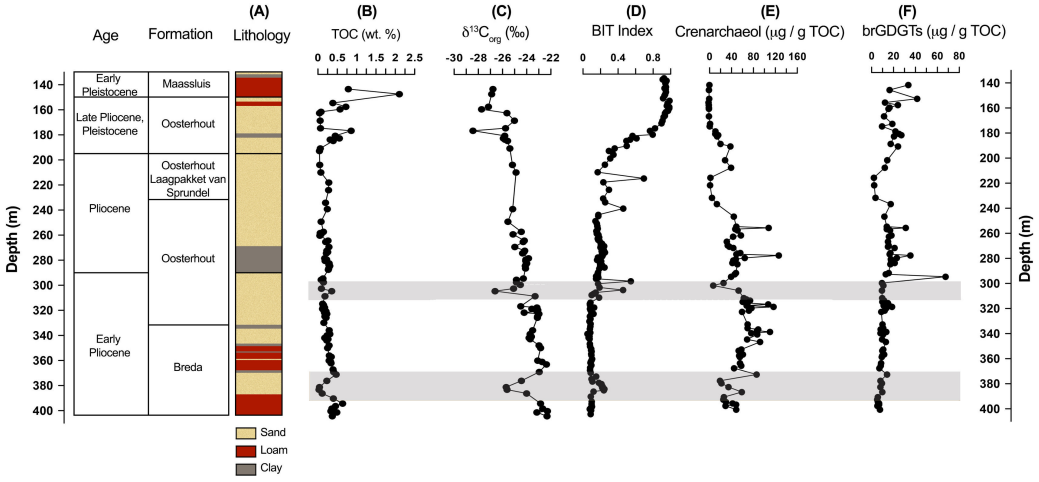

Fig. 4. Depth, age, and formation of the Hank sediments plotted with: (A) lithology, (B) total organic carbon (TOC) content, (C) $\delta^{13}C_{org}$, (D) BIT index, (E) crenarchaeol concentration (TOC-normalised), and (F) brGDGT concentration (TOC-normalised). The brGDGT concentrations represent the sum of all brGDGTs measured (Ia-IIIc′). The two shaded intervals represent Pliocene events discussed in the text

Table 1. Biostratigraphic age model for the Hank Core. Note: ages correlating ranges for MIS 95 and 97 are based on the benthic isotope stratigraphy stack (Lisiecki and Raymo, 2005).

Dinocyst event	Depth (m)	Age (Period)	Age (Ma)	Location	Reference
Acme *Operculodinium israelianum*	133–136	Early Pleistocene, MIS 95 (Unit N3b)	2.407–2.427	Netherlands, North Sea	Meijer et al., 2006; Noorbergen et al., 2015
Acme *Impagidinium multiplexum*	150	Early Pleistocene, MIS 97 (Unit N2b)	2.452–2.477	Netherlands, North Sea	Meijer et al., 2006; Noorbergen et al., 2015
LOD *Barssidinium* spp.	157	Late Pliocene	2.58	Netherlands, North Sea	Kuhlmann et al., 2006
LOD *Barssidinium pliocenicum*[1]	190	Late Pliocene	2.58	Netherlands, North Sea	Kuhlmann et al., 2006
			2.6	Eastern North Atlantic, DSDP 610A	De Schepper and Head, 2008, 2009
LOD *Operculodinium? eirikianum*[2]	201	Late Pliocene	2.6	Eastern North Atlantic, DSDP 610A	De Schepper and Head, 2008, 2009
			3.0	Norwegian Sea, ODP 642B	De Schepper et al., 2015, 2017
LOD *Invertocysta lacrymosa*[3]	265	Late Pliocene	2.72–2.74	Eastern North Atlantic, DSDP 610A	De Schepper and Head, 2008, 2009
		Mid Pliocene	3.27	Norwegian Sea, ODP 642B	De Schepper et al., 2015, 2017
LOD *Melitasphaeridium choanophorum*[4]	330	Late Pliocene	3.0	Eastern North Atlantic, DSDP 610A	De Schepper and Head, 2008, 2009
		Mid Pliocene	3.3	Norwegian Sea, ODP 642B	De Schepper et al., 2015, 2017
LOD *Operculodinium tegillatum*[5]	340	Early Pliocene	3.71	Eastern North Atlantic, DSDP 610A	De Schepper and Head, 2008, 2009
			4.6	Norwegian Sea, DSDP 642B	De Schepper et al., 2015, 2017

LOD *Reticulatosphaera actinocoronata*[6]	355	Early Pliocene	*ca.* 4.4	Northern North Atlantic, DSDP Site 611	Mudie, 1987; Baldauf et al. (1987)
			4.64	Norwegian Sea, DSDP 642B	De Schepper et al., 2015, 2017

[1] Despite several reports on younger occurrences than 2.6 Ma outside the Dutch part of the North Sea for the genus *Barssidinium*, there is consistent evidence from multiple Dutch wells to maintain the magnetostratigraphically calibrated Gauss/Matuyama boundary (Kuhlmann et al., 2006). The dating is verified by the occurrences in the eastern North Atlantic (De Schepper and Head, 2009).
[2] The higher occurrence of *Operculodinium? eirikianum* is reported in ODP 642B at 3.0 Ma (De Schepper et al., 2015, 2017) and in the North Atlantic at 2.6 Ma (De Schepper and Head, 2008, 2009).
[3] The higher occurrence of *Invertocysta lacrymosa* is reported for the North Atlantic at 2.72-2.74 Ma (De Schepper and Head, 2008, 2009) and in the Norwegian Sea at 3.27 Ma (De Schepper et al., 2015, 2017). The former age of the event was followed in Belgium (Louwye and De Schepper, 2010).
[4] For the North Sea area, the LOD of *Melitasphaeridium choanophorum* was indicated at 3.6 Ma (Dybkjaer and Piasecki, 2010; Kuhlmann et al., 2006). The age assessment for the Danish sector of the North Sea is likely too old (De Schepper et al., 2017). In the Norwegian Sea the event is magnetostratigraphically calibrated to 3.27 Ma (De Schepper et al., 2017). In DSDP Site 610 the highest persistence occurrence of this taxon goes up to 3.0 Ma (De Schepper and Head, 2008).
[5] The LOD of *Operculodinium tegillatum* is recorded in the Nordic Seas at ca. 4.6 Ma (De Schepper et al., 2015, 2017) and in the North Atlantic at 3.71 Ma (De Schepper and Head, 2008, 2009). The latter age is followed in the North Sea at 3.71 Ma (Louwye and De Schepper, 2010).
[6]The LOD of *Reticulosphaera actinocoronata* at 4.64 Ma in the Norwegian Sea and at 4.45 Ma in the Iceland Sea corresponds to the well-established North Atlantic, including the North Sea area at 4.4-4.5 Ma (Louwye et al., 2004; Schreck et al., 2012; De Schepper et al., 2015; 2017).

3.3 GDGT concentrations and proxies

Crenarchaeol and brGDGTs are present in all 155 samples analyzed, although brGDGTs IIIb, IIIb′, IIIc, and IIIc′ were below the detection limit in 47 samples. Crenarchaeol and total brGDGT concentrations are normalized to TOC to enable comparison of the abundances of the compounds, regardless of changes in lithology. The concentration of crenarchaeol varies between 0.2–130 μg g^{-1} TOC, and shows a marked decrease starting in the Late Pliocene (190 m; Fig. 4E). The summed concentration of all brGDGTs varies between 1.5–67 μg g^{-1} TOC, and brGDGTs generally occur in higher concentration from the Late Pliocene onwards (<200 m, Fig. 4F), apart from one spike in the record (~300 m). As a result, values for the BIT index are generally low (<0.2) in the Pliocene, apart from two intervals where the values of the BIT index increase to ~0.25–0.5 (386–

376 and 305–300 m; shaded intervals, Fig. 4D). BIT index values then increase to a maximum of 0.98 ± 0.02 for Pleistocene sediments.

4. Discussion

4.1 Provenance of organic matter in the North Sea Sediments

During the Mid-Miocene, sediment supply to the North Sea basin was primarily dominated by the Eridanos river system, which drained the Fennoscandia and the Baltic States (Gibbard and Lewin, 2016). In the late Miocene (Tortonian), the proto Rhine-Meuse river system emerged, which drained the low-lying topography of central Europe (Wong et al., 2007). Due to the close proximity of the Hank site to the proto Rhine-Meuse river system (Fig. 2), it is assumed that the terrestrial OM delivered to this part of the southern North Sea basin is mostly derived from that river system.

The higher $\delta^{13}C_{org}$ values (-22 to -24‰) in the Pliocene section indicate a primarily marine origin of the OM, with a relatively smaller input from terrestrial sources (Tyson, 1995). The trend towards more depleted $\delta^{13}C_{org}$ values of < -26‰ in the Pleistocene suggests that the prevailing source of OM to the sediment changes to a terrestrial origin (i.e. soil and/or higher plant OM; Tyon, 1995) in this interval (<200 m). In addition, OM produced in rivers during transport may also contribute to the sedimentary $\delta^{13}C_{org}$ signal. However, this contribution is hard to identify, as there is no vast difference in $\delta^{13}C_{org}$ values of soil OM vs. river-produced OM (Cloern et al., 2002). Nevertheless, the clear shift in OM provenance from marine to terrestrial occurring at a core depth of ca. 200 m combined with the age model and lithology provides evidence that the Hank site became more deltaic during this time. Furthermore, two distinct shifts in $\delta^{13}C_{org}$ in the Pliocene section of the record represent periods with increased terrestrial OM input. This can be explained by a temporary lowering of the sea level, leading to marine regression, thus rendering the Hank site location closer to shore during these intervals (Fig. 4C, shaded intervals). Higher BIT index values, as

well as increased abundances in terrestrial palynomorphs during both intervals also indicate an increase in terrestrial OM input at this time. Finally, the lithology of the core supports the argument that the Hank site was shallow(er) in these two intervals due to the presence of sandy deposits.

Hence, periods of high BIT/low $\delta^{13}C_{org}$ values indicate that the shore was likely closer to the Hank site, as a result of a lower sea level related to an increase in global ice volume. This is similar to what has been observed for the Last Glacial Maximum in the Bay of Biscay, where high BIT indices were recorded during the sea-level low stand, which placed the paleo-coastline considerably closer to the site (Ménot et al., 2006). Due to the relatively low resolution of the current age model and the difficulties in making a straightforward benthic $\delta^{18}O$ record for shallow, coastal locations, we cannot directly assign the shaded intervals to specific events. From this point, the lower interval (385–375 m) is referred to as the 'Early Pliocene Event', and the upper interval (320–300 m) is referred to as the 'Late Pliocene Event'. Given the absence of indicators to suggest that the Miocene is reached at the base of the succession, the Early Pliocene Event occurs between 5.33–4.4 Ma. The age model also indicates that the Late Pliocene Event occurs between ~3.6–2.7 Ma. The large shift and leveling off of the BIT index and $\delta^{13}C_{org}$ records starting at 200 m likely reflects the onset of the NH glaciations that mark the Pleistocene (~2.6 Ma). The large increase in ice volume on the NH led to significant sea level lowering (Lisiecki and Raymo, 2005), which stranded the Hank site and consequently removed marine influence on the site.

4.2 Identifying sources of brGDGTs in the North Sea Basin

The covarying BIT and $\delta^{13}C_{org}$ records, and the recent findings on the in-situ production of brGDGTs in marine systems indicate the possibility of a mixed terrestrial and marine contribution of brGDGTs to the sediments (Peterse et al., 2009a; De Jonge et al., 2014b; Sinninghe Damsté, 2016). It is likely that the

processes governing the distribution of brGDGTs produced in marine systems differ from those in soils, and that temperatures derived from brGDGTs in marine sediments may not capture the MAT of the surrounding catchment. It is therefore essential to identify the contribution of marine-produced brGDGTs and to correct for their influence on the MAT record.

As a first step in assessing the sources of brGDGTs, the fractional abundances of the North Sea Basin brGDGTs are plotted in a ternary diagram and compared with data from the global soil calibration set (De Jonge et al., 2014a), following the approach of Sinninghe Damsté (2016). This shows that the fractional abundances of the North Sea Basin brGDGTs plot offset from the soils (Fig. 5), suggesting a marine brGDGT contribution to North Sea Basin sediments. However, comparison of these data with brGDGT data from the two coastal marine locations that have been analyzed with the improved chromatography method so far, i.e. Svalbard fjords and the Berau River delta, Indonesia (Sinninghe Damsté, 2016), indicates that the offset from the soil data is relatively small (Fig. 5). In comparison with the Svalbard and Berau sites, for which in situ production of brGDGTs has been suggested to be the predominant source (Peterse et al., 2009a; Sinninghe Damsté, 2016), brGDGTs from the coastal North Sea appear to be mostly soil-derived. When considering the data in more detail, sediments with BIT index values >0.3 plot closer to the soil data than those with BIT index values <0.3 (Fig. 5). Also, the Pliocene sediments with higher BIT index values (Fig. 4, shaded intervals) plot closer to the soil data (Fig. 5). This is in good agreement with our earlier interpretation that higher values of the BIT index and depleted $\delta^{13}C_{org}$ reflect increased input of terrestrial OM, including soil-derived brGDGTs. Nevertheless, it also indicates that in sections with lower BIT index values marine in-situ production is probably modifying the brGDGT distribution.

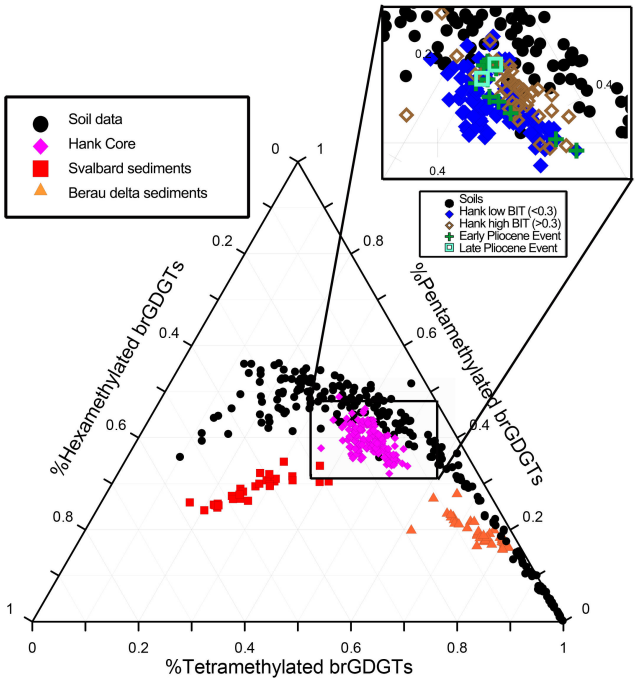

Fig. 5. Ternary diagram of the fractional abundances of the tetramethylated (% tetra), pentamethylated (% penta), and hexamethylated (% hexa) brGDGTs in the Hank core (magenta diamonds), the global soil calibration dataset (black circles), Svalbard fjord sediments (red squares), and the Berau Delta (orange triangles). The inset shows the Hank data separated into BIT index values>0.3 (brown open diamonds) and BIT index values<0.3 (dark blue closed diamonds) for comparison to the soil dataset. The two Pliocene events are indicated by green crosses (Early Pliocene event) and light blue open squares (Late Pliocene event).

To further elucidate trends in the downcore variations in brGDGT concentration and distribution, principal component analysis (PCA) was performed on the fractional abundances of the brGDGTs. Principal component PC1 described 54% of the variance in the dataset, whereas PC2 describes 15% (Fig. 6). The acyclic 5-methyl brGDGTs Ia, IIa, and IIIa all score negatively on PC1, whereas all cyclic brGDGTs score positively (Fig. 6). This indicates a distinct relationship between PC1 and the brGDGTs with cyclopentane moieties. Indeed, when the $\#rings_{tetra}$ is compared to the PC1 scores, a strong positive correlation is observed ($r^2 = 0.75$).

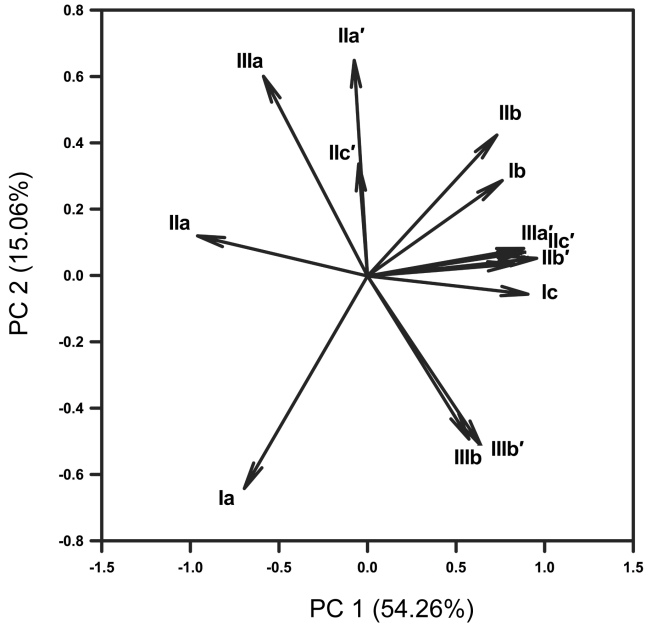

Fig. 6. PCA analysis based on fractional abundances of all 15 brGDGTs of the Hank core sediments. Species scores of the 15 brGDGTs on the first two PCs. Roman numerals refer to the structures from Fig. 1.

The $\#rings_{tetra}$ has been found to vary from 0–0.7 in soils from the global soil calibration set (De Jonge et al., 2014a), but exceeds these values in coastal marine sediments with considerable in situ brGDGT production, likely because the pore waters of marine sediments are alkaline (Peterse et al., 2009a; Sinninghe Damsté, 2016), and brGDGT production at higher pH tends to result in the production of higher relative amounts of cyclopentane-containing brGDGTs (Weijers et al., 2007a; Peterse et al., 2012). A contribution of marine in-situ produced brGDGTs to marine sediments in coast-shelf transects from the Berau Delta, East China Sea shelf system, and the Iberian margin was clearly reflected by zones where $\#rings_{tetra}$ >0.7, which was consequently proposed as an indicator value for coastal marine sediments that possess a primarily non-soil source input (Sinninghe Damsté, 2016). In the North Sea basin sediments, the $\#rings_{tetra}$ ranges from 0.20–0.59 (Fig. 7B). Although these values are within the range for soils in

the global calibration set, soils with #rings$_{tetra}$ >0.4 are mostly alkaline soils (pH >7), often occurring in arid deserts (De Jonge et al., 2014a). The majority of the soils in the catchment area of the Hank site are unlikely to be alkaline in nature (Reuter et al., 2008), and the average soil pH value for soils in North Western Europe is 6.5 (global soil dataset, excluding Sweden, Ireland, Norway, and Scotland, De Jonge et al., 2014a). Thus, the fact that #rings$_{tetra}$ exceeds 0.4 for parts of the record more likely implies that the brGDGT distribution in these intervals has a marine overprint. However, as the Hank #rings$_{tetra}$ record is consistently <0.7, a substantial proportion of brGDGTs is soil-derived, particularly for the Pleistocene sediments (average #rings$_{tetra}$ ~0.3; Fig. 7B). Furthermore, #rings$_{tetra}$ generally increases with depth, where higher values particularly in the Pliocene sediments suggest that there may be a contribution of marine produced brGDGTs (Fig. 7B).

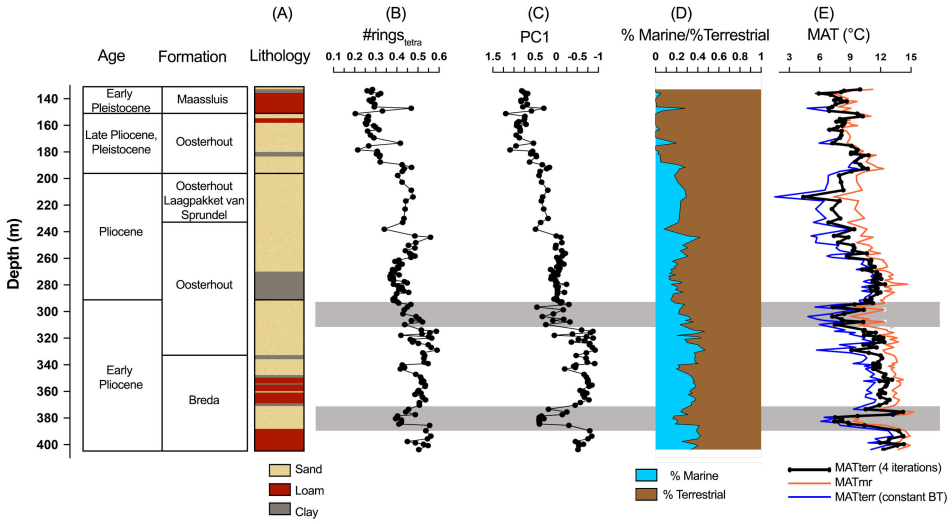

Fig. 7. Depth, age, and formation of the Hank sediments plotted with brGDGT proxies. (A) Lithology, (B) #rings$_{tetra}$, (C) PC1, (D) % Marine/% Terrestrial, and (E) MAT records (orange line for the MAT$_{mr}$ record, dark blue line for the MAT$_{terrestrial}$ calculated with constant bottom water temperature, and solid black line with circle symbols for the MAT$_{terrestrial}$ using the iteration method) of the Hank sediments are plotted against depth. The two shaded bars represent Pliocene events discussed in the text.

It is apparent that the PC1 varies in concert with $\#rings_{tetra}$ over depth, and they both follow the patterns of the BIT index and $\delta^{13}C_{org}$ records: all Pleistocene samples scoring positively on PC1, and the majority of Pliocene samples scoring negatively (Fig. 7B,C). Indeed, in a cross plot of BIT index vs. $\#rings_{tetra}$ (r^2 = 0.68; Fig. 8), the depths with high BIT index (>0.9) occurring in the Pleistocene have $\#rings_{tetra}$ between ~0.25–0.3, typical values for acidic soils. Furthermore, the two intervals with increased terrestrial input recognized in the BIT index and $\delta^{13}C_{org}$ records (Fig. 4C, D) have positive values on PC1. The covariance of the BIT index, $\delta^{13}C_{org}$, $\#rings_{tetra}$ and PC1 records indicates that the variation in marine and terrestrial brGDGT contribution to the North Sea sediments is the dominant factor determining the variance in the dataset. This suggests that in the Hank sediments, a more negative score on PC1 and a higher $\#rings_{tetra}$ can be used as indicators of marine in situ brGDGT production.

Consequently, we applied the $\#rings_{tetra}$ record to disentangle the marine and terrestrial sources of the brGDGTs in the North Sea basin using two end-member modeling. A soil end-member value of $\#rings_{tetra}$ = 0.29 was chosen based on the $\#rings_{tetra}$ for the sediments with highest soil input (BIT index >0.9) under the assumption that pH of the soils in the hinterland did not change substantially over the period studied. The samples chosen for the soil end-member (n = 23) all occur in the late Pliocene/early Pleistocene interval of the core, during which mean annual precipitation (MAP, a controlling factor for soil pH) in the Lower Rhine Basin did not change significantly (1000 mm/year ±100; Mosbrugger et al., 2005). The marine end-member was set at 0.93, based on the $\#rings_{tetra}$ in the marine sediments from Svalbard, where the brGDGT distribution represents almost exclusively marine in-situ production (Peterse et al., 2009a; Sinninghe Damsté, 2016). Using these end-members, the $\#rings_{tetra}$ record was translated into a record indicating the relative contributions of soil vs. marine brGDGTs (Fig. 7D). This record indicates on average ~35% marine contribution during the Pliocene, and ~0-27% during the Pleistocene. The two Pliocene

intervals with presumed lower sea level and increased terrestrial input (shaded intervals, Figs. 4 and 7) are also characterized by a lower contribution of marine brGDGTs ($\Delta_{terrestrial\text{-}marine} \sim 20\%$).

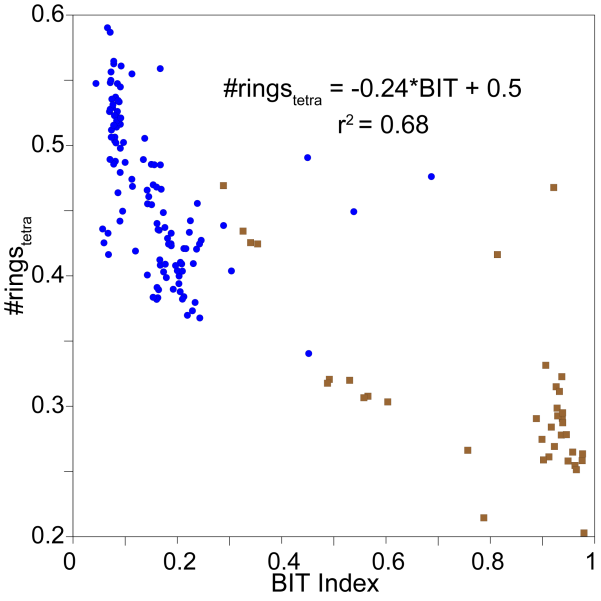

Fig. 8. $\#Rings_{tetra}$ values for Hank sediments plotted against corresponding BIT index values, with linear fit equation and coefficient of determination (r^2) shown. Samples plotted as blue circles occur at sediment core depths >200 m and samples plotted in brown squares occur at core depths <200 m.

4.3 BrGDGT-based MAT reconstruction

Application of the latest soil transfer function of De Jonge et al. (2014a) to brGDGTs in the Hank core generates a record of MAT_{mr} reflecting a temperature range of 7–15 °C (Fig. 7E, orange line). Overall, MATs decrease steadily towards the Pleistocene, with additional notable cooler periods (ΔT = 3–5 °C) corresponding with the Early and Late Pliocene events discussed earlier (shaded intervals; Fig. 7E). The period directly after the Late Pliocene event represents a warm period, which is connected with a thick clay interval in the lithology (300–280 m; Fig. 4A), pointing to a relatively higher sea level.

However, this MAT reconstruction is only valid if the brGDGTs are predominantly derived from soil, whereas the values of $\#rings_{tetra}$ indicate that brGDGT sources to the North Sea basin vary throughout the record. Hence, to obtain the 'true' terrestrial MAT (MAT_{terr}) signal, the marine contribution to the brGDGT distribution must be removed from the MAT record. This can be achieved with the use of two transfer functions: one for soils, for which the recent MBT′5Me – MAT global soil calibration data set will be used (De Jonge et al., 2014a), and a second, new function reflecting in-situ production in coastal marine sediments. The MBT′5Me index for the Hank sediments represents a mix of the marine ($MBT'5Me_{marine}$) and terrestrial ($MBT'5Me_{terrestrial}$) inputs. Consequently, the MAT_{terr} record can be obtained by subtracting the marine contribution to the 'mixed' MBT′5Me values.

The first step for this procedure is to create the function needed to transfer coastal marine brGDGT distributions to marine water temperatures, similar to the transfer function for the global soil calibration set of De Jonge et al. (2014a). In situ water temperatures are used instead of air temperatures, due to the fact that the temperature response of brGDGTs produced in the marine environment is more likely to record in situ water temperature rather than air temperature. So far, 'novel' brGDGT data (i.e. including the separate integration of 5- and 6-methyl brGDGT isomers) is only available for two coastal marine sites, i.e. Svalbard (Peterse et al., 2009a) and the Berau delta (Sinninghe Damsté, 2016). Based upon the low BIT index values (<0.1) and high values of $\#rings_{tetra}$ (>0.7), these authors concluded that the brGDGT distribution at these two sites is predominantly composed of in situ produced brGDGTs (Peterse et al., 2009a; Sinninghe Damsté, 2016).

Although the number of global sites is limited, they conveniently represent a polar and tropical environment, stretching the reach of the temperature range, thus preventing extrapolation of the regression line. In addition, available brGDGT data from one surface sediment located in the Tagus drainage basin off

the coast of Portugal was added (Warden et al., 2016). We supplemented this mid-latitude datapoint with surface sediments from the Portuguese margin (Zell et al., 2015), of which those characterized by a low BIT index (<0.1) and a high value of $\#rings_{tetra}$ (>0.7) were reanalyzed using the new chromatography method (Hopmans et al., 2016).

In order to formulate the regression model, MBT′5Me values from the Berau delta (n = 11), Svalbard (n = 28), Portuguese margin (n = 9) sites were plotted against in situ bottom water temperatures at the respective sites, reflecting the depth at which the surface sediments were obtained. It is therefore assumed that the MBT′5Me value represented by these three sites represents a 100% marine signal of brGDGT production. We use bottom water temperatures from ca. 40–90 m for the shallow Berau delta, 200–300 m for Svalbard, and 300–1000 m for the samples from the Portuguese margin (Peterse et al., 2009a; Zell et al., 2015; Sinninghe Damsté, 2016).

The resulting linear regression fit produced the following coastal marine transfer function (Fig. 9):

$$BWT = 59.5 * MBT'5Me_{marine} - 23.7 \qquad (R^2 = 0.95) \qquad (5)$$

Where BWT is the bottom water temperature. The marine transfer function possesses a slightly steeper slope than the soil calibration line (Fig. 9). This translates into larger changes in the high (MBT′5Me >0.7) and low (MBT′5Me <0.4) ends of the calibration compared to the soil calibration line.

Subsequently, the MBT′5Me index can be corrected for the contribution of marine brGDGTs by separating the terrestrial and marine contributions to the total brGDGT pool:

$$MBT'5Me_{total} = \%terrestrial\ brGDGTs * MBT'5Me_{terrestrial} + \%marine\ brGDGTs * MBT'5Me_{marine} \qquad (6)$$

Where $MBT'5Me_{marine}$ is described by Eq. 5, $MBT'5Me_{total}$ is the index measured on the sediment samples, and the %marine and %terrestrial brGDGTs are

calculated as described in Section 4.2. To estimate MBT′5Me$_{marine}$, a BWT must be chosen that reflects the bottom water temperature of the North Sea in the Pliocene. The current average BWT (11.5 °C) of the North Sea at 30 m depth is determined by the winter minimum of 6–7 °C and the summer maximum of 16–17 °C (Johnson et al., 2009; Boyer et al., 2013). During the Pliocene, ostracod assemblages in the Coralline Crag Formation in England, with an estimated paleodepth of greater than 50 m, suggest winter minimum and summer maximum seafloor temperatures of 11 and 18 °C, respectively (Hodgson and Funnel, 1987; Johnson et al., 2009). Using the average of the summer and winter Pliocene temperatures proposed by Johnson et al. (2009), we estimate the Pliocene BWT for the North Sea as 14.5 °C, i.e. ~3 °C higher than present. The use of a constant BWT results in a constant MBT′5Me$_{marine}$ value (0.64) that is used in Eq. 6 to correct MBT′5Me$_{total}$. The measured MBT′5Me$_{total}$ and constant MBT′5Me$_{marine}$ values are then combined with the %Terrestrial/%Marine ratios to determine MBT′5Me$_{terrestrial}$. The corrected temperature record is obtained by applying the soil transfer function for MAT and MBT′5Me, as described by De Jonge et al. (2014a; Fig. 7E, blue line):

$$MAT_{terr} = 31.5 * MBT'5Me_{terrestrial} - 8.6 \qquad (R^2 = 0.66) \qquad (7)$$

This calculation does not take into account the fact that the BWT is likely to change over time as a response to regional climate changes. As it is quite likely that the BWT of the coastal North Sea did change over the course of the Pliocene and the Pleistocene, we used the MAT$_{terr}$ record generated to predict BWT in a series of iterations. The present day difference in temperature between the annual mean temperature of the bottom water of the North Sea (~11.5 °C) and the MAT of the Netherlands (~10 °C) was calculated (ΔT = 1.5 °C; van Engelen et al., 2001; Boyer et al., 2013) and this ΔT was assumed to also hold for the Pliocene and the Pleistocene. This allows calculating BWT from MAT$_{terr}$ and feed newly calculated BWTs for each individual sediment horizon back into the calculation. Starting with a constant bottom water temperature of 14.5 °C a series of four

iterations were performed after which the calculated MAT_{terr} for each individual sediment horizon did not change substantially (<0.6 °C) from its predecessor value. The corrected MAT_{terr} record (Fig. 7E, solid black line with circle symbols) varies between 4 and 14 °C, showing a distinctly lower range of temperatures (ΔT = 10 °C) than the MAT_{terr} record using a constant BWT value (ΔT = 12 °C; Fig. 7E). In both records the general cooling trend from older to younger sediments is evident.

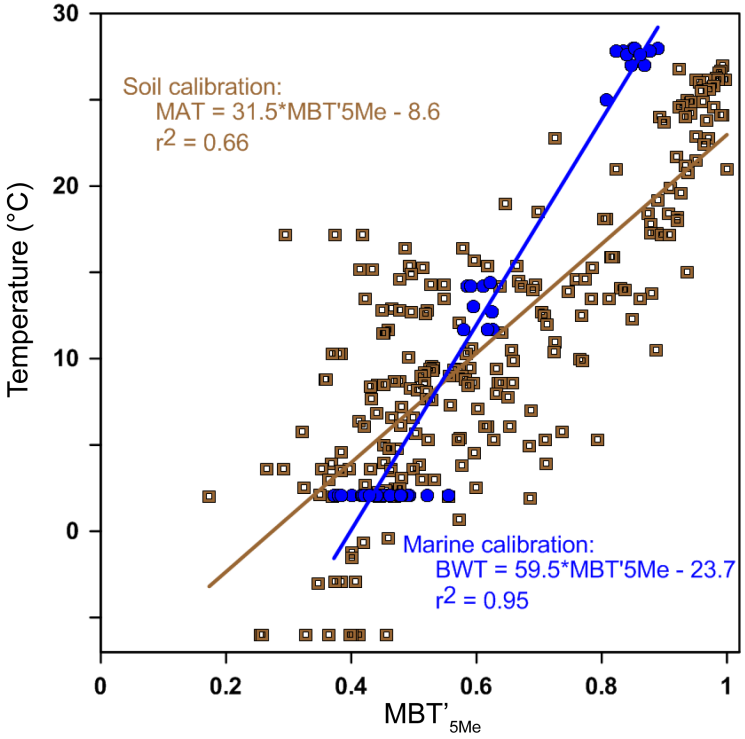

Fig. 9. Cross plot and regression lines for the MBT´5Me value versus measured MAT for the soil calibration data set (open brown squares) and versus BWT for the Svalbard (Peterse et al., 2009a), Berau Delta (Sinninghe Damsté, 2016), and Portuguese margin sediments (reanalyzed from Zell et al., 2015; Warden et al 2016; blue circles).

A number of assumptions are made to arrive at the final MAT_{terr}, some of which cannot be fully explored regarding the error they propagate through to the estimation of temperature. These include the assumptions i) that all terrestrial OM

is derived from the Rhine-Meuse river system, and ii) that the MBT′5Me value of the three reference sites (Svalbard, Berau delta, and Portuguese margin) represents a 100% marine signal. Assumption i) would require a detailed study of the OM composition in the different river catchments that discharge into the North Sea Basin during the Pliocene, which is beyond the scope of this paper, and assumption ii) cannot be confirmed as long as the exact producer(s) of brGDGTs remain(s) unknown. The most important assumptions that can be addressed with regards to the error on reconstructed temperatures are iii) estimating the Pliocene BWT of the North Sea, and iv) the temperature difference between the continental and bottom water temperatures in the North Sea, ΔT. We explore the error in our estimate of Pliocene BWT by also carrying out the correction steps outlined above for a cooler (11.5 °C) and warmer (17.5 °C) BWT, which results in maximum deviations of -1.3 °C and 1.5 °C respectively. Secondly, we explore the error associated with slightly different values for ΔT by re-doing the iteration for a smaller (0.5 °C) and larger ΔT (3 °C). The errors associated with different ΔT maximize at -0.46 °C for a larger ΔT and 0.31 °C for a smaller ΔT. Taking all the errors associated with correcting the MAT record into account, shows that they fall well within the calibration error of the brGDGT temperature proxy (4.6 °C; De Jonge et al., 2014a). This calibration error reflects a systematic error most likely affecting calculated absolute temperatures in a similar way. Note that the timing, as well as the direction of the changes in the temperature record are not influenced by the assumptions made, and can thus be considered reliable.

4.4 Pliocene air temperature evolution in NW Europe

Our final, corrected continental temperature record (MAT_{terr}) retains the original pattern of the MAT_{mr} record, with higher temperatures in the Pliocene and a gradual cooling that is initiated in the Late Pliocene and carries on into the Early Pleistocene (Fig. 7E). This gradual cooling trend is in strong agreement with existing global climate records, for example the global benthic oxygen isotope

stack (Lisiecki and Raymo, 2005). Hence, despite the large number of assumptions made in the correction of the temperature record, the method proposed here leads to encouraging results.

The MAT_{terr} record indicates that MAT was ~ 12–14 °C during the Early Pliocene (Fig. 7E), which matches well with the brGDGT-derived temperatures of 14 °C reported for South-eastern Netherlands during the same period (Donders et al., 2009; using the calibration of Weijers et al., 2007a). The temperatures also match those recorded in Central Europe, using an approach based on the occurrence of seeds, fruits, and leaf remnants in continental sedimentary records (13 °C; Mosbrugger et al., 2005).

The two colder (Δ 5–7 °C) periods in the Pliocene interval present in the initial MAT_{mr} record are retained in the MAT_{terr} record (shaded intervals, Fig. 7E). These two periods occur simultaneously with the Early Pliocene event and Late Pliocene event (shaded intervals, Fig. 4), which were associated with a lower sea level. Given this synchroneity, the timing of the Early and Late Pliocene events fit the framework for Pliocene glaciations composed by De Schepper et al. (2014). The authors identified a Pliocene glacial at 4 Ma (Fronval and Jansen, 1996; St John and Krissek, 2002; De Schepper et al., 2014), which could correspond with the occurrence of the Early Pliocene event in our record. Our multi-proxy records thus support the existence of (a) glaciation(s) during the early Pliocene (De Schepper et al., 2014), and provide the first evidence that the influence of the early Pliocene glaciations on the Northern Hemisphere reached into the North-western European continent.

Furthermore, we also tentatively link the Late Pliocene event with either the Pliocene glacial at 3.6 Ma (De Schepper et al., 2014), or the well-documented M2 glacial (Lisiecki and Raymo, 2005; Mudelsee and Raymo, 2005; Naish and Wilson; 2009). The depth and age of the Late Pliocene event indicates a substantial cool event lasting significantly longer than the M2 event (3312–3264 ka), such that this glacial might be combination of two or more glacials in this

record (possibly the 3.6 Ma glacial and the M2; De Schepper et al., 2014). The amplitude of the cooling of the late Pliocene glacial(s) (ΔT ~4 °C) is comparable to that of ~3–6 °C for the M2 glaciation recorded by alkenone- and Mg/Ca-derived SSTs at DSDP site 610 and IODP site U1308 in the North Atlantic (De Schepper et al., 2013), as well as with that reflected by pollen assemblages from Lake Elgygytgyn in NE Russia (Brigham-Grette et al., 2013). Alkenone SST records of the M2 glaciation in a tropical SST stack show lower amplitudes of 2.5 °C (Herbert et al., 2010), so the MAT_{terr} record at this North Western European location also supports the interpretation of a greater latitudinal temperature gradient during the Pliocene.

We speculate that the mPWP is represented by the interval of 295–263 m, and occurs directly after the Late Pliocene Glacial. The interval associated with the mPWP is characterized by sustained elevated MATs (10.5–12.0 °C; Fig. 7E). When absolute temperatures are compared with the present MAT in NW Europe (~9.5 °C), they largely match the global mPWP temperature estimates of 2–3 °C warmer than the present day determined by the PRISM group (Dowsett et al., 2012). The warmer climate is also reflected in the BIT index, $\delta^{13}C_{org}$, and lithology records, which indicate a larger marine influence at the study location. MATs are furthermore comparable with MPWP temperature estimates based on pollen spectra from the Lower Rhine Basin (14.1 ± 0.2 °C, 3.6–2.6 Ma; Utescher et al., 2000), Germany (13.9 ± 0.5 °C, 3.2–2.6 Ma; Uhl et al., 2007), and south-east England (12.8 ± 1.3 °C, 3–2.6 Ma; Head, 1998). The HadAM3 GCM model for the mid-Pliocene (Pope et al., 2000; Haywood et al., 2002) produces a temperature estimate of 13.8 ± 0.4 °C for the region of west Germany (Salzmann et al., 2008), which is slightly higher than reflected by the brGDGTs at Hank. All current paleodata (including the Hank MAT_{terr} record) suggest that the climate in Northwestern Europe was approximately 2–6 °C warmer than present in the Pliocene.

Following the Plio-Pleistocene transition, MATs decrease, coinciding with an increase in BIT index values and depletion in $\delta^{13}C_{org}$. The high amplitude temperature variations (ΔT = 5 °C) indicate the onset of the glacial-interglacial cycles of the Pleistocene (Raymo et al., 2006). Temperatures in this section of the record (6–11 °C) lie in the median between the reconstructed pollen-based mean temperature of coldest and warmest month (MTC and MTW) estimates for the Netherlands during the Tiglian (~0 and ~18 °C, respectively; Zagwijn, 1963; Pross and Klotz, 2001).

5. Conclusions

Bulk OM and brGDGT data in a sediment core from the North Sea basin indicates that the average number of cyclopentane rings ($\#rings_{tetra}$) can be used to identify and disentangle the provenance of brGDGTs in coastal marine sediments. Subsequent use of a newly developed coastal marine brGDGT temperature calibration and end member modeling can improve the reliability of brGDGT-based MAT reconstructions by correcting for marine contributions to the brGDGT pool in these settings. Applying these correction steps to the Pliocene section of the sediment core leads to a continental record (MAT_{terr}) of Pliocene temperature evolution in North Western Europe. The MAT_{terr} record indicates that NW Europe was approximately 1–2 °C warmer than present during the mPWP. Furthermore, the influence of two early Pliocene glaciations could be identified. The occurrence of these early Pliocene glaciations is supported by a simultaneous increase in BIT index value and a decrease (2–3‰) in $\delta^{13}C_{org}$ values, likely caused by sea level lowering due to waxing ice sheets on the NH. The good fit of our corrected MAT_{terr} record with existing global climate records indicates the promise of our method to resolve the influence of mixed brGDGT sources in coastal marine sediments on continental MAT reconstruction. Before the correction method can be widely applied, additional brGDGT data from coastal shelf environments is needed to strengthen the coastal marine brGDGT

temperature calibration. This is currently hampered by to the limited number of studies that measure the 5- and 6- methyl brGDGTs separately in these specific settings.

Acknowledgements

We like to thank Dr. Stijn De Schepper and an anonymous reviewer for their comments, which greatly helped to improve this manuscript. The authors thank Natasja Welters and Arnold van Dijk for assistance with TOC and $\delta^{13}C_{org}$ analyses, and Denise Dorhout for re-analysis of the Portuguese margin samples. The work was supported by funding from the Netherlands Earth System Science Center (NESSC) through a gravitation grant (NWO 024.002.001) from the Dutch Ministry for Education, Culture and Science to JSSD. NWO grant #834.11.006 enabled the purchase of the UHPLC-MS system used for GDGT analyses.

Chapter 5

A new age model for the Pliocene of the Southern North Sea Basin: evidence for asynchronous shifts of marine and terrestrial climate

Emily Dearing Crampton-Flood, Lars Noorbergen, Damian Smits, R. Christine Boschman, Timme H. Donders, Dirk K. Munsterman, Johan ten Veen, Francien Peterse, Luc Lourens, Jaap S. Sinninghe Damsté.

Under review at *Climate of the Past Discussions*.

Abstract

The mid-Pliocene Warm Period (mPWP, 3254–3025 ka) represents the most recent interval in Earth's history where atmospheric CO_2 levels were similar to today. The reconstruction of sea surface temperatures (SSTs) and modeling studies have shown that global temperatures were 2–4 °C warmer than present. However, detailed reconstructions of marginal seas and/or coastal zones that enable linking climate evolution in the marine realm to that on the continents are lacking. This is due in part to the absence of precise age models for coastal zones, as they are generally dynamic systems with varying sediment and fresh water inputs. Here, we present a multi-proxy record of Pliocene climate change in the coastal Southern North Sea Basin (SNSB) based on the sedimentary record from the Hank borehole, the Netherlands. The marginal marine setting of the Hank borehole during the late Pliocene provides an excellent opportunity to correlate marine and terrestrial signals, due to continental sediment input mainly from the proto-Rhine-Meuse river. We improve the existing low-resolution palynology-based age model for the Hank borehole using oxygen stable isotope measurements ($\delta^{18}O$) of the endobenthic foraminiferal species *Cassidulina laevigata*, integrated with biochrono- and seismostratigraphy. Identification of hiatuses and freshwater effects in the record allows us to accurately isolate glacial-interglacial climate signals that can be linked to a reference global benthic $\delta^{18}O$ stack. In tandem with the biostratigraphic age control this results in an age framework for the SNSB for the Late Pliocene (~3200–2800 ka). Our multi-proxy reconstruction for the mPWP shows a strong agreement between lipid biomarker and palynology-based terrestrial temperature proxies, which suggest a stable climate, 1–2 °C warmer than present. In the marine realm, however, biomarker-based SSTs show a large range of variation (10 °C). Nevertheless, the fluctuation is comparable to other SST records from the North Atlantic and Nordic Seas, suggesting that a common factor, most likely variations in the North Atlantic Current, exerted a strong influence over SSTs in the North Atlantic at this time.

1. Introduction

The Pliocene epoch (5.33–2.6 Ma) is a frequently targeted interval for palaeoenvironmental reconstructions because it is considered an analogue for future climate change. For example, atmospheric CO_2 concentrations (380–420 ppmv; Seki et al., 2010; Zhang et al., 2013) and continental configurations during the Pliocene were largely similar to present. Detailed proxy and model comparisons for the so-called mid-Piacenzian Warm Period (mPWP, 3254–3025 ka) have been the focus of the Pliocene Research, Interpretation and Synoptic Mapping (PRISM) group (Dowsett et al., 2010, 2013), and reveal that global temperatures were on average 2–4 °C warmer than present (Haywood et al., 2013). This makes the mPWP an excellent interval to investigate a warmer world associated with the scenarios for the (near) future summarized by the Intergovernmental Panel on Climate Change (IPCC, 2014).

Our understanding of Pliocene climate is largely based on sea surface temperature (SST) reconstructions (e.g. Dowsett et al., 2012), which indicate that global SSTs were 2–6 °C warmer than present. Only a few temperature records exist for the terrestrial realm (Zagwijn, 1992; Salzmann et al., 2013), which also indicate climate was warmer than present, however, these temperatures are less well constrained. There are even fewer studies that examine the phase relations and amplitude of variability in coupled land-sea changes (e.g. Kuhlmann et al., 2006), although this information is of key interest for understanding heat transport and the hydrological cycle during the Pliocene. Sediments on continental shelves receive inputs from both the terrestrial and marine environment, and could thus contain an archive of land-sea climate evolution. The North Sea Basin shelf is a site that potentially hosts a combined record of SST evolution and climate change in the North Western (NW) European continent during the Pliocene due to input of terrestrial material by large European rivers and the active subsidence that provides sediment accumulation space (Gibbard, 1988). Moreover, significant warming of its waters since the

second half of the 20th century (0.6 °C rise on average in the period 1962–2001; Perry et al., 2005) indicates the sensitivity of the area for recording climate change. The region has been a type area for Pliocene and early Pleistocene terrestrial stages (see overview in Zagwijn, 1992), but most studied sections lack absolute dating and land-sea correlation as they target deltaic deposits (Donders et al., 2007; Kemna and Westerhoff, 2007). However, the shallow marine deposits of the Southern North Sea Basin (SNSB) allow better chronostratigraphy building through integrated paleomagnetic, isotope, and biostratigraphic approaches (e.g. Kuhlmann et al., 2006; Noorbergen et al., 2015; Donders et al., 2018).

Despite the promising preconditions that should enable Pliocene climate reconstruction using the sedimentary archive of the SNSB, the generation of an independently calibrated age model for coastal zone sediments is often complicated by complex interactions between sea level, sediment supply, and biotic factors (e.g. Krantz, 1991; Jacobs, 2008; Noorbergen et al., 2015; Donders et al., 2018), which may alter sedimentation rates or cause hiatuses resulting from periods with erosion or non-deposition. Indeed, the Pliocene SNSB was a dynamic system in which multiple westward advances of the Eridanos and Rhine-Meuse Rivers generated clinoform successions (Jansen et al., 2004; Kuhlmann and Wong, 2008; Harding, 2015), and the sedimentary record thus needs to be critically evaluated on its stratigraphic continuity before it can be compared with records from adjacent areas, such as the Nordic Seas and the North Atlantic. Munsterman (2016) reported a Pliocene-age sequence of coastal marine sediments from Hank, located in the South West of the Netherlands. The current age framework for the sequence is based on first (FODs) and last occurrence dates (LODs) of dinoflagellate cysts (Dearing Crampton-Flood et al., 2018). Due to the lack of an independent age constraint in the SNSB, FODs and LODs were inferred from those in the Nordic Seas and the North Atlantic, introducing an unknown range of age uncertainty to the biostratigraphic age model (Dearing

Crampton-Flood et al., 2018). Furthermore, the resolution of the age model is too low (9 biostratigraphic age tie points for the period ~ 4.5–2.5 Myr) to identify possible hiatuses or changes in deposition, preventing comparison of the record to other archives from the Northern Hemisphere.

The established method for age model construction involves measuring the stable oxygen isotope content ($\delta^{18}O$) of foraminiferal tests and matching the variability to a global benthic $\delta^{18}O$ reference stack, such as LR04 (Lisiecki and Raymo, 2005). However, in more coastal settings this method is complicated due to isotopically lighter fresh water input, which alters the $\delta^{18}O$ value of the foraminfera tests (Delaygue et al., 2001; Lubinski et al., 2001). Recently, Noorbergen et al. (2015) were successful in creating a tuned age model for the early Quaternary shallow marine interval of borehole Noordwijk, also located in the SNSB, using the $\delta^{18}O$ values of endobenthic foraminifera (*Bulimina aculeata*, *Cassidulina laevigata*, and *Elphidiella hannai*). The depth habitat of endobenthic foraminifera in the sediment shelters these species from disturbances, such as reworking by bottom currents and freshwater input. Although vital and microhabitat effects still influenced the absolute $\delta^{18}O$ values of these foraminifera and caused an offset towards more positive values, the trends in $\delta^{18}O$ at Noordwijk clearly resembled those of LR04 (Lisiecki and Raymo, 2005; Noorbergen et al., 2015).

In this study, we follow the approach of Noorbergen et al. (2015) and use $\delta^{18}O$ values of the endobenthic foraminifera *Cassidulina laevigata* in the Hank borehole to improve the current low-resolution biostratigraphic age model for the Pliocene SNSB of Dearing Crampton-Flood et al. (2018). Reconstruction of the age model is further supported by the identification of hiatuses based on seismic information and gamma ray logging. Subsequently, we complement the existing terrestrial air temperature record for Pliocene NW Europe based on soil bacterial membrane lipid distributions stored in the Hank sediments (Dearing Crampton-Flood et al., 2018), with multi-proxy records of SST, relative land cover, and

terrestrial input based on lipid biomarker proxies, pollen, and dinoflagellate cysts. This enables us to directly compare marine and terrestrial climate evolution of the SNSB and continental NW Europe during the mid-Piacenzian Warm Period for the first time.

2. Methods

2.1 Geological setting and study site

The Pliocene North Sea was confined by several landmasses, except towards the North, where it opened into the Atlantic (Ziegler, 1990). At times, there may have also been a connection via the English Channel to the North Atlantic (Funnel, 1996). In addition to a main marine water supply via the North Atlantic, the Eridanos River, draining the Fennoscandian shield, and the Rhine-Meuse River, draining North Western Europe delivered freshwater to the North Sea (Fig. 1). The proto-Rhine-Meuse river system existed for a large part of the Pliocene, although it did not drain the Alps until the latest Pliocene (Boenigk, 2002). During the Pliocene, the sediment supply by the Eridanos River system to the southern area of the SNSB was limited, such that the Rhine-Meuse river system was the predominant source of sediments in the Roer Valley Rift system (Westerhoff, 2009). The water depth of the North Sea during the Pliocene and the Pleistocene was approximately 100–300 m in the central part of the basin (Donders et al., 2018).

The study site (51°43′N, 4°55′E) is located within the current Rhine-Meuse-Scheldt delta in the municipality of Hank, the Netherlands. The Hank site is located within the Roer Valley Rift: a region that experienced relatively high tectonic subsidence during the late Cenozoic (Van Balen et al., 2000). The current drainage area of the Rhine-Meuse-Scheldt river system is 221,000 km^2, however it was likely smaller in the Pliocene (van den Brink et al., 1993; Boenigk, 2002). Air-lifting well technology was used to drill the Hank borehole (B44E0146) to a

base of 404 m in 2001. Intervals were drilled every 1 m, such that each sample taken from the meter intervals is an integrated mixture. One advantage of this drilling technique is that it leads to smoothed records. The gamma ray log of the borehole is readily accessible from an online database (dinoloket.nl). In addition, a seismic section is available and covers an east-west transect of the River Meuse (Maas2002 survey, nlog.nl). The lithology of the Hank borehole (Fig. 2a) is described by the Geological Survey of the Netherlands (TNO) and Dearing Crampton-Flood et al. (2018). In short, the base of the succession corresponds to the upper part of the shallow marine Breda Formation, followed by the sandy, occasionally silty and clay-rich marine delta front deposits sometimes containing shell fragments, or so-called 'crags', belonging to the Oosterhout Formation. The overlying Maassluis Formation contains silty shell-bearing deltaic to estuarine deposits. For this study, the interval 404–136 m was considered, covering ~4.5 to ~2.5 Myr based on the biostratigraphic age model of Dearing Crampton-Flood et al. (2018).

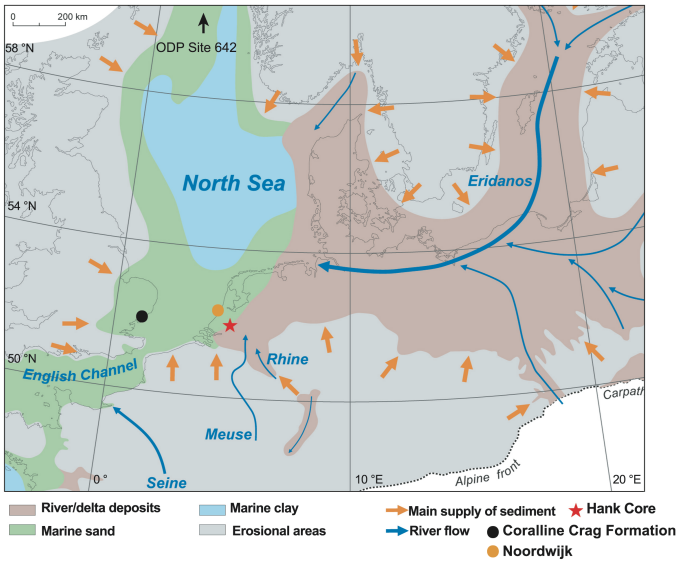

Fig. 1. Pliocene paleogeography in the North Sea basin (Gibbard and Lewin, 2003; Knox et al., 2010). The location of the Hank borehole is denoted by a red star. Major river and sediment inputs are represented by blue and orange arrows, respectively. Other locations mentioned in the text are indicated. Figure modified from Gibbard and Lewin (2016).

2.2 Stable isotopes

Sediment samples (n = 269) from the interval between 404 and 136 m were washed and passed over a series of sieves, after which the >125 µm and >63 µm fractions were collected and dried at 40 °C. Well preserved foraminifera of the endobenthic species *Cassidulina laevigata* (i.e. shiny tests) of around the same size were picked from the >125 µm fraction. Due to the scarcity of foraminifera in some samples, tests were left uncrushed in order to conserve enough material for isotope analysis. The foraminifera were washed ultrasonically in water before weighing, and between 10 and 60 µg of intact tests were weighed per sample. The $\delta^{18}O$ and $\delta^{13}C$ values were measured on a Thermo Gas Bench II (Thermofisher Scientific) connected to a Delta V mass spectrometer. An in-house NAXOS standard and an internationally accepted NBS-19 standard ($\delta^{18}O$ = -2.20‰, $\delta^{13}C$ = 1.95‰) were used to calibrate measured isotope ratios to the Vienna Pee Dee Belemnite (VPDB) standard. Oxygen isotope ratios were calculated according to the following equation (replacing $\delta^{18}O$ by $\delta^{13}C$ for the calculation of carbon isotope ratios):

$$\delta^{18}O = \frac{\delta^{18}O_{\,s} - \delta^{18}O_{\,standard}}{\delta^{18}O_{\,standard}} * 1000‰ \qquad (1)$$

Where:

- $\delta^{18}O$ resembled the eventual data (in ‰) used for comparison with the benthic oxygen isotope stack (Lisiecki and Raymo; 2005).
- $\delta^{18}O_s$ was the isotope value of the sample measured by the mass spectrometer.
- $\delta^{18}O_{standard}$ was the isotope value measured on the standard.

Outliers were identified when measurements exceeded the range of the upper and lower boundaries of the standard deviation added to and subtracted from a 7 point moving average of the isotope record. Since the isotope analysis is coupled, the corresponding value of $\delta^{18}O$ or $\delta^{13}C$ was removed if either value was identified as an outlier.

2.3 Palynology

Organic-walled dinoflagellates that form a cyst during their life cycle are referred to as dinocysts, and they are preserved in sediments (Head, 1996). Dinocyst assemblages in marine sediments are linked to infer environmental parameters such as temperature and productivity in surface waters (Rochon et al., 1999; Zonneveld et al., 2013), and can be used as such to reconstruct past climate changes in downcore sediment records (e.g. Pross and Brinkhuis, 2005; Hennissen et al., 2014, 2017). Terrestrial palynomorphs are derived from vegetation and are delivered to coastal marine sediments through wind or river runoff. The pollen and spore (or sporomorph) assemblage in a downcore sediment record like the coastal marine Hank site can thus indicate the type of vegetation in the nearby continent, which can then be used to infer precipitation and/or temperature regimes of the source area (e.g. Heusser and Shackleton, 1979; Donders et al., 2009; Kotthoff et al., 2014).

Standard palynological techniques were used to process 82 selected samples. HCl and HF digestion followed by 15 µm sieving were carried out according to Janssen and Dammers (2008). Both marine dinocysts and spores were counted under a light microscope at 400x magnification until a minimum of 200 specimens were found. Rare species were identified during a final scan of the microscope slide. For dinocysts, the taxonomy of Williams et al. (2017) is used.

Some dinocyst taxa prefer cooler (sub)polar waters, hence we may take the sum of those taxa and use that as an indicator for SST in the SNSB. We calculate % cold-adapted dinocysts as the sum of the following species over the sum of all dinocysts in the Hank borehole: *Bitectatodinium* spp., *Habibacysta tectata, Filisphaera filifera, Headinium* spp., *Filisphaera* spp., *Islandinium* spp., *Habibacysta* spp., *Islandinium euaxum,* and *Bitectatonium tepikiense* following the approach adopted by Versteegh and Zonneveld (1994), Donders et al. (2009), De Schepper et al. (2011), and Donders et al. (2018).

A subset of 25 samples was analysed for detailed pollen assemblages to provide independent long-term trends in climate and vegetation cover. Late Neogene pollen types can, in most cases, be related to extant genera and families (e.g. Donders et al., 2009; Larsson et al., 2011). Percent abundances are calculated based on total pollen and spores excluding bisaccate taxa, freshwater algae, and *Osmunda* spores due to peak abundance in one sample of the latter. Bisaccate pollen abundances are excluded because they are heavily influenced by on- to offshore trends (Mudie and McCarthy, 1994), and therefore do not primarily represent tree abundance.

The terrestrial/marine (T/(T+M)) ratio of palynomorphs takes the sum of all sporomorphs and divides by the sum of all sporomorphs and dinocysts. The sum of sporomorphs excludes bisaccate taxa. The T/M ratio is commonly used as a relative measure of sea level variations and therefore distance to the coast (e.g. Donders et al., 2009; Kotthoff et al., 2014).

2.4 Lipid biomarkers and proxies

We use three independent organic temperature proxies for sea surface temperature based on different lipid biomarkers. The TEX_{86} is a proxy based on the temperature sensitivity of isoprenoidal glycerol dialkyl glycerol tetraethers (isoGDGTs), membrane lipids of marine archaea (Schouten et al., 2002). An increase in the relative abundance of isoGDGTs containing more cyclopentane moieties was found to correlate with SSTs (Schouten et al., 2002). Several transfer functions exist to translate TEX_{86} values into SSTs (e.g. Kim et al., 2010; Tierney and Tingley, 2014). Here we use the global core-top calibration of Kim et al. (2010). Since isoGDGTs are also produced in soils, albeit in minor amounts, they may alter the marine temperature signal during periods with large contributions from land. The relative input of (fluvially discharged) terrestrial organic matter (OM) can be determined using the ratio of branched GDGTs (brGDGTs), which are produced in soils (Sinninghe Damsté et al., 2000; Weijers

et al., 2007) and rivers (Zell et al., 2013a), with crenarchaeol, an isoGDGT exclusively produced by marine Thaumarchaeota (Sinninghe Damsté et al., 2002). This ratio is quantified in the Branched and Isoprenoid Tetraether (BIT) index (Hopmans et al., 2004), where high BIT indicates a high continental OM input and a low BIT indicates a predominantly marine source of OM. A BIT index >0.3 is generally used as a cut-off for the validity of TEX_{86}-based SST estimates (Weijers et al., 2006). Secondly, the $U^{K'}_{37}$ index is used as a proxy for SST based on the degree of unsaturation of C_{37} alkenones produced by marine haptophyte algae (Prahl and Wakeham, 1987). An increased abundance of the tri- relative to the di-unsaturated C_{37} alkenones, expressed as the $U^{K'}_{37}$ index, is linked with decreasing temperature, an adaptation thought to retain membrane fluidity in cooler environments (Marlowe et al., 1984). $U^{K'}_{37}$ values can be converted to SSTs using the global core top calibration of Müller et al. (1998), with a calibration error of 1.5 °C. Finally, SSTs can be reconstructed based on the relative distribution of long chain diols, which are dihydroxylated lipids with 22–38 carbon atoms. The C_{28} 1,13- C_{30} 1,13- and C_{30} 1,15 diols are most commonly found in seawater, and have a putative phytoplankton source (Volkman et al., 1992; Rampen et al., 2007, 2011). The distribution of these three diols are used to formulate the long chain diol index (LDI), which can be converted to SST using the calibration of Rampen et al. (2012), of which the calibration error is 2.0 °C. Furthermore, since freshwater eustigmatophyte algae produce C_{32} diols (Volkman et al., 1992, 1999; Gelin et al., 1997), the percentage of the C_{32} diol versus that of the marine C_{28} 1,13- C_{30} 1,13- and C_{30} 1,15 diols used in the LDI can be used as an indicator for freshwater discharge (Lattaud et al., 2017).

Sediments (n = 155) were previously extracted and processed according to procedures outlined in Dearing Crampton-Flood et al. (2018). The polar fractions, containing GDGTs, were analysed on an Agilent 1260 Infinity ultra-high performance liquid chromatography instrument (UHPLC) coupled to an Agilent 6130 single quadrapole mass detector with settings following Hopmans et

al. (2016). Injection volume of each sample was 10 µL. GDGTs were separated using two silica Waters Acquity UPLC HEB Hilic (1.7 µm, 2.1 mm x 150 mm) columns (30 °C). A flow rate of 0.2 ml/min was used for isocractic elution: starting with 82% A and 18% B for 25 min, then a linear gradient to 70% A and 30% B for 25 min (A= hexane, B=hexane:isopropanol 9:1, *v*/*v*). Prior to mass detection, atmospheric pressure chemical ionisation (APCI) with the following source conditions was used: vaporizer temperature 400 °C, gas temperature 200 °C, capillary voltage 3500 V, drying gas (N_2) flow 6L/min, nebulizer pressure 25 psi, corona current 5.0 µA. Selected ion monitoring (SIM) was used to detect $[M-H]^+$ ions of the isoGDGTS: *m*/*z* 1302, 1300, 1298, 1296, 1292.

After GDGT analysis, polar fractions were silylated by the addition of N,O-bis(trimethylsilyl)trifluoroacetamide (BSTFA) and pyridine (60 °C, 20 min). A Thermo trace gas chromatograph (GC) coupled to a Thermo DSQ mass spectrometer (MS) was used to analyse long chain diol distributions in SIM mode (*m*/*z* 299, 313, 327, 341) at the Royal NIOZ. The temperature program was: 70 °C for one min, then ramp to 130 °C at 20 °C/min, then ramp to 320 °C at 4 °C/min, then held for 25 minutes.

Ketone fractions, containing the C_{37} alkenones, were analysed using gas chromatography with flame ionisation detection (GC-FID). Samples were injected (1 µL) manually on a Hewlett Packard 6890 series GC system equipped with a CP-Sil-5 fused silica capillary column (25 m x 0.32 mm, film thickness 0.12 µm) and a 0.53 mm pre-column. The oven temperature program was similar to that used for long chain diol analysis.

3. Results

3.1 Stable isotopes of *Cassidulina laevigata*

Foraminifera preservation in the intervals 404–386 and 204–136 meters was either very low or non-existent. Furthermore, foraminifera were challenging to

pick in the crag material (220–205 m, Fig. 2c). The $\delta^{18}O_{cass.}$ values of foraminifera in the remaining intervals before and after outlier removal ranges from -1.0–3.2‰ and 0.3–2.9‰, respectively (Fig. 2c). The variability in $\delta^{18}O_{cass.}$ values between peaks and adjacent troughs in the Hank record ranges from ~ 0.9–1.8‰. The stable carbon isotope record varies between -2.2–0.6‰ (Fig. 2d). The variability in the $\delta^{13}C_{cass.}$ record ranges from ~0.3–2.3‰, inside the moving average range. Discounting the sample at 206 m, the variability in the $\delta^{13}C_{cass.}$ record is similar than that of the $\delta^{18}O_{cass.}$ record (~1‰, Fig. 2d). The interval with the most outliers for carbon and oxygen isotopes was 311–303 m, where all samples exceeded the upper and lower range of values calculated using the 7-point average (Sect. 2.2).

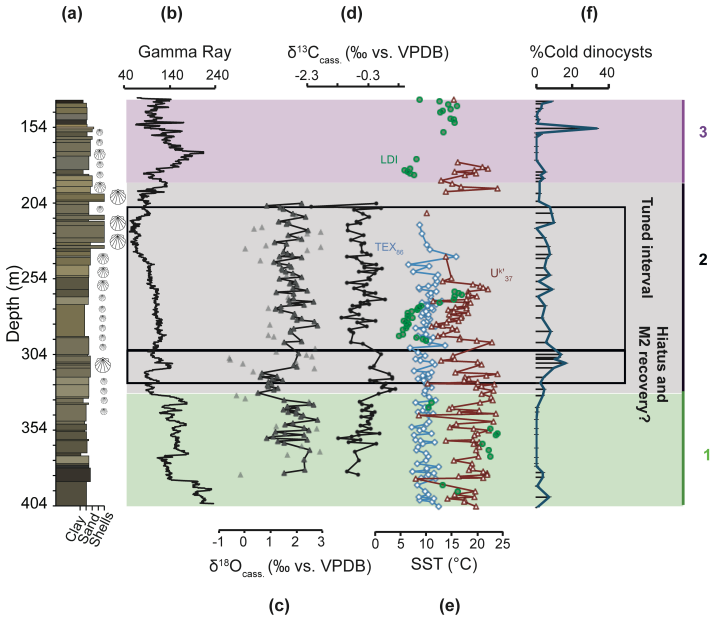

Fig. 2. Marine proxies for the Hank borehole. (a) The depth and lithology of the Hank sediments (shell abundance qualitatively indicated). (b) The smoothed gamma ray (GR) log (dinoloket.nl). (c) Stable oxygen and (d) stable carbon isotope records for the endobenthic *Cassidulina laevigata*. Outliers in the $\delta^{18}O$ record are indicated by grey triangles. (e) SST records based on TEX_{86} (blue diamonds), $U^{K'}_{37}$ (red triangles), and LDI (green circles). (f) %Cold taxa of dinoflagellate cysts. The intervals corresponding to the A (green), B (grey), and C (purple) depths discussed in the text are indicated. The tuned interval and the position of the hiatus marking the M2 are represented by a black line.

3.2 Palynology

The palynomorphs in the Hank sediments are well preserved. The borehole can be divided into three main intervals according to the (co)dominance of the marine/terrestrial palynomorphs: A, B, and C, which roughly correspond to the early Pliocene (A), mid-Pliocene (B) and late Pliocene/early Pleistocene (C). In the deepest part of the borehole (404–330 m, A), the marine component of the palynomorph assemblage clearly exceeds the terrestrial, as evidenced by the low T/M values (Fig. 3c). An isolate sporomorph peak and (sub)polar dinocyst peak is visible at 383 m (Figs. 2f, 3c). The B interval from 330–187 m shows a fluctuating ratio between the marine and terrestrial elements (Fig. 3c). The cold-adapted dinocysts also show fluctuations indicating alternating warmer and cooler periods (Fig. 2f). One striking feature is the increase in number of cold-adapted dinocysts and the *Osmunda* acme at 305 m (Figs. 2f, 3c). The third interval C spans the upper part of the borehole (187–136 m), and sporomorphs in particular dominate the spectra from 187 m upward, visible by the consistently high T/M (Fig. 3c). Interval C shows an increased occurrence of coastal marine genera, like *Lingulodinium*. The increased gamma ray values at ~175 m (Fig 2b) are the result of the abundance of (shell) concretions, not clays, and as such, do not indicate a more distal environment but rather a development toward a more proximal environment. At 154–153 m, the marine indicators in the borehole are reduced to just 0.5% of the total sum of palynomorphs. However, the highest abundance of cold-adapted dinocysts, mostly composed of taxa like *Habibacysta tectata*, is at 154 m (Fig. 2f). This depth is also marked by the complete disappearance of several (sub)tropical species from the Pliocene, like the genus *Barssidinium* spp. with an LOD at 157 m (Dearing Crampton-Flood et al., 2018). The uppermost (154–136 m) interval indicates an estuarine to deltaic environment, due to the presence of freshwater and brackish water algae species *Pediastrum* and *Botryococcus*. In contrast, the freshwater indicators are (almost) absent in

intervals A and B. The assemblages of interval C are also characterized by a fluctuating abundance of cold-adapted dinocysts (Fig. 2f).

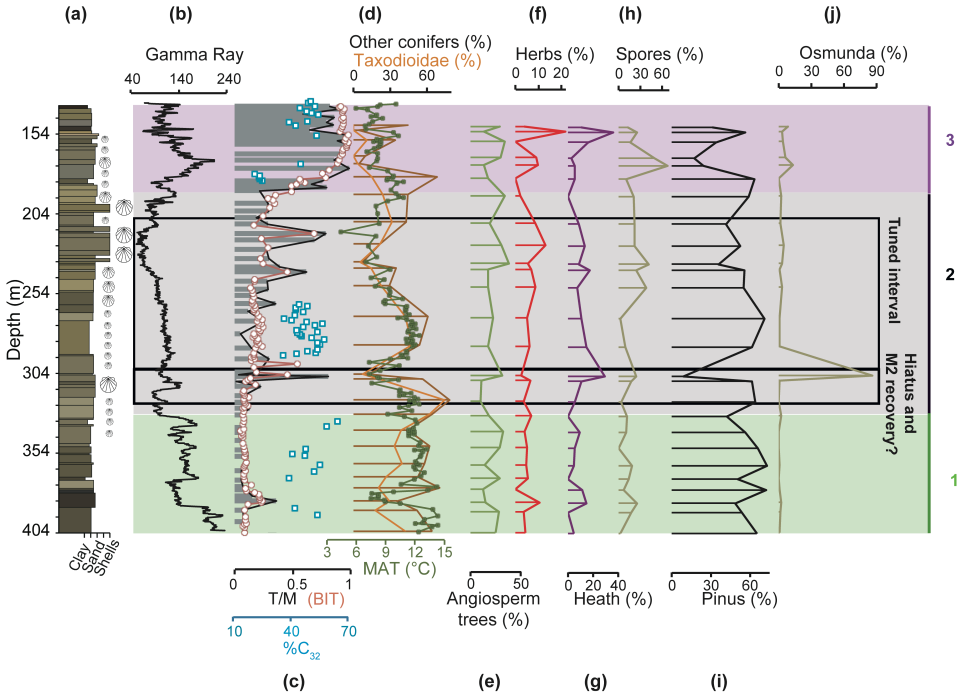

Fig. 3. Terrestrial proxies for the Hank borehole. (a) The depth and lithology of the Hank sediments, with shell material qualitatively indicated by shell symbols. (b) The smoothed gamma ray (GR) log (from dinoloket.nl), (c) the relative input of terrestrial organic material to the Hank sediments based on the terrestrial/marine ratio of palynomorphs (black line), the Branched and Isoprenoid Tetraether (BIT) index (orange circles), and the $\%C_{32}$ diol (blue squares). Pollen records expressed as % of total pollen: (d) Other conifers (brown line), Taxodioidae (orange line) and MAT (°C; green line; Dearing Crampton-Flood et al., 2018), (e) angiosperm trees, (f) herbs, (g) heath, (h) spores, (i) Pinus, and (j) Osmunda. The intervals corresponding to the A (green), B (grey), and C (purple) depths discussed in the text are indicated. The tuned interval and the position of the hiatus marking the M2 are represented by a black line.

The pollen assemblages are dominated by tree pollen, particularly conifers (*Pinus, Picea, Abies, Taxodioidae*-type, including *Glyptostrobus* and *Taxodium*, *Sciatopitys,* and *Tsuga*), but with increasing proportions of grasses (Poaceae, Cyperaceae), and heath (Ericales) in interval B, and significantly increased amounts of fern spores from 260 m and up (Fig. 3). The angiosperm

tree abundances averages about 20% and shows no significant long-term change towards the top of the sequence. The angiosperm tree pollen record is diverse, although few taxa are continuously present, and consists mostly of *Quercus robur*-type with significant proportions of *Pterocarya*, *Fagus, Carpinus* and, above 240 m, *Ulmus* (Fig. 3e). The Taxodioidae-type shows a distinct long-term decline superimposed by three shorter minima in the end of interval B and beginning of C, occurring at 205, 235 and 170 m (Fig. 3d).

3.3 Lipid biomarkers and proxies

IsoGDGTs are present in high abundances throughout the borehole, as evidenced by the high total organic carbon (TOC)-normalized concentrations of crenarchaeol (0.2–130 µg g^{-1} TOC; Dearing Crampton-Flood et al., 2018; Fig. 3c). SSTs are reconstructed for those sediments where BIT <0.3, i.e. between 404 and 219 m. The trends in the SSTs calculated from the Bayesian calibration (Tierney and Tingley, 2014) and the Kim et al. (2010) calibration are the same, however, the absolute values differ (Fig. S1). TEX_{86}^{H}-reconstructed SSTs range between 7 and 13 °C, but do not show a clear trend over time (Fig. 2e).

Alkenones are present in the majority of the samples in the interval 404–250 m, however, they are below the detection limit in many of the overlying sediments from 250–200 m. Alkenones re-emerge in the interval from 197–178 m. The $U^{K'}_{37}$ index values range between 0.30–0.83, and correspond to an SST range of 8–24 °C (Fig. 2e). In the early Pliocene (A), the $U^{K'}_{37}$ SST record shows the largest fluctuations in temperature (ΔT = 15 °C), and an average SST of 19 °C. Similar variability (ΔT = 14 °C) is observed in B (middle-late Pliocene), although the average SST drops slightly to 17 °C. Alkenones are present around or below the detection limit in C (late Pliocene/early Pleistocene), so no SSTs can be calculated. Notably, $U^{K'}_{37}$ SSTs show a warming of 11 °C during the interval between 290–260 m (Fig. 2e).

Long chain diols used for calculation of the LDI index are below the detection limit in a large proportion of the Hank borehole. SSTs can be reconstructed for only a few samples in sections A and C, and they show scattered temperatures with a range of 13 °C (Fig. 2e). The sediments in section B contain enough diols to enable a semi-continuous SST reconstruction. The range of LDI SSTs in B is 4–18 °C (Fig. 2e). The record shows a strong warming trend of 10–12 °C from 295–263 m, coeval with the trend in the $U^{K'}_{37}$ record (Fig. 2). The $\%C_{32}$ diol is generally high (~36–57%) in A and B (Early-Mid Pliocene; Fig 3c), indicating a modest to strong freshwater input (cf. Lattaud et al., 2017). The $\%C_{32}$ diol slightly decreases (10%) over 294–264 m, indicating a gradually decreasing influence of riverine OM and/or an increase in the abundance of the C_{28} 1,13- C_{30} 1,13- and C_{30} 1,15 marine diols. In section C, the $\%C_{32}$ diol exhibits a strong increasing (21–59%) trend (187–136 m; Fig. 3).

4. Discussion

4.1 Age model reconstruction

4.1.1 Environmental setting and seismic profile

The changes in depositional environment in the Hank borehole from open marine to coastal marine, and successively estuarine conditions are based upon the BIT, TOC, and $\delta^{13}C_{org}$ records presented in Dearing Crampton-Flood et al. (2018), and the biological changes in the abundances of typical marine (dinocysts and test linings of foraminifera), estuarine/freshwater algae species, and sporomorph assemblages (Munsterman, 2016), summarised in the T/M ratio. A transition of marine OM during the Pliocene to more terrestrial OM input towards the Pleistocene starts approximately at 190 m as evidenced by these indicators (Fig. 3c).

The ~15 km east to west seismic profile of the Meuse River, including the location of the Hank borehole, spans a depth of >500 m (Maas2002 survey, nlog.nl; Fig. 4). Comparison of the formations of the Hank borehole with the

seismic depth profile in Fig. 4 indicates that the Breda Formation at 404–370 m is characterized by horizontal-reflection patterns, likely indicating shallow marine conditions. The eastern continuation of the seismic line reveals that these horizontal strata can be interpreted as shelf toesets of westward prograding deltaic clinoforms.

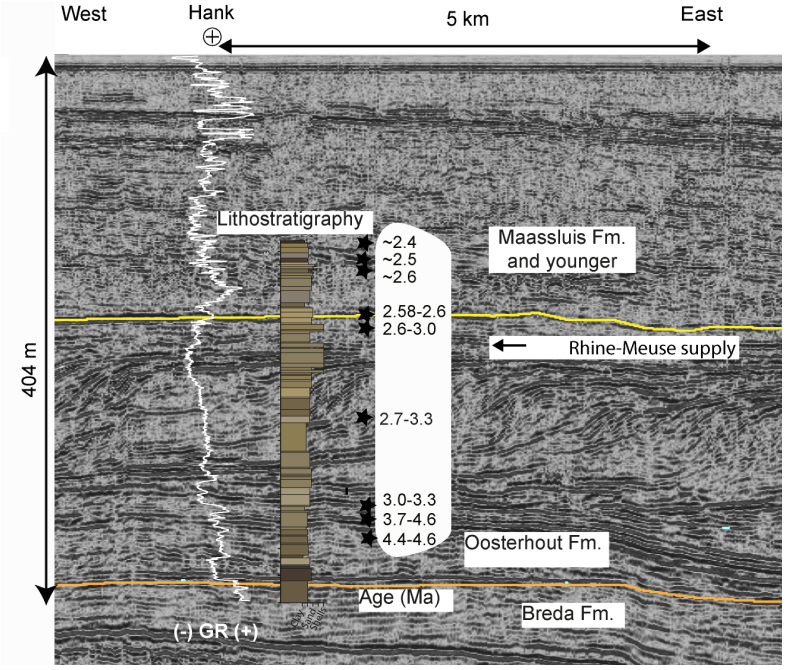

Fig. 4. Seismic east to west depth profile at the River Maas (from Maas2002 survey, nlog.nl) with the location of the Hank borehole (B44E0146) and corresponding formations indicated. The smoothed Gamma ray log (from dinoloket.nl, white), and lithology of the borehole are provided for context. Stars and age ranges refer to the biostratigraphic age model of Dearing Crampton-Flood et al. (2018). The orange and yellow lines represent the boundaries of the Breda and Oosterhout (revised), and the Oosterhout and Maassluis formations, respectively.

The transition to the overlying Oosterhout Formation is marked by a distinct angular unconformity referred to as the Late Miocene Unconformity (LMU; Munsterman et al., unpublished data; Fig. 4). The seismic data of the overlying Oosterhout Formation (Mid-Late Pliocene) indicates a twofold subdivision. The lower unit of the subdivision at 370–319 m is characterized by

convex downward reflection patterns that correspond to an open marine signature (with corresponding low sedimentation rates). This is confirmed by the transition to finer grained sediments (silts) over 381–352 m attributed to a more distal setting (Fig. 2a). This interval is also characterized by an increased abundance of dinocysts with a preference for open marine conditions, like the genus *Spiniferites*. The facies of interval 352–338 m indicates shallow to open marine conditions with a temperate to (sub)tropical SST. A coarsening upward trend is corroborated by the gradual decrease in gamma ray values. In the second Oosterhout unit from 319–157 m the environment is shallow marine, and several stacked clinoform sets are visible in the seismic profile (Fig. 4). The transition between the two Oosterhout units is clearly visible as a downlap surface around 319–313 m that corresponds to a possible hiatus (Fig. 4). Above this transition, an increase in water depth to ~200 m can be deduced from the height of the clinoforms where the topsets represent the fluvial distributary system and the clinoform breaks the coastlines. The topset beds in borehole Hank show an abundance of shell crag facies material corroborating the near shore setting (Figs. 2a, 4). The stratigraphic stacking is first purely progradational (clinoforms) and changes to both progradational and aggradational higher up, suggesting progressive fluvial influence replacing the marine environment. In the Hank borehole, this change is marked by a distinct clay layer at 292–271 m (Fig. 2a). In the upper part of the second Oosterhout Formation at depths of 260 m and upwards, the increased proportion of heath and grasses is generally considered indicative of colder and drier terrestrial climate (Faegri et al., 1989; Fig. 3). The decrease in Taxodioidae-type pollen over section B and the Oosterhout to the Maassluis Formations further indicates a cooling terrestrial climate, and is classically recognized as the top Pliocene (Late Reuverien) in the continental zonation of Zagwijn (1960), although in the onshore type area the sequences are most likely fragmented time intervals bounded by several hiatuses (Donders et al., 2007). Strikingly, both the MAT record (Dearing Crampton-Flood et al.,

2018) and the Taxodioidae-type pollen covary throughout the record (Fig. 4d), following the same trends as the Taxodioidae pollen record for the coeval Brunssumian, Reuverian, and Praetiglian stages (Zagwijn et al., 1992). This provides an opportunity to anchor the record of Zagwijn et al. (1992) to the chronology of the Hank borehole and to link it to marine records.

At the transition of the Oosterhout Formation to the Maassluis Formation, concave downward reflection patterns may reflect channel incisions into the topsets of the Oosterhout Formation (Fig. 4). The Maassluis Formation (late Pliocene-early Pleistocene, <2.6 Ma) is composed of horizontal and channel-like strata in the seismic profile (Fig. 4). The environment of the Maassluis Formation becomes more fluvio-deltaic, characterized by the decreased abundance of dinoflagellate cysts and steep rise in the number of sporomorphs, manifested by the high T/M values (Fig. 3c). Further warm-temperate trees in the Maassluis interval of the record such as *Carya, Liquidambar, Nyssa* disappeared in NW Europe in the earliest Pleistocene (Donders et al., 2007).

4.1.2 Chronological constraints

Based upon the age model of Dearing Crampton-Flood et al. (2018), it is clear that the sample resolution is too low to resolve a stable isotope tuning on Milankovitch time scales for the older succession including the Breda and lower Oosterhout Formations (404–330 m). In contrast, the sample resolution is sufficient (i.e. < 6 kyr) for the depth interval above 298 m. A dramatic decrease in sedimentation rate in the initial age model (Dearing Crampton-Flood et al., 2018) is coupled with a hiatus indicated by a sequence boundary (SB) in the seismic profile (Fig. 4) around ~330 m. The biostratigraphic age model places this interval within the scope of the M2 glacial event (~3.30 Ma; Dearing Crampton-Flood, 2018). This is further supported by the absence of excursions towards heavier values in the $\delta^{18}O_{cass.}$ record for any point in the interval deeper than 300 m (Fig. 2c). Due to the M2 being a globally recognized event (De Schepper et al.,

2014), this indicates that a hiatus likely exists over the most acute part of the glacial. A Pliocene benthic $\delta^{18}O$ record adjacent to the NS in the Nordic Seas (ODP hole 642B; Risebrobakken et al., 2016) also does not record any strong evidence of the M2 event, and the authors also postulated that the M2 might have occurred during a hiatus in the borehole. Evidence indicates a large sea level drawdown of 70 m in the North Sea (Miller et al., 2011) during the M2 that would have led to a hiatus. In addition, equivocal temperature/assemblage signals in the Coralline Crag Formation are hypothesized to be a result of sea-level change associated with the M2, which would have decreased or ceased sedimentation entirely (Williams et al., 2009). This indicates that sedimentation in the SNSB was sensitive to disturbance due to its shallow depth. Overall, the combined climate data from the Nordic Seas, East of England, and the Hank borehole site indicate that a significant hiatus (~ 319–313 m at Hank) occurred in the interconnecting basins. Thus, the coolest interval (with the presumed lowest sea level) of the M2 is not recorded.

The Plio-Pleistocene transition (2.6 Ma) occurs between 200–154 m in the Hank borehole (Dearing Crampton-Flood et al., 2018). This transition is accompanied by a peak in gamma ray values at ~175 m (Fig. 2b). The upper (Plio-Pleistocene transition) and lower (M2 event) boundaries identified here provide a contextual framework to construct a higher resolution age model for the mPWP (3254–3025 ka) using stable isotopes of *Cassidulina laevigata*. The open marine signature and relatively horizontally deposited clinoform sets in the second unit of the Oosterhout subdivision from ~305–200 m (Fig. 4) should be suitable for age model reconstruction. However, the coastal marine depositional setting for the Hank borehole in the chosen interval (upper Oosterhout Formation) during the late Pliocene/Early Pleistocene strongly indicates that successions are likely not continuous, but are stacks representing short time windows (cf. Donders et al., 2007). It is likely that these short time windows share common features, e.g. warmer or cooler intervals. This indicates that tuning the $\delta^{18}O_{cass.}$

record at the Hank borehole to the LR04 stack (Lisiecki and Raymo, 2005) should correlate either the warmer or cooler intervals.

4.1.3 Age model tuning

The absolute values of the oxygen isotope measurements on *Cassidulina laevigata* recorded in Hank are substantially lower by approximately 1–1.5‰ than the composite benthic $\delta^{18}O$ values in the LR04 stack (Lisiecki and Raymo, 2005), as well as those of a nearby Pliocene benthic oxygen isotope record from the Nordic Seas (~2–3‰; Risebrobakken et al., 2016). The offset in absolute values is unlikely due to a species-dependant effect, as $\delta^{18}O_{cass.}$ values in a nearby Quaternary-age core from Noordwijk (Noorbergen et al., 2015) are comparable to the LR04 stack (Lisiecki and Raymo, 2005). Hence, the relatively low $\delta^{18}O$ values of the Hank record likely reflect the influence of freshwater input at this site, which is proximal to the mouth of the paleo Rhine (e.g. Delaygue et al., 2001; Lubinski et al., 2001; Fig. 1). Furthermore, the large $\delta^{18}O_{cass.}$ variability in the Hank record (0.9–1.8‰) compared to that in the LR04 stack record (0.2–0.7‰ during the Pliocene; Lisiecki and Raymo, 2005) indicates that the shallow and relatively fresh(er) North Sea is more sensitive to climate disturbance than ocean bottom waters. Thus, changes in salinity linked to sensitivity in freshwater input affect the oxygen isotopes incorporated into *Cassidulina* species, regardless of the endobenthic habitat.

For tuning purposes, a detailed understanding of the North Sea hydrogeography and circulation patterns during the Pliocene must be taken into consideration. During cold periods, the North Sea circulation slows due to the reduced sea level and inflow of Atlantic water (Kuhlmann et al., 2006). Stratification in the North Sea due to freshwater input from rivers combined with the sluggish circulation and weak influence of the Atlantic waters make cooler periods problematic to tune to due to a $\delta^{18}O_{cass.}$ signature that is probably highly localized and erratic. Moreover, Donders et al. (2007) noted that the coldest phase

of glacials of the Plio-Pleistocene climate development of coastal areas in the NS is likely to be marked by substantial hiatuses caused by non-deposition and erosion. During warmer periods, an increased freshwater input from river outflows is also expected, due to the supposedly wetter climate conditions during interglacials. However, Kuhlmann et al. (2006) linked warmer periods in the Pliocene in the central section of the Southern North Sea with the occurrence of *Cassidulina laevigata*, whose habitat in the modern North Sea is located in the northern part with a strong connection to the Atlantic (Murray, 1991). Thus, tuning the warmer periods in the $\delta^{18}O_{cass.}$ record at the Hank site with warm periods in the LR04 benthic stack is preferable due to the strong(er) connection to the Atlantic (Kuhlman, 2004), resulting in a relatively more regional signature of the $\delta^{18}O_{cass.}$ values (Kuhlmann et al., 2006). Moreover, the chance of disturbance/hiatuses that affect the continuity of the sediment record at Hank is decreased in warmer periods, thus making them suitable for tuning.

Using the above reasoning, the sample with the lowest $\delta^{18}O_{cass.}$ value in each cycle between 300–200 m in the Hank record can be tuned to the lowest $\delta^{18}O$ value between the M2 and the Plio-Pleistocene boundary (Sect. 4.1.2) in the LR04 stack, presuming that the low $\delta^{18}O$ values in the Hank borehole represent the warmest part of each interglacial. Further investigation in the variation of the $\delta^{18}O_{cass.}$ cycles in the Hank borehole isotope record reveals unique saw tooth structures, representing a different pattern than the more symmetrical pattern of cyclicity that is seen in the Pleistocene. Specifically, cycles G19, G17, and G15 display these reversed saw-tooth patterns in the global benthic stack, and help pinpoint corresponding cycles in the Hank borehole record (Fig. 5). Hence, starting from the initial age constraints, we correlate lower values in our $\delta^{18}O_{cass.}$ record to those in the global benthic LR04 stacked record (Fig. 5). The reconstructed time window spans ~3200–2800 ka, and thus most of the mPWP. Based on the tuned oxygen isotope age model, the LOD of *Invertocysta*

lacrymosa and *Operculodinium? eirikianum* can be constrained to ~3045 and 2600–2782 ka, respectively (see Dearing Crampton-Flood et al., 2018).

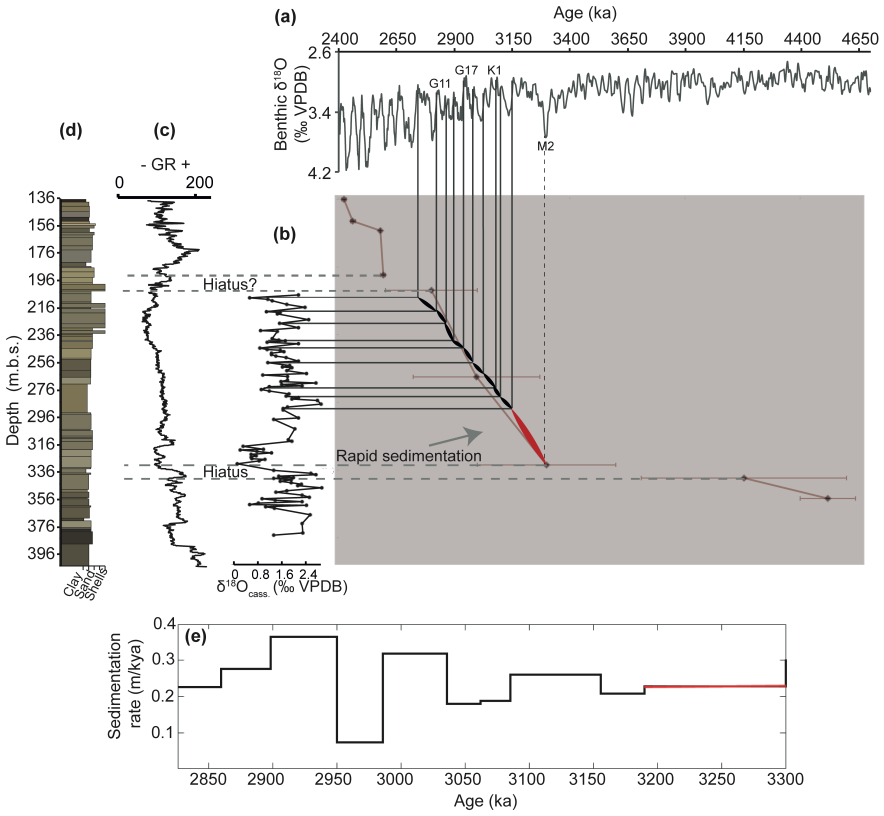

Fig. 5. Age framework for the Pliocene Southern North Sea Basin. Correlations of the interglacials of the (a) LR04 stack (Lisiecki and Raymo, 2005) to the interglacials in the (b) $\delta^{18}O_{cass.}$ record for Hank. (c) Smoothed gamma ray (GR), (d) lithology, and depth of Hank sediments. Grey lines indicate tie points based on $\delta^{18}O$ values, whereas the red tie point is based on biostratigraphy. The other biostratigraphic age points (Dearing Crampton-Flood et al., 2018) are given in purple. (e) The sedimentation rate for the tuned interval of Hank.

4.2 SST proxy comparison

Despite the fact that all three lipid biomarker proxies (TEX_{86}, $U^{K'}_{37}$, and LDI) are calibrated to SST, the records that they generate show remarkable differences and are offset in temperature (Fig. 2e). Interestingly, the TEX_{86}^{H}-derived SST record remains relatively stable throughout the tuned interval, whereas the $U^{K'}_{37}$ and

LDI-based records show large variability (Fig. 2e). The Pliocene TEX_{86}^{H} SSTs are 10 °C on average, which is the same temperature as the modern mean SST of the North Sea (Locarnini et al., 2013), and contrasts with other North Sea Pliocene temperature estimates based on ostracod, mollusc, foraminiferal, and dinocyst assemblages (Wood et al., 1993; Kuhlman et al., 2006; Johnson et al., 2009; Williams et al., 2009), all suggesting that the SST of the North Sea was 2–4 °C warmer than present at that time. Given the shallow water depth of the SNSB in the Pliocene (50–200 m; Hodgson and Funnel, 1987; Long and Zalasiewicz, 2011) at the Hank site, it seems unlikely that the isoGDGTs are influenced by the contribution of a subsurface isoGDGT-producing community. This can be further confirmed by calculating the ratio of isoGDGT-2/isoGDGT-3 ([2]/[3]; Taylor et al., 2013), whose value increases with increasing isoGDGT input from subsurface dwelling archaea. The [2]/[3] ratio in the Hank borehole is 2.1 on average, and always well below the value associated with a deep-water archaea community overprint (>5; Taylor et al., 2013). Instead, the low TEX_{86}^{H} SSTs are likely a result of seasonal production of isoGDGTs. In the modern North Sea the main period of Thaumarchaeotal blooms and associated isoGDGT production is in the winter months where ammonia is available and competition with phytoplankton is minimal (Herfort et al., 2006; Pitcher et al., 2011), which likely introduces a cold bias in TEX_{86}-based SST estimates for the SNSB.

Conversely, $U^{K'}_{37}$ reconstructed SSTs are 16 °C on average, and thus 2–4 °C higher than the temperature estimates based on ostracod, mollusc, and foraminiferal assemblages (Wood et al., 1993; Kuhlmann et al., 2006; Johnson et al., 2009; Williams et al., 2009) and ca. 6 °C higher than modern annual mean SST. These higher-than-expected $U^{K'}_{37}$ SSTs could in part be caused by a species effect as a result of a contribution from alkenones produced by freshwater haptophyte algae that have little to no correlation of $U^{K'}_{37}$ with temperature (Theroux et al., 2010; Toney et al., 2010). Moreover, the influence of freshwater input on salinity may alter the main alkenone producing communities in coastal

regions (Fujine et al., 2006; Harada et al., 2008), and thus affect the reliability of SST estimates based on the open ocean calibration specifically adapted for Group III alkenone producers (e.g. *Emiliania huxleyi*). Indeed, strong temperature fluctuations of 10 °C in a Holocene $U^{K'}_{37}$ record from the Sea of Okhotsk were linked to periods with low sea surface salinity, which were in turn correlated to high $U^{K'}_{37}$-derived SSTs (Harada et al., 2008). In contrast, a recent study showed that alkenone producers in particulate organic matter (POM) in a coastal bay in Rhode Island were unaffected by a lower salinity, further illustrated by the excellent match of the 300-year $U^{K'}_{37}$ SST record with instrumental temperature records, despite the proximity of the sample sites to the river (Salacup et al., 2019). Although the high variability in the $U^{K'}_{37}$ SST record and the higher-than-expected reconstructed temperatures at Hank fit with a freshwater input as observed in the Sea of Okhotsk, low BIT index values and T/M ratios in the Hank borehole (Fig. 3) suggest that the organic matter has a primarily marine origin. In addition, the absence of the $C_{37:4}$ alkenone in the Hank sediments, a biomarker tentatively linked with coastal or freshwater haptophytes (Cacho et al., 1999), suggests that the $U^{K'}_{37}$ should mostly represent SSTs. However, a moderate relation between the $\%C_{32}$ diol and $U^{K'}_{37}$ derived SST throughout the tuned record ($n = 26$; $R^2 = 0.32$), suggests that freshwater input may at times have influenced the $U^{K'}_{37}$ SSTs.

Alternatively, the higher $U^{K'}_{37}$ SSTs can be a result of increased production in the spring or summer (Chapman et al., 1996; Rodrigo-Gámiz et al., 2014). Indeed, summer temperatures in the Oosterhout Formation (Ouwerkerk, Netherlands) and contemporaneous Lillo Formation in Belgium (Valentine et al., 2011) recorded from benthic bivalves range from 14.9–20.4 °C, which is similar to the range of $U^{K'}_{37}$ SSTs in Fig. 2e. This would mean that summer SSTs were high and very variable during the Pliocene. Although quite variable in the earlier (~3250–3150 ka) part of the tuned record, $U^{K'}_{37}$ SSTs warmed by approximately

10 °C over the latter part of the tuned interval from 3150 to 3000 ka (Fig. 6d). In line with the winter-biased and warmer season-biased interpretation of the TEX_{86} and $U^{K'}_{37}$ reconstructed SSTs, respectively, comparison of the average reconstructed TEX_{86} (10 °C) and $U^{K'}_{37}$ (16°C) SSTs in the mPWP interval shows good agreement with the PRISM3 model reconstructions for February (10.4 °C) and August (16.7 °C; Dowsett et al., 2009).

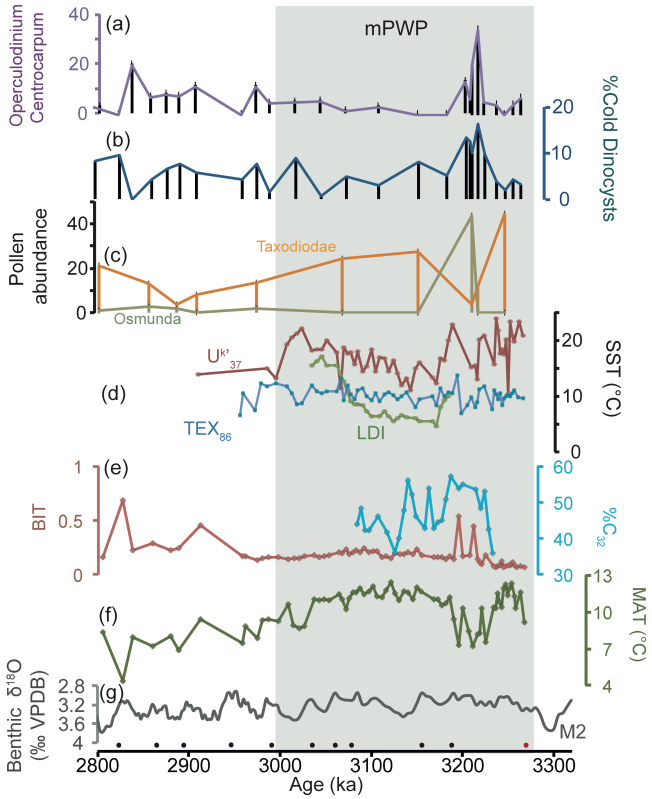

Fig. 6. Climate proxy records for the Southern North Sea Basin around the mPWP. Age tie points based on oxygen isotope stratigraphy (black) and biostratigraphy (red) are indicated. (a) The relative abundance of *Operculodinium centrocarpum* expressed as a percent total dinocysts as marker for the North Atlantic Current. (b) %Cold dinocysts, (c) pollen abundances for Taxodioidae (red) and Osmunda (blue) as a percentage of the pollen sum, (d) SST records based on the TEX_{86}, $U^{k'}_{37}$ and LDI proxies, (e) the relative input of terrestrial organic material to the Hank sediments based on the Branched and Isoprenoid Tetraether (BIT) index (Dearing Crampton-Flood et al., 2018) and the input of fresh water based on $\%C_{32}$ diol, (f) mean air temperature based on brGDGT-paleothermometry (Dearing Crampton-Flood et al., 2018), and (g) the benthic oxygen isotope stack of Lisiecki and Raymo (2005).

Finally, the LDI record is not complete over the whole depth interval due to low abundances of long chain diols in various parts of the record. Nevertheless, the LDI-based SSTs show the same warming trend from ~3150–3000 ka as the $U^{K'}_{37}$ record (Fig. 6d). LDI SSTs are first 2 °C cooler than the TEX_{86} record, and then increase toward the same SSTs as in the $U^{K'}_{37}$ record (Fig. 6d). Large discrepancies of 9 °C between TEX_{86} and LDI-derived SSTs have been observed in the Quaternary of South Eastern Australia (Lopes dos Santos et al., 2013), which the authors attributed to seasonal production of isoGDGTs in the cooler months and long chain diols in the warmer months. In late Pliocene sediments from the central Mediterranean, LDI SST estimates were slightly lower than $U^{K'}_{37}$ SSTs, however this was within the error range of the proxies (Plancq et al., 2015). Due to the recent advent of the LDI proxy, and the scarcity of other multi-proxy studies (De Bar et al., 2018; Lattaud et al., 2018) comparing the LDI to $U^{K'}_{37}$ and TEX_{86} SSTs in the same sediment samples, further discussion on this topic is limited.

5. Late Pliocene climate evolution in the Southern North Sea Basin

5.1 The M2 event and recovery

The M2 event is most likely incomplete, or absent in the Hank record, and is marked by a hiatus that is also recognized in sequences from the Coralline Crag in the English North Sea and the Nordic Seas (Fig. 1, Williams et al., 2009; Risebrobakken et al., 2016). Nevertheless, in the sediments occurring above the hiatus marked by the sequence boundary in Fig. 4, large variability in $\delta^{18}O_{cass.}$ indicates fluctuating climate conditions that may be associated with the onset or the recovery of the M2. The fluctuations match those in the records of the BIT index and $\delta^{13}C$ of organic matter (see Dearing Crampton-Flood et al., 2018), which indicate a closer proximity of the coast to the site, likely as a result of sea level change. The major peak of *Osmunda* spores (outside of pollen percentage

sum) after the hiatus at ~3210 ka (306 m) could then represent a pioneer phase of marsh vegetation related to a rapid sea level lowering. The (sub)polar dinocyst acme and increase of *Operculodinium centrocarpum* (Figs. 2, 6a) at 305 m may then represent the restoration of the location of the Hank site to a more distal marine setting within the confinement of the Rhine Valley Graben. The acme of *Osmunda* spores coincides with the occurrence of dinocysts characteristic of (sub)polar watermasses at ~3210 ka, further indicating cold conditions (Fig. 6). In addition, the distinct decrease in Taxodioidae-type pollen at the same time indicates that climate conditions were also cold(er) on the continent (Fig. 6c), which is supported by low terrestrial mean air temperatures of 6 °C, independently reconstructed based on brGDGTs (Fig. 6f; Dearing Crampton-Flood et al., 2018). In contrast, all SST reconstructions remain stable during this M2 deglaciation/recovery period (Fig. 6d), suggesting that cold periods on land are better recorded in the sedimentary record than those in the marine realm. Indeed, terrestrial proxies represent an integrated signal over longer time and larger space (NW Europe), compared to that of the marine proxies, which are confined to the shallow SNSB basin and potentially only record warm periods (Sect. 4.1.3).

5.2 The mid-Piacenzian Warm Period

The mPWP is almost entirely covered by the age-tuned interval of the Hank record, which starts after the hiatus that marks the M2 event. The sea level drop associated with the M2 event may have decreased the inflow of Atlantic bottom water currents originating from the Northern opening of the North Sea (Kuhlmann et al., 2006). After the M2 event, isostasy may have then slowly opened a new connection to the North Atlantic via the English Channel, which would have allowed the inflow of relatively warmer and saline Atlantic Water fed by the North Atlantic Current (NAC) into the North Sea (Funnel, 1996). The occurrence of such an inflow is supported by the high abundance of dinocysts

from *Operculodinium centrocarpum*, that is generally used as a tracer for the NAC (Boessenkool et al., 2001; De Schepper et al., 2009; Fig. 6a), present after the hiatus associated with the M2 event at ~3210 ka (305 m). The amount of *Operculodinium centrocarpum* cysts then decreases to zero and gradually re-emerges from 3150 ka on (Boessenkool et al., 2001; De Schepper et al., 2009; Fig. 6a), indicating a fluctuating influence of the NAC.

The presence of Taxodioidae-type pollen (*Taxodium, Glyptostrobus*) throughout most of the mPWP (Fig. 6c) indicates that land temperatures were generally not low enough for prolonged winter frosts. Minimum Taxodioidae-type pollen abundance of 10% has been associated with a mean temperature of the coldest month of >5 °C (Fauquette et al., 1998). The terrestrial temperature record of Dearing Crampton-Flood et al. (2018) and the increased proportion of Taxodioidae-type pollen (Fig. 6) support the presumed relatively stable climate conditions on land during the mPWP (Draut et al., 2003; Lisiecki and Raymo, 2005). Based on these pollen species, Zagwijn et al. (1992) inferred mean July temperatures between 15–20 °C for the Reuverian of the Netherlands (corresponding to the Piacenzian defined by the International Commission on Stratigraphy, 3.6–2.58 Ma), with short lived cool pulses of ~12 °C, that can also be recognized in the brGDGT MAT record (Fig. 6f).

In contrast to the stable terrestrial climate, the LDI and $U^{K'}_{37}$ SST records indicate that SSTs were highly variable during the mPWP (Fig. 6d). The large amplitude of the variation in the SST records may be a result of the at the time relatively shallow coastal location of Hank, which is sensitive to warming and cooling. The proximity to of the site to freshwater input may also play a role, however this cannot be confirmed (Sect. 4.3). Notably, the high variability in SSTs during the mPWP at the Hank site is also seen in all other currently available $U^{K'}_{37}$ SST records from the North Atlantic (Lawrence et al., 2009; Naafs et al., 2010; Bachem et al., 2017; Clotten et al., 2018). The proposed scenarios for

the high variability in these $U^{K'}_{37}$ SST records range from a change in the strength of the NAC (Lawrence et al., 2009; Naafs et al., 2010), orbital forcing (Lawrence et al., 2009; Bachem et al., 2017) and ocean gateway changes (Bachem et al., 2017). In addition, the high variability in the $U^{K'}_{37}$ record from the Iceland Sea record was linked to the frequent occurrence of spring sea ice cover and ice-free summers linked to freshwater input (Clotten et al., 2018). Thus, the high variability of $U^{K'}_{37}$ SSTs at the Hank Site during the Pliocene is most likely due to a combination of freshwater influence, the shallow depth of the SNSB, and changes in the direction and strength of the NAC. Orbital forcing may play a role in pacing the variation of the NAC (Naafs et al., 2010), although this investigation requires further analysis, which is not possible in the Hank borehole due to the shorter tuned interval. Nevertheless, the common factor among the records discussed here is the influence of variations in the position of the NAC, which thus seems most likely responsible for the variation in all five $U^{K'}_{37}$ SST records discussed above.

In contrast, the variability of the $U^{K'}_{37}$ SSTs is not reflected in the TEX_{86} record, which may be due to the winter signal they record (Sect. 4.3). Regardless, a common feature of the $U^{K'}_{37}$ and LDI SST records is the gradual warming between ~3150–3000 ka (Fig. 6d), which is seen most clearly in the LDI record. Before the SST warming, $\%C_{32}$ diol decreases slowly from 3200–3100 ka (Fig. 6e), indicating a decrease in freshwater discharge and/or an increased distance to the coast. The low T/M ratios and the presence of a clay layer from 292–271 m in Fig. 3c (corresponding to 3170–3070 ka; Fig. 6) at this time further indicate increased marine influence, likely as a result of sea level rise. Differences in the degree of warming recorded by the organic SST proxies may be attributed to the lateral transport of certain biomarkers (Benthien and Müller, 2000; Ohkouchi et al., 2002). For example, the change in currents in the North Sea after the M2 event, bringing in warmer waters from the North Atlantic may have brought alkenones and/or diols with a warmer signature to the SNSB, resulting in the high

SSTs reflected by the $U^{K'}_{37}$ and LDI proxies. Regardless, the high variability and warming trend in two out of the three organic SST proxies in the Pliocene North Sea indicate that the area encompassing the North Atlantic, Nordic Seas, and North Sea was very sensitive to changing currents, probably as a result of the strength and/or direction of the NAC.

5. Conclusions

The age framework for the mid-Pliocene Southern North Sea Basin (SNSB) constructed here reveals that the M2 glacial is represented as a hiatus, confirming interpretations at proximal sites in the Nordic Seas and the English North Sea coast. Our terrestrial multi-proxy records show a consistent signal between lipid biomarker temperatures and pollen assemblages, which show stable terrestrial temperatures of 10–12 °C, and the continued presence of warm-adapted tree species during the mPWP. Importantly, the chronology presented here allows placing earlier terrestrial temperature reconstructions for Pliocene NW Europe (Zagwijn et al., 1992) in time. Conversely, sea surface temperatures were variable, which may be caused by the sensitivity of the shallow Pliocene North Sea to climate change and the influence of freshwater input on lipid biomarker SST proxies. Nevertheless, the variability in SSTs matches that in all other currently available SST records from the North Atlantic and Nordic Seas, indicating that the marine realm was highly dynamic during the mPWP, probably as a result of shifting currents caused by a reorganization/diversion of the North Atlantic Current after the M2. Thus, our multi-proxy approach for the first time reveals that land-sea climate evolution in the SNSB was asynchronous during the mPWP.

Acknowledgements

The authors would like to thank Nico Janssen for processing palynological samples, Giovanni Dammers and Natasja Welters for preparation of foraminifera samples, Arnold van Dijk for help with isotope measurements, and Anita van Leeuwen and Dominika Kasjaniuk for assistance in the organic geochemistry lab. Stefan Schouten and Anchelique Mets at the Royal NIOZ assisted with the analysis of long chain diols. This work was supported by funding from the Netherlands Earth System Science Center (NESSC) through gravitation grant NWO 024.002.001 from the Dutch Ministry for Education, Culture and Science to Jaap S. Sinninghe Damsté and Lucas Lourens.

Chapter 6

BayMBT: A Bayesian calibration model for branched glycerol dialkyl glycerol tetraethers in soils and peats

Emily Dearing Crampton-Flood, Jessica E. Tierney, Francien Peterse, Frédérique M.S.A. Kirkels, Jaap S. Sinninghe Damsté.

In revision for *Geochimica et Cosmochimica Acta*.

Abstract

Accurate temperature records for the deep geological past are a vital component of paleoclimate research. Distributional changes of branched glycerol dialkyl glycerol tetraether (brGDGT) lipids in sedimentary archives are a promising proxy indicators to infer pastcontinental air temperatures. However, the 'orphan' status of the brGDGTs, the potential effect of parameters other than temperature on their relative distribution, and the uneven geographical distribution of the soil sample locations used for calibration contribute to the high uncertainty of brGDGT proxy calibration (RMSE ± 5 °C). Here, we expand the soil dataset from the previous calibration(s) with new and published soil and peat data. We use Bayesian statistics to calibrate the relationship of the 5-methyl brGDGTs (MBT′5Me) and mean annual air temperature (MAAT). The addition of warm (>28 °C) soils from India substantially increases the upper limit of the Bayesian (BayMBT) calibration from ~25 °C to ~29 °C, aiding in the generation of temperature records for past greenhouse climates, such as the Eocene. The BayMBT model also effectively minimizes the structured MAAT residuals prevalent in previous calibrations, therefore giving the opportunity to explore confounding factors on the calibration. We formulate a set of alternative calibration models to test the effect of specific environmental parameters and show that soils at mid-latitudes with seasonalities above 20 °C are not well described by the BayMBT model. We find that the MBT′5Me index is best correlated to the average temperature of all months above 0 °C, called the $BayMBT_0$ model. This finding supports the hypothesis that brGDGT production ceases or slows down in the winter months. However, a persistent feature of the BayMBT model and previous calibrations is the significant scatter at mid-latitudes. This scatter is speculatively linked with a possible overlap or divergence of microbial brGDGT-producing communities in these locations. Finally, we stress the need for further studies and brGDGT biological provenance studies in order to address specific issues regarding this proxy.

1. Introduction

The generation of high-fidelity temperature records for both recent and deep time is an important component of paleoclimate research. The distribution of branched glycerol dialkyl glycerol tetraethers (brGDGTs; Sinninghe Damsté et al., 2000; Weijers et al., 2006), membrane-spanning lipids of a yet unknown (group of) soil-dwelling producer(s), are a promising proxy for continental temperatures (Weijers et a., 2007a) and have been widely applied to reconstruct climate up to the deep geological past (Weijers et al., 2007b; Inglis et al., 2017; Dearing Crampton-Flood et al., 2018; Miller et al., 2018). The basic structure of brGDGTs consists of two long (C_{28}) alkanes with variable numbers of cyclopentane rings (0–2) and methyl side chains (4–6), which are linked to glycerol moieties on either end via ether bonds. Prior work has indicated that the stereochemistry of the glycerol moieties points toward a bacterial origin (Weijers et al., 2006) and that the producers may be heterotropic facultative aerobes derived from *Acidobacteria* (Weijers et al. 2009, 2010). A recent mesocosm experiment found that brGDGT production increased in response to low oxygen conditions and glucose addition following nutrient starvation (Martínez-Sosa and Tierney, 2019), supporting the lifestyle inferences of Weijers et al. (2009). Indeed, the simplest brGDGT structure, Ia, was identified in two species of *Acidobacteria* (Sinninghe Damsté et al., 2011). However, the origin of the other brGDGT compounds remains enigmatic (Sinninghe Damsté et al., 2018).

Weijers et al. (2007a) discovered the link between the degree of methyl branching (MBT; methylation of branched tetraethers) with temperature and soil pH. The authors also observed that the number of cyclopentane rings is related to soil pH (CBT; cyclisation of branched tetraethers) and formulated an empirical proxy (MBT/CBT) to reconstruct past mean annual air temperatures (MAATs) and soil pH. An improvement in brGDGT analysis led to the discovery of brGDGT isomers, which have methyl groups located on either the C-5 or C-6 position of the alkyl chain (De Jonge et al., 2013, 2014a). Reanalysis of soil

samples with the new method resulted in a revised form of the MBT index: the MBT′5Me index, which recognizes that only the 5-methyl brGDGTs respond to temperature (De Jonge et al., 2014a).

Despite the strong link of brGDGTs with temperature and soil pH, it is reasonably likely that other factors such as temperature seasonality, precipitation, and microbial community composition affect the relative distribution of brGDGTs in soils (Menges et al., 2014; Ding et al., 2015; Dang et al., 2016). However, due to the limited information on the biological source of brGDGTs, pure culture experiments on brGDGT producers have not been performed to test this. Instead, the direct influence of temperature on brGDGTs in soils has been studied in geothermally heated soils, altitudinal transects, or mesocosm experiments, but the producers remain enigmatic (e.g. Sinninghe Damsté et al., 2008; Peterse et al., 2009b; Huguet et al., 2014). Additionally, most bacterial taxa in soils remain under-studied (Ramirez et al., 2014). Nonetheless, recent research into the microbial diversity and composition of global soil datasets suggests that soil pH and MAAT are the dominant controls on bacterial communities in a wide range of locations and biomes (Delgado-Baquerizo et al., 2017; Oliverio et al., 2017).

Four substantial challenges exist for the brGDGT temperature proxy in its current form. First, the proxy becomes 'saturated' (i.e. MBT′5Me = 1) at temperatures above ca. 25 °C, limiting the application of the proxy in past greenhouse climates (De Jonge et al., 2014a; Naafs et al., 2017a). Second, there is evidence for soil moisture content exerting an effect on the methylation patterns of brGDGTs in arid areas (Dang et al., 2016). In light of this observation, the most recent calibration of MBT′5Me with temperature (Naafs et al., 2017a) imposed a cut-off based on the relative proportion of 6-methyl brGDGTs expressed as the Isomer Ratio (IR), first introduced by De Jonge et al. (2014b):

$$\mathrm{IR} = \frac{[\mathrm{IIa}'] + [\mathrm{IIb}'] + [\mathrm{IIc}'] + [\mathrm{IIIa}'] + [\mathrm{IIIb}'] + [\mathrm{IIIc}']}{[\mathrm{IIa}'] + [\mathrm{IIb}'] + [\mathrm{IIc}] + [\mathrm{IIIa}'] + [\mathrm{IIIb}'] + [\mathrm{IIIc}'] + [\mathrm{IIa}] + [\mathrm{IIb}] + [\mathrm{IIc}] + [\mathrm{IIIa}] + [\mathrm{IIIb}] + [\mathrm{IIIc}]} \quad (1)$$

Naafs et al. (2017a) removed soils with an IR > 0.5, i.e. about 50 % of the dataset, and proposed to use the cut-off as a method of screening environmental archives for the applicability of the proxy. However, use of this cut-off would preclude application of the brGDGT proxy in many sedimentary environments. The third challenge is that some of the previous calibration models (e.g. De Jonge et al., 2014a) tend to under-predict temperatures for warmer soils and vice versa due to regression dilution. This can be alleviated by using Deming regression (Naafs et al., 2017a), but this technique requires an *a priori* assumption of the analytical error for MBT′5Me and MAAT, which are not well constrained. The fourth challenge is related to the relatively high RMSE of the proxy and the corresponding large range of MAAT residuals at mid-latitudes (30–50°; e.g. Fig. 11 in De Jonge et al., 2014a). This may reflect 1) a seasonal bias, as brGDGT production might increase during the warmer summer months (e.g. Deng et al., 2016); 2) the heterogeneous nature of soils; 3) the difference between soil temperatures that influence brGDGTs and air temperatures; and/or 4) microbial diversity of brGDGT producers.

Naafs et al. (2017a) considered growing degree days above freezing (GDD), a measure of annual soil heat accumulation, and the moisture index (MI) of soils as potentially better indicators for the conditions that soil bacteria experience. A new transfer function including these parameters resulted in a lower RMSE (4.1 °C) and improved model fit (R^2 = 0.76; Naafs et al., 2017a). Regardless, the error on brGDGT-based temperature estimates is still substantial, demonstrating that we still do not have a full understanding of the factors influencing brGDGT methylation.

Here, we use Bayesian statistics to construct a general calibration model for the MBT′5Me index vs. MAAT in order to provide a calibration that propagates observational and parametric uncertainties. With the Bayesian approach, the MBT′5Me index can be treated as the dependent variable in the calibration model, respecting the etiological relationship between MBT′5Me and

MAAT. Bayes' rule can then be used to invert the relationship between the two variables, in order to predict MAAT values from a given MBT′5Me value, i.e. the goal of a paleoclimatological study. Previous calibrations using ordinary least squares (OLS) regression and Deming regression treated MBT′5Me as the independent variable. Given the scatter in the MBT′5Me-MAAT relationship, this will result in severe regression dilution if using OLS, and mild dilution in the Deming case, if the uncertainty in the observations is underestimated.

Besides, the mounting evidence for controls other than MAAT on the brGDGT temperature proxy calls for an exploration of the variance in MBT′5Me indices that is not explained by MAAT. Here, we explore patterns in the residuals of the Bayesian calibration model with regard to presumably confounding environmental parameters, namely: temperature seasonality, mean annual precipitation (MAP), precipitation seasonality, and soil pH. We also explore other Bayesian calibration models that take these environmental parameters into account and discuss their suitability for certain datasets.

2. Methods

2.1 Surface soil dataset

The soil brGDGT data used in this study are listed in Table 1. All data consist of fully separated 5-methyl and 6-methyl brGDGT isomers. For this study, 66 new soils from India, Russia, New Zealand, and China were added to the global soil data compilation set of Naafs et al. (2017a) to extend the spatial distribution of the calibration dataset (Fig. 1A). Recently published soil data from Northern China (Wang et al., 2016), and data from 96 globally distributed peatlands (Naafs et al., 2017b) were also added to the dataset. Due to the statistical similarity of the peat-specific calibration (Naafs et al., 2017b) and the soil calibrations (De Jonge et al., 2014a, Naafs et al., 2017a), there is no strong evidence that these datasets should be separated (Fig. 1B; Appendix A). We also find no difference in the

Pearson correlation coefficient of the MBT′5Me index with MAAT between the soil and peat dataset (n = 663, r = 0.79) and the soil-only dataset (n = 567, r = 0.79).

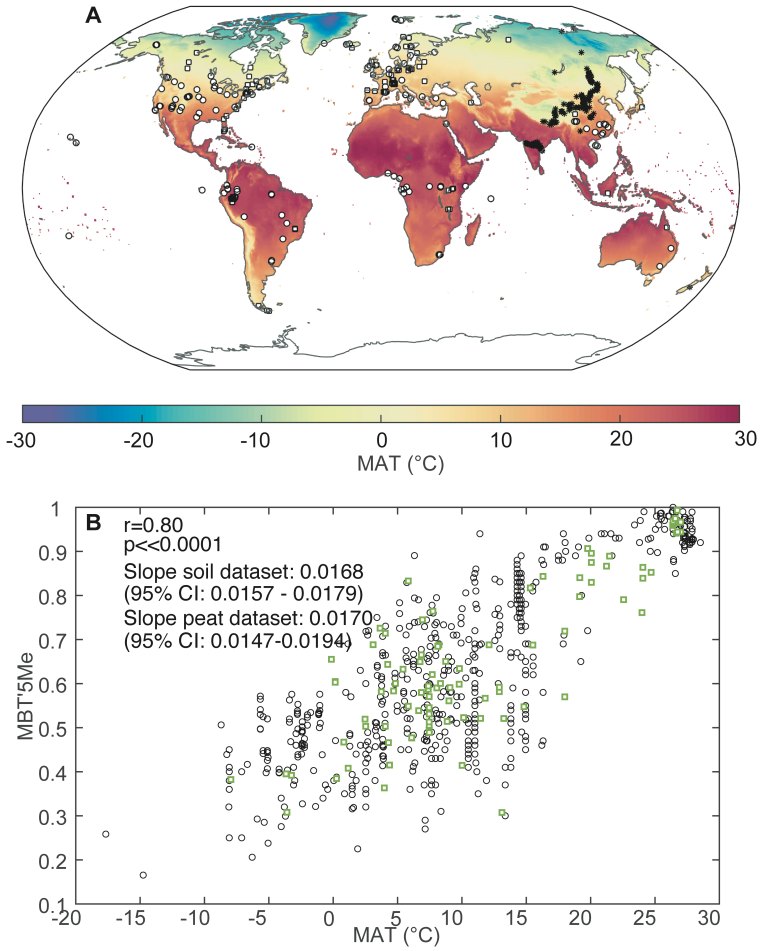

Fig. 1. (A). Global distribution of the soils used in the study. Soils analysed for the previous calibration are represented by circles (De Jonge et al., 2014a), soils added for consideration for this calibration are represented by black stars (Xiao et al., 2015; Yang et al., 2015; Lei et al., 2016; Ding et al., 2016; Wang et al., 2016; this study), and peats are represented by squares (Naafs et al., 2017b). (B) Plot of measured MBT′5Me indices for global soils (black circles) and peats (green squares) versus MAAT. Pearson correlation coefficients (r) and p values are shown. Instrumental MAAT is obtained from the CRU TS v. 3.24.01 dataset (Harris et al., 2014).

Table 1. Number, location, and references for soils and peats used for the Bayesian calibration of MBT′5Me and instrumental MAAT

Number of Soils/Peats*	**Location**	**Reference(s)**
229	Globally distributed	Weijers et al. (2007a), Peterse et al. (2012), De Jonge et al. (2014a)
46	India	This study
4	Russia/Siberia	This study
1	New Zealand	This study
15	China	This study
27	China	Xiao et al. (2015)
26	China	Yang et al. (2015)
27	China	Ding et al. (2015)
44	China	Lei et al. (2016)
148	China	Wang et al. (2016)
96*	Globally distributed	Naafs et al. (2017b)
N=663		

Previously, Naafs et al. (2017a) found that excluding soils with a high proportion of 6-methyl brGDGTs (IR>0.5) improved calibration statistics. However, in our expanded dataset, we find that the Pearson correlation coefficient between MBT′5Me and instrumental MAAT only nominally increases if the soils/peats with an IR >0.5 are removed, going from 0.79 (whole dataset, n =663) to 0.80 (IR <0.5, n = 311). Therefore, in the interest of retaining as much data as possible, we included both peats and soils with IR >0.5 in the Bayesian calibration model.

All new soils were freeze-dried, homogenized, and extracted (3x) using dichloromethane (DCM):methanol (9:1, *v/v*) with an accelerated solvent extractor (ASE 350, Dionex™) for 5 minutes at 100 °C and 7.6 x 10^6 Pa. The soils from

China (n = 15) were extracted at The Institute of Botany at the Chinese Academy of Sciences (Beijing). The extracts were dried under a gentle stream of N_2 prior to separation into apolar and polar fractions using an activated Al_2O_3 column with hexane:DCM (9:1, *v/v*) and DCM:methanol (1:1, *v/v*). Internal standard (IS, $GTGT_{46}$) was added to the polar fraction (Huguet et al., 2006). For GDGT analysis, the polar fraction was dried under N_2, re-dissolved in hexane:isopropanol 99:1 (*v/v*), and filtered through a 0.45 µm PTFE filter. Samples were analysed with an Agilent 1260 Infinity ultra high performance liquid chromatography (UHPLC) coupled to an Agilent 6130 single quadrupole mass detector using the method of Hopmans et al. (2016). The system consists of two silica Waters Acquity UPLC BEH Hilic (1.7 µm, 2.1 mm x 150 mm) columns maintained at 30 °C, with a guard column of the same material preceding the first column. GDGTs were separated using isocratic elution at 0.2 ml/min, starting with 82% A and 18% B for 25 min, followed by a linear gradient to 70% A and 30% B for 25 min, where A=hexane and B=hexane:isopropanol 9:1. Sample injection volumes were 10 µL. GDGTs were ionized using atmospheric pressure chemical ionization with the following source conditions: gas temperature 200 °C, vaporizer temperature 400 °C, drying gas (N_2) flow 6L/min, capillary voltage 3500 V, nebulizer pressure 25 psi, corona current 5.0 µA.

BrGDGTs were identified using selected ion monitoring (SIM) mode using detection of the $[M\text{-}H]^+$ ions at *m/z* 1050, 1048, 1046, 1036, 1034, 1032, 1022, 1020, 1018. The internal standard was detected at *m/z* 744. Samples were integrated manually using the Chemstation software B.04.02.

2.2 The MBT′5Me index

We used MBT′5Me rather than the MAT_{mr} function to infer MAAT from the distribution of brGDGTs, as the MBT′5Me incorporates only 5-methyl brGDGTs, which have the strongest relationship with MAAT (De Jonge et al., 2014a), and is

a straightforward index for the degree of methylation, the presumed biophysical response to temperature. In contrast, the MAT_{mr} regression is based on statistical derivation alone. The formula for MBT′5Me is defined as:

$$MBT'5Me = \frac{Ia+Ib+Ic}{Ia+Ib+Ic+IIa+IIb+IIc+IIIa} \quad (2)$$

2.3 Environmental parameters

Due to the scarcity of in situ soil temperature logger data, MBT′5Me indices in this study were compared to mean annual air temperatures (MAATs). Nearest instrumental MAATs to the data sites (determined by chordal distance) were extracted from the 0.5° gridded CRU TS v. 3.24.01 dataset (Harris et al., 2014). As the turnover time for brGDGTs in soils is on the order of decades (Peterse et al., 2010; Weijers et al., 2010, 2011; Huguet et al., 2014), we used climatological monthly and annual mean temperatures averaged over January 1901 to December 2015. The chordal distance between the MBT′5Me observations and the centroid of the nearest MAAT observation is smaller than 40 km for all sites (median 21 km; Appendix B), except for one case: USA-10 in Hawaii, where it is 48 km. Using this method to estimate MAATs leads to a homogeneous temperature collection, which is preferable to compilation using different datasets/weather stations, as was done in previous work (Weijers et al., 2007a; Peterse et al., 2012; De Jonge et al., 2014a). Nevertheless, comparison of the gridded MAAT with the instrumental MAAT from the dataset of De Jonge et al. (2014a) shows a good relation ($r = 0.90$; $p < 0.0001$), with comparable values (average difference of 0.47 °C).

Instrumental precipitation data (MAP for each month) was also taken from the CRU TS v. 3.24.01 dataset (Harris et al., 2014). Extraction of the precipitation data and assignment to the MBT′5Me values followed the same method as above. In case that two or more soils fall within the same gridbox used to estimate MAAT, average MBT′5Me values were taken to avoid weighting the

regression exercises (cf. Tierney and Tingley, 2018), leaving the total number of soil 'packets' considered in this study as 343. This formatted dataset (n = 343) is used for the construction of the Bayesian regression model (BayMBT) and all following exercises.

2.4 Bayesian regression model (BayMBT)

Bayes' theorem (or Bayes' rule) is a method to determine the probability or outcome of an event given some prior knowledge (e.g. a hypothesis) that might be related to the outcome. Bayes' rule in the general form is:

$$\mathrm{p(hypothesis|data)} = \frac{\mathrm{p(data|hypothesis)\,p(hypothesis)}}{\mathrm{p(data)}} \quad (3)$$

Where p(hypothesis|data) is the posterior probability, p(hypothesis) is the prior probability, p(data|hypothesis) is the likelihood, and p(data) is the marginal likelihood.

Following the approach of Tierney and Tingley (2014), who obtained a calibration model to estimate sea surface temperatures based on isoprenoidal GDGTs, Bayes' rule is applied twice here: once to infer regression parameters between MBT′5Me and instrumental MAAT, and second to predict MAAT from MBT′5Me values.

The first application of Bayes' rule is used to infer the parameters of a linear regression model of the general form:

$$\mathbf{Y} = \mathbf{X\beta} + \epsilon \quad (4)$$

$$\epsilon \sim \mathrm{N}(0, \sigma^2, \mathbf{I}) \quad (5)$$

Where Y is a n x 1 vector of MBT′5Me values, X is a n x 2 matrix of corresponding instrumental MAATs (where the second column is a column of ones), β is a 2 x 1 vector of the regression parameters (i.e. slope and intercept) and ϵ is a n x 1 vector of the error, which is normally distributed around zero with a variance of σ^2. By assigning the Y parameter as MBT′5Me and the X parameter

as instrumental MAAT, the relationship between MBT′5Me and instrumental MAAT is formulated in the etiologically correct way.

Bayesian inference of the parameters is thus:

$$p(\boldsymbol{\beta}, \sigma^2 \mid \mathbf{Y}) = p(\mathbf{Y}|\boldsymbol{\beta}, \sigma^2) * p(\boldsymbol{\beta}, \sigma^2) \quad (6)$$

Where $p(\boldsymbol{\beta},\sigma^2 \mid \mathbf{Y})$ is the posterior probability of the regression parameters $\boldsymbol{\beta}$ and σ^2 given the values of MBT′5Me, $p(\mathbf{Y} \mid \boldsymbol{\beta},\sigma^2)$ is the likelihood of the MBT′5Me values given the regression parameters, and $p(\boldsymbol{\beta},\sigma^2)$ is the prior on the regression parameters. The priors on $\boldsymbol{\beta}$ and σ^2 are conjugate (Multivariate Normal and Inverse Gamma, respectively) and the resulting conditional posteriors are:

$$\boldsymbol{\beta} \mid \cdot \sim \mathrm{N}(\boldsymbol{\Psi}\mathbf{V}, \mathbf{V}) \quad (7)$$

Where

$$\boldsymbol{\Psi} = \mu_0\sigma_0^{-2}\mathrm{I} + \mathbf{X}^{\mathrm{T}}\mathbf{Y}\sigma_{\mathrm{n}}^{-2} \quad (8)$$

$$\mathbf{V} = (\sigma_0^{-2}\mathrm{I} + \mathbf{X}^{\mathrm{T}}\mathbf{X}\sigma_{\mathrm{n}}^{-2})^{-1} \quad (9)$$

And

$$\sigma_{\mathrm{n}}^2 \sim \mathrm{IG}(\mathrm{a}, \mathrm{b}) \quad (10)$$

Where

$$\mathrm{a}: \mathrm{a}_{\emptyset} + \frac{\mathrm{N}}{2} \quad (11)$$

$$\mathrm{b}: \left(\mathrm{b}_{\emptyset} + \frac{1}{2}\right) * (\mathbf{Y} - \mathrm{X}\boldsymbol{\beta})^{\mathrm{T}}(\mathbf{Y} - \mathrm{X}\boldsymbol{\beta}) \quad (12)$$

μ_0 and σ_0 are priors on $\boldsymbol{\beta}$, and $a_{\emptyset}$ and $b_{\emptyset}$ are priors on σ^2_n. We use a Gibbs sampler to draw from these conditional posterior distributions of $\boldsymbol{\beta}$ and σ^2 (Gelman et al., 2003) and generate an ensemble of possible values of the slopes, intercepts, and error variances of the calibration model.

The second application of Bayes' rule, i.e. the step used to invert the relationship between the X and Y variables to estimate MAAT, is the 'prediction model', which takes the form:

$$p(\mathbf{MAAT}|\mathbf{MBT}, \boldsymbol{\beta}, \sigma^2) \propto p(\mathbf{MBT}|\mathbf{MAAT}, \boldsymbol{\beta}, \sigma^2) * p(\mathbf{MAAT}) \quad (13)$$

Where $p(\mathbf{MAAT} \mid \mathbf{MBT},\boldsymbol{\beta},\sigma^2)$, $p(\mathbf{MBT} \mid \mathbf{MAAT},\boldsymbol{\beta},\sigma^2)$ and $p(\mathbf{MAAT})$ are the posterior probability, the likelihood, and the prior, as above.

The full conditional posterior is:

$$\mathbf{MAAT} \mid \cdot \propto \mathrm{N}(\boldsymbol{\Psi}\mathbf{V}, \mathbf{V}) \quad (14)$$

Where

$$\boldsymbol{\Psi} = \mu_M \sigma_M^{-2} \mathrm{I} + \boldsymbol{\beta}^{\mathrm{T}} \mathbf{Y} \sigma^{-2} \quad (15)$$

$$\mathbf{V} = (\sigma_M^{-2} + \boldsymbol{\beta}^{\mathrm{T}} \boldsymbol{\beta} \sigma^{-2})^{-1} \quad (16)$$

Inference of MAAT proceeds by plugging in each paired slope, intercept, and error variance value into the conditional posterior such that the uncertainties in the regression parameters are propagated through to the estimation.

The second application of the Bayesian model requires the choice of a prior mean (μ_M) and a prior standard deviation (σ_M) in order to predict MAATs from MBT′5Me values. For the inferences in this work, the prior mean is set to the mean of modern MAATs across all soil locations (10 °C). The prior standard deviation is set to triple the standard deviation across modern MAATs (30 °C). A large standard deviation is chosen to ensure the MAAT predictions are dominated by the MBT′5Me-MAAT regression model (see discussions in Tierney and Tingley, 2014, 2018).

3. Results

The prior and posterior distributions for the slope, intercept and error variance of the Bayesian calibration model based on the MBT′5Me index, i.e. BayMBT, are shown in Fig. 2A. The posterior distributions are greater in probability density and far narrower than the prior distributions, meaning that the likelihood exerts the bulk of control on the posterior, rather than the prior.

The RMSE of predicted temperatures using the BayMBT model is higher than the RMSE of previous calibrations using OLS and Deming regressions (Table 2; De Jonge et al., 2014a; Naafs et al., 2017a). This is part because, in contrast with OLS, the uncertainties in the slope and intercept are captured by the Bayesian inference, but it is also likely due to the expanded dataset considered here. Nevertheless, the upper limit for the BayMBT model is substantially higher

than previous calibrations (ΔT ~5 °C, Table 2), increasing the range of temperatures that may be predicted when using the BayMBT model (Fig. 2B). This increased upper limit arises from a slightly steeper slope (from MBT′5Me and instrumental MAAT) of the expanded soil dataset as well as the elimination of regression dilution. For instance, the BayMBT upper limit is much greater than that calculated with OLS using the same dataset (24.8 °C, not shown). It is likely that the addition of the Indian soils with MAATs exceeding 26–27 °C contributes to the steeper slope in the Bayesian regression model. The lower limit of the calibration is also brought down substantially (ΔT ~10 °C, Table 2). This is the result of the addition of soils from Siberia, extending the low end of the MBT′5Me range from MBT′5Me = 0.35 (De Jonge et al., 2014a) to MBT′5Me = 0.17.

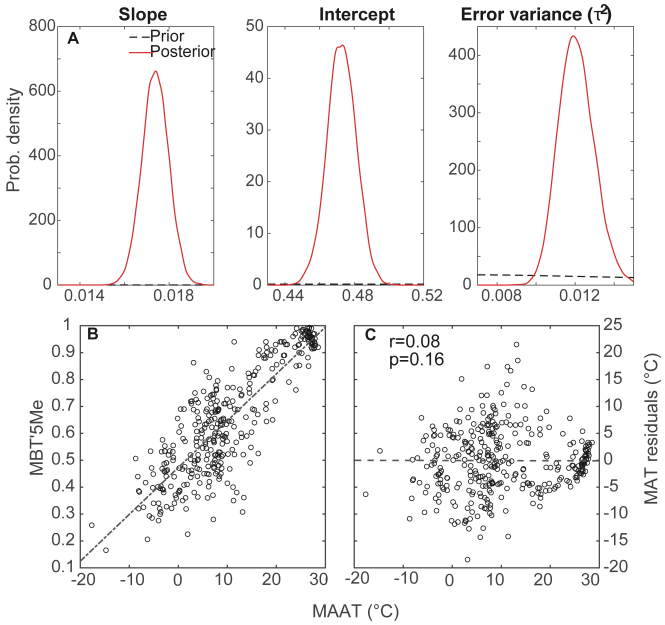

Fig. 2. (A) Plot of prior (dotted black lines) and posterior (solid red lines) probability density functions for the slope, intercept, and error variance of the BayMBT calibration model. (B) Plot of the Bayesian regression model with fitted line (dashed grey line). (C) BayMBT MAAT residuals plotted against instrumental MAAT (CRU TS v. 3.24.01 dataset; Harris et al., 2014). The Pearson correlation coefficient and p value are shown.

A comparison of MAAT residuals from the BayMBT model (Fig. 2C) with Fig. 9D of De Jonge et al. (2014a) shows that the leaning trend in MAT residuals is resolved, as revealed by the low Pearson correlation coefficient (r = 0.08, Fig. 2C). This is due to the fact that the Bayesian approach treats MBT′5Me as the dependent variable, which eliminates the regression dilution prevalent in the previous calibrations. However, the scatter (MAAT residuals ranging from -18 to 22 °C) at sites with MAATs between 0 and 15 °C (i.e. soils residing at mid-latitudes; Fig. 2C) remains a large source of uncertainty in the calibration.

Table 2. The BayMBT and extended set of Bayesian regression models for predicting MAAT in global soils and peats. Instrumental MAAT values are obtained from the CRU TS v. 3.24.01 dataset (Harris et al., 2014).

Model	n	R^2	Variance in residuals (MAAT)	RMSE (°C)	Upper limit (MBT′5Me =1)	Lower limit (MBT′5Me =0)
BayMBT	343	0.64	36.4	6.0	29.9	-25.6
BayMBTLowSeas	168	0.76	21.7	4.6	29.3	-19.2
BayMBTHighSeas	175	0.13	36.6	6.0	26.9	-25.1
$BayMBT_0$	343	0.70	14.2	3.8	27.1	0.9
$BayMBT_{-5}$	343	0.68	18.3	4.3	27.6	-3.5
$BayMBT_{-10}$	343	0.64	24.4	4.9	27.8	-7.7
BayMBT500	229	0.71	26.3	5.1	28.7	-22.9
BayMBT500 + MAT>0 °C	229	0.74	14.6	3.8	27.5	-13.2
BayMBTIR	256	0.64	35.3	5.9	30.2	-24.6

4. Discussion

4.1 Identifying confounding factors on BayMBT model residuals

The extremely large range of MAAT residuals (~40 °C; Fig. 2C) for soils located at mid-latitudes indicates that MAAT alone fails to explain a substantial portion

of the MBT′5Me variance. Here, we explore whether other environmental parameters, namely temperature seasonality, soil pH, and the magnitude and timing of precipitation, may explain this scatter, while recognizing that covariance between environmental variables (e.g. pH vs. MAP and MAAT vs. MAP) could hinder the attribution of variance to a single factor.

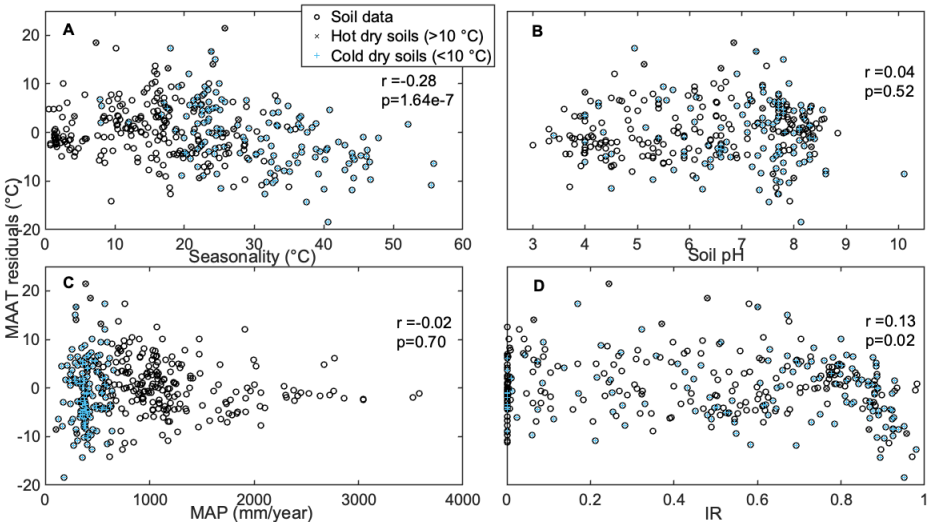

Fig. 3. (A-D) MAAT residuals (observed–predicted MAT estimates) of BayMBT model plotted against temperature seasonality, Soil pH, MAP, and IR. Arid soils (<600 mm/year) are plotted as blue plus signs (<10 °C) and black crosses (>10 °C), respectively.

4.1.1 Temperature seasonality

Seasonal variation in temperature (temperature of warmest month–temperature of coldest month) explains some of the variance of the BayMBT MAAT residuals (r = -0.28; Fig. 3A). BayMBT overestimates temperatures in soils with high seasonality, which is consistent with a bias of the proxy toward summer temperatures, following the assumption that soil bacteria may preferentially produce brGDGTs during the growing season in summer (Rueda et al., 2009; Deng et al., 2016). However, there are indications that microbial biomass synthesis in soils also continues under frozen conditions (Nedwell, 1999; Drotz et

al., 2010) and no seasonal variations in brGDGT distributions were observed in mid-latitude soils over the course of a year (Weijers et al., 2011). Thus, these contrasting observations warrant further investigation into the effect of seasonality on brGDGT distributions in soils.

4.1.2 Soil pH

Soil pH is the first control on the distribution and abundance of soil microbes in soils (Lauber et al. 2009), and therefore may have an important bearing on the MAAT residuals of the BayMBT model. For instance, pH has an influence on the degree of cyclisation of brGDGTs (expressed in the CBT index; Weijers et al., 2007a) and the relative abundance of 6-methyl isomers (De Jonge et al., 2014a; Dang et al., 2016). Although the calibrations using the MBT′5Me index only include 5-methyl brGDGTs, a possible pH effect on the degree of cyclisation may not be unexpected. Overall, the BayMBT model performs better on acidic soils (pH <6) than alkaline soils (pH >6), as seen by the larger variance of residuals for alkaline soils compared to acidic soils (37.9 vs. 27.7; Fig. 3B; $p = 0.04$). From Fig. 3B and C it also seems that dry (<600 mm/year), alkaline soils with MAAT <10 °C are particularly difficult for the BayMBT model to predict (null hypothesis rejected in F-test in favor of alternative hypothesis that the population variance of dry and alkaline soils is greater than that of wet and acidic soils). Coincidentally, those soils are located in areas which (i) are located at high altitudes (average 1364 m), and (ii) occur at mid-to-high latitudes (31 to 78 °N). 67% of these alkaline soils/peats with MAAT <10 °C are located in China. These Chinese soils are further associated with a high seasonality (>25 °C), and a grassland biome. Therefore, while pH may be a meaningful factor dictating the scatter of MAAT residuals, co-variance with other environmental variables makes the prediction of the scatter unclear. As most of the alkaline soils were associated with high temperature seasonality, it is probable that temperature seasonality has a stronger effect on the large scatter of MAAT residuals.

Interestingly, reductions in soil pH are known to reduce bacterial diversity in soils, which, on a speculative level, may refine the bacterial response to temperature (Lauber et al., 2009), and may explain why the acidic soils perform better in the BayMBT model (Fig. 3B). However, a more detailed discussion on this point is hampered due to missing information on the identity of brGDGT producers.

4.1.3 MAP

4.1.3.1 Amount of precipitation

Interestingly, the relationship of MAP to the MAAT residuals in Fig. 3C does not possess a significant Pearson correlation coefficient ($r = 0.02$). However, this is most likely an artifact of the significant correlation between MAAT and MAP throughout the dataset ($r = 0.65$; $p < 0.0001$). Previous studies have shown that MAAT is severely underestimated (>20 °C) in soils with low precipitation and high elevation (<500 mm/year; Peterse et al., 2012; Dirghangi et al., 2013; Menges et al., 2013; De Jonge et al., 2014a). However, in Figs. 3C and 4A, dry soils cluster almost symmetrically around 0 °C in the BayMBT model. The symmetrical distribution is also a result of treating the MBT′5Me index as the dependent variable, and indicates that regression dilution in the previous calibrations was primarily responsible for the underestimation of MAAT in dry soils (e.g. Peterse et al., 2012). However, the largest spread of MAAT residuals in Fig. 3C is indeed associated with dry soils (MAP <600 mm/year; $p = 1.8e10^{-4}$), suggesting that MAP has some bearing on MAT residuals. The highest residuals for the dry soils are associated with warmer instrumental MAATs (black crosses, Fig. 3C), however the low number of those soils ($n = 15$) precludes any statistical test to determine if this is meaningful. Furthermore, the dry soils associated with higher (>5 °C) residuals (Fig. 4A) consist of a large range of IR values, and thus do not allow excluding one particular range of values (i.e. either high or low IR

values). An F test shows that the variance in residuals for the soils with IR >0.5 is not greater than the variance for soils with IR <0.5, and Fig. 3D does not suggest that a cut-off of IR >0.5 is appropriate for this expanded dataset. However, Fig. 3D indicates a trend in MAAT residuals at IR values >0.8, with almost all MAT residuals having negative values. Thus, the non-random behavior in the MAAT residuals at IR >0.8 suggest that perhaps a revised cut-off may be necessary in a modified calibration model of BayMBT (explored further below).

4.1.3.2 Timing of precipitation

The distribution of rainfall throughout the year is another factor that could influence the communities of brGDGT-producing soil bacteria, and thus the brGDGT distribution of a soil. For instance, a short duration of precipitation may lead to seasonally arid conditions, therefore exerting moisture stress on soil microbes. Furthermore, the timing of precipitation in relation to that of the warmer months and growing season could also influence brGDGT distributions. Using the monthly MAP data, the difference in MAP between the month with the maximum amount of rainfall with the overall average amount of rainfall throughout the year was calculated and used to estimate the seasonality of precipitation (SoP, MAP_{max}-$\overline{MAP}$). Thus, a low SoP is indicative of a region/soil with an overall low MAP throughout the year, or a region where MAP is constant throughout the year. On the other hand, a high SoP may indicate that rainfall may be concentrated in one time of the year, such as regions that have a heavily distinct 'wet' and 'dry' season. Ergo, the SoP index can aid in interpreting whether a potential production bias is present for regions experiencing various timings of precipitation.

We do not observe a strong correlation between SoP and the residuals; however soils in regions with relatively low SoPs (<100) have a larger scatter in MAT residuals associated with the model (Fig. 4C), and the variance of the residuals is correlated with SoP ($r = -0.24$, $p = 1.02e\text{-}4$), however slightly less so

with MAP (<600 mm/year; r = 0.15, p = 0.07). In general, soils >20 °C associated with high SoPs (>100) perform better, with MAT residuals within a 5 °C range (typical RMSE of the proxy; Fig. 4C). This indicates that warm soils located in regions with a seasonally heavy rainfall have brGDGT distributions which estimate MAT relatively well. However, because these soils are associated with high MAT and associated lower range of temperature seasonality, it is not surprising that predicted MAT is more accurately reconstructed because a bias toward any season would not be immediately perceived.

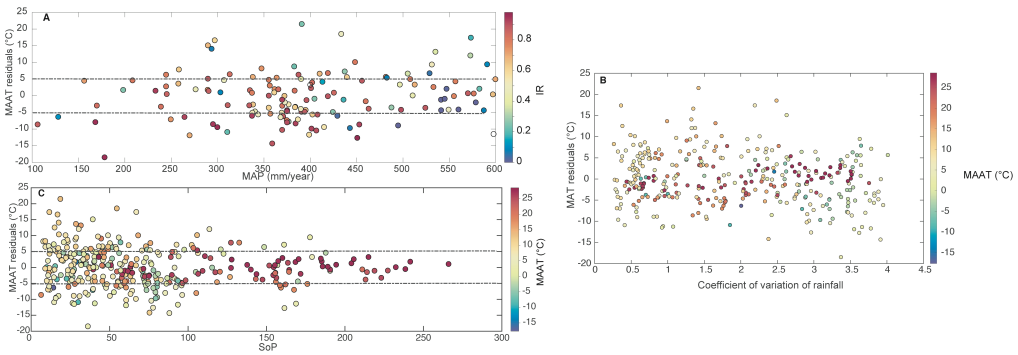

Fig. 4. (A) MAAT residuals of dry (<600 mm/year) soils plotted against MAP with circle color fill indicating IR value. (B) MAAT residuals plotted against the coefficient of variation of rainfall (MAP), with circle color fill indicating MAAT. (C) MAAT residuals plotted against the seasonality of precipitation (SoP) index, with circle color fill indicating MAAT.

4.1.4 Saturation of the BayMBT model at high temperature

A subtle feature of the soils/peats >20 °C in Fig. 2C is that they appear to contain some evidence of non-random distribution in their MAT residuals. This becomes more evident when the MAAT residuals of the soils/peats >20 °C are plotted against MAAT, seasonality, MAP, altitude, soil pH, and IR (Fig. 5). Several cutoffs (25, 20, 15°C; not shown) are considered, and 20 °C is the cutoff that consists of a reasonable number of soils (n = 88) and shows the most distinctive trend in MAAT residuals. This subset of the data shows clear relationships

between MAAT residuals and MAAT (r = 0.43), seasonality (r = 0.36), soil pH (r = 0.60), MAP (r = -0.47) and IR (r = 0.21). No clear relationship with altitude (r = -0.17) was observed for these soils (as is the case for the whole dataset, r = 0.15).

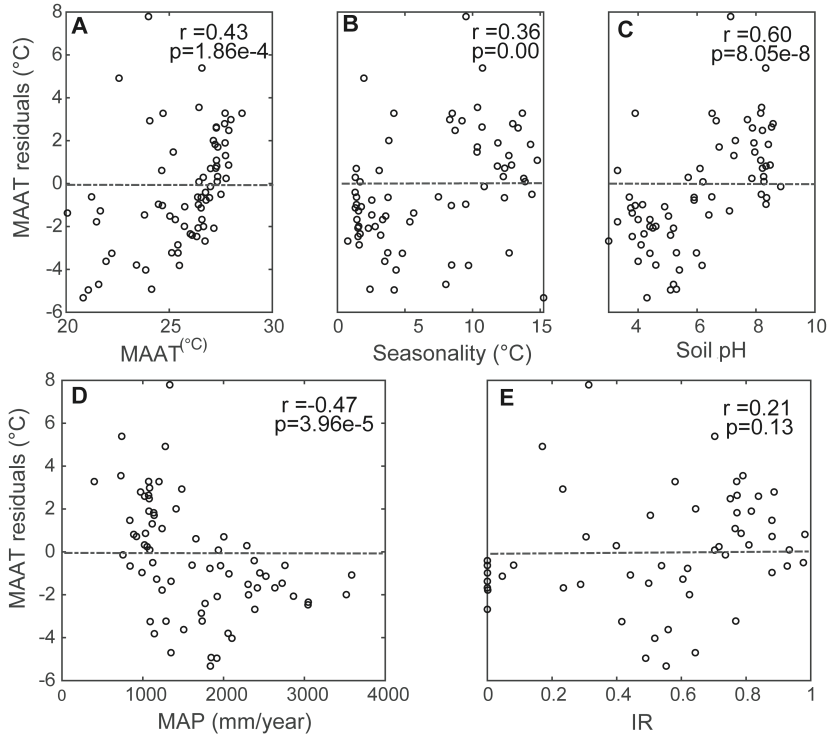

Fig. 5. (A-E) Crossplots of MAAT residuals (BayMBT) of soils >20 °C with (A) MAAT, (B) seasonality, (C) Soil pH, (D) MAP, and (E) IR. Pearson correlation coefficients and p values are indicated.

The trends in Fig. 5 may indicate that above a certain threshold temperature (i.e. between 15–25 °C), the MBT′5Me signal represents a complex interplay between the magnitude and timing of precipitation, and temperature seasonality. In particular, BayMBT overestimates MAAT (on average 1.6 ± 0.3 °C) for warm soils linked with high MAP (>2000 mm/year, e.g. tropical rainforests; Fig. 5D). Alternatively, the trends in residuals in Fig. 5 may indicate that the proxy becomes non-linearly sensitive to MAAT as it approaches its saturation point. This raises the question as to whether an adjustment of the

MBT′5Me index to deal with non-linearity is needed at this higher end of the calibration, or indeed whether a nonlinear calibration is necessary. However, data from India dominate the warm end of the calibration dataset; other warm locations are underrepresented. Thus, fitting a non-linear function at this time might unduly bias a global regression towards Indian soils. A further consideration is that the absolute saturation temperature for this proxy is not explicitly known, given that the bacteria responsible for producing brGDGTs have not been cultured in a laboratory. It is therefore important to note that the upper limit of 29 °C proposed in this study may therefore not be a true limit insofar as the bacteria responsible for synthesizing brGDGTs may continue to do so at higher temperatures.

4.2 Assessing the influence of confounding factors on the BayMBT model performance

To test the sensitivity of the BayMBT model for the potentially confounding factors discussed above, we developed seven sub-models using different subsets of the soil dataset. Given that seasonality accounts for a significant part of the residual variance, we explored modified regression models that consider seasonal variation, the timing and length of the growing season, and days without freezing. The effect of a large temperature shift throughout the annual cycle is tested with the BayMBTHighSeas model, which excludes all soils/peats with low seasonality. A cut-off of 20 °C was chosen based upon the discussion in Section 4.1.1 and Fig. 3A. Conversely, the BayMBTLowSeas model excludes soils with seasonality >20 °C. The next set of models, i.e. the $BayMBT_0$, $BayMBT_{-5}$, and $BayMBT_{-10}$ models, calibrate the MBT′5Me index to the average temperature of all months above 0, -5, and -10 °C, respectively. These models are designed to test the effect of the production of brGDGTs in soils in higher latitudes/altitudes, where the production days may be directly related to the days where temperature

does not drop below a certain threshold value. This investigation is functionally similar to the growing degree days parameter investigated by Naafs et al. (2017a), which they found to result in a slightly better R^2 value and a reduction in the range of low temperature residuals.

The aridity factor (Section 4.1.3) is tested with the BayMBT500 model, which excludes all soils/peats with MAP values <500 mm/year, i.e. dry, arid soils. To test the effect of including soils with an increased abundance of 6-methyl brGDGTs, the BayMBTIR model excludes all soils with IR >0.8, based upon the pattern of residuals in Fig. 3D. The dataset for each of these models comprises at least 168 soils (Table 2).

4.2.1 Influence of temperature seasonality

The BayMBTLowSeas model has a R^2 value of 0.76, whereas the R^2 of the BayMBTHighSeas model is 0.13 (Table 2), thus it seems that seasonal biases in MAAT estimates are more pronounced in soils where seasonality exceeds 20 °C, regardless of location or latitude (Fig. 3A). Soils with large seasonality (n = 175) occur in both mid to high latitudes (Fig. 6), although there are only 15 soils with seasonality >20 °C located in 'high' latitudes (>60°N, in Finland, Russia, Sweden, Canada, USA, Iceland, and Svalbard).

Both BayMBTHighSeas and BayMBTLowSeas models considered here are associated with a high RMSE (6.0 and 4.6 °C, respectively), and contain a large degree of scatter in the proxy that affects the accuracy of predicted MAATs. In comparison, the $BayMBT_0$ and $BayMBT_{-5}$ models possess improved RMSE values (3.8–4.3 °C). However, the coefficient of determination value (R^2) for the $BayMBT_0$ is only marginally higher than that of the BayMBT model (Table 2, Fig. 7). The $BayMBT_{-5}$ and $BayMBT_{-10}$ models do not exhibit any advantage over the $BayMBT_0$, however, the $BayMBT_{-5}$ model still performs better than the BayMBT and BayMBTHighSeas models in terms of R^2 and RMSE values.

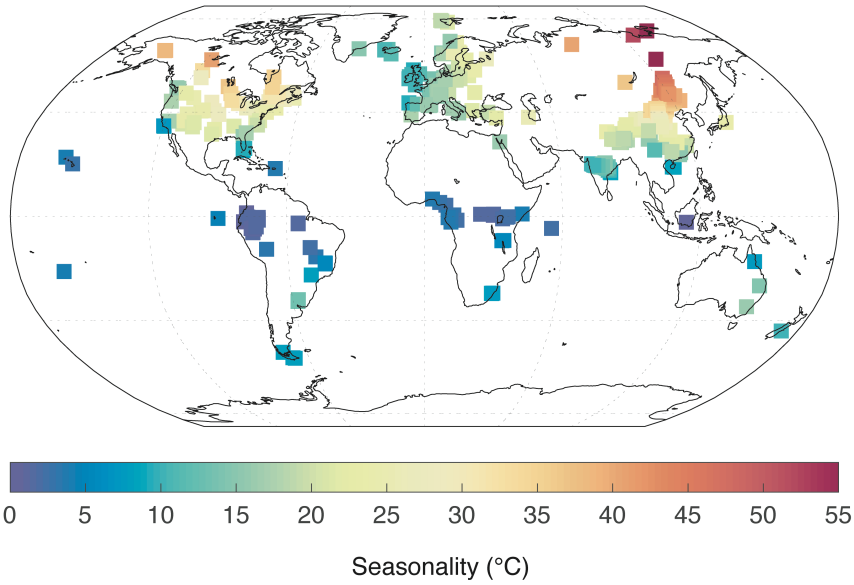

Fig. 6. Global map showing soils plotted with corresponding values for seasonality (obtained from CRU TS v. 3.24.01; Harris et al., 2014).

The improvements in the threshold-based models suggest that temperatures above the freezing point of water (0 °C) more accurately describe variation in MBT′5Me. Indeed, a study that examined the seasonal variation of bacterial communities in the active layer of permafrost from Svalbard demonstrated that the strongest changes in community structure recorded by DNA and RNA- based analyses occurred during the freezing in October and the spring thaw in May (Schostag et al., 2015). If brGDGT producers were part of one or both of those distinct winter and summer communities, it raises the hypothesis as to whether brGDGTS produced by bacteria in the summer months are better recorders of temperature.

4.2.2 Influence of precipitation amount and seasonality

The BayMBT500 model has a higher R^2 value ($R^2 = 0.71$) and lower RMSE (5.1 °C) than the BayMBT model, and the variance in residuals is decreased compared

to the BayMBT model (Table 2). However, this improvement likely arises from the reduced size of the dataset. Furthermore, the BayMBT model does not structurally underestimate MAAT in arid regions, as was the case in previous calibrations (Fig. 3C). Therefore, we find little justification for adopting BayMBT500.

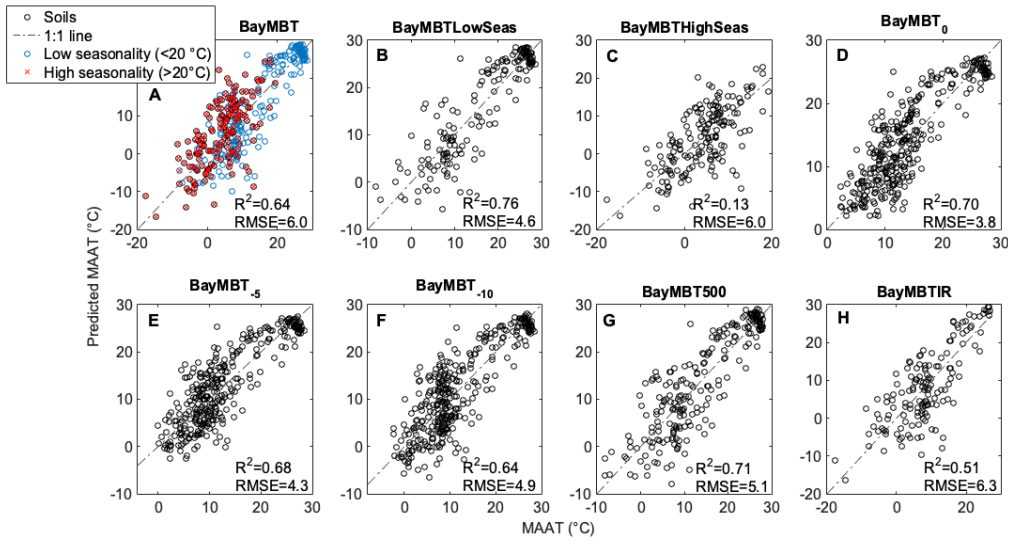

Fig. 7. Plots of instrumental MAAT vs. predicted MAAT for the eight Bayesian regression models. (A) the BayMBT model, with high (>20 °C, red cross) and low (<20, blue circle) seasonalities plotted separately. (B) the BayMBTLowSeas, (C) BayMBTHighSeas, (D) $BayMBT_0$, (E) $BayMBT_{-5}$, (F) $BayMBT_{-10}$, (G) BayMBT500, and (H) BayMBTIR models, respectively. A 1:1 reference line is added and coefficient of determination (R^2) and RMSE values are shown.

The BayMBTIR model has similar values for the coefficient of determination (R^2 = 0.64) and RMSE (5.9 °C, Table 2) to the original BayMBT model. Ergo, even though there seems to be a trend in the residuals at high IR values (Fig. 3D), removing the soils with IR >0.8 does not substantially improve the prediction of MAAT for global soils/peats. Thus, the BayMBTIR model does not offer an immediate advantage over the BayMBT model and the increased proportion of 6-methyl brGDGTs in soils as calculated by the IR index does not

appear to have a substantial impact on calibration of the brGDGT paleotemperature proxy.

4.3 Remaining scatter in the BayMBT model

Despite the better performance of the BayMBT$_0$ model, which reduces part of the scatter at mid-latitudes, the source of the persistent remaining scatter remains elusive. One possible source of this scatter is the potential offset between soil and air temperature (Weijers et al., 2011). This offset is not equal everywhere, and could account for a large proportion of residual scatter in Figs. 2C and 3. For example, Grundstein et al. (2005) found that the annual thermal offset with MAAT for soils from North Dakota experiencing a seasonal snow cover ranged between 1.5 and 4 °C, over the study period 1990 – 2001. For the soils in this study that experience snow cover, the influence of snowpack insulation on the offset between soil/air temperatures could play a significant role on predicted temperatures using the BayMBT model. Furthermore, soil temperature is not always measured, which makes reducing the scatter without these data a difficult undertaking. Consequently, these arguments indicate that MAAT is not the best temperature parameter to compare MBT′5Me indices to, and they provide support for the utilization of the BayMBT$_0$ model as an alternative calibration to predict temperatures for months >0 °C.

A second source for the large scatter at mid-latitudes could relate to the microbial community composition in soils, which may be different in cold and warm, or high and low seasonality soils (Delgado-Baquerizo et al., 2016, 2017). For instance, different communities could have distinct relations to temperature (Oliverio et al., 2017). A comprehensive investigation into this aspect is hindered by the fact that microbial communities and lipid composition in soils are not commonly analyzed together, and in fact are studied by two different fields of research. Furthermore, brGDGTs have only been identified in 2 out of 46 strains

of *Acidobacteria* (Sinninghe Damsté et al., 2018), and most of the brGDGT structures are still 'orphans'. A recent study by Oliverio et al. (2017) compared the phylotype response of temperature-sensitive soil microbes and found that the relative abundance of most (13 out of 15) phylotypes within the family *Koribacteraceae* in *Acidobacteria* decreased as temperature increases. This observation was found to hold true for other families (*Acidobacteriaceae* and *Soilbacteres*) within the *Acidobacteria* phylum, as well as some families within the *Proteobacteria* phylum, which are the two most dominant soil phyla in the Northern Hemisphere (Oliverio et al., 2017). Hence, a decrease in abundance of brGDGT producing soil bacteria in soils, and the increase of other bacteria which produce brGDGTs with distributions that have a slightly different relation to temperature, could change the dynamics of the MBT′5Me-MAAT relationship. Soils located in a region where a certain threshold temperature is reached may thus have two or more different communities of brGDGT producing bacteria with different responses to temperature change and, therefore, may, speculatively, contribute to the scatter of the BayMBT calibration.

In temperate zones (i.e. the possible convergence of different brGDGT-producing soil bacterial communities), the diversity of soil bacteria is expected to be very high, particularly in the Northern Hemisphere (Delgado-Baqueriz et al., 2016). In particular, the largest scatter around mid-latitudes in the BayMBT model is associated with soils with high seasonality >20 °C (Fig. 7A). Indeed, only 32% (53/168) of soils in the BayMBTLowSeas model reside in mid-latitudes, compared to 98% (172/175) of soils in the BayMBTHighSeas model, which may indicate that the increased diversity of brGDGT-producing soil bacteria residing at mid-latitudes leads to the scatter and low R^2 of the BayMBTHighSeas model. This finding raises two questions: (i) is there a threshold temperature at which the measured MBT′5Me signal changes, e.g. from a 'cold' to a 'warm', or 'low' to 'high' seasonality calibration? and (ii) how can it be quantified? Due to the dramatically higher R^2 value of the BayMBTLowSeas

model compared to the BayMBTHighSeas model (Table 2), the source of the scatter in the latter is more likely due to multiple bacterial communities at soils residing at mid- (and possibly high) latitudes. On a microbial level, it is not implausible that severe temperature disturbance through strong seasonal contrasts could have such an effect. However, the large scatter of (all) the calibration(s) will remain a feature as long as the individual responses to temperature of the brGDGT-producing bacteria are not fully constrained.

5. BayMBT paleoclimate application

The fact that the $BayMBT_0$ model is inclusive of all soils considered, together with the lower RMSE (3.8 °C) and lowest variance of MAAT residuals indicates that it is the most suitable calibration to apply to paleoclimate datasets. Besides, the $BayMBT_0$ model also takes the strong effect of temperature seasonality and potential seasonality of brGDGT production on the calibration models into account. Thus, we test the performance of the $BayMBT_0$ on brGDGTs in an Eocene lignite sequence from Western Europe (Inglis et al., 2017), as well as on brGDGTs in Pliocene sediments from the North Sea Basin, after correction for a possible in situ marine overprint (Dearing Crampton-Flood et al., 2018). We compare the reconstructed temperatures of these two records using the $BayMBT_0$ model with temperatures obtained using the De Jonge et al. (2014a) and Naafs et al. soil (2017a) and peat (2017b) calibrations.

5.1 Eocene climate in Western Europe

The consequence of the high upper limit of the BayMBT models (i.e. 27 °C for $BayMBT_0$) is that they can be applied to reconstruct temperatures during greenhouse periods of Earth's history, such as the Eocene. To illustrate, a recent study that used brGDGTs in a lignite sequence from western Europe to reconstruct paleotemperatures for the Eocene concluded that the magnitude for

early Eocene warming (2–3 °C) was likely a minimum estimate, as reconstructed temperatures reached up to 26 °C, thus reaching the upper limit of the proxy (Inglis et al., 2017). In contrast, temperature reconstructions for the Bighorn Basin, Wyoming based on leaf physiognomy indicate that the amplitude of warming was much larger, in the order of 4–6 °C (Wilf, 2000). This is also corroborated by TEX_{86} sea surface temperature (SST) reconstructions, which also show a warming of 4–6 °C for the same time interval in both the Western Siberian Sea (Frieling et al., 2014), and the South West Pacific (Hollis et al., 2012, Bijl et al., 2013; Inglis et al., 2015).

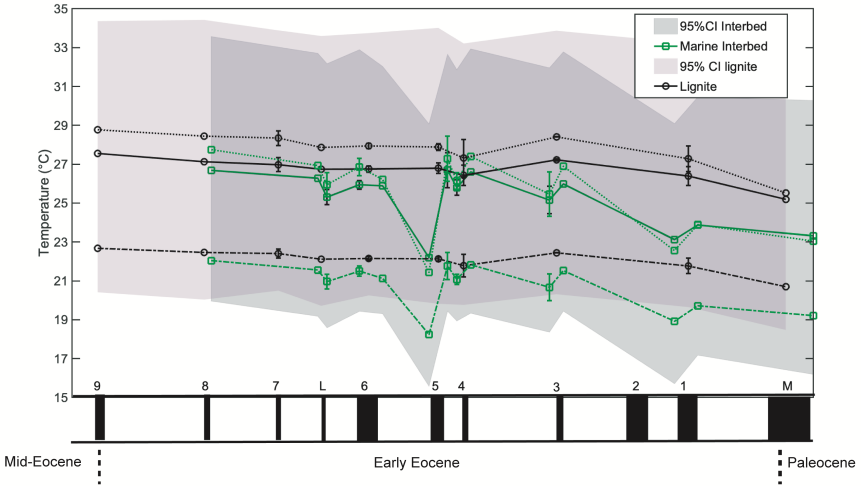

Fig. 8. Reconstructed continental temperatures during the Eocene from a series of lignites (black circles) and marine interbeds (green squares) located in the Schöningen Südfeld mine (Inglis et al., 2017). Lignite seam/marine interbed alterations and approximate ages are indicated. Note seam thickness not to scale. Temperatures reconstructed using the MBT′5Me based MAT calibrations of Naafs et al. (2017b; dotted lines), De Jonge et al. (2014a; dashed lines) and $BayMBT_0$ calibrations (solid lines). The 95 % confidence intervals for the lignite and marine interbed $BayMBT_0$ temperatures are shaded in purple and grey, respectively. Error bars are based on standard deviations of multiple samples.

Application of the $BayMBT_0$ model to reconstruct paleotemperatures in this record may potentially result in a more comparable amount of warming and thus improve the record. Due to the deep-time application, modern MAATs could not be used to estimate the prior mean. Instead, an average of the MAT_{mr}

temperatures presented in Inglis et al. (2017; 24 °C) and a suitably high prior standard deviation were chosen (15), so as not to place too much emphasis on the prior mean.

Interestingly, the $BayMBT_0$ model yields a similar estimate for the magnitude of early Eocene warming (2–3 °C) as the original MAT_{mr} and MBT′5Me-based (De Jonge et al., 2014a) temperature records (main seam to seam 3; Fig. 8; Inglis et al., 2017). Indeed, the upper limit of the $BayMBT_0$ is also reached at 27 °C, so the magnitude of early Eocene warming using this calibration may still be underestimated. The magnitude of warming using the peat calibration (Naafs et al., 2017b) is slightly higher, at 4 °C. The average early Eocene temperature of ~27 °C (Seams 3–9) predicted using $BayMBT_0$ is 4–5 °C warmer than MBT′5Me estimates using the De Jonge et al. (2014a) calibration, but 1–2 °C lower than the Naafs et al. (2017b) peat calibration (Fig. 8).

The closer absolute estimates of the $BayMBT_0$ model and the Naafs et al. (2017b) peat calibration, which has a higher saturation temperature of ~29 °C, confirms the suitability of the $BayMBT_0$ model for these types of temperature reconstructions. However, the peat calibration in this case is more able to reconstruct temperatures in the lignites, which regularly go above 27 °C (the saturation temperature of $BayMBT_0$). The absolute reconstructed continental temperatures using the $BayMBT_0$ model and the peat calibration (Naafs et al., 2017b) better fit with TEX_{86}-based early Eocene sea surface temperature reconstructions, indicating that also continental temperatures were above 25 °C at mid- and high latitudes (Frieling et al., 2014).

5.2 Pliocene climate of Northwestern Europe

A recent terrestrial temperature reconstruction of the Pliocene Northwestern Europe indicated that temperatures during the Early-Mid Pliocene were mostly stable, and fluctuated between 10–13 °C (Dearing Crampton-Flood et al., 2018).

A decrease in temperatures of ~3 °C is visible in the younger part of the record, and corresponds to the Plio-Pleistocene transition. Temperatures in the corrected record of Dearing Crampton-Flood et al. (2018) were largely comparable with temperatures reconstructed from pollen assemblages in Northwestern Europe (13–14 °C; Head, 1998; Uhl et al., 2007; Utescher et al., 2000). Thus, application of the BayMBT$_0$ model may further reduce the error associated with this record, and further constrain the temperature estimates for the Pliocene of NW Europe. The published temperature record of Dearing Crampton-Flood et al. (2018) has been corrected for possible marine overprint by 'subtracting' the marine MBT′5Me value from the total 'mixed' MBT′5Me values in the sediments. We use the corrected MBT′5Me indices, representing the terrestrial component as input for the BayMBT$_0$ model. Furthermore, a prior mean of 10 °C (modern MAAT of the Netherlands) and a prior standard deviation of 15 were chosen as model input.

The trends in the records generated by all three methods are practically identical (Fig. 9). However, BayMBT$_0$ reconstructed temperatures are higher than those of the De Jonge et al. (2014a) and Naafs et al. (2017a) soil calibrations, by 1–3 and 3–4 °C, respectively. This difference may be due to the different temperatures (i.e. all months above zero vs. annual average temperatures) that are reconstructed by the calibrations. However, pollen assemblages in this region indicate that it is unlikely that the temperatures in the Netherlands went below zero for extended amounts of time during the Pliocene (Zagwijn, 1963; Pross and Klotz, 2002), which indicates that to a large extent, the temperatures reconstructed using the BayMBT$_0$ and the De Jonge et al. (2014a) and Naafs et al. (2017a) calibrations can be directly compared. All records show a decrease in MAAT from the early Pliocene to the Pleistocene/late Pliocene, reflecting the global climate cooling that took place that the end of the Pliocene.

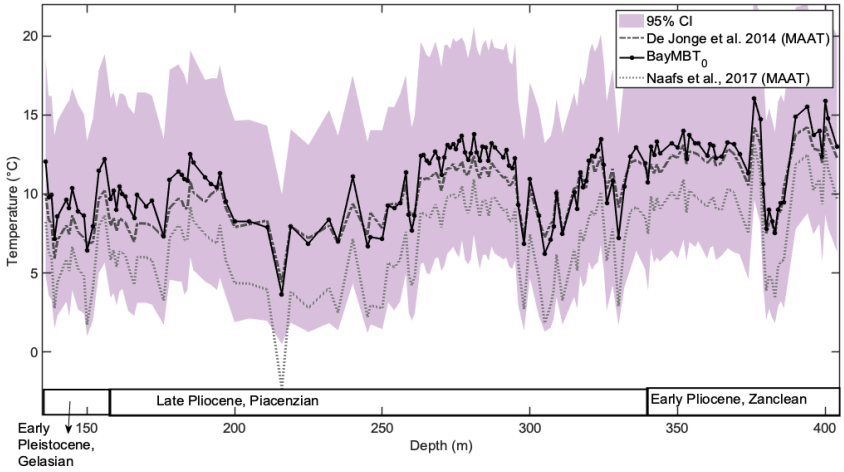

Fig. 9. Reconstructed temperatures for the Pliocene marine sediment sequence from the Hank core located in the Netherlands (Dearing Crampton-Flood et al., 2018). The $BayMBT_0$ (black line with black circles), De Jonge et al. (grey dashed line; 2014a), and Naafs et al. (dotted line; 2017a) calibrations based on a corrected MBT′5Me index are plotted against depth and relative ages based on a biostratigraphic age model of Dearing Crampton-Flood et al. (2018). The 95% confidence intervals for the $BayMBT_0$ temperatures are shaded in purple.

The slightly higher absolute $BayMBT_0$-derived temperatures for the Early and Late Pliocene (~13–16 °C) fit well with reconstructed temperatures based on pollen from Germany, England and the Lower Rhine Basin (Head, 1998; Uhl et al., 2007; Utescher et al., 2000). Moreover, temperatures from the $BayMBT_0$ model actually better agree with temperature estimates for the mid-Pliocene in Germany (13.8 ± 0.4 °C) based on the HadAM3 GCM model (Pope et al., 2000; Haywood et al., 2002; Salzmann et al., 2008) compared to the calibration used in Dearing Crampton-Flood et al. (2018). The absolute temperatures from the $BayMBT_0$ record are also associated with a smaller error (3.8 °C) than the original record, therefore increasing the reliability of the Pliocene temperature record for inclusion into climate models.

6. Conclusions

Our study presents the BayMBT model that utilizes Bayes' rule to calibrate the relationship between MBT′5Me and MAAT. The BayMBT model encompasses an expanded dataset that includes both soils and peats, and improves the coverage of the Asian continent. In this new model, the regression dilution of previous calibrations is removed, allowing for a more detailed investigation of the effects of confounding factors on the MBT′5Me for soils/peats. The largest MAAT residuals of the BayMBT model belong to mid-latitude soils with a high seasonality (>20 °C). The large scatter may speculatively be attributed to two or more co-existing communities of brGDGT-producing soil bacteria. A series of modified calibrations indicates that the most accurate temperature reconstructions can be obtained using the $BayMBT_0$ model. We propose to apply this model to paleo-datasets, providing the temperature record outcome is properly interpreted as the mean temperature of all months above 0 °C. Finally, we stress the need for studies measuring both DNA and lipids to make a step forward in constraining the temperature control on brGDGT production in soils and resolving the large scatter of MAAT residuals at mid-latitudes.

MATLAB code

The MATLAB code for the BayMBT and $BayMBT_0$ models are available on the GITHUB repository of J.E.T (https://github.com/jesstierney).

Acknowledgements

The work was supported by funding from the Netherlands Earth System Science Center (NESSC) through a gravitation grant (NWO 024.002.001) from the Dutch Ministry for Education, Culture and Science to JSSD. JET was supported by National Science Foundation grant EAR-1603674. FP acknowledges funding from ETH Fellowship FEL-36 11-1 (New Zealand soil), NWO Veni grant 863.13.016 (Indian soils), and KNAW China Exchange Program grant 530-6CDP17 (Chinese soils). We would like to thank Sebastian Breitenbach (Ruhr-University Bochum) for soil collection in Siberia. Thanks to Tian Ma and Jingjing Guo (Institute of Botany, Chinese Academy of Sciences) for help with extractions of the Chinese soils.

Appendix A

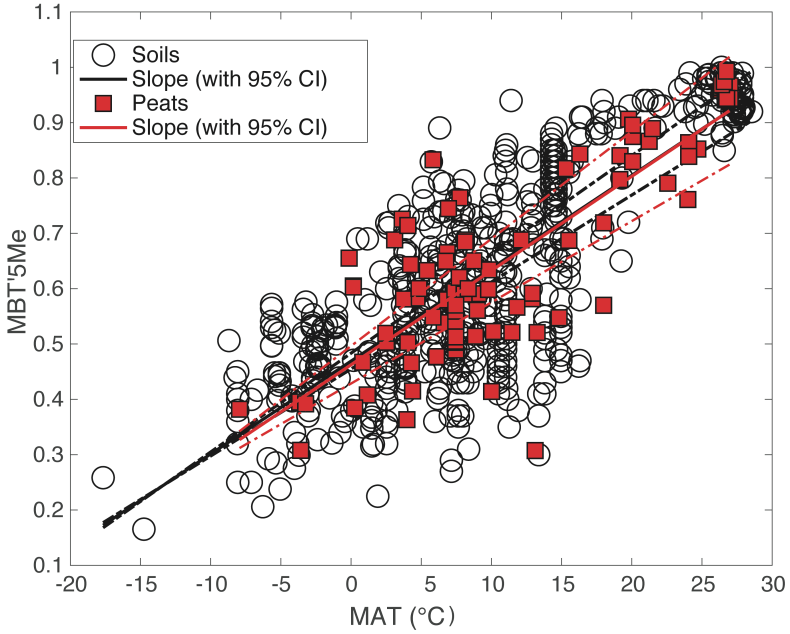

Fig. A1. Statistical similarity of the Peat (Naafs et al., 2017b) and soil calibrations

Appendix B

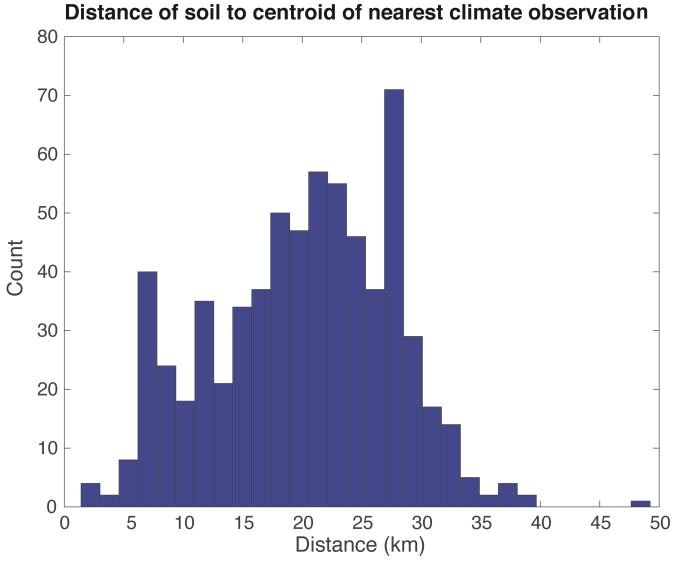

Fig. A2. Histogram of chordal distances between soil locations and gridboxes from CRU MAAT dataset (Harris et al., 2014)

References

Bachem, P.E., Risebrobakken, B., Schepper, S.D. and McClymont, E.L. (2017). Highly variable Pliocene sea surface conditions in the Norwegian Sea, Climate of the Past 13, 1153-1168.

Badger, M.P., Schmidt, D.N., Mackensen, A. and Pancost, R.D. (2013). High-resolution alkenone palaeobarometry indicates relatively stable pCO2 during the Pliocene (3.3–2.8 Ma). Philosophical Transactions of the Royal Society A 371, 20130094.

Bailey, I.W. and Sinnott, E.W. (1916). The climatic distribution of certain types of angiosperm leaves. American Journal of Botany 3, 24-39.

Baldauf, J.G., Thomas, E., Clement, B., Takayama, T., Weaver, P.P.E., Backman, J., Jenkins, G., Mudie, P.J. and Westbergsmith, M. (1987). Magnetostratigraphic and biostratigraphic synthesis, Deep-Sea Drilling Project LEG-94. Initial Reports of the Deep Sea Drilling Project 94, 1159-1205.

Bendle, J.A., Weijers, J.W., Maslin, M.A., Sinninghe Damsté, J.S., Schouten, S., Hopmans, E.C., Boot, C.S. and Pancost, R.D. (2010). Major changes in glacial and Holocene terrestrial temperatures and sources of organic carbon recorded in the Amazon fan by tetraether lipids. Geochemistry, Geophysics, Geosystems 11. doi:10.1029/2010GC003308

Benthien, A. and Müller, P.J. (2000). Anomalously low alkenone temperatures caused by lateral particle and sediment transport in the Malvinas Current region, western Argentine Basin. Deep Sea Research Part I: Oceanographic Research Papers 47, 2369-2393.

Bentley Sr, S.J., Blum, M.D., Maloney, J., Pond, L. and Paulsell, R. (2016). The Mississippi River source-to-sink system: Perspectives on tectonic, climatic, and anthropogenic influences, Miocene to Anthropocene. Earth-Science Reviews 153, 139-174.

Bernabo, J.C. (1981). Quantitative estimates of temperature changes over the last 2700 years in Michigan based on pollen data. Quaternary Research 15, 143-159.

Bijl P.K., Bendle, J.A., Bohaty S.M., Pross J., Schouten S., Tauxe L., Stickley C.E., McKay R.M., Röhl U., Olney M. and Sluijs A. (2013). Eocene cooling linked to early flow across the Tasmanian Gateway. Proceedings of the National Academy of Sciences 110, 9645-9650.

Birks, H.J.B. and Seppä, H. (2004a). Pollen-based reconstructions of late-Quaternary climate in Europe–progress, problems, and pitfalls. Acta Palaeobotanica 44, 317-334.

Birks, H.J.B., Jones, V.J., and Rose, N.L. (2004b). Recent environmental change and atmospheric contamination on Svalbard as recorded in lake sediments–synthesis and general conclusions. Journal of Paleolimnology 31, 531-546.

Boenigk, W. (2002). The Pleistocene drainage pattern in the Lower Rhine basin. Netherlands Journal of Geoscience 81, 201-209.

Boessenkool, K.P., Van Gelder, M.J., Brinkhuis, H. and Troelstra, S.R. (2001). Distribution of organic-walled dinoflagellate cysts in surface sediments from transects across the Polar Front offshore southeast Greenland. J. Quaternary Sci.: Published for the Quaternary Research Association 16, 661-666.

Boyer, T.P., J. I. Antonov, O. K. Baranova, C. Coleman, H. E. Garcia, A. Grodsky, D. R. Johnson, R. A. Locarnini, A. V. Mishonov, T.D. O'Brien, C.R. Paver, J.R. Reagan, D. Seidov, I. V. Smolyar, and M. M. Zweng. (2013). World Ocean Database 2013, NOAA Atlas NESDIS 72, S. Levitus, Ed., A. Mishonov, Technical Ed.; Silver Spring, MD, 209 pp.

Brassell, S.C., Eglinton, G., Marlowe, I.T., Pflaumann, U. and Sarnthein, M. (1986). Molecular stratigraphy: a new tool for climatic assessment. Nature 320, 129.

Brierley, C.M., Fedorov, A.V., Liu, Z., Herbert, T.D., Lawrence, K.T. and LaRiviere, J.P. (2009). Greatly expanded tropical warm pool and weakened Hadley circulation in the early Pliocene. Science 323, 1714-1718.

Brigham-Grette, J., Melles, M., Minyuk, P., Andreev, A., Tarasov, P., DeConto, R., Koenig, S., Nowaczyk, N., Wennrich, V., Rosén, P. and Haltia, E. (2013). Pliocene warmth, polar amplification, and stepped Pleistocene cooling recorded in NE Arctic Russia. Science 340, 1421-1427.

Buckles, L.K., Weijers, J.W., Verschuren, D., and Sinninghe Damsté, J.S. (2014). Sources of core and intact branched tetraether membrane lipids in the lacustrine environment: Anatomy of Lake Challa and its catchment, equatorial East Africa. Geochimica et Cosmochimica Acta 140, 106-126.

Butman, D. and Raymond, P.A. (2011). Significant efflux of carbon dioxide from streams and rivers in the United States. Nature Geoscience 4, 839.

Cacho, I., Pelejero, C., Grimalt, J.O., Calafat, A. and Canals, M. (1999). C 37 alkenone measurements of sea surface temperature in the Gulf of Lions (NW Mediterranean). Organic Geochemistry 30, 557-566.

Castañeda, I.S. and Schouten, S. (2011). A review of molecular organic proxies for examining modern and ancient lacustrine environments. Quaternary Science Reviews 30, 2851-2891.

Chapman, M.R., Shackleton, N.J., Zhao, M. and Eglinton, G. (1996). Faunal and alkenone reconstructions of subtropical North Atlantic surface hydrography and paleotemperature over the last 28 kyr. Paleoceanography 11, 343-357.

Cloern, J. E., Canuel, E. A., and Harris, D. (2002). Stable carbon and nitrogen isotope composition of aquatic and terrestrial plants of the San Francisco Bay estuarine system. Limnology and Oceanography 47, 713-729.

Clotten, C., Stein, R., Fahl, K. and De Schepper, S. (2018). Seasonal sea ice cover during the warm Pliocene: Evidence from the Iceland Sea (ODP Site 907). Earth and Planetary Science Letters 481, 61-72.

Coleman, J.M. (1988). Dynamic changes and processes in the Mississippi River delta. Geological Society of America Bulletin 100, 999-1015.

Conte, A., Papale, M., Amalfitano, S., Mikkonen, A., Rizzo, C., De Domenico, E., Michaud, L., and Lo Giudice, A. (2018). Bacterial community structure along the subtidal sandy sediment belt of a high Arctic fjord (Kongsfjorden, Svalbard Islands). Science of the Total Environment 619-620, 203-211.

Coope, G.R. (1970). Interpretations of Quaternary insect fossils. Annual review of entomology 15, 97-121.

Cox, R.T., Lumsden, D.N. and Van Arsdale, R.B. (2014). Possible relict meanders of the Pliocene Mississippi River and their implications. The Journal of Geology 122, 609-622.

Crowley, T.J. (1996). Pliocene climates: the nature of the problem. Marine Micropaleontology 27, 3-12.

Curry, W.B., Shackleton, N.J. and Richter, C. (1995). Leg 154. Synthesis. Proceedings ODP, Initial Reports 154, 421-442.

Dang X., Yang H., Naafs B. D. A., Pancost R. D., and Xie S. (2016). Evidence of moisture control on the methylation of branched glycerol dialkyl glycerol tetraethers in semi-arid and arid soils. Geochimica et Cosmochimica Acta 189, 24-36.

Dansgaard, W., Johnsen, S.J., Clausen, H.B., Dahl-Jensen, D., Gundestrup, N., Hammer, C.U. and Oeschger, H. (1984). North Atlantic climatic oscillations revealed by deep Greenland ice cores. Climate Processes and Climate Sensitivity 29, 288-298.

Davis, B. A., Brewer, S., Stevenson, A. C., and Guiot, J. (2003). The temperature of Europe during the Holocene reconstructed from pollen data. Quaternary Science Reviews 22, 1701-1716.

De Bar, M.W., Stolwijk, D.J., McManus, J.F., Sinninghe Damsté, J.S. and Schouten, S. (2018). A Late Quaternary climate record based on long-chain diol proxies from the Chilean margin. Climate of the Past 14, 783-1803.

De Jonge, C., Hopmans, E.C., Stadnitskaia, A., Rijpstra, W.I.C., Hofland, R., Tegelaar, E. and Sinninghe Damsté, J.S. (2013). Identification of novel penta-and hexamethylated branched glycerol dialkyl glycerol tetraethers in peat using HPLC–MS2, GC–MS and GC–SMB-MS. Organic Geochemistry 54, 78-82.

De Jonge, C., Hopmans, E.C., Zell, C.I., Kim, J.H., Schouten, S. and Sinninghe Damsté, J.S. (2014a). Occurrence and abundance of 6-methyl branched glycerol dialkyl glycerol tetraethers in soils: Implications for palaeoclimate reconstruction. Geochimica et Cosmochimica Acta 141, 97-112.

De Jonge, C., Stadnitskaia, A., Hopmans, E.C., Cherkashov, G., Fedotov, A. and Sinninghe Damsté, J.S. (2014b). In situ produced branched glycerol dialkyl glycerol tetraethers in suspended particulate matter from the Yenisei River, Eastern Siberia. Geochimica et Cosmochimica Acta 125, 476-491.

De Jonge, C., Stadnitskaia, A., Hopmans, E.C., Cherkashov, G., Fedotov, A., Streletskaya, I.D., Vasiliev, A.A. and Sinninghe Damsté, J.S. (2015). Drastic changes in the distribution of branched tetraether lipids in suspended matter and sediments from the Yenisei River and Kara Sea (Siberia): Implications for the use of brGDGT-based proxies in coastal marine sediments. Geochimica et Cosmochimica Acta 165, 200-225.

De Schepper, S., Head, M. J., and Louwye, S. (2004). New dinoflagellate cyst and incertae sedis taxa from the Pliocene of northern Belgium, southern North Sea Basin. Journal of Paleontology 78, 625-644.

De Schepper, S. and Head, M.J. (2008). Age calibration of dinoflagellate cyst and acritarch events in the Pliocene–Pleistocene of the eastern North Atlantic (DSDP Hole 610A). Stratigraphy 5, 137-161.

De Schepper, S., Head, M.J. and Groeneveld, J. (2009a). North Atlantic Current variability through marine isotope stage M2 (circa 3.3 Ma) during the mid-Pliocene. Paleoceanography and Paleoclimatology 24, https://doi.org/10.1029/2008PA001725.

De Schepper, S., and Head, M. J. (2009b). Pliocene and Pleistocene dinoflagellate cyst and acritarch zonation of DSDP Hole 610A, eastern North Atlantic. Palynology 33, 179-218.

De Schepper, S., Fischer, E.I., Groeneveld, J., Head, M.J. and Matthiessen, J. (2011). Deciphering the palaeoecology of Late Pliocene and Early Pleistocene dinoflagellate cysts. Palaeogeography, Palaeoclimatology, Palaeoecology 309, 17-32.

De Schepper, S., Groeneveld, J., Naafs, B.D.A., Van Renterghem, C., Hennissen, J., Head, M. J., Louwye, S., Fabian, K. (2013). Northern hemisphere glaciation during the globally warm early late Pliocene. PLoS One 8, e81508.

De Schepper, S., Gibbard, P.L., Salzmann, U. and Ehlers, J. (2014). A global synthesis of the marine and terrestrial evidence for glaciation during the Pliocene Epoch. Earth-Science Reviews 135, 83-102.

De Schepper, S., Schreck, M., Beck, K.M., Matthiessen, J., Fahl, K., & Mangerud, G. (2015). Early Pliocene onset of modern Nordic Seas circulation related to ocean gateway changes. Nature Communications 6. doi:10.1038/ncomms9659

De Schepper, S., Beck, K. M., & Mangerud, G. (2017). Late Neogene dinoflagellate cyst and acritarch biostratigraphy for Ocean Drilling Program Hole 642B, Norwegian Sea. Review of Palaeobotany and Palynology 236, 12-32.

De Wet, G. A., Castañeda, I. S., DeConto, R. M., & Brigham-Grette, J. (2016). A high-resolution mid-Pleistocene temperature record from Arctic Lake El'gygytgyn: a 50 kyr super interglacial from MIS 33 to MIS 31? Earth and Planetary Science Letters 436, 56-63.

Dearing Crampton-Flood, E., Peterse, F., Munsterman, D. and Sinninghe Damsté, J.S. (2018). Using tetraether lipids archived in North Sea Basin sediments to extract North Western European Pliocene continental air temperatures. Earth and Planetary Science Letters 490, 193-205.

Delaygue, G., Bard, E., Rollion, C., Jouzel, J., Stiévenard, M., Duplessy, J.C. and Ganssen, G. (2001). Oxygen isotope/salinity relationship in the northern Indian

Ocean. Journal of Geophysical Research-Oceans 106, 4565-4574.

Delgado-Baquerizo M., Maestre F. T., Reich P. B., Trivedi P., Osana, Y., Liu Y. R., Hamonts K., Jeffries T.C. and Singh B. K. (2016). Carbon content and climate variability drive global soil bacterial diversity patterns. Ecological Monographs 86, 373-390.

Delgado-Baquerizo M., Bissett A., Eldridge D. J., Maestre F. T., He J. Z., Wang J. T., Hamonts K., Liu Y.R., Singh B.K. and Fierer N. (2017). Palaeoclimate explains a unique proportion of the global variation in soil bacterial communities. Nature Ecology & Evolution 1, 1339.

Deng L., Jia G., Jin C., and Li S. (2016). Warm season bias of branched GDGT temperature estimates causes underestimation of altitudinal lapse rate. Organic Geochemistry 96, 11-17.

Ding, S., Xu, Y., Wang, Y., He, Y., Hou, J., Chen, L. and He, J.S. (2015). Distribution of branched glycerol dialkyl glycerol tetraethers in surface soils of the Qinghai–Tibetan Plateau: implications of brGDGTs-based proxies in cold and dry regions. Biogeosciences 12, 3141-3151.

Dirghangi S. S., Pagani M., Hren M. T., and Tipple B. J. (2013). Distribution of glycerol dialkyl glycerol tetraethers in soils from two environmental transects in the USA. Organic Geochemistry 59, 49-60.

Donders, T.H., Kloosterboer-van Hoeve, M.L., Westerhoff, W., Verreussel, R.M. and Lotter, A.F. (2007). Late Neogene continental stages in NW Europe revisited. Earth-Science Reviews 85, 161-186.

Donders, T.H., Weijers, J.W.H., Munsterman, D.K., Kloosterboer-van Hoeve, M.L., Buckles, L.K., Pancost, R.D., Schouten, S., Sinninghe Damsté, J.S. and Brinkhuis, H. (2009). Strong climate coupling of terrestrial and marine environments in the Miocene of northwest Europe. Earth and Planetary Science Letters 281, 215-225.

Donders, T.H., van Helmond, N.A., Verreussel, R., Munsterman, D., ten Veen, J., Speijer, R., Weijers, J.W., Sangiorgi, F., Peterse, F., Reichart, G.J. and Sinninghe Damsté, J.S. (2018). Land-sea coupling of early Pleistocene glacial cycles in the southern North Sea exhibit dominant Northern Hemisphere forcing. Climate of the Past 14, 397-411.

Dorale, J.A., Edwards, R.L., Alexander, E.C., Shen, C.C., Richards, D.A. and Cheng, H. (2004). Uranium-series dating of speleothems: current techniques, limits, & applications. In Studies of Cave Sediments (177-197). Springer, Boston, MA.

Dowsett, H., Thompson, R., Barron, J., Cronin, T., Fleming, F., Ishman, S., Poore, R., Willard, D. and Holtz Jr, T. (1994). Joint investigations of the Middle Pliocene climate I: PRISM paleoenvironmental reconstructions. Global and Planetary Change 9, 169-195.

Dowsett, H.J., Robinson, M.M. and Foley, K.M. (2009). Pliocene three-dimensional global ocean temperature reconstruction. Climate of the Past 5, 769-783.

Dowsett, H., Robinson, M., Haywood, A.M., Salzmann, U., Hill, D., Sohl, L.E., Chandler, M., Williams, M., Foley, K. and Stoll, D.K. (2010). The PRISM3D paleoenvironmental reconstruction. Stratigraphy 7, 123-139.

Dowsett, H.J., Robinson, M.M., Haywood, A.M., Hill, D.J., Dolan, A.M., Stoll, D.K., Chan, W.L., Abe-Ouchi, A., Chandler, M.A., Rosenbloom, N.A. and Otto-Bliesner, B.L. (2012). Assessing confidence in Pliocene sea surface temperatures to evaluate predictive models. Nature Climate Change 2, 365.

Dowsett, H.J., Robinson, M.M., Stoll, D.K., Foley, K.M., Johnson, A.L., Williams, M. and Riesselman, C.R. (2013). The PRISM (Pliocene palaeoclimate) reconstruction: time for a paradigm shift. Philosophic Transactions of the Royal Society A 371, 20120524.

Draut, A.E., Raymo, M.E., McManus, J.F. and Oppo, D.W. (2003). Climate stability during the Pliocene warm period. Paleoceanography 18, https://doi.org/10.1029/2003PA000889.

Drotz S. H., Sparrman T., Nilsson M. B., Schleucher J., and Öquist M. G. (2010). Both catabolic and anabolic heterotrophic microbial activity proceed in frozen soils. Proceedings of the National Academy of Sciences 107, 21046-21051.

Dybkjaer, K., and Piasecki, S. (2010). Neogene dinocyst zonation for the eastern North Sea Basin, Denmark. Review of Palaeobotany and Palynology 161, 1-29.

Elsik, W.C., Late Neogene palynomorph diagram, northern Gulf of Mexico. Gulf Coast Association of Geological Societies Transactions 19, 509-528

Emiliani, C. (1955). Pleistocene temperatures. The Journal of Geology 63, 538-578.

Faegri, K., Iversen, J., Kaland, P. E., and Krzywinski, K. (1989). Text book of pollen analysis, IV Edition, The Blackburn Press, New Jersey, USA, 328.

Fauquette, S., Guiot, J. and Suc, J.P. (1998). A method for climatic reconstruction of the Mediterranean Pliocene using pollen data. Palaeogeography, Palaeoclimatology, Palaeoecology 144, 183-201.

Figueiredo, J.J.J.P., Hoorn, C., Van der Ven, P. and Soares, E. (2009). Late Miocene onset of the Amazon River and the Amazon deep-sea fan: Evidence from the Foz do Amazonas Basin. Geology 37, 619-622.

Freymond, C.V., Peterse, F., Fischer, L.V., Filip, F., Giosan, L. and Eglinton, T.I. (2017). Branched GDGT signals in fluvial sediments of the Danube River basin: Method comparison and longitudinal evolution. Organic Geochemistry 103, 88-96.

Frieling J., Iakovleva A.I., Reichart G.J., Aleksandrova G.N., Gnibidenko Z.N., Schouten S. and Sluijs A. (2014). Paleocene–Eocene warming and biotic response in the epicontinental West Siberian Sea. Geology 42, 767-770.

Fronval, T., and Jansen, E. (1996). Late Neogene paleoclimates and paleoceanography in the Iceland-Norwegian Sea: evidence from the Iceland and Vøring Plateaus. In Proceedings of the Ocean Drilling Program. Scientific Results 151, 455-468.

Fujine, K., Yamamoto, M., Tada, R. and Kido, Y. (2006). A salinity-related occurrence of a novel alkenone and alkenoate in Late Pleistocene sediments from

the Japan Sea. Organic Geochemistry 37, 1074-1084.

Funnell, B.M. (1996). Plio-Pleistocene palaeogeography of the southern North Sea basin (3.75-0.60 Ma). Quaternary Science Reviews 15, 391-405.

Galloway, W.E., Whiteaker, T.L. and Ganey-Curry, P. (2011). History of Cenozoic North American drainage basin evolution, sediment yield, and accumulation in the Gulf of Mexico basin. Geosphere 7, 938-973.

Gelin, F., Boogers, I., Noordeloos, A.A., Sinninghe Damsté, J.S., Riegman, R. and De Leeuw, J.W. (1997). Resistant biomacromolecules in marine microalgae of the classes Eustigmatophyceae and Chlorophyceae: geochemical implications. Organic Geochemistry 26, 659-675.

Gelman A. (2003). A Bayesian Formulation of Exploratory Data Analysis and Goodness-of-fit Testing. International Statistical Review 71, 369-382.

Gibbard, P.L. (1988). The history of the great northwest European rivers during the past three million years. Philosophic Transactions of the Royal Society London B, 318, 559-602.

Gibbard, P.L. and Lewin, J. (2003). The history of the major rivers of southern Britain during the Tertiary. Journal of the Geological Society London 160, 829-845.

Gibbard, P.L. and Lewin, J. (2016). Filling the North Sea Basin: Cenozoic sediment sources and river styles (André Dumont medallist lecture 2014). Geol. Belg., http://dx.doi.org/10.20341/gb.2015.017.

Graumlich, L.J. and Brubaker, L.B. (1986). Reconstruction of annual temperature (1590–1979) for Longmire, Washington, derived from tree rings. Quaternary Research 25, 223-234.

Grundstein A., Todhunter P., and Mote T. (2005). Snowpack control over the thermal offset of air and soil temperatures in eastern North Dakota. Geophysical Research Letters 32. DOI: 10.1029/2005GL022532

Guiot, J. (1990). Methodology of the last climatic cycle reconstruction in France from pollen data. Palaeogeography, Palaeoclimatology, Palaeoecology 80, 49-69.

Harada, N., Sato, M. and Sakamoto, T. (2008). Freshwater impacts recorded in tetraunsaturated alkenones and alkenone sea surface temperatures from the Okhotsk Sea across millennial-scale cycles. Paleoceanography 23, https://doi-org.proxy.library.uu.nl/10.1029/2006PA001410.

Harding, R. (2015). Evolution of the Giant Southern North Sea Shelf-Prism: Testing sequence stratigraphic concepts and the global sea level curve with full-three dimensional control. Doctoral dissertation, The University of Manchester (United Kingdom).

Harris, I. P. D. J., Jones, P. D., Osborn, T. J., and Lister, D. H. (2014). Updated high-resolution grids of monthly climatic observations–the CRU TS3. 10 Dataset. International Journal of Climatology 34, 623-642.

Harvey, H.R., Fallon, R.D. and Patton, J.S. (1986). The effect of organic matter and oxygen on the degradation of bacterial membrane lipids in marine sediments. Geochimica et Cosmochimica Acta 50, 795-804.

Haug, G.H. and Tiedemann, R. (1998). Effect of the formation of the Isthmus of Panama on Atlantic Ocean thermohaline circulation. Nature 393, 673.

Haywood A.M., Valdes P.J., Francis J.E. and Sellwood B.W. (2002). Global middle Pliocene biome reconstruction: A data/model synthesis. Geochemistry, Geophysics, Geosystems, 3, 1-18.

Haywood, A.M., Hill, D.J., Dolan, A.M., Otto-Bliesner, B.L., Bragg, F., Chan, W.L., Chandler, M.A., Contoux, C., Dowsett, H.J., Jost, A. and Kamae, Y. (2013). Large-scale features of Pliocene climate: results from the Pliocene Model Intercomparison Project. Climate of the Past 9, 191-209.

Haywood, A.M., Dowsett, H.J. and Dolan, A.M. (2016a). Integrating geological archives and climate models for the mid-Pliocene warm period. Nature Communications 7, 10646.

Haywood, A. M., Dowsett, H. J., Dolan, A. M., Chandler, M. A., Hunter, S. J., and Lunt, D. J. (2016b). The Pliocene Model Intercomparison Project (PlioMIP) Phase 2: scientific objectives and experimental design. Climate of the Past 12, 663.

He, M., Zheng, H., Huang, X., Jia, J. and Li, L. (2013). Yangtze River sediments from source to sink traced with clay mineralogy. Journal of Asian Earth Sciences 69, 60-69.

Head, M.J., Norris, G., and Mudie, P. J. (1989). New species of dinocysts and a new species of acritarch from the upper Miocene and lowermost Pliocene, ODP Leg 105, Site 646, Labrador Sea. In Proceedings of the Ocean Drilling Program, Scientific Results 105, 453-466.

Head, M.J. (1996). Modern dinoflagellate cysts and their biological affinities, in: Palynology: Principles and Application, Vol. 3, edited by: Jansonius, J. and McGregor, D. C., American Association of Stratigraphic Palynologists Foundation, College Station, Texas, USA, 1197–1248.

Head, M.J. (1998). Pollen and dinoflagellates from the Red Crag at Walton-on-the-Naze, Essex: evidence for a mild climatic phase during the early Late Pliocene of eastern England. Geological Magazine 135, 803-817.

Heiri, O., Lotter, A.F., Hausmann, S. and Kienast, F. (2003). A chironomid-based Holocene summer air temperature reconstruction from the Swiss Alps. The Holocene 13, 477-484.

Hendy, C.H. and Wilson, A.T. (1968). Palaeoclimatic data from speleothems. Nature 219, 48.

Hennissen, J.A., Head, M.J., De Schepper, S. and Groeneveld, J. (2014). Palynological evidence for a southward shift of the North Atlantic Current at ~2.6 Ma during the intensification of late Cenozoic Northern Hemisphere glaciation. Paleoceanography and Paleoclimatology 29, 564-580.

Hennissen, J.A., Head, M.J., De Schepper, S. and Groeneveld, J. (2017). Dinoflagellate cyst paleoecology during the Pliocene–Pleistocene climatic transition in the

North Atlantic. Palaeogeography, Palaeoclimatology, Palaeoecology 470, 81-108.

Herbert, T. D., Peterson, L. C., Lawrence, K. T., and Liu, Z. (2010). Tropical ocean temperatures over the past 3.5 million years. Science 328, 1530-1534.

Herfort, L., Schouten, S., Boon, J.P., Woltering, M., Baas, M., Weijers, J.W., and Sinninghe Damsté, J.S. (2006). Characterization of transport and deposition of terrestrial organic matter in the southern North Sea using the BIT index. Limnology and Oceanography 51, 2196-2205.

Heusser, L. E. and Shackleton, N. J. (1979). Direct marinecontinental correlation: 150,000-year oxygen isotope-pollen record from the North Pacific. Science 204, 837–839.

Hodgson, G.E. and Funnell, B.M. (1987). Foraminiferal biofacies of the early Pliocene Coralline Crag. Micropalaeontology of Carbonate Environments. British Micropalaeontological Society Series. Ellis Horwood Ltd., Chichester, UK, 44-73.

Hollis C.J., Taylor K.W., Handley L., Pancost R.D., Huber M., Creech J.B., Hines B.R., Crouch E.M., Morgans H.E., Crampton J.S. and Gibbs S. (2012). Early Paleogene temperature history of the Southwest Pacific Ocean: Reconciling proxies and models. Earth and Planetary Science Letters 349, 53-66.

Hop, H., Pearson, T., Hegseth, E.N., Kovacs, K.M., Wiencke, C., Kwasniewski, S., Eiane, K., Mehlum, F., Gulliksen, B., Wlodarska-Kowalczuk, M., and Lydersen, C. (2002). The marine ecosystem of Kongsfjoren, Svalbard. Polar Research 21, 167-208.

Hopmans, E.C., Weijers, J.W., Schefuß, E., Herfort, L., Sinninghe Damsté, J.S. and Schouten, S. (2004). A novel proxy for terrestrial organic matter in sediments based on branched and isoprenoid tetraether lipids. Earth and Planetary Science Letters 224, 107-116.

Hopmans, E.C., Schouten, S. and Sinninghe Damsté, J.S. (2016). The effect of improved chromatography on GDGT-based palaeoproxies. Organic Geochemistry 93, 1-6.

Hughes, M.K. (2002). Dendrochronology in climatology–the state of the art. Dendrochronologia, 20, 95-116.

Huguet, C., Hopmans, E.C., Febo-Ayala, W., Thompson, D.H., Sinninghe Damsté, J.S. and Schouten, S. (2006). An improved method to determine the absolute abundance of glycerol dibiphytanyl glycerol tetraether lipids. Organic Geochemistry 37, 1036-1041.

Huguet A., Francez A. J., Jusselme M. D., Fosse C., and Derenne S. (2014). A climatic chamber experiment to test the short term effect of increasing temperature on branched GDGT distribution in Sphagnum peat. Organic Geochemistry 73, 109-112.

Inglis G.N., Farnsworth A., Lunt D., Foster G.L., Hollis C.J., Pagani M., Jardine P.E., Pearson P.N., Markwick P., Galsworthy A.M. and Raynham L. (2015). Descent toward the Icehouse: Eocene sea surface cooling inferred from GDGT distributions. Paleoceanography and Paleoclimatology 30, 1000-1020.

Inglis G.N., Collinson M.E., Riegel W., Wilde V., Farnsworth A., Lunt D.J., Valdes P., Robson B.E., Scott A.C., Lenz O.K. and Naafs B.D.A. (2017). Mid-latitude continental temperatures through the early Eocene in western Europe. Earth and Planetary Science Letters 460, 86-96.

IPCC, 2014: Climate Change 2014: Synthesis Report. Contribution of Working Groups I, II and III to the Fifth Assessment Report of the Intergovernmental Panel on Climate Change [Core Writing Team, R.K. Pachauri and L.A. Meyer (eds.)]. IPCC, Geneva, Switzerland, 151 pp.

IPCC, 2018: Global warming of 1.5°C. An IPCC Special Report on the impacts of global warming of 1.5°C above pre-industrial levels and related global greenhouse gas emission pathways, in the context of strengthening the global response to the threat of climate change, sustainable development, and efforts to eradicate poverty [V. Masson-Delmotte, P. Zhai, H. O. Pörtner, D. Roberts, J. Skea, P.R. Shukla, A. Pirani, W. Moufouma-Okia, C. Péan, R. Pidcock, S. Connors, J. B. R. Matthews, Y. Chen, X. Zhou, M. I. Gomis, E. Lonnoy, T. Maycock, M. Tignor, T. Waterfield (eds.)]. In Press.

Jacobs, Z. (2008). Luminescence chronologies for coastal and marine sediments. Boreas 37, 508-535.

Jansen, H.S.M., Huizer, J., Dijkmans, J.W.A., Mesdag, C. and Van Hinte, J.E. (2004). The geometry and stratigraphic position of the Maassluis Formation (western Netherlands and southeastern North Sea). Netherlands Journal of Geosciences 83, 93-99.

Janssen, N., and Dammers, G. (2008). Sample Processing for Pre-Quaternary Palynology. Internal TNO Report.

Jernas, P., Klitgaard-Kristensen, D., Husum, K., Koç, N., Tverberg, V., Loubere, P., Prins, M., Dijkstra, N., and Gluchowska, M. (2018). Annual changes in Arctic fjord environment and modern benthic foraminiferal fauna: Evidence from Kongsfjorden, Svalbard. Global and Planetary Change 163, 119-140.

Jimenez-Moreno, G., Head, M. J., and Harzhauser, M. (2006). Early and Middle Miocene dinoflagellate cyst stratigraphy of the central Paratethys, central Europe. Journal of Micropalaeontology 25, 113-139.

Johnson, A.L., Hickson, J.A., Bird, A., Schöne, B.R., Balson, P.S., Heaton, T.H. and Williams, M. (2009). Comparative sclerochronology of modern and mid-Pliocene (c. 3.5 Ma) Aequipecten opercularis (Mollusca, Bivalvia): an insight into past and future climate change in the north-east Atlantic region. Palaeogeography, Palaeoclimatology, Palaeoecology 284, 164-179.

Jourabchi, P., Meile, C., Pasion, L.R., and Van Cappellen, P. (2008). Quantitative interpretation of pore water O2 and pH distributions in deep-sea sediments. Geochimica et Cosmochimica Acta 72, 1350-1364.

Jouzel, J., Lorius, C., Petit, J.R., Genthon, C., Barkov, N.I., Kotlyakov, V.M. and Petrov, V.M. (1987). Vostok ice core: a continuous isotope temperature record over the last climatic cycle (160,000 years). Nature 329, 403.

Jouzel, J., Masson-Delmotte, V., Cattani, O., Dreyfus, G., Falourd, S., Hoffmann, G., Minster, B., Nouet, J., Barnola, J.M., Chappellaz, J. and Fischer, H. (2007). Orbital and millennial Antarctic climate variability over the past 800,000 years. Science 317, 793-796.

Joyce, J.E., Tjalsma, L.R. and Prutzman, J.M. (1990). High-resolution planktic stable isotope record and spectral analysis for the last 5.35 MY: Ocean Drilling Program Site 625 northeast Gulf of Mexico. Paleoceanography 5, 507-529.

Keeling, Ralph, F., Keeling, and Charles, D., (2017). Atmospheric Monthly In Situ CO2 Data – Mauna Loa Observatory, Hawaii. In Scripps CO2 Program Data. UC San Diego Library Digital Collections. http://doi.org/10.6075/J08W3BHW

Keigwin, L.D., Curry, W.B., Lehman, S.J. and Johnsen, S. (1994). The role of the deep ocean in North Atlantic climate change between 70 and 130 kyr ago. Nature 371, 323.

Keisling, B.A., Castañeda, I.S., and Brigham-Grette, J. (2017). Hydrological and temperature change in Arctic Siberia during the intensification of Northern Hemisphere Glaciation. Earth and Planetary Science Letters 457, 136-148.

Keller, G. (1978). Late Neogene biostratigraphy and paleoceanography of DSDP Site 310 Central North Pacific and correlation with the Southwest Pacific. Marine micropaleontology 3, 97-119.

Kemna, H.A. and Westerhoff, W.E. (2007). Remarks on the palynology-based chronostratigraphical subdivision of Pliocene terrestrial deposits in NW-Europe. Quaternary International 164, 184-196.

Kemp, D.B., Robinson, S.A., Crame, J.A., Francis, J.E., Ineson, J., Whittle, R.J., Bowman, V. and O'Brien, C. (2014). A cool temperate climate on the Antarctic Peninsula through the latest Cretaceous to early Paleogene. Geology 42, 583-586.

Kim, J.H., Schouten, S., Buscail, R., Ludwig, W., Bonnin, J., Sinninghe Damsté, J.S., and Bourrin, F. (2006). Origin and distribution of terrestrial organic matter in the NW Mediterranean (Gulf of Lions): Exploring the newly developed BIT index. Geochemistry, Geophysics, Geosystems 7.https://doi.org/10.1029/2006GC001306.

Kim, J.H., Ludwig, W., Schouten, S., Kerhervé, P., Herfort, L., Bonnin, J., and Sinninghe Damsté, J.S. (2007). Impact of flood events on the transport of terrestrial organic matter to the ocean: a study of the Têt River (SW France) using the BIT index. Organic Geochemistry 38, 1593-1606.

Kim, J.H., Van der Meer, J., Schouten, S., Helmke, P., Willmott, V., Sangiorgi, F., Koç, N., Hopmans, E.C. and Sinninghe Damsté, J.S. (2010). New indices and calibrations derived from the distribution of crenarchaeal isoprenoid tetraether lipids: Implications for past sea surface temperature reconstructions. Geochimica et Cosmochimica Acta 74, 4639-4654.

Kirkels, F.M.S.A., Ponton, C., Galy, V., West, A.J., Feakins, S.J., Peterse, F.. From Andes to Amazon: assessing branched tetraether lipids as tracers for soil OC in the Madre de Dios River system. In prep.

Knox, R.W.O'B., Bosch, J.H.A., Rasmussen, E.S., Heilmann-Clausen, C., Hiss, M., De Lugt, I.R., Kasiński, J., King, C., Köthe, A., Słodkowska, B., Standke, G. and Vandenberghe, N. (2010). Cenozoic. In Doornenbal, J.C. & Stevenson, A.G. (eds), Petroleum geological atlas of the Southern Permian Basin area. EAGE Publications b.v., Houten, 211-223.

Koga, Y., Nishihara, M., Morii, H., and Akagawa-Matsushita, M. (1993). Ether polar lipids of methanogenic bacteria: structures, comparative aspects, and biosyntheses. Microbiology and Molecular Biology Reviews 57, 164-182.

Kotthoff, U., Greenwood, D. R., McCarthy, F. M. G., MüllerNavarra, K., Prader, S., and Hesselbo, S. P. (2014). Late Eocene to middle Miocene (33 to 13 million years ago) vegetation and climate development on the North American Atlantic Coastal Plain (IODP Expedition 313, Site M0027), Climate of the Past 10, 1523–1539.

Kovach, W.L. and Spicer, R.A. (1996). Canonical correspondence analysis of leaf physiognomy: a contribution to the development of a new palaeoclimatological tool. Paleoclimates 2, 125-138.

Krantz, D.E. (1991). A chronology of Pliocene sea-level fluctuations: The US Middle Atlantic Coastal Plain record. Quaternary Science Reviews 10, 163-174.

Kuhlmann, G. (2004). High resolution stratigraphy and paleoenvironmental changes in the southern North Sea during the Neogene – an integrated study of Late Cenozoic marine deposits from the northern part of the Dutch offshore area. PhD Thesis, Utrecht University (The Netherlands).

Kuhlmann, G., Langereis, C., Munsterman, D., van Leeuwen, R.J., Verreussel, R., Meulenkamp, J. and Wong, T. (2006). Chronostratigraphy of Late Neogene sediments in the southern North Sea Basin and paleoenvironmental interpretations. Palaeogeography, Palaeoclimatology, Palaeoecology 239, 426-455.

Kuhlmann, G. and Wong, T.E. (2008). Pliocene paleoenvironment evolution as interpreted from 3D-seismic data in the southern North Sea, Dutch offshore sector. Marine and Petrology Geology 25, 173-189.

Lammertsma, E.I., Troelstra, S.R., Flores, J.A., Sangiorgi, F., Chemale, F., do Carmo, D.A. and Hoorn, C. (2018). Primary productivity in the western tropical Atlantic follows Neogene Amazon River evolution. Palaeogeography, Palaeoclimatology, Palaeoecology 506, 12-21.

Lara, A. and Villalba, R. (1993). A 3620-year temperature record from Fitzroya cupressoides tree rings in southern South America. Science 260, 1104-1106.

Larsson, L.M., Dybkjær, K., Rasmussen, E.S., Piasecki, S., Utescher, T. and Vajda, V. (2011). Miocene climate evolution of northern Europe: A palynological investigation from

Denmark. Palaeogeography, Palaeoclimatology, Palaeoecology 309, 161-175.

Lattaud, J., Kim, J.H., De Jonge, C., Zell, C., Sinninghe Damsté, J.S. and Schouten, S. (2017). The C 32 alkane-1, 15-diol as a tracer for riverine input in coastal seas. Geochimica et Cosmochimica Acta 202, 146-158.

Lattaud, J., Lo, L., Huang, J.J., Chou, Y.M., Gorbarenko, S.A., Sinninghe Damsté, J.S. and Schouten, S. (2018). A Comparison of Late Quaternary Organic Proxy-Based Paleotemperature Records of the Central Sea of Okhotsk. Paleoceanography and Paleoclimatology 33, 732-744.

Lauber C. L., Hamady M., Knight R., and Fierer N. (2009). Pyrosequencing-based assessment of soil pH as a predictor of soil bacterial community structure at the continental scale. Applied and environmental microbiology 75, 5111-5120.

Lawrence, K.T., Herbert, T.D., Brown, C.M., Raymo, M.E. and Haywood, A.M. (2009). High-amplitude variations in North Atlantic sea surface temperature during the early Pliocene warm period. Paleoceanography 24. https://doi.org/10.1029/2008PA001669.

Lear, C.H., Elderfield, H. and Wilson, P.A. (2000). Cenozoic deep-sea temperatures and global ice volumes from Mg/Ca in benthic foraminiferal calcite. Science 287, 269-272.

Lei Y., Yang H., Dang X., Zhao S., and Xie S. (2016). Absence of a significant bias towards summer temperature in branched tetraether-based paleothermometer at two soil sites with contrasting temperature seasonality. Organic Geochemistry 94, 83-94.

Li, Z., Peterse, F., Wu, Y., Bao, H., Eglinton, T.I. and Zhang, J. (2015). Sources of organic matter in Changjiang (Yangtze River) bed sediments: preliminary insights from organic geochemical proxies. Organic Geochemistry 85, 11-21.

Libby, L.M. and Pandolfi, L.J. (1974). Temperature dependence of isotope ratios in tree rings. Proceedings of the National Academy of Sciences 71, 2482-2486.

Limoges, A., de Vernal, A. and Van Nieuwenhove, N. (2014). Long-term hydrological changes in the northeastern Gulf of Mexico (ODP-625B) during the Holocene and late Pleistocene inferred from organic-walled dinoflagellate cysts. Palaeogeography, Palaeoclimatology, Palaeoecology 414, 178-191.

Lisiecki, L.E. and Raymo, M.E. (2005). A Pliocene-Pleistocene stack of 57 globally distributed benthic δ18O records. Paleoceanography 20. https://doi-org.proxy.library.uu.nl/10.1029/2004PA001071

Liu, W., Huang, Y., An, Z., Clemens, S.C., Li, L., Prell, W.L. and Ning, Y. (2005). Summer monsoon intensity controls C4/C3 plant abundance during the last 35 ka in the Chinese Loess Plateau: carbon isotope evidence from bulk organic matter and individual leaf waxes. Palaeogeography, Palaeoclimatology, Palaeoecology 220, 243-254.

Liu, X.L., Zhu, C., Wakeham, S.G., and Hinrichs, K.U. (2014). In situ production of branched glycerol dialkyl glycerol tetraethers in anoxic marine water columns. Marine Chemistry 166, 1-8.

Locarnini, R. A., A. V. Mishonov, J. I. Antonov, T. P. Boyer, H. E. Garcia, O. K. Baranova, M. M. Zweng, C. R. Paver, J. R. Reagan, D. R. Johnson, M. Hamilton, and D. Seidov. (2013). World Ocean Atlas 2013, Volume 1: Temperature. S. Levitus, Ed., A. Mishonov Technical Ed.; NOAA Atlas NESDIS 73, 40.

Long, P.E. and Zalasiewicz, J.A. (2011). The molluscan fauna of the Coralline Crag (Pliocene, Zanclean) at Raydon Hall, Suffolk, UK: palaeoecological significance reassessed. Palaeogeography, Palaeoclimatology, Palaeoecology 309, 53-72.

Loomis, S.E., Russell, J.M., Heureux, A.M., D'Andrea, W.J., and Sinninghe Damsté, J.S. (2014). Seasonal variability of branched glycerol dialkyl glycerol tetraethers (brGDGTs) in a temperate lake system. Geochimica et Cosmochimica Acta 144, 173-187.

Lopes Dos Santos, R.A., Spooner, M.I., Barrows, T.T., De Deckker, P., Sinninghe Damsté, J.S. and Schouten, S. (2013). Comparison of organic (UK'37, TEXH86, LDI) and faunal proxies (foraminiferal assemblages) for reconstruction of late Quaternary sea surface temperature variability from offshore southeastern Australia. Paleoceanography 28, 377-387.

Lorius, C., Raynaud, D., Petit, J.R., Jouzel, J. and Merlivat, L. (1984). Late-glacial maximum-Holocene atmospheric and ice-thickness changes from Antarctic ice-core studies. Annals of Glaciology 5, 88-94.

Louwye, S., Head, M. J., and De Schepper, S. (2004). Dinoflagellate cyst stratigraphy and palaeoecology of the Pliocene in northern Belgium, southern North Sea Basin. Geological Magazine 141, 353-378.

Louwye, S., and De Schepper, S. (2010). The Miocene–Pliocene hiatus in the southern North Sea Basin (northern Belgium) revealed by dinoflagellate cysts. Geological Magazine, 147, 760-776.

Lubinski, D.J., Polyak, L. and Forman, S.L. (2001). Freshwater and Atlantic water inflows to the deep northern Barents and Kara seas since ca 13 14C ka: foraminifera and stable isotopes. Quaternary Science Reviews 20, 1851-1879.

Marlowe, I.T., Green, J.C., Neal, A.C., Brassell, S.C., Eglinton, G. and Course, P.A. (1984). Long chain (n-C37–C39) alkenones in the Prymnesiophyceae. Distribution of alkenones and other lipids and their taxonomic significance. British Phycological Journal 19, 203-216.

Martinez, J.M., Guyot, J.L., Filizola, N. and Sondag, F. (2009). Increase in suspended sediment discharge of the Amazon River assessed by monitoring network and satellite data. Catena 79, 257-264.

Martínez-Botí, M.A., Foster, G.L., Chalk, T.B., Rohling, E.J., Sexton, P.F., Lunt, D.J., Pancost, R.D., Badger, M.P.S. and Schmidt, D.N. (2015). Plio-Pleistocene climate sensitivity evaluated using high-resolution CO 2 records. Nature 518, 49.

Martínez-Sosa P. and Tierney J.E. (2019). Lacustrine brGDGT response to microcosm and mesocosm incubations. Organic Geochemistry 127, 12-22.

Masson-Delmotte, V. Schulz, M. Abe-Ouchi A., Beer J. , A.Ganopolski A., González Rouco J.F., Jansen, E. Lambeck, K. Luterbacher, J. Naish, T., Osborn, T., Otto-Bliesner, B., Quinn T. , Ramesh R. , Rojas M. , Shao X., Timmermann, A.. Information from Paleoclimate Archives T.F. Stocker, D. Qin, G.K. Plattner, M. Tign or, S.K. Allen, J. Boschung, A. Nauels, Y. Xi a, V. Bex, P.M. Midgley (Eds.), Climate Change 2013: The Physical Science Basis. Contribution of Working Group I to the Fifth Assessment Report of the Intergovernmental Panel on Climate Change, Cambridge University Press, Cambridge, United Kingdom and New York, NY, USA (2013)

Meijer, T., Cleveringa, P., Munsterman, D. K., and Verreussel, R.M.C.H. (2006). The Early Pleistocene Praetiglian and Ludhamian pollen stages in the North Sea Basin and their relationship to the marine isotope record. Journal of Quaternary Science 21, 307-310.

Menges J., Huguet C., Alcañiz J.M., Fietz S., Sachse D. and Rosell-Melé A. (2014). Influence of water availability in the distributions of branched glycerol dialkyl glycerol tetraether in soils of the Iberian Peninsula. Biogeosciences 11, 2571.

Ménot, G., Bard, E., Rostek, F., Weijers, J. W., Hopmans, E. C., Schouten, S., and Sinninghe Damsté, J. S. (2006). Early reactivation of European rivers during the last deglaciation. Science 313, 1623-1625.

Miller, K.G., Mountain, G.S., Wright, J.D. and Browning, J.V. (2011). A 180-million-year record of sea level and ice volume variations from continental margin and deep-sea isotopic records. Oceanography 24, 40-53.

Miller, K.G., Wright, J.D., Browning, J.V., Kulpecz, A., Kominz, M., Naish, T.R., Cramer, B.S., Rosenthal, Y., Peltier, W.R. and Sosdian, S. (2012). High tide of the warm Pliocene: Implications of global sea level for Antarctic deglaciation. Geology 40, 407-410.

Miller D.R., Habicht M.H., Keisling B.A., Castañeda I.S. and Bradley R.S. (2018). A 900-year New England temperature reconstruction from in situ seasonally produced branched glycerol dialkyl glycerol tetraethers (brGDGTs). Climate of the Past 14, 1653-1667.

Moreira, A. and Fageria, N. K. (2009). Soil chemical attributes of Amazonas state, Brazil. Communications in Soil Science and Plant Analysis 40, 2912-2925.

Mosbrugger, V. and Utescher, T. (1997). The coexistence approach—a method for quantitative reconstructions of Tertiary terrestrial palaeoclimate data using plant fossils. Palaeogeography, Palaeoclimatology, Palaeoecology 134, 61-86.

Mosbrugger, V., Utescher, T., and Dilcher, D.L. (2005). Cenozoic continental climatic evolution of Central Europe. Proceedings of the National Academy of Sciences of the United States of America 42, 14964-14969.

Mudelsee, M., and Raymo, M.E. (2005). Slow dynamics of the Northern Hemisphere glaciation. Paleoceanography, 20.

Mudie, P.J., (1987). Palynology and dinoflagellate biostratigraphy of deep-sea drilling project leg-94, Site-607 and site-611, North-Atlantic Ocean. Initial Reports of the Deep Sea Drilling Project 94, 785.

Mudie, P. J. and McCarthy, F. M. G. (1994). Late Quaternary pollen transport processes, western North Atlantic: Data from box models, cross-margin and N-S transects. Marine Geology 118, 79–105.

Müller, P.J., Kirst, G., Ruhland, G., Von Storch, I. and Rosell-Melé, A. (1998). Calibration of the alkenone paleotemperature index U 37 K′ based on core-tops from the eastern South Atlantic and the global ocean (60 N-60 S). Geochimica et Cosmochimica Acta 62, 1757-1772.

Munsterman, D.K. (2016). Towards a higher resolution: The Plio-Pleistocene palynostratigraphy of well B44E0146 (Hank), interval 45-404 m. Extended and updated version, including an additional set of 20 samples. TNO report 2016 R11106: 17.

Murray, J.W. (2014). Ecology and palaeoecology of benthic foraminifera. Routledge, 1: 408.

Naafs, B.D.A., Stein, R., Hefter, J., Khélifi, N., De Schepper, S. and Haug, G.H. (2010). Late Pliocene changes in the North Atlantic current. Earth and Planetary Science Letters 298, 434-442.

Naafs, B.D.A., Gallego-Sala, A.V., Inglis, G.N., and Pancost, R.D. (2017a). Refining the global branched glycerol dialkyl glycerol tetraether (brGDGT) soil temperature calibration. Organic Geochemistry 106, 48-56.

Naafs, B.D.A., Inglis, G.N., Zheng, Y., Amesbury, M.J., Biester, H., Bindler, R., Blewett, J., Burrows, M.A., del Castillo Torres, D., Chambers, F.M., and Cohen, A.D. (2017b). Introducing global peat-specific temperature and pH calibrations based on brGDGT bacterial lipids. Geochimica et Cosmochimica Acta 208, 285-301.

Naafs, B.D.A., Rohrssen, M., Inglis, G.N., Lähteenoja, O., Feakins, S.J., Collinson, M.E., Kennedy, E.M., Singh, P.K., Singh, M.P., Lunt, D.J., and Pancost, R.D. (2018). High temperatures in the terrestrial mid-latitudes during the early Palaeogene. Nature Geoscience 11, 766.

Naish, T.R., and Wilson, G.S. (2009). Constraints on the amplitude of Mid-Pliocene (3.6–2.4 Ma) eustatic sea-level fluctuations from the New Zealand shallow-marine sediment record. Philosophical Transactions of the Royal Society of London A: Mathematical, Physical and Engineering Sciences, 367, 169-187.

Nedwell D. B. (1999). Effect of low temperature on microbial growth: lowered affinity for substrates limits growth at low temperature. FEMS Microbiology Ecology 30, 101-111.

Noorbergen, L.J., Lourens, L.J., Munsterman, D.K. and Verreussel, R.M.C.H. (2015). Stable isotope stratigraphy of the early Quaternary of borehole

Noordwijk, southern North Sea. Quaternary International 386, 148-157.
Nürnberg, D., Bijma, J. and Hemleben, C. (1996). Assessing the reliability of magnesium in foraminiferal calcite as a proxy for water mass temperatures. Geochimica et Cosmochimica Acta 60, 803-814.
O'Brien, G., O'Keefe, P., Rose, J. and Wisner, B. (2006). Climate change and disaster management. Disasters 30(1), 64-80.
Ohkouchi, N., Eglinton, T.I., Keigwin, L.D. and Hayes, J.M. (2002). Spatial and temporal offsets between proxy records in a sediment drift. Science 298, 1224-1227.
Oliverio A. M., Bradford M. A., and Fierer N. (2017). Identifying the microbial taxa that consistently respond to soil warming across time and space. Global Change Biology 23, 2117-2129.
Pancost, R.D. and Sinninghe Damsté, J.S. (2003). Carbon isotopic compositions of prokaryotic lipids as tracers of carbon cycling in diverse settings. Chemical Geology 195, 29-58.
Perry, A.L., Low, P.J., Ellis, J.R. and Reynolds, J.D. (2005). Climate change and distribution shifts in marine fishes. Science 308, 1912-1915.
Peterse, F., Kim, J.H., Schouten, S., Kristensen, D.K., Koç, N. and Sinninghe Damsté, J.S. (2009a). Constraints on the application of the MBT/CBT palaeothermometer at high latitude environments (Svalbard, Norway). Organic Geochemistry 40, 692-699.
Peterse F., Schouten S., van der Meer J., van der Meer M.T. and Sinninghe Damsté, J.S. (2009b). Distribution of branched tetraether lipids in geothermally heated soils: implications for the MBT/CBT temperature proxy. Organic Geochemistry 40, 201-205.
Peterse F., Nicol G. W., Schouten S., and Sinninghe Damsté, J. S. (2010). Influence of soil pH on the abundance and distribution of core and intact polar lipid-derived branched GDGTs in soil. Organic Geochemistry 41, 1171-1175.
Peterse, F., Prins, M.A., Beets, C.J., Troelstra, S.R., Zheng, H., Gu, Z., Schouten, S. and Sinninghe Damsté, J.S, (2011). Decoupled warming and monsoon precipitation in East Asia over the last deglaciation. Earth and Planetary Science Letters 301, 256-264.
Peterse F., van der Meer J., Schouten S., Weijers J. W., Fierer N., Jackson R. B., Kim J.H. and Sinninghe Damsté, J.S. (2012). Revised calibration of the MBT–CBT paleotemperature proxy based on branched tetraether membrane lipids in surface soils. Geochimica et Cosmochimica Acta 96, 215-229.
Pitcher, A., Hopmans, E.C., Schouten, S., and Sinninghe Damsté, J.S. (2009). Separation of core and intact polar archaeal tetraether lipids using silica columns: insights into living and fossil biomass contributions. Organic Geochemistry 40, 12-19.
Pitcher, A., Wuchter, C., Siedenberg, K., Schouten, S. and Sinninghe Damsté, J.S. (2011). Crenarchaeol tracks winter blooms of ammonia-oxidizing Thaumarchaeota in the coastal North Sea. Limnology and Oceanography 56, 2308-2318.
Plancq, J., Grossi, V., Pittet, B., Huguet, C., Rosell-Melé, A. and Mattioli, E. (2015). Multi-proxy constraints on sapropel formation during the late Pliocene of central Mediterranean (southwest Sicily). Earth and Planetary Science Letters 420, 30-44.
Pope V.D., Gallani M.L., Rowntree P.R. and Stratton R.A. (2000). The impact of new physical parametrizations in the Hadley Centre climate model: HadAM3. Climate Dynamics 16, 123-146.
Prahl, F.G. and Wakeham, S.G. (1987). Calibration of unsaturation patterns in long-chain ketone compositions for palaeotemperature assessment. Nature 330, 367.
Pross J. and Klotz S. (2002). Palaeotemperature calculations from the Praetiglian/Tiglian (Plio–Pleistocene) pollen record of Lieth, northern Germany: implications for the climatic evolution of NW Europe. Global and Planetary Change 34, 253-267.
Pross, J. and Brinkhuis, H. (2005). Organic-walled dinoflagellate cysts as paleoenvironmental indicators in the Paleogene; a synopsis of concepts. Palaeontologische Zeitschrift 79, 53-59.
Ramirez K. S., Leff J. W., Barberán A., Bates S. T., Betley J., Crowther T. W., Kelly E.F., Oldfield E.E., Shaw E.A., Steenbock C. and Bradford M. A. (2014). Biogeographic patterns in below-ground diversity in New York City's Central Park are similar to those observed globally. Proceedings of the Royal Society B 281, 20141988.
Rampen, S.W., Schouten, S., Wakeham, S.G. and Sinninghe Damsté, J.S. (2007). Seasonal and spatial variation in the sources and fluxes of long chain diols and mid-chain hydroxy methyl alkanoates in the Arabian Sea. Organic Geochemistry 38, 165-179.
Rampen, S.W., Schouten, S. and Sinninghe Damsté, J.S. (2011). Occurrence of long chain 1, 14-diols in Apedinella radians. Organic Geochemistry 42, 572-574.
Rampen, S.W., Willmott, V., Kim, J.H., Uliana, E., Mollenhauer, G., Schefuß, E., Sinninghe Damsté, J.S. and Schouten, S. (2012). Long chain 1, 13- and 1, 15-diols as a potential proxy for palaeotemperature reconstruction. Geochimica et Cosmochimica Acta 84, 204-216.
Reimers, C.E., Ruttenberg, K.C., Canfield, D.E., Christiansen, M.B., and Martin, J.B. (1996). Porewater pH and authigenic phases formed in the uppermost sediments of the Santa Barbara Basin. Geochimica et Cosmochimica Acta 60, 4037-4057.
Raymo, M.E., Lisiecki, L.E. and Nisancioglu, K.H. (2006). Plio-Pleistocene ice volume, Antarctic climate, and the global δ18O record. Science 313, 492-495.
Reuter, H. I., Lado, L. R., Hengl, T., and Montanarella, L. (2008). Continental-scale digital soil mapping using European soil profile data: soil pH. Hamburger Beiträge zur Physischen Geographie und Landschaftsökologie 19, 91-102.
Riahi, K., Grübler, A. and Nakicenovic, N. (2007). Scenarios of long-term socio-economic and environmental development under climate stabilization. Technological Forecasting and Social Change 74, 887-935.

Richardson, D.C., Newbold, J.D., Aufdenkampe, A.K., Taylor, P.G. and Kaplan, L.A. (2013). Measuring heterotrophic respiration rates of suspended particulate organic carbon from stream ecosystems. Limnology and Oceanography: Methods 11, 247-261.

Risebrobakken, B., Andersson, C., De Schepper, S. and McClymont, E.L. (2016). Low-frequency Pliocene climate variability in the eastern Nordic Seas. Paleoceanography 31, 1154-1175.

Rochon, A., Vernal, A.D., Turon, J.L., Matthießen, J. and Head, M.J. (1999). Distribution of recent dinoflagellate cysts in surface sediments from the North Atlantic Ocean and adjacent seas in relation to sea-surface parameters. American Association of Stratigraphic Palynologists Contribution Series 35, 1-146.

Rodrigo-Gámiz, M., Martínez-Ruiz, F., Rampen, S.W., Schouten, S. and Sinninghe Damsté, J.S. (2014). Sea surface temperature variations in the western Mediterranean Sea over the last 20 kyr: A dual-organic proxy (UK′ 37 and LDI) approach. Paleoceanography 29, 87-98.

Rohde, R., Muller, R.A., Jacobsen, R., Muller, E., Perlmutter, S., Rosenfeld, A., Wurtele, J., Groom, D. and Wickham, C. (2013). A new estimate of the average Earth surface land temperature spanning 1753 to 2011. Geoinformatics and Geostatistcs: An Overview 1: 1. of 7, 2.

Rueda G., Rosell-Melé A., Escala M., Gyllencreutz R., and Backman J. (2009). Comparison of instrumental and GDGT-based estimates of sea surface and air temperatures from the Skagerrak. Organic Geochemistry 40, 287-291.

Salacup, J.M., Farmer, J.R., Herbert, T.D. and Prell, W.L. (2019). Alkenone Paleothermometry in Coastal Settings: Evaluating the Potential for Highly Resolved Time Series of Sea Surface Temperature. Paleoceanography and Paleoclimatology 34, 164-181.

Salzmann, U., Haywood, A.M., Lunt, D.J., Valdes, P.J. and Hill, D.J. (2008). A new global biome reconstruction and data-model comparison for the middle Pliocene. Global Ecology and Biogeography 17, 432-447.

Salzmann, U., Dolan, A.M., Haywood, A.M., Chan, W.L., Voss, J., Hill, D.J., Abe-Ouchi, A., Otto-Bliesner, B., Bragg, F.J., Chandler, M.A. and Contoux, C. (2013). Challenges in quantifying Pliocene terrestrial warming revealed by data–model discord. Nature Climate Change 3, 969.

Schostag M., Stibal M., Jacobsen C.S., Bælum J., Taş N., Elberling B., Jansson J.K., Semenchuk P. and Priemé A. (2015). Distinct summer and winter bacterial communities in the active layer of Svalbard permafrost revealed by DNA-and RNA-based analyses. Frontiers of Microbiology 6, 399.

Schouten, S., Hopmans, E.C., Schefuß, E. and Sinninghe Damsté, J.S. (2002). Distributional variations in marine crenarchaeotal membrane lipids: a new tool for reconstructing ancient sea water temperatures? Earth and Planetary Science Letters 204, 265-274.

Schouten, S., Forster, A., Panoto, F.E. and Sinninghe Damsté, J.S. (2007). Towards calibration of the TEX86 palaeothermometer for tropical sea surface temperatures in ancient greenhouse worlds. Organic Geochemistry 38, 1537-1546.

Schouten, S., Eldrett, J., Greenwood, D.R., Harding, I., Baas, M. and Sinninghe Damsté, J.S. (2008). Onset of long-term cooling of Greenland near the Eocene-Oligocene boundary as revealed by branched tetraether lipids. Geology 36, 147-150.

Schouten, S., Hopmans, E.C. and Sinninghe Damsté, J.S. (2013). The organic geochemistry of glycerol dialkyl glycerol tetraether lipids: a review. Organic Geochemistry 54, 19-61.

Schreck, M., Matthiessen, J., and Head, M.J. (2012). A magnetostratigraphic calibration of Middle Miocene through Pliocene dinoflagellate cyst and acritarch events in the Iceland Sea (Ocean Drilling Program Hole 907A). Review of Palaeobotany and Palynology 187, 66-94.

Seki, O., Foster, G.L., Schmidt, D.N., Mackensen, A., Kawamura, K. and Pancost, R.D. (2010). Alkenone and boron-based Pliocene pCO 2 records. Earth and Planetary Science Letters 292, 201-211.

Shakun, J.D., Raymo, M.E. and Lea, D.W. (2016). An early Pleistocene Mg/Ca-δ18O record from the Gulf of Mexico: Evaluating ice sheet size and pacing in the 41-kyr world. Paleoceanography 31, 1011-1027.

Sinninghe Damsté, J.S., Hopmans, E.C., Pancost, R.D., Schouten, S. and Geenevasen, J.A. (2000). Newly discovered non-isoprenoid glycerol dialkyl glycerol tetraether lipids in sediments. Chemical Communications 17, 1683-1684.

Sinninghe Damsté, J.S., Schouten, S., Hopmans, E.C., van Duin, A.C. and Geenevasen, J.A. (2002). Crenarchaeol the characteristic core glycerol dibiphytanyl glycerol tetraether membrane lipid of cosmopolitan pelagic crenarchaeota. Journal of Lipid Research 43, 1641-1651.

Sinninghe Damsté, J.S., Rampen, S., Irene, W., Rijpstra, C., Abbas, B., Muyzer, G. and Schouten, S. (2003). A diatomaceous origin for long-chain diols and mid-chain hydroxy methyl alkanoates widely occurring in Quaternary marine sediments: Indicators for high-nutrient conditions. Geochimica et Cosmochimica Acta 67, 1339-1348.

Sinninghe Damsté J.S., Ossebaar J., Schouten S. and Verschuren D. (2008). Altitudinal shifts in the branched tetraether lipid distribution in soil from Mt. Kilimanjaro (Tanzania): Implications for the MBT/CBT continental palaeothermometer. Organic Geochemistry 39, 1072-1076.

Sinninghe Damsté, J.S., Ossebaar, J., Abbas, B., Schouten, S., and Verschuren, D. (2009). Fluxes and distribution of tetraether lipids in an equatorial African lake: constraints on the application of the TEX86 palaeothermometer and BIT index in lacustrine settings. Geochimica et Cosmochimica Acta 73, 4232-4249.

Sinninghe Damsté, J.S., Rijpstra, W.I.C., Hopmans, E.C., Weijers, J.W., Foesel, B.U., Overmann, J. and Dedysh, S.N. (2011). 13, 16-Dimethyl

octacosanedioic acid (iso-diabolic acid): A common membrane–spanning lipid of Acidobacteria subdivisions 1 and 3. Applied and Environmental Microbiology, AEM-00466.

Sinninghe Damsté, J.S., Rijpstra, W.I.C., Hopmans, E.C., Foesel, B.U., Wüst, P.K., Overmann, J., Tank, M., Bryant, D.A., Dunfield, P.F., Houghton, K., and Stott, M.B. (2014). Ether- and ester-bound iso-diabolic acid and other lipids in members of Acidobacteria subdivision 4. Applied and environmental microbiology 80, 5207-5218.

Sinninghe Damsté, J.S. (2016). Spatial heterogeneity of sources of branched tetraethers in shelf systems: the geochemistry of tetraethers in the Berau River delta (Kalimantan, Indonesia). Geochimica et Cosmochimica Acta 186, 13-31.

Sinninghe Damsté, J.S., Rijpstra, W.I.C., Foesel, B.U., Huber, K.J., Overmann, J., Nakagawa, S., Kim, J.J., Dunfield, P.F., Dedysh, S.N. and Villanueva, L. (2018). An overview of the occurrence of ether-and ester-linked iso-diabolic acid membrane lipids in microbial cultures of the Acidobacteria: Implications for brGDGT paleoproxies for temperature and pH. Organic Geochemistry 124, 63-76.

Sparkes, R.B., Doğrul Selver, A., Bischoff, J., Talbot, H.M., Gustafsson, Ö., Semiletov, I.P., Dudarev, O.V. and van Dongen, B.E. (2015). GDGT distributions on the East Siberian Arctic Shelf: implications for organic carbon export, burial and degradation. Biogeosciences 12. https://doi.org/10.5194/bg-12-3753-2015

St John, K.E., and Krissek, L.A. (2002). The late Miocene to Pleistocene ice-rafting history of southeast Greenland. Boreas 31, 28-35.

Super, J.R., Chin, K., Pagani, M., Li, H., Tabor, C., Harwood, D.M. and Hull, P.M. (2018). Late Cretaceous climate in the Canadian Arctic: Multi-proxy constraints from Devon Island. Palaeogeography, Palaeoclimatology, Palaeoecology 504, 1-22.

Svendsen, H., Beszczynska-Møller, A., Hagen, J.O., Lefauconnier, B., Tverberg, V., Gerland, S., Børre Ørbæk, J., Bischof, K., Papucci, C., Zajaczkowski, M., and Azzolini, R. (2002). The physical environment of Kongsfjorden–Krossfjorden, an Arctic fjord system in Svalbard. Polar research 21, 133-166.

Taylor, K.W., Huber, M., Hollis, C.J., Hernandez-Sanchez, M.T. and Pancost, R.D. (2013). Re-evaluating modern and Palaeogene GDGT distributions: Implications for SST reconstructions. Global and Planetary Change 108,158-174.

Theroux, S., D'Andrea, W.J., Toney, J., Amaral-Zettler, L. and Huang, Y. (2010). Phylogenetic diversity and evolutionary relatedness of alkenone-producing haptophyte algae in lakes: implications for continental paleotemperature reconstructions. Earth and Planetary Science Letters 300, 311-320.

Thöle, H., Gaedicke, C., Kuhlmann, G. and Reinhardt, L. (2014). Late Cenozoic sedimentary evolution of the German North Sea–A seismic stratigraphic approach. Newsletter of Stratigraphy 47, 299-329.

Tierney, J.E., and Russell, J.M. (2009). Distributions of branched GDGTs in a tropical lake system: implications for lacustrine application of the MBT/CBT paleoproxy. Organic Geochemistry 40, 1032-1036.

Tierney, J.E. and Tingley, M.P. (2014). A Bayesian, spatially-varying calibration model for the TEX86 proxy. Geochimica et Cosmochimica Acta 127, 83-106.

Tierney J.E. and Tingley M.P. (2018). BAYSPLINE: a new calibration for the alkenone paleothermometer. Paleoceanography and Paleoclimatology 33, 281-301.

Tipple, B.J. and Pagani, M. (2010). A 35Myr North American leaf-wax compound-specific carbon and hydrogen isotope record: implications for C 4 grasslands and hydrologic cycle dynamics. Earth and Planetary Science Letters 299, 250-262.

Toney, J.L., Huang, Y., Fritz, S.C., Baker, P.A., Grimm, E. and Nyren, P. (2010). Climatic and environmental controls on the occurrence and distributions of long chain alkenones in lakes of the interior United States. Geochimica et Cosmochimica Acta 74, 1563-1578.

Tyson R.V. (1995). Sedimentary Organic Matter. Organic Facies and Palynofacies, first ed. Chapman & Hall, London.

Uhl, D., Klotz, S., Traiser, C., Thiel, C., Utescher, T., Kowalski, E. and Dilcher, D.L. (2007). Cenozoic paleotemperatures and leaf physiognomy—a European perspective. Palaeogeography, Palaeoclimatology, Palaeoecology 248, 24-31.

Urey, H.C. (1947). The thermodynamic properties of isotopic substances. Journal of the Chemical Society (Resumed), 562-581.

Utescher, T., Mosbrugger, V. and Ashraf, A.R. (2000). Terrestrial climate evolution in northwest Germany over the last 25 million years. Palaios 15, 430-449.

Valentine, A., Johnson, A.L., Leng, M.J., Sloane, H.J. and Balson, P.S. (2011). Isotopic evidence of cool winter conditions in the mid-Piacenzian (Pliocene) of the southern North Sea Basin. Palaeogeography, Palaeoclimatology, Palaeoecology 309, 9-16.

Van Adrichem Boogaert, H.A., and Kouwe, W.F.P. WFP (1993–1997). Stratigraphic nomenclature of the Netherlands; revision and update by RGD and NOGEPA.

Van Balen, R.T., Houtgast, R.F., Van der Wateren, F.M., Vandenberghe, J. and Bogaart, P.W. (2000). Sediment budget and tectonic evolution of the Meuse catchment in the Ardennes and the Roer Valley Rift System. Global and Planetary Change 27, 113-129.

Van de Vossenberg, J.L., Ubbink-Kok, T., Elferink, M.G., Driessen, A.J. and Konings, W.N. (1995). Ion permeability of the cytoplasmic membrane limits the maximum growth temperature of bacteria and archaea. Molecular Microbiology 18, 925-932.

van de Vossenberg, J.L., Driessen, A.J., da Costa, M.S. and Konings, W.N. (1999). Homeostasis of the membrane proton permeability in Bacillus subtilis grown at different temperatures. Biochimica et Biophysica Acta (BBA)-Biomembranes 1419, 97-104.

Van den Brink, F.W.B., De Leeuw, J.P.H.M., Van der Velde, G. and Verheggen, G.M. (1992). Impact of hydrology on the chemistry and phytoplankton development in floodplain lakes along the Lower Rhine and Meuse. Biogeochemistry 19, 103-128.

van Engelen, A. F., Buisman, J., and IJnsen, F. (2001). A millennium of weather, winds and water in the low countries, in: Jones, P.D., Ogilvie, A.E.J., Davies, T.D., Briffa, K.R. (Eds.), History and Climate, Springer, US, 101-124.

van Soelen, E.E., Kim, J.H., Santos, R.V., Dantas, E.L., de Almeida, F.V., Pires, J.P., Roddaz, M. and Sinninghe Damsté, J.S. (2017). A 30 Ma history of the Amazon River inferred from terrigenous sediments and organic matter on the Ceará Rise. Earth and Planetary Science Letters 474, 40-48

Van Vuuren, D.P., Eickhout, B., Lucas, P.L. and Den Elzen, M.G.J. (2006). Long-term multi-gas scenarios to stabilise radiative forcing—exploring costs and benefits within an integrated assessment framework. The Energy Journal, 201-233.

Van Vuuren, D.P., Den Elzen, M.G., Lucas, P.L., Eickhout, B., Strengers, B.J., Van Ruijven, B., Wonink, S. and van Houdt, R. (2007). Stabilizing greenhouse gas concentrations at low levels: an assessment of reduction strategies and costs. Climatic Change 81, 119-159.

Velle, G., Brodersen, K.P., Birks, H.J.B. and Willassen, E. (2010). Midges as quantitative temperature indicator species: Lessons for palaeoecology. The Holocene 20, 989-1002.

Verschuren, D., Sinninghe Damsté, J.S., Moernaut, J., Kristen, I., Blaauw, M., Fagot, M., Haug, G.H. and CHALLACEA project members (2009). "Half-precessional dynamics of monsoon rainfall near the East African Equator." Nature 462, 637-641.

Versteegh, G.J. and Zonneveld, K.A. (1994). Determination of (palaeo-) ecological preferences of dinoflagellates by applying detrended and canonical correspondence analysis to Late Pliocene dinoflagellate cyst assemblages of the south Italian Singa section. Review of Palaeobotany and Palynology 84, 181-199.

Volkman, J.K., Barrett, S.M., Dunstan, G.A. and Jeffrey, S.W. (1992). C30 C32 alkyl diols and unsaturated alcohols in microalgae of the class Eustigmatophyceae. Organic Geochemistry 18, 131-138.

Volkman, J.K., Barrett, S.M. and Blackburn, S.I. (1999). Eustigmatophyte microalgae are potential sources of C29 sterols, C22–C28 n-alcohols and C28–C32 n-alkyl diols in freshwater environments. Organic Geochemistry 30, 307-318.

Walker, I.R., Mott, R.J. and Smol, J.P. (1991). Allerød—Younger Dryas lake temperatures from midge fossils in Atlantic Canada. Science 253, 1010-1012.

Wang H., Liu W., and Lu H. (2016). Appraisal of branched glycerol dialkyl glycerol tetraether-based indices for North China. Organic Geochemistry 98, 118-130.

Ward, N.D., Keil, R.G., Medeiros, P.M., Brito, D.C., Cunha, A.C., Dittmar, T., Yager, P.L., Krusche, A.V. and Richey, J.E. (2013). Degradation of terrestrially derived macromolecules in the Amazon River. Nature Geoscience 6, 530.

Warden, L., Kim, J.H., Zell, C., Vis, G.J., Stigter, H.D., Bonnin, J. and Sinninghe Damsté, J.S. (2016). Examining the provenance of branched GDGTs in the Tagus River drainage basin and its outflow into the Atlantic Ocean over the Holocene to determine their usefulness for paleoclimate applications. Biogeosciences 13, 5719-5738.

Warden, L., Moros, M., Weber, Y., and Sinninghe Damsté, J.S. (2018). Change in provenance of branched glycerol dialkyl glycerol tetraethers over the Holocene in the Baltic Sea and its impact on continental climate reconstruction. Organic Geochemistry 121, 138-154.

Weber, Y., De Jonge, C., Rijpstra, W.I.C., Hopmans, E.C., Stadnitskaia, A., Schubert, C.J., Lehmann, M.F., Sinninghe Damsté, J.S., and Niemann, H. (2015). Identification and carbon isotope composition of a novel branched GDGT isomer in lake sediments: Evidence for lacustrine branched GDGT production. Geochimica et Cosmochimica Acta 154, 118-129.

Weijers, J.W., Schouten, S., Hopmans, E.C., Geenevasen, J.A., David, O.R., Coleman, J.M., Pancost, R.D. and Sinninghe Damsté, J.S. (2006a). Membrane lipids of mesophilic anaerobic bacteria thriving in peats have typical archaeal traits. Environmental Microbiology 8, 648-657.

Weijers, J.W., Schouten, S., Spaargaren, O.C. and Sinninghe Damsté, J.S. (2006b). Occurrence and distribution of tetraether membrane lipids in soils: Implications for the use of the TEX86 proxy and the BIT index. Organic Geochemistry 37, 1680-1693.

Weijers, J.W., Schouten, S., van den Donker, J.C., Hopmans, E.C. and Sinninghe Damsté, J.S. (2007a). Environmental controls on bacterial tetraether membrane lipid distribution in soils. Geochimica et Cosmochimica Acta 71, 703-713.

Weijers, J.W., Schefuß, E., Schouten, S. and Sinninghe Damsté, J.S. (2007b). Coupled thermal and hydrological evolution of tropical Africa over the last deglaciation. Science 315, 1701-1704.

Weijers, J.W., Schouten, S., Sluijs, A., Brinkhuis, H. and Sinninghe Damsté, J.S. (2007c). Warm arctic continents during the Palaeocene–Eocene thermal maximum. Earth and Planetary Science Letters 261, 230-238.

Weijers, J.W., Panoto, E., van Bleijswijk, J., Schouten, S., Rijpstra, W.I.C., Balk, M., Stams, A.J. and Sinninghe Damsté, J.S. (2009). Constraints on the biological source (s) of the orphan branched tetraether membrane lipids. Geomicrobiology Journal 26, 402-414.

Weijers, J.W.H., Wiesenberg, G.L.B., Bol, R., Hopmans, E.C. and Pancost, R.D. (2010). Carbon isotopic composition of branched tetraether membrane lipids in soils suggest a rapid turnover and a heterotrophic life style of their source organism (s). Biogeosciences 7, 2959-2973.

Weijers, J.W., Bernhardt, B., Peterse, F., Werne, J.P., Dungait, J.A., Schouten, S., and Sinninghe Damsté, J.S. (2011). Absence of seasonal patterns in MBT–CBT indices in mid-latitude soils. Geochimica et Cosmochimica Acta 75, 3179-3190.

Westerhoff, W.E. (2009). Stratigraphy and sedimentary evolution: The lower Rhine-Meuse system during the Late Pliocene and Early Pleistocene (southern North Sea Basin). PhD Thesis, Vrije Universiteit Amsterdam (The Netherlands).

White, D.C., Davis, W.M., Nickels, J.S., King, J.D. and Bobbie, R.J. (1979). Determination of the sedimentary microbial biomass by extractible lipid phosphate. Oecologia 40, 51-62.

Wilf P. (2000). Late Paleocene–early Eocene climate changes in southwestern Wyoming: Paleobotanical analysis. Geological Society of America Bulletin 112, 292-307.

Wilkens, R., Westerhold, T., Drury, A.J., Lyle, M., Gorgas, T. and Tian, J. (2017). Revisiting the Ceara Rise, equatorial Atlantic Ocean: isotope stratigraphy of ODP Leg 154. Climate of the Past 13, 779-793.

Williams, M., Haywood, A.M., Harper, E.M., Johnson, A.L., Knowles, T., Leng, M.J., Lunt, D.J., Okamura, B., Taylor, P.D. and Zalasiewicz, J. (2009). Pliocene climate and seasonality in North Atlantic shelf seas. Philosophic Transactions of the Royal Society A 367, 85-108.

Williams, G.L., Fensome, R.A. & Macrae, R.A. (2017). Lentin and Williams index of fossil 523 dinoflagellates. American Association of Stratigraphic Palynologists, Contribution series, 48: 1097.

Wolfe, J.A. (1995). Paleoclimatic estimates from Tertiary leaf assemblages. Annual Review of Earth and Planetary Sciences 23, 119-142.

Wong, T.E., Batjes, D.A., and de Jager, J. (Eds.). (2007). Geology of the Netherlands. Amsterdam: Royal Netherlands Academy of Arts and Sciences.

Wood, A.M., Whatley, R.C., Cronin, T.M. and Holtz, T. (1993). Pliocene palaeotemperature reconstruction for the southern North Sea based on Ostracoda. Quaternary Science Reviews 12, 747-767.

Woodbury, H.O., Murray Jr, I.B., Pickford, P.J. and Akers, W.H. (1974). Pliocene and Pleistocene depocenters, outer continental shelf, Louisiana and Texas. Stratigraphy and Petroleum Potential of the Northern Gulf: (Part II of a Seminar on) the Gulf of Mexico, 182-194.

Woodward, F.I. (1987). Stomatal numbers are sensitive to increases in CO2 from pre-industrial levels. Nature 327, 617.

Wuchter, C., Schouten, S., Coolen, M.J. and Sinninghe Damsté, J.S. (2004). Temperature-dependent variation in the distribution of tetraether membrane lipids of marine Crenarchaeota: Implications for TEX86 paleothermometry. Paleoceanography 19. https://doi-org.proxy.library.uu.nl/10.1029/2004PA001041

Xiao W., Xu Y., Ding S., Wang Y., Zhang X., Yang H., Wang G. and Hou J. (2015). Global calibration of a novel, branched GDGT-based soil pH proxy. Organic Geochemistry 89, 56-60.

Xie, S., Chen, F., Wang, Z., Wang, H., Gu, Y. and Huang, Y. (2003). Lipid distributions in loess-paleosol sequences from northwest China. Organic Geochemistry 34, 1071-1079.

Xie, S.P., Deser, C., Vecchi, G.A., Ma, J., Teng, H. and Wittenberg, A.T. (2010). Global warming pattern formation: Sea surface temperature and rainfall. Journal of Climate 23, 966-986.

Xie, S., Liu, X.L., Schubotz, F., Wakeham, S.G., and Hinrichs, K.U. (2014). Distribution of glycerol ether lipids in the oxygen minimum zone of the Eastern Tropical North Pacific Ocean. Organic Geochemistry 71, 60-71.

Yang, G., Zhang, C.L., Xie, S., Chen, Z., Gao, M., Ge, Z. and Yang, Z. (2013). Microbial glycerol dialkyl glycerol tetraethers from river water and soil near the Three Gorges Dam on the Yangtze River. Organic Geochemistry 56, 40-50.

Yang, H., Lü, X., Ding, W., Lei, Y., Dang, X. and Xie, S. (2015). The 6-methyl branched tetraethers significantly affect the performance of the methylation index (MBT') in soils from an altitudinal transect at Mount Shennongjia. Organic Geochemistry 82, 42-53.

Zagwijn, W.H. (1960). Aspects of the Pliocene and Early Pleistocene vegetation in the Netherlands. Mededelingen Geologische Stichting, C 3, 1-78.

Zagwijn W.H. (1963). Pollen-analytic investigations in the Tiglian of the Netherlands. Geol. Stichting Meded. 16, 49-69.

Zagwijn, W.H. (1992). The beginning of the ice age in Europe and its major subdivisions. Quaternary Science Reviews 11, 583-591.

Zell, C., Kim, J.H., Moreira-Turcq, P., Abril, G., Hopmans, E.C., Bonnet, M.P., Sobrinho, R.L. and Sinninghe Damsté, J.S. (2013a). Disentangling the origins of branched tetraether lipids and crenarchaeol in the lower Amazon River: Implications for GDGT-based proxies. Limnology and Oceanography 58, 343-353.

Zell, C., Kim, J.H., Abril, G., Sobrinho, R., Dorhout, D., Moreira-Turcq, P. and Sinninghe Damsté, J. (2013b). Impact of seasonal hydrological variation on the distributions of tetraether lipids along the Amazon River in the central Amazon basin: implications for the MBT/CBT paleothermometer and the BIT index. Frontiers in Microbiology 4, 228.

Zell, C., Kim, J.H., Hollander, D., Lorenzoni, L., Baker, P., Silva, C.G., Nittrouer, C. and Sinninghe Damsté, J.S. (2014a). Sources and distributions of branched and isoprenoid tetraether lipids on the Amazon shelf and fan: Implications for the use of GDGT-based proxies in marine sediments. Geochimica et Cosmochimica Acta 139, 293-312.

Zell, C., Kim, J.H., Balsinha, M., Dorhout, D., Fernandes, C., Baas, M., and Sinninghe Damsté, J.S. (2014b). Transport of branched tetraether lipids from the Tagus River basin to the coastal ocean of the Portuguese margin: consequences for the interpretation of the MBT'/CBT paleothermometer. Biogeosciences 11, 5637-5655.

Zell, C., Kim, J.H., Dorhout, D., Baas, M. and Sinninghe Damsté, J.S. (2015). Sources and distributions of branched tetraether lipids and crenarchaeol along the Portuguese continental margin: Implications for the BIT index. Continental Shelf Research 96, 34-44.

Zhang, Y.M., and Rock, C.O. (2008). Membrane lipid homeostasis in bacteria. Nature Reviews Microbiology 6, 222.

Zhang, C., Wang, J., Wei, Y., Zhu, C., Huang, L. and Dong, H. (2012). Production of branched tetraether lipids in the lower Pearl River and estuary: effects of extraction methods and impact on bGDGT proxies. Frontiers in Microbiology 2, 274.

Zhang, Y.G., Pagani, M., Liu, Z., Bohaty, S.M. and DeConto, R. (2013). A 40-million-year history of atmospheric CO2. Philosophic Transactions of the Royal Society A 371, 20130096.

Zhu, C., Weijers, J.W., Wagner, T., Pan, J.M., Chen, J.F. and Pancost, R.D. (2011). Sources and distributions of tetraether lipids in surface sediments across a large river-dominated continental margin. Organic Geochemistry 42, 376-386.

Zhu, R., Ding, W., Hou, L., and Wang, Q. (2014). Matrix-bound phosphine and phosphorus fractions in surface sediments of Arctic Kongsfjorden, Svalbard: effects of glacial activity and environmental variables. Chemosphere 103, 240-249.

Ziegler, P.A. (1990). Geological Atlas of Western and Central Europe. (2nd edn), Geological Society Publishing House, 239.

Zonneveld, K.A., Marret, F., Versteegh, G.J., Bogus, K., Bonnet, S., Bouimetarhan, I., Crouch, E., de Vernal, A., Elshanawany, R., Edwards, L. and Esper, O., 2013. Atlas of modern dinoflagellate cyst distribution based on 2405 data points. Review of Palaeobotany and Palynology 191, 1-197.

“We can only see a short distance ahead, but we can see plenty there that needs to be done” – Alan Turing

Acknowledegements

This PhD thesis would have never come to fruition if it weren't for an initial spark of interest which took place in 2013 at Bristol University, during one of Rich Pancost's lectures for third year chemists. As a chemistry student, I was completely unaware how (organic) chemical techniques could be applied to solve critical issues in the past, present, and future climates. Rich's enthusiasm and approachability attracted me to the field of organic geochemistry which I have had the pleasure of calling my field for the last 5 years. For that initial spark, and subsequent meeting in Boston Tea Party on Park Street where we discussed master's projects, I thank you Rich! I also want to thank everyone there at Bristol who made my experience unforgettable, especially JP, David and Gordon, among others.

The transition to Utrecht University was quite daunting for me but was made so much easier and extraordinary (in a good way) by the presence of Francien and Jaap. Jaap, your Dutch humor (which surprisingly didn't take me long to get used to) and unwavering motivation to produce the best science possible are nothing short of an inspiration. Francien, your top-notch feedback and enthusiasm to get things done really left their (positive!) mark on me and set me up with a good toolbox to continue on into science! You've also been incredibly supportive of my decision to continue on in science. Both of you have encouraged me to ask critical questions about the science others, and more importantly, I am doing and for that I thank you. I am very grateful to Stefan also for stepping in and being a positive (and Zen) influence for the last few months of my thesis preparation.

I would like to thank the reading committee for their assessment on this thesis: Prof. Wout Krijgsman, Prof. Erin McClymont, Prof. Luc Lourens, Dr. David Naafs, and Prof. Dr. Lex Bouwman.

Jess, I'd like to thank you for inviting me to Arizona to come and learn the basics of Bayesian statistics with you. Your patience and help with MATLAB

and coding for an absolute beginner is greatly appreciated. I'd also like to thank all the co-authors whose expertise, time, and collaboration led to significant improvements to my manuscripts to what they are today. I am massively in debt to Dirk Munsterman, who provided me with my first samples to measure and has been a close collaborator since the start of my PhD. I'd especially like to thank Timme, Luc, Lars Noorbergen and Johan ten Veen for providing my interdisciplinary training and advice.

I am grateful to the technicians in UU and NIOZ that have been helpful over the course of these last 4 years: Dominika Kasjaniuk, Anita van Leeuwen, Arnold van Dijk, Denise van Doorhout, Desmond Eefting, and Klaas Nierop. Thanks also to Ellen Hopmans who let me use the prep HPLC system at NIOZ, your enthusiasm for technical instrumentation is unmatched!

I'd like to thank all of my colleagues in NESSC, and Mirjam for organizing the NESSC days conferences. Big thanks to Loes, Carolien, Anne, Robin, Joshua, Cait, Michiel, Els, Bregje, Itzel, Shaun and Luke for working with me on the NESSC workboard. Conference buddies: Gabriella and Julie, thanks for that boozy night at my first conference at IMOG 2015 (are the pictures still on Yuki's camera?!). Carolien: I will remember our fun days and evenings in Zaragoza at the PAGES 2017 meeting with the poster sessions in the evening with wine. Nadine: thanks for being a good conference travel buddy and for putting up with my tardy post-midnight entrance to our shared room at Gordon 2018! I look forward to spending more conferences with you all in the future. Thanks also to all the colleagues in Geowetenschappen at Utrecht that I've come to know over the past four years. Finally, I would also like to thank Loes (again), Frédérique and Allix (briefly!) for being office buddies with me. Our small organic geochemistry group at Utrecht was made much more gezellig with your presence.

Finally, a word to thank my family for being so supportive from the start of my academic career until now. I love you all | Je vous aime tous | Vi amo tutti.

About the author

Emily Katherine Louise Honora Dearing Crampton-Flood was born in 1992 in Liverpool, the United Kingdom. She received an MSci in Chemistry at the University of Bristol (2010–2014), where she was first introduced to the field of organic geochemistry and paleoclimate during a Masters project. After her undergraduate degree, she moved to the Netherlands to complete an internship at the laboratory of the Operation for the Prohibition of Chemical Weapons (OPCW) in The Hague, where she developed a deep appreciation for the application of analytical chemistry to solve societal problems. Her keen interest in the fields of organic geochemistry and paleoclimate led her to apply for a PhD at Utrecht University under supervision of Jaap S. Sinninghe Damsté and Francien Peterse.

Her PhD is an exploration through the generation of reliable terrestrial temperature records for a key interval in Earth's history which can be considered an analogue for the future: the Pliocene. The results of this multidisciplinary work are presented in this manuscript.

Emily has been living in Manchester since March 2019, where she is pursuing a postdoctoral project which aims to produce records of terrestrial temperatures for the Cretaceous-Paleogene boundary.